Development and Characterization of Drug Delivery Systems for Oral and Intravaginal Applications

Tentor, Fabio

Publication date:
2018

Document Version
Publisher's PDF, also known as Version of record

DTU Nanotech
Department of Micro- and Nanotechnology

Development and Characterization of Drug Delivery Systems for Oral and Intravaginal Applications

Fabio Tentor

PhD Thesis

30th November, 2018

DTU Nanotech – Department of Micro- and Nanotechnology

Technical University of Denmark

Building 345C

2800 Kongens Lyngby

DENMARK

Danmarks Grundforskningsfond Danish National Research Foundation
IDUN
VILLUM FONDEN

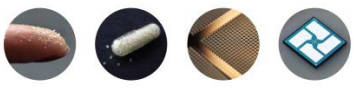

To my loved ones

To my family,

To my friends,

To my girlfriend

"Everyone sees what you appear to be, few experience what you really are."

- Niccolò di Bernardo dei Machiavelli -

Contents

Preface

The thesis here presented represents a partial requirement for obtaining a PhD degree from the Technical University of Denmark (DTU). The project was funded by the Danish National Research Foundation (grant no. DNRF122) and by the Villum Fonden (grant no. 9301) within the framework of the 'IDUN' project.

The research was carried out in the Department of Micro- and Nanotechnology (DTU Nanotech) from the 1st of December 2015 to thes 30th of November 2018. The PhD project was supervised by Professor Anja Boisen and co-supervised by Professor Kristoffer Almdal and Postdoc Sanjukta Bose Goswami.

Kongens Lyngby,
30th November, 2018
Fabio Tentor

Acknowledgements

First of all, I would like to acknowledge my supervisor, Prof. Anja Boisen, for making all of the work presented in my thesis possible. She has been a fantastic leader and a great example to follow.

I acknowledge my co-supervisors, Kristoffer Almdal and Sanjukta Bose Goswami, for supporting me during my work, for always being active in giving me feedbacks and for pushing me to become a better scientist.

A special thank goes to Associate Prof. Stephan Sylvest Keller for always being there to support us with great advises: your calm and joyful attitude has been exceptionally valuable for me during these 3 years.

I would like to thank the Nanoprobes, the amazing group I have had the luck to join within the frame of the “IDUN” center of excellence. Working with you has been an incredible experience as in you I did not find fellow colleagues only, but true friends to rely on. In some ways, the Nanoprobes group has truly been a local family to me. I will always happily remember all the laughs we have shared. I have learnt a lot from you during the last three years and for this I am most grateful.
I would like to thank all the people I have had the pleasure to work with and, in particular to: Chiara Mazzoni, Claudio Cecone, Sophie Strindberg Andersen and Peter Emil Larsen for the enjoyable and successful collaboration, Tommy Alstrøm, for your great help with the statistical analyses and Roman Slipets and Oleksii Ilchenko for your contribution with your incredible knowledge of Raman spectroscopy.

I thank Prof. Lars Berglund, Anna Svagan Hanner, Thomas Paulraj and the rest of group of the Wallenberg Wood Science Center at the Department of fiber and polymer technology for their support during my external stay at the Royal Institute of Technology (Stockholm, Sweden).

I would also like to thank Prof. Sergio Paoletti, Prof. Eleonora Marsich, Pasquale Sacco and the rest of group of the BiomatLab of the Department of life sciences, for their help during my external stay at the University of Trieste (Trieste, Italy).

A sincere thank goes to my students: Boris Spessotto, Giorgia Siccardi, Anastasia Antalaki, Jorge Alberto Sevilla Moreno and Sandra Junquera Navarrete: having the chance of contributing to your personal and scientific growth was priceless. Thank you for the continuous effort you have put in your projects and for your positive and open attitude. I am very proud of you. I am sure a bright future awaits you.

Thanks to our fantastic technicians: Lasse, Per, Christina, Lotte, Sara and Lars for helping me and the group, you have made our life in the lab incredibly easier. A special thank goes also to the administrative staff at Nanotech, one of the most helpful, optimistic and enthusiast group I have had the pleasure to interact with.

Thanks to my friends here in Denmark, for making my stay here unforgettable and to my friends in the rest of the world as your support during the past three years, despite the distance, has been incredibly important.

Thanks to Lidia. Thank you for supporting me, for fighting by my side, for believing in me and for pushing me to do better. Thank you for the laughs we have shared and for the tears we have shared. Without you, these years would have not been nearly has memorable as they are.

And, finally, I would like to thank my family. Thanks to my mother Dorina and to my father Nordio for giving me the possibility of studying and for teaching me how to become a better person. All of this would have not been possible without your support. Thanks to my sister Chiara and David for helping me during more difficult times. Thanks to my grandparents Giovanni and Olinda for your unconditional love and for reminding me what is truly important in life.

Abstract

Drug delivery systems are important medical tools that can effectively improve therapeutic outcomes. Establishing new drug delivery systems, to enhance the effectiveness of active pharmaceutical ingredients, is extremely important. It is moreover essential to consider the benefits of using a specific material for providing the drug delivery system with desired properties taking into account the route of administration that has to be used. Among the various routes of administration, the oral one is the preferred by the patients and with the highest compliance. Oral drug delivery is however limited by physiological barriers that determine a reduction in bioavailability. Nowadays, oral administration is performed using tablets and capsules. The interest towards new oral drug delivery systems based on micro-fabricated devices is, however, increasing.

Within the frame of this PhD project, microcontainers were deployed as an alternative oral drug delivery system. Microcontainers have been extensively studied in the past years, some question have, however, yet to be answered.

As a first goal of the PhD project, the addition of a water soluble sacrificial layer, included during the microcontainers fabrication, has been explored to improve the handling of the microcontainers. The compatibility of this layer with the loading and coating of microcontainers was also assessed. The resulting formulation has been tested *in vivo* and *ex vivo*. The effect of tuning the loading method in terms of different release profiles was also assessed. Finally, the 3D distribution of the active pharmaceutical ingredients within the microcontainers was visualized by Raman spectroscopy, evaluating the effect of changing the microcontainers sizes.

A second goal of the PhD project was to develop an intravaginal drug delivery system able to exploit the intravaginal environment for improving the retention time of the formulation. To reach this objective, an AL and CH mucoadhesive and biocompatible membrane was fabricated and tested *in vitro*. The membrane demonstrated to possess good mechanical properties and to slowly degrade in a simulated vaginal medium, remaining intact for up to one month.

The third goal of the PhD project involved the fabrication of polymeric nanoparticles. Polymeric nanoparticles have been extensively studied and used for several applications by many research groups. The focus of this study was to evaluate the possibility of using an ultrasonic spray coater as a novel technique for continuously producing polymeric nanoparticles in a controlled fashion. In this work, the parameters controlling the ultrasonic spray coater were also modulated to elucidate their influence upon the nanoparticles size distribution.

Resumé på Dansk

Drug delivery systemer er vigtige medicinske redskaber der effektivt forbedrer resultatet af medicinske behandlinger. Etableringen af nye drug delivery systemer er vigtig i forhold til at forøge effekten af aktive farmaceutiske ingredienser. Derudover er det essentielt, at overveje hvilke fordele specifikke materialer kan have på drug delivery systemet i forhold til at opnå de ønskede egenskaber og med tanke på administrationsvejen. Af samtlige administrationsveje, er oral indtagelse den fortrukne hos patienter og samtidig den administrationsvej med størst compliance. Oral drug delivery er dog forbundet med fysiologiske barrierer som giver en reduceret biologisk tilgængelighed. For tiden er tabletter og kapsler de fortrukne orale drug delivery systemer, men interessen for nye mikro-fabrikerede enheder er stigende.

I dette PhD projekt testes mikrocontainere som et alternativt oral drug delivery system. Mikrocontainere er blevet udførligt beskrevet de seneste år, men der er stadig ubesvarede spørgsmål.

Det første mål for dette PhD projekt var, at undersøge om tilføjelsen af et vandopløseligt aftageligt lag, under fabrikationen af mikrocontainerne, kunne forbedre håndteringen af mikrocontainerne. Kompatibiliteten med loading og coating af mikrocontainerne blev vurderet. Det endelige design blev testet både in vivo og ex vivo. Effekten af forskellige loading metoder på stofferens release-profiler blev bestemt. Slutteligt blev 3D distributionen af de aktive farmaceutiske ingredienser visualiseret med Raman spektroskopi for at evaluere effekten af varierende mikrocontainer størrelse.

Dernæst var målet at udvikle et intravaginalt drug delivery system, i stand til at udnytte det intravaginale miljø og derigennem forbedre retentionstiden for formuleringen. En alginat og chitosan mucoadhesive og biokompatibel membran blev derfor fabrikeret og testet in vitro. Membranen demonstrerede gode mekaniske egenskaber samt en langsom nedbrydning i et simuleret vaginalt miljø, varende op mod en måned.

Det tredje og sidste mål for dette PhD projekt var fabrikationen af polymeriske nanopartikler. Polymeriske nanopartikler er vel undersøgt og bruges til mange formål af flere forskellige forskningsgrupper. Fokus i dette studie var at evaluere muligheden for brugen af en ultrasonisk spray coater som en ny teknik til kontrolleret kontinuerlig produktion af polymeriske nanopartikler. Derigennem blev de kontrollerende parametre for den ultrasoniske spray coater også moduleret for, at synliggøre parametrenes indflydelse på nanopartiklernes størrelsesfordeling.

List of abbreviations

AL	Alginate
API	Active Pharmaceutical Ingredient
AUC	Area Under the Curve
BCS	Biopharmaceutical Classification System
BHI	Brain Hearth Infusion
BNPs	Blank Nanoparticles
CCD	Charge-Coupled Device
CFU	Colony Forming Unit
CH	Chitosan
CM	Confocal Microscopy
COX	cyclooxygenase
DCM	Dichloromethane
DDS	Drug Delivery System
DI-water	Deionized Water
DLS	Dynamic Light Scattering
EE%	Encapsulation Efficiency Percentage
EPR	Enhanced Permeation and Retention
FDA	Food and Drug Administration
G.v.	*Gardnerella vaginalis*
GDL	D-(+)-Glucono-delta-lactone
HP	Hot Punching
HPLC	High-Performance Liquid Chromatography
HPMC	Hydroxypropylmethyl cellulose
LB	Luria-Bertani
LNPs	Loaded Nanoparticles
MCs	Microcontainers
MDR	Multi Drug Resistance

NPs	Nanoparticles
PAA	Polyacrylic Acid
PBS	Phosphate Buffered Saline
PCL	poly-δ caprolactone
PDI	Polydispersity Index
PDMS	Poly-di-methylsiloxane
PEC	Polyelectrolyte Complex
PFOR	Pyruvate: Ferrodoxin Oxidoreductase
PVP	Polyvinylpyrrolidone
ROS	Reactive Oxygen Species
RP-HPLC	Reverse Phase – High Performance Liquid Chromatography
RPM	Revolutions Per Minute
RT	Room Temperature
S.a.	*Staphilococcus aureus*
$scCO_2$	Supercritical Carbon Dioxide
SD	Standard Deviation
SE	Secondary Electrons
SEM	Scanning Electron Microscopy
SME	Small Molecular Entities
Tg	Glass Transition Temperature
Tmax	Time at which the maximum concentration was reached
TPP	Tripolyphosphate pentabasic
XrμCT	X-ray Micro Computed Tomography
XRPD	X-ray Powder Diffraction

List of definitions

Adhesion	Tendency of two materials to cling together due to mechanical and intermolecular interactions.
Amorphous	A non-crystalline material that lacks long range order.
Antimicrobial	A molecule able to induce microbial death.
Bioavailability	The fraction of an administered active pharmaceutical ingredient that reaches the systemic circulation.
Compliance	Tendency of a patient to follow medical advice.
Crystal	A material which components are arranged geometrically to form a crystal lattice and manifest long range order.
Cytotoxicity	Negative effect on cells, where cell damage is induced by the interaction between a molecule/material and cells.
Enteral Administration	Route of drug administration that implies the absorption of the medication in the GI tract.
Excipient	Component added to a drug to grant additional properties to the formulation such as: increase rate of dissolution of the drug, stabilize the formulation and improve absorption.
First Pass Metabolism	Process by which the bioavailability of a drug is significantly reduced before distributing in the body. In oral drug delivery, the first pass metabolism is caused by the enzymes present in the intestine and in the liver.
Glass Transition Temperature	Temperature at which a material changes from a hard and relatively brittle state to a rubber-like state.
Parenteral Administration	Any route of drug administration that is not enteral
Polyelectrolyte Complex	Material formed due to the electrostatic interaction between oppositely charged particles (e.g. polymer-polymer, polymer-drug and polymer-drug-polymer).

Prodrug	Inactive precursor of a drug. These molecules are activated when metabolized in the body (e.g. in the liver).
Relative Oral Bioavailability	A measure of the amount of an active pharmaceutical ingredient that has reached the blood stream compared to a control (e.g. an intravenous administration).
Roughness	Given a surface, its roughness is quantified by the deviations in the direction of the normal vector from its ideal form.
Solid Dispersion	Physical mixture of an active pharmaceutical ingredient and excipients.
$\mathbf{T_{max}}$	Time at which the maximum concentration of a drug is detected in the blood stream.

List of publications

Paper I	**From Concept to *in vivo* testing: Microcontainers for oral drug delivery** C. Mazzoni*, F. Tentor*, S. S. Andersen, L. H. Nielsen, S. S. Keller, T. S. Alstrøm, C. Gundlach, A. Müllertz, P. Marizza, A. Boisen *Journal of Controlled Release*, vol. 268, pp. 343–351, 2017 *joint first authorship
Paper II	**Release of ketoprofen from microcontainers - influence of the loading method** F. Tentor*, C. Mazzoni*, L. Leonardi, P. Marizza, R. S. Petersen, S. S. Keller, A. Boisen Manuscript submitted to *Biomedical Microdevice* *joint first authorship
Paper III	**Where is the drug? - Quantitative 3D distribution analyses of confined drug-loaded polymer matrices** Chiara Mazzoni, Fabio Tentor, Anastasia Antalaki, Rasmus Due Jacobsen, Jacob Mortensen, Roman Slipets, Oleksii Ilchenko, Stephan Sylvest Keller, Line Hagner Nielsen, Anja Boisen Manuscript submitted to *Advanced Materials Technologies*
Paper IV	**Long lasting mucoadhesive membrane based on AL and CH for intravaginal drug delivery** Fabio Tentor, Giorgia Siccardi, Pasquale Sacco, Danilo Demarchi, Eleonora Marsich, Kristoffer Almdal, Sanjukta Bose Goswami, Anja Boisen Manuscript submitted to *ACS Biomaterials science and engineering*

Paper V	**Ultrasonic spray coating: a novel, continuous and tunable method for the fabrication of polymeric nanoparticles** F. Tentor, P.E. Larsen, S. Basak, N. Kamaly, K. Almdal, S.B. Goswami, A. Boisen Manuscript to be submitted to *Lagmuir*

Contributions to the papers

Paper I	I designed, planned and performed the experiments, together with Chiara Mazzoni. I wrote the manuscript together with Chiara Mazzoni.
Paper II	I performed part of the experimental work and data analyses in close collaboration with Chiara Mazzoni. I and Chiara Mazzoni wrote the scientific article.
Paper III	I participated in the formulation of the scientific question and in the design of experiment. I performed part of the experiments and supervised Anastasia Antalaki who significantly contributed to the experimental work. I reviewed the manuscript.
Paper IV	I defined the project, the scientific question and the experimental design. I performed the experiments and supervised Giorgia Siccardi, who significantly contributed to the work by performing parts of the experimental work. I wrote the manuscript.
Paper V	I defined the project, the scientific question and the experimental design. I performed the experiments and wrote the manuscript. Peter Emil Larsen and Kristoffer Almdal greatly contributed with the data analysis of the dynamic light scattering measurements.

List of conference contributions

I	**Microcontainers for intestinal drug delivery** F. Tentor, C. Mazzoni, S. S. Keller, P. Marizza, A. Boisen *11th Central European Symposium on Pharmaceutical Technology (CESPT)* September 22 – 24, 2016, Belgrade, Serbia
II	**Microcontainers as effective drug delivery vehicles: advances in the drug loading** P. Marizza, L. Leonardi, C. Mazzoni, F. Tentor, R. Singh Petersen, Z.Abid, A.Boisen *11th Central European Symposium on Pharmaceutical Technology (CESPT)* September 22 – 24, 2016, Belgrade, Serbia
III	**Microcontainers improve the Relative Oral Bioavailability of Ketoprofen** F. Tentor, C. Mazzoni, S. S. Andersen, L. H. Nielsen, S. S. Keller, T. S. Alstrøm, Carsten Gundlach, Anette Müllertz, Paolo Marizza, Anja Boisen *2017 Controlled Release Society Annual Meeting & Exposition (CRS)* July 16 – 19, 2017, Boston, U.S.A.
IV	**Distribution and quantitative analyses of poorly water soluble drugs loaded by supercritical CO2 impregnation in microcontainers with different sizes** Chiara Mazzoni, Fabio Tentor, Anastasia Antalaki, Rasmus Due Jacobsen, Jacob Mortensen, Roman Slipets, Oleksii Ilchenko, Stephan Sylvest Keller, Line Hagner Nielsen, Anja Boisen *Micro Nano Engineering (MNE)* September 24 – 27, 2018, Copenhagen, Denmark

1. Introduction

1.1 Motivation

This work describes the development and characterization of drug delivery systems (DDS) for oral and intravaginal applications.

Novel DDS are continuously developed with the aim of improving current therapies[1]. This objective can be reached in several ways, including an increase in patients´ compliance. Compliance (also known as adherence) corresponds to the tendency of patients to follow medical advises and prescriptions[2]. Turning an injectable formulation into an oral formulation can effectively increase patients´ compliance, due to, among other things, the avoidance of needle usage which is commonly associated with pain and is a cause of fear in a significant portion of the population[3]. Oral drug delivery is, overall, the preferred route of administration by the patients. Within this research field, numerous research groups have put their focus on improving oral DDS, for example protecting the formulation from the harsh gastrointestinal tract (GI-tract)[4–6] environment. Commercially available oral formulations come in different forms: powdered formulations, pre-dispersed in water (e.g. ketoprofen[7]), may be one of the simpler formulations. Tablets also represent a very common formulation. Tablets are obtained by compressing powdered mixtures of, for example, active pharmaceutical ingredients (APIs) and excipients. Tablets can be tuned to release the API with different kinetics in accordance to the needs of the therapy and can be coated with pH sensitive coatings to protect the formulation during its travel in the GI-tract[8]. Capsules are another highly common DDS available in the market. In this case the formulation, that can be either solid or liquid, is included inside a gelatin (or e.g. hydroxypropyl cellulose, HPMC) shell[9]. As per tablets, capsules can also be coated to protect the formulation in the GI-tract and provide release in the intestine[10].

Due to the technological advancements in the past years and to the desire of improving drug delivery, an increased interest in adopting new technologies and approaches for the production of pharmaceutical formulations has arisen. As a consequence, this led to the development of microdevices as novel drug carriers for oral delivery[11]. An example of a

top-down technology, historically deployed in the field of electronics and imported in the field of pharmaceutics, is photolithography and etching. Ahmed et al.[12] developed, in 2001, a prototype SiO_2 based microdevice as a novel DDS. Chirra et al.[13,14] were instead able to demonstrate the beneficial effect of using microdevices for improving the relative oral bioavailability of acyclovir compared to a control formulation. Also in this case, photolithography and etching were deployed to fabricate microdevices of poly methylmethacrylate (PMMA). Fox et al.[15] took a step forward and were able to introduce nanostraws in microdevices similar to those developed by Chirra et al.[14]. These nanostraws determined an increased adhesion to the mucus and facilitated drug loading due to passive diffusion. The development of microdevices for oral drug delivery has, however, several limitations: the fabrication process is not trivial and requires dedicated instrumentation, the loading of APIs can be complicated and the quantities loaded may not be sufficient or may require an excessive amount of microdevices to be swallowed to reach therapeutic ranges. Focusing the attention on the loading of microdevices, in the case of Chirra et al.[14], for example, only 1.54 ng of acyclovir could be loaded in each microdevice, requiring a high number of microdevices to be dosed to reach therapeutic ranges. This is generally due to the small volumes of the cavities of these microdevices[13]. Within the frame of microdevices for drug delivery, the usage of microcontainers (MCs) for oral administration has been, instead, one of the focal points of the research carried out in our group and has been extensively studied. In respect to the microdevices aforementioned described, MCs present a bigger cavity, of around 7 nL[16]. The increased volume allowed for the loading of higher API quantities. MCs can be loaded using several techniques, including supercritical carbon dioxide ($scCO_2$) impregnation[17,18], inkjet printing[19], powder embossing[20] and a simpler, manual approach[21]. Moreover, Nielsen et al.[22] highlighted the increased stabilization of amorphous indomethacin when confined in MCs. In this PhD project the exploration of MCs as oral DDS was continued by: i) addressing the handling of MCs after loading with API and coating with pH sensitive coatings, ii) determining the effect of changing the loading method towards the release profile of the included API and iii) evaluating the distribution of the API in the MCs after $scCO_2$ impregnation, determining the effect of confinement.

As a second aim of this PhD project, intravaginal DDS were developed. During the design and development of a new DDS, the material choice can be tailored upon the administration route chosen and on the desired characteristics of the formulation. With respect to the development of intravaginal DDS, a major focus over the years has been to develop formulations with improved residence times. The residence time of conventional formulations such as, for example, suppositories, is generally short. The formulation is in fact progressively removed due to physiological vaginal fluid loss. This causes a reduction in the bioavailability[23]. To improve the residence time Dobaria et al.[24], for instance, developed a membrane, constituted of hydroxypropyl cellulose (HPMC), which was able to resist in the vaginal cavity for 8 h. Various studies lack, however, an important characterization step, which is the evaluation of the degradation rate of the DDS in a simulated vaginal fluid[25,26]. To improve the residence time of an intravaginal DDS, we developed an alginate (AL) based membrane which is stabilized in the vaginal environment due to the presence of Ca^{2+} ions in the vaginal fluid[27]. As a model disease, bacterial vaginosis was addressed with such system, a common infection in women in their reproductive age, which symptoms are: vaginal discharge, risk of miscarriage and preterm birth. This disorder is associated with an abnormal growth of *Staphilococcus aureus* (S.a.) and *Gardnerella vaginalis* (G.v.)[28–30].

A different type of DDS investigated in the framework of the PhD project is nanoparticles (NPs). These are generally aimed at targeting drugs towards a specific cell type to improve the efficacy of the therapy. These formulations can be used as intravenous formulations[31] but could also be used for other applications[32], in conjunction, for example to MCs[33]. In particular, regarding polymeric NPs, several research groups have studied their fabrication and the possibility of deploying these DDS for various pathological conditions. These NPs are formed, exploiting the interaction between oppositely charged polymers, to form polyelectrolyte complexes (PECs)[34]. The fabrication of polymeric NPs can be performed using several approaches (discussed hereafter in paragraph 3.3.1). With the intention of addressing the issues present in the already existing fabrication methods, the development of NPs by means of an ultrasonic spray coater was investigated. Additionally, this study

shed light over the effect of tuning the ultrasonic spray coater parameters on the NPs size distribution.

1.2 Summary of the research

During this PhD project, DDS for oral and intravaginal drug delivery were developed. With respect to oral drug delivery an investigation on the use of MCs as DDS was performed. Different aspects of the MCs were investigated in Paper I, II and III, focusing on different scientific questions.

In Paper I, we evaluated the possibility of fabricating SU-8 MCs on a sacrificial, water soluble layer made of polyacrylic acid (PAA) to improve the handling of MCs. These MCs were then utilized to understand the compatibility of the sacrificial layer with the secondary steps necessary to obtain a MCs based formulation. First of all, the MCs were manually filled with polyvinylpyrrolidone (PVP), already used in previous studies. Ketoprofen (chosen as a poorly soluble model drug) was then impregnated in PVP by means of $scCO_2$ impregnation. The ketoprofen loaded MCs were subsequently coated with a pH sensitive coating to protect the formulation from the harsh gastric environment. The loaded and coated MCs were then detached from the Si wafer exploiting the presence of the water soluble sacrificial layer and collected into gelatin capsules to be dosed orally to rats. The amount of ketoprofen in the blood was compared to a control formulation.

In Paper II, the effect of loading MCs with different techniques was investigated. The MCs loading by means of hot punching (HP) of a poly-δ caprolactone (PCL) film including ketoprofen was compared to the loading of ketoprofen with $scCO_2$ impregnation MCs filled with PCL by means of HP. The differences between the two methods were evaluated by performing *in vitro* release studies.

In Paper III, MCs of different sizes filled with PVP were subjected to $scCO_2$, loading either ketoprofen or naproxen. The aim of this study was to evaluate the distribution of the API within the polymeric matrix; this was performed using a custom-made 3D Raman spectroscope.

In Paper IV, the development of an intravaginal DDS, in the form of a membrane based on AL and chitosan (CH), was performed. The aim of this work was to improve the

intravaginal residence time by exploiting the physiological intravaginal environment, rich in Ca^{2+} ions[27]. The membrane has been characterized to obtain information regarding its mechanical and biological properties.

In Paper V, a nanoparticles-based-formulation was developed using an ultrasonic spray coater. The NPs, constituted of AL and CH, have been characterized by means of dynamic light scattering (DLS) and scanning electron microscopy (SEM).

1.3 Organization of the thesis

The thesis is divided into 5 chapters, with the intention of guiding the reader through the rationale behind the work performed. The chapters provide an overview of the main scientific topics and research fields that were the focus of the PhD project.

Chapter 2 introduces the concept of drug delivery and discusses the various routes of administration with particular focus on the oral and the intravaginal route of administration, describing their advantages, disadvantages and limitations. Information on the APIs used in the PhD project is also included.

Chapter 3 provides an initial overview of the concept of DDS and then moves onto describing different types of DDS. The chapter is divided into three main parts. In the first part, microdevices are described as carriers for APIs. Furthermore, the main results of the PhD thesis, falling within the topic of microdevices, are presented. In the second part the focus is dedicated towards the usage of membranes as DDS, describing the most significant results achieved. In the last part of the chapter, NPs-based DDS are described. In particular, a closer look at the fabrication of polymeric NPs is taken, motivated by the results obtained during the PhD project.

Chapter 4 describes the experimental methods used during the PhD project and introduces the theory behind each technique.

Chapter 5 concludes the thesis with a summary and a discussion of the results achieved and includes the future perspective of this work.

The Appendix contains the published scientific articles, the submitted manuscripts and the manuscripts in preparation written throughout the PhD project.

2. Drug delivery: an overview

Drug delivery is defined as the approach, technique or formulation used to deliver an API to the patients with the aim of reaching therapeutic concentrations in a safe manner[1,35].

2.1 Active pharmaceutical ingredients

With the term API a class of molecules and macromolecules that can be used in the treatments of different diseases is defined. These molecular entities are also generally referred to as "drugs", although the meaning of this word normally identifies the combination of an API and excipients to constitute the formulation. Throughout this thesis, the words API and drug will be, nevertheless, used as interchangeable, whereas the term formulation will be used to refer to the combination of APIs and excipients.

APIs can be classified into different categories. With small molecular entities (SME) a group of molecules, with molecular weights lower than 900 Da, is indicated[36]. Conversely to SME, drugs that are represented by complex glycoproteins, having much higher molecular weights, are included in the category known as biologics (or Biopharmaceuticals)[37]. Biologics are drugs manufactured, extracted or semi-synthesized from biological sources (e.g. insulin, blood factors, and vaccines)[38]. An important difference between SME and biologics is their stability in biological media, generally lower for the latter and their cost of production, usually higher for latter.

APIs can be further distinguished in those that are active prior to dosage and those that instead require a modification to become active[39]. This is obtained by exploiting the activity of physiological enzymes that chemically modify the prodrug (inactive drug) turning it into its active counterpart.

Two of the most important characteristics of APIs are i) the solubility in aqueous media and ii) their ability of permeating biological barriers. These two properties correlate to the bioavailability of the drug after administration and must be taken into consideration during the design of new DDS. The biopharmaceutical classification system[40] (BCS) divides APIs into four classes in accordance to their solubility and permeability. Class I, is attributed when both the solubility and permeability are high, ii) class II, when the

solubility is low but the permeability is high, iii) class III, when the solubility is high but the permeability is low and iv) class IV, when both the solubility and permeability are low.
In the last decades an increasing number of new APIs, falling in Class II of the BCS, have been developed[41]. As these drugs manifest poor solubility, it has been necessary to focus on the possible ways of enhancing their solubility to improve their bioavailability[42].
A scheme of the BCS classification systems can be seen in Figure 1.

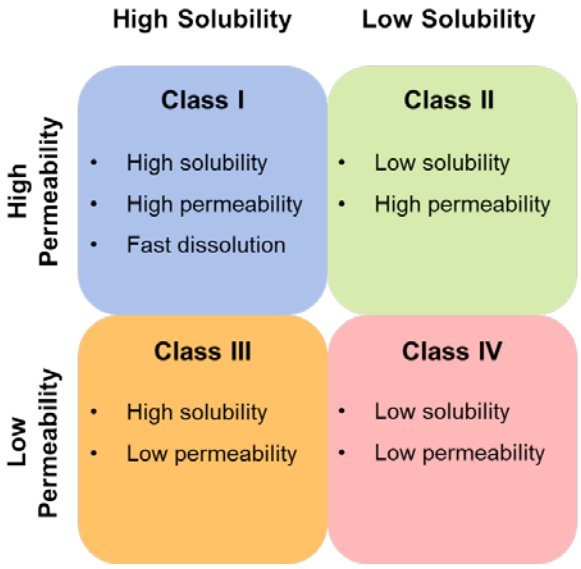

Figure 1 – Schematic representation of the BCS.

The solubility of a molecule is defined as the maximum amount of it that can be solubilized in a known volume of a known liquid, constituting a uniform phase. Solubility is generally expressed as the amount of solute in grams dissolved in 100 g of solvent at a known temperature. The solubility of molecules (e.g. APIs) in a solvent is dependent on the chemical properties of both solute and solvent.
In fact, for non-polar molecules in aqueous media, as the formation of hydrogen bonds between the solute and the solvent are not possible or can only be formed partially, poor water solubility is recorded. Aside from the chemical structure, the crystal structure of molecular entities and their physical forms (solid vs liquid), play a role in their rate of dissolution[43].

The rate of dissolution is represented by the speed at which a molecule solubilizes in the solvent at a known temperature and is dependent on the solubility of the molecule and on its physical form and crystallinity[44,45].

Crystals are highly organized and stable solid states of matter that are formed due to the intermolecular interaction between copies of the same molecule. APIs in their crystalline solid state are less soluble than their amorphous counterpart and present a lower free energy; their interaction with solvents is limited. The amorphous state is, conversely, a non-organized and unstable (or metastable) solid state. The reduced level of interaction between the molecules of the API allows for a higher solubility, as more molecules are free to interact with the surrounding environment (e.g. biological fluids) to reduce the level of free energy. The dimension of the crystals also characterize the rate of dissolution; indeed, the smaller the particles, the higher the dissolution rate is, as the surface area increases. The Noyes-Whitney equation (Equation 1) shows the calculation of the dissolution rate[44].

$$\frac{dm}{dt} = \frac{D \cdot A \cdot (C_S - C)}{L} \quad (1)$$

Where dm/dt is the dissolution rate, D represents the diffusion coefficient, A is the interface surface area between the solute and the solvent, C_s is the mass concentration of the solute at its surface layer, C represents the mass concentration of the solute in the bulk dissolution medium and L is the diffusion layer thickness (region where the concentrations are different from their value in the bulk solution).

As different APIs where used during the PhD project, these will be discussed individually, underlying their differences.

2.1.1 Ketoprofen and Naproxen

Ketoprofen ((RS)-2-(3-benzoylphenyl)-propionic acid) and naproxen ((+)-(S)-6-Methoxy-α-methyl-2-naphthaleneacetic acid) are non-steroidal anti-inflammatory drugs (NSAID) which fall in the Class II of the BCS (Figure 2)[7,46]. Ketoprofen and naproxen are used for

their analgesic and antipyretic properties. These drugs are generally prescribed for the treatment of pain deriving from arthritis and in case of severe toothaches, but can also be used to address musculoskeletal and nerve pain. Ketoprofen and naproxen execute their action by reversely inhibiting the enzymes cyclooxygenase-1 and cyclooxygenase-2 (COX-1 and COX-2); this determines a reduction in the proinflammatory prostaglandin precursors production[47,48]. These API can be prescribed as an oral formulation, topical patch, cream, gel, spray or ointment. As it concerns oral administration, ketoprofen and naproxen are rapidly and well-absorbed orally, with a plasma concentration peak occurring within 30 min to 2 h[7,46].

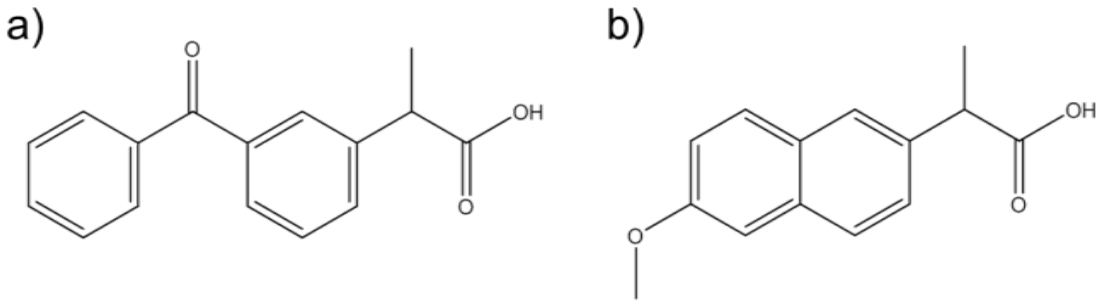

Figure 2 – Chemical structure of ketoprofen (a) and chemical structure of naproxen (b).

2.1.2 Metronidazole

Metronidazole (1-(2-hydroxy-1-ethyl)-2-methyl-5-nitroimidazole) is an antibacterial and antiprotozoal prodrug lying into the Class I of the BCS (Figure 3)[49]. Metronidazole is used to treat bacterial infections, such as vaginitis, amebiasis, trichomonas infections and giardiasis. This drug can be prescribed as an oral formulation and as a cream but it can also be administered intravenously[50,51].

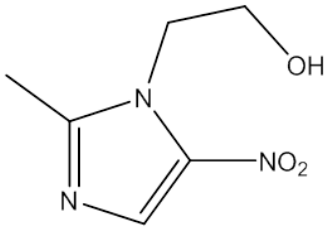

Figure 3 – Chemical structure of metronidazole.

In the form presented in Figure 3, metronidazole is non-active. To exert its antimicrobial and antiprotozoal properties, metronidazole has to reach the bacterial cytoplasm, where the reducing environment, typical of the metabolism of anaerobic and micro-aerophilic bacteria and protozoans, reduces the imidazole nitro group to a nitro radical. This radical competes with the electron acceptors of anaerobic organism for the electrons produced by the pyruvate: ferrodoxin oxidoreductase (PFOR) enzyme pathway. The energy metabolism of anaerobes is consequently hindered and, as a consequence, the replication, transcription and repair processes of DNA are compromised, leading to cell death. As metronidazole and oxygen both strive for the electrons formed during metabolism of energy, the presence of oxygen decreases metronidazole cytotoxicity and reduces activation[51–53].

2.1.3 Furosemide

Furosemide[54,55] (2-Furfurylamino-4-chloro-5-sulfamoylbenzoic acid) is a diuretic used in the treatment of fluid build-up due to heart failure, liver scarring, kidney disease and to reduce blood pressure (Figure 4). Being poorly soluble but manifesting high permeability, furosemide lies in the Class II of the BCS. Furosemide inhibits the luminal Na-K-Cl cotransporter in the ascending limb of the loop of Henle of the nephrons (Figure 4) determining a loss of sodium, potassium and chloride in the urine.

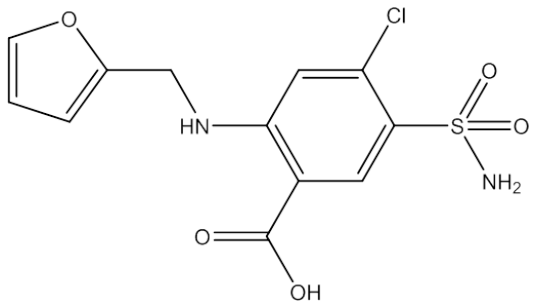

Figure 4 – Chemical structure of furosemide.

2.1.4 Enhancing the rate of dissolution of APIs

As already mentioned above, the rate of dissolution of an API is an important characteristic that can be enhanced to improve their bioavailability. Several ways have been studied in the

past years to improve the dissolution rate of APIs. A very common method to achieve this objective is to stabilize the drug in its amorphous solid state[56]. This can be done exploiting different techniques. APIs can, for example, be heated up above the melting temperature and quickly quenched with liquid nitrogen to preserve the amorphous state obtained during melting. This process can be coupled with a grinding step of the frozen API to obtain a fine powder (using a mortar and pestle or a ball-mill machine)[16,57]. Generally, however, as the amorphous state of a molecule is less stable than its crystalline counterpart, it tends to re-crystallize over time. To reduce the rate of re-crystallization, excipients can be added to the formulation, obtaining a solid dispersion[58,59]. Very common excipients used in the pharmaceutical industry are, e.g. PVP[60] (Figure 5) and PCL (Figure 6).

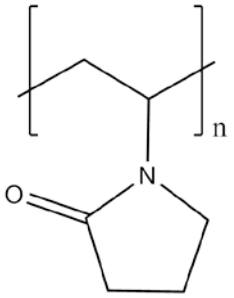

Figure 5 – Chemical structure of PVP

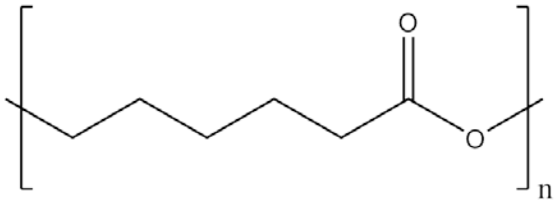

Figure 6 – Chemical structure of PCL

PVP is extremely soluble in aqueous media and is in fact used as a solubility enhancer in drug formulations. It has also been demonstrated how coupling an API in its amorphous state and PVP determines an improved stability of the formulation with a reduced rate of re-crystallization[61]. This is possible thanks to the interactions occurring between the API and PVP. A method that couples the addition of a polymer, such as PVP or PCL with a

thermal treatment, is, for example, hot-melt extrusion[62], where the formulation (drug + excipient) is heated up above the glass transition temperature (Tg) or above the melting temperature of the compounds and extruded through a nozzle after extensive mixing[63]. This technique is highly efficient, with high-throughput and is potentially continuous. A different method that can be used to couple an API with a polymer is the use of $scCO_2$ impregnation, this technique exploit the ability of $scCO_2$ to solubilize a drug which is then impregnated into a polymer matrix[17,18,64]. This technique will be further addressed in the thesis as it represents a significant portion of the PhD project.

A different method to stabilize the amorphous state of a drug, is the inclusion of it in micro-sized reservoirs called MCs. Nielsen et al.[22] demonstrated, in fact, that a slower rate of recrystallization was seen for indomethacin included in MCs compared to pure powder. Aside from changing the physical state of APIs, to increase the dissolution rate of formulations it is possible to tune the formulation size. By reducing the size of the formulation, the ratio between surface and volume increases significantly and the rate of dissolution increases accordingly.

2.2 Administration Routes

APIs can be delivered to the patients using different administration routes: each one bestowing advantages and disadvantages. Administration routes are generally separated into two distinct categories: i) enteral routes of administration and ii) parenteral routes of administration.

Within enteral administration, all routes that involve the consumption of APIs in the gastrointestinal tract are included. Enteral administration thereby includes the oral, rectal, sub-lingual, sub-labial and buccal administration. The parenteral route, as the name explicates, refers instead to all administration routes that are not enteral, the medications are administered directly to the mucosa (or accessible epithelia) or injected with a needle or a catheter. Injections can be performed in several different locations, depending on the disease and the condition of the patient, some of these are: intravenous, subcutaneous and intramuscular.

As in this PhD thesis, both oral and intravaginal DDS were developed, these two routes of administration will be further discussed.

2.2.1 Oral administration

The oral administration of pharmaceuticals has several advantages and is the preferred route by the patients[65]. The reason why the oral route of administration is more easily accepted by the patients lies in its intrinsic easiness. Swallowing a tablet or capsule is in fact extremely similar to the daily process of eating food. Moreover, compared to injections, oral administration is painless. Indeed, the fear of needles is not to be underestimated as it is present in a significant portion of the adult population and is very common in children[66]. The reduced compliance due to the fear of needles may determine the worsening of diseases with a consequent negative impact in the patients´ quality of life and on the healthcare system. The substitution of injected medication to oral medication is also pushed by the potential reduction of the hazardous wastes production. Finally, in countries under development, were the resources are poor and the logistics of transportation are complicated, reducing the number of medications requiring the usage of syringes and needles represents a priority.

Nonetheless, designing formulations for oral drug delivery is not trivial. First of all, an important difference between injections and oral administration lies in the bioavailability. When an API is injected into the blood stream, all of it is available. Conversely, when a drug is administered orally, the absorption of the API in the blood stream occurs after absorption in the intestine and after the first pass metabolism. This generally causes a reduction in the bioavailability of the API and, as a consequence, higher dosages may be required to reach the therapeutic range for that specific drug. When a drug is taken through the oral route, it has first to be able to resist the oral environment, where the pH is neutral, or slightly alkaline, and the presence of enzymes may degrade the API[67]. The formulation has, then, to be small enough to be swallowed with ease and pass safely through the esophagus, reaching the stomach. In the stomach, the presence of enzymes and the low pH (1 - 3.5 in fasted state and 3 - 6 in fed state)[68–70] (Figure 7), may degrade the formulation before its absorption. This is particularly crucial for biologics, such as insulin

and other proteins that, if not protected, are degraded to smaller peptides, as it occurs for food. Protecting the API from the harsh gastric environment is thereby fundamental. Once reached the small intestine, the formulation has to be designed for releasing the API in the appropriate intestinal region. For most APIs, this is represented by the small intestine (duodenum, jejunum and ileum) where the absorption is higher due to the high surface area available by the presence of *villi* and *microvilli*[71]. Even if the controlled release is achieved, it is also important to consider, during formulation design, that the pH of the small intestine varies between 5.5 and 8[68] and that the presence of bile salts and enzymes could affect the formulation or the API prior to absorption. The last barrier a formulation encounters before reaching the enterocytes (intestinal epithelium) is represented by the mucus layer[72,73]. Mucus is secreted by the Goblet cells in the intestine and its building blocks are mucins: highly glycosylated proteins rich in disulfide bonds and comprising a highly negative and a hydrophobic domain. Mucus is constituted by two separated layers, the first one is a firmly adherent layer, closer to the epithelium and the second one is represented, instead, by a loosely adherent mucus layer. The intestinal mucus is continuously produced, with a variable turnover from few minutes to hours. The presence of mucus in the intestine is extremely important as it acts as lubricant and prevents infections from microorganisms. Mucus can, however, interfere with the formulation, blocking the API before reaching the intestinal epithelium and thereby its absorption. Finally, the formulation has to degrade over time or has to be excreted safely with the feces.

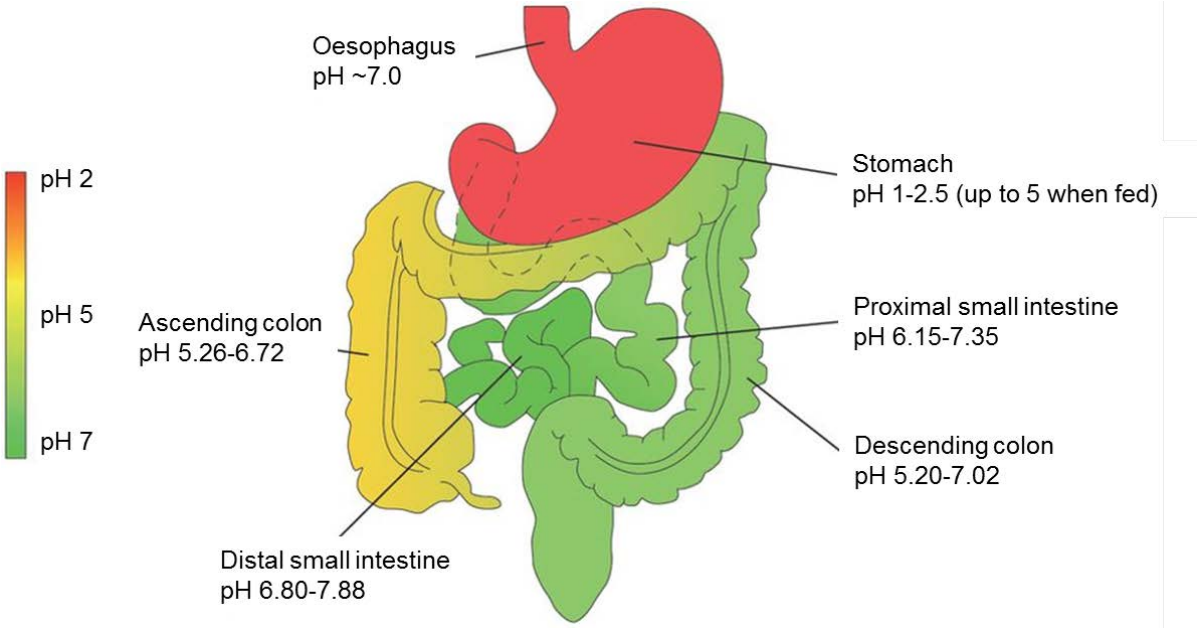

Figure 7 – Representation of the human stomach, small intestine and large intestine with the relative pH found in each region. Figure taken from[69] with permission.

2.2.2 Intravaginal administration

The intravaginal route of administration is considered as a favorable site for the local[74] and the systemic delivery of drugs[75]. Intravaginal formulations can thereby be designed for systemic delivery but also for topical/mucosal delivery. In the first case, when a formulation is administered to the vaginal mucosa, the API dissolves in the vaginal fluid and undergoes trans-membrane penetration. The possibility of exploiting intravaginal drug delivery as a route for systemic delivery has been extensively studied. The poor absorption of molecules by the vaginal mucosa remains a challenge that has to be dealt with[75]. Moreover, an important disadvantage in the context of intravaginal drug delivery, is the patient to patient variance: personal hygiene, irritation, porosity, vaginal microflora, viscosity and thickness of the vaginal mucus together with the volume and the pH of the vaginal fluid, all can vary significantly between patients and, thus, the same formulation might not behave in the same manner[76].

Nevertheless, an advantage of administering drugs intravaginally for systemic delivery is found in the avoidance of needle usage (comparing to injections) and in the avoidance of first pass metabolism (comparing to oral administration). In the second scenario, the API is released in the vaginal cavity and exerts its effect *in situ*. Antifungal, antiviral, antibacterial, antiprotozoal and spermicidal agents have all been used as *in situ* formulations to treat common diseases. As an example, vaginal candidiasis, a common bacterial infection (caused by the presence of *Candida albicans* in the vagina), is treated by means of local delivery. Aerobic vaginitis, an alteration of the physiological microflora, often evidenced by inflammation symptoms and presence of pathogens, especially *Streptococcus galactiae* and *Escherichia coli* is another critical problem treated with local delivery.

3. Drug delivery systems

DDS are formulations that, combining APIs and excipients, are used in drug delivery to target specific cells[77], or a specific area of the body and to control the release of the drug over time[78]. When developing novel DDS it is, for obvious reasons, important to consider the administration route that has to be used. As described previously (Chapter 2.2), in fact, different administration routes present different limitations that must be considered during the design of the DDS. Nevertheless, the usage of DDS, more complex than common formulations, has the potential of greatly improving the therapy outcome. Important examples, where the design of novel DDS greatly impacted the outcome of therapies, can be found in the literature. In 1995, Doxil®, was approved by the Food and Drug Administration (FDA) as the first nano-DDS for the treatment of cancer[31]. Doxil® is a DDS constituted of a pegylated liposome encapsulating doxorubicin, a known API used in cancer treatment. This DDS showed several advantages: i) being in the nano-sized range, the enhanced permeation and retention effect (EPR) could be exploited for delivering the API at the tumor site, where, due to the high expression of vascular endothelial growth factor (VEGF) the vascularization is abnormal and leaky[79], ii) prolonged circulation in the blood stream was achieved and iii) a significant reduction in the adverse effects, specifically towards the heart, was obtained. Xu et al.[80], on the other hand, developed an injectable DDS based on nano-porous Si encapsulating doxorubicin. This DDS was able to accumulate preferentially in the metastasis sites of triple negative breast cancer (liver and lungs) thanks to its geometrical design, internalize in tumor cells, escaping the endosomes and avoiding the multi drug resistance (MDR) to finally cause cancer cell death.

In the past years, several types of DDS have been developed, each of these granting additional features to the formulation. DDS can be classified in multiple ways. As in the PhD project the focus was kept on different types of drug carriers, constituting the base of the DDS, a classification based on this seems appropriate. By drug carrier, the substrate used in the design of the DDS, which improves the safety and/or the effectiveness of the final formulation, is defined. This terminology is generally associated with nano-particulate

DDS, such as liposomes[31,81] and polymeric NPs[32,82,83], this definition fits, nevertheless, other types of substrates, as in example: patches and microdevices encapsulating an API.

In the next paragraphs, a deeper look at some drug delivery carriers, specifically microdevices, membranes (or patches) and nano-particulate systems, will be taken.

3.1 Microdevices

Pushed by the improvements in technology and by the desire of improving oral drug delivery, DDS based on the use of microdevices, as carriers, have emerged. Several research groups contributed in the development of this field of research, exploiting different fabrication techniques[11]. To give some examples, Chirra et al.[14] were successful in demonstrating the advantages of using planar microdevices to improve the oral bioavailability of acyclovir (class III drug in the BCS) compared to a solution in mice. Fox et al.[15], instead, focused their attention on porous nanostructured delivery substrates comprising nanostraws. These increased the adhesion to the mucus and facilitated the drug loading via diffusion inside the nanostraws.

In this work, a MCs based formulation was used to improve oral drug delivery. These MCs are cylindrical shaped reservoirs with a cavity in the micrometer scale and a volume in the nanoliter range. The size of these MCs can be adjusted to obtain deeper, shorter or larger MCs. MCs are fabricated with the negative photoresist SU-8, an epoxy resin. The fabrication of MCs has been explained in previous publications[19,84]. Briefly, a layer of SU-8 is spin coated over a 4-in. Si wafer and cured with UV light, the desired pattern is obtained using a shadow mask to selectively illuminate the substrate. The fabricated MCs are distributed in arrays of 25x25 pieces on a Si wafer (seen as squares/chips in Figure 8).

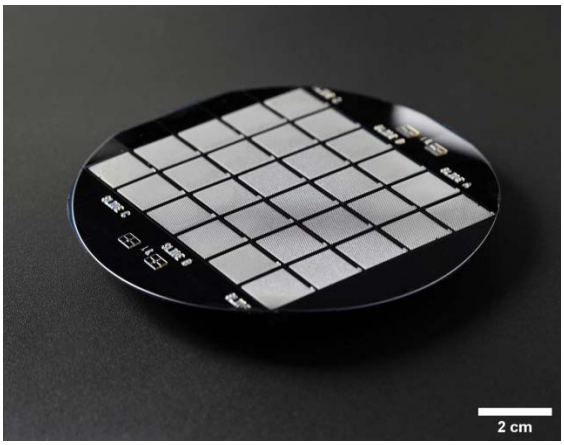

Figure 8 – Picture showing a Si wafer with MCs distributed in an array of 5x6 chips of 25x25 MCs.

MCs for oral drug delivery have been extensively investigated by our group. Marizza et al.[17–19] evaluated the use of $scCO_2$ impregnation and of inkjet printing to load APIs in MCs. Nielsen et al.[22] demonstrated a significant improvement in the stability of the amorphous state of indomethacin when confined in MCs compared to unconfined powder. Nielsen et al.[11,85] also showed how the relative oral bioavailability of furosemide in rats was higher than a control formulation and how it was possible to include spray dried cubosomes in the MCs. Abid et al.[20], developed a method for loading powder formulations in the MCs in a more controlled manner in respect to the previously used manual approach[21]. Overall, several works were conducted in order to shed light on the advantages of MCs as carriers for oral drug delivery. Several issues, however, persisted. SU-8 is, for instance, a non-biodegradable and non FDA approved material for oral drug delivery. Trying to address this issue, Nielsen et al.[86] worked on microwells of poly-L-lactic acid (PLLA) including furosemide and covered with a pH sensitive coating as a starting point for future works on the fabrication of biocompatible and biodegradable MCs.

In this work, we focused our attention on some of the other issues related to MCs, being: i) the handling of the MCs, ii) the loading of MCs and iii) the deposition of pH sensitive coatings over the MCs to protect the API from the harsh gastric environment.

In regards to the handling of the MCs, a study on SU-8 MCs fabricated on a water soluble sacrificial layer of polyacylic acid (PAA) is described in Paper I[16]. Figure 9 depicts an example of a MCs chip on a sacrificial layer of PAA.

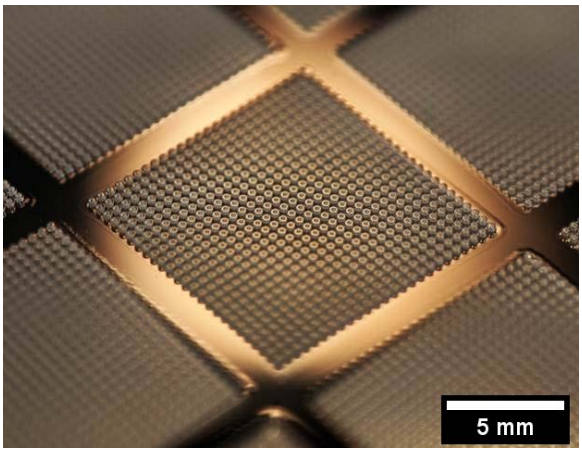

Figure 9 – Picture of a MCs chip fabricated over a sacrificial layer of PAA.

The presence of PAA facilitated the collection of MCs loaded with ketoprofen by means of $scCO_2$ impregnation and coated with a pH sensitive coating. This was possible by soaking the MCs chips in water, acidified to prevent disruption of the coating.

To protect the formulation inside the MCs, an ultrasonic spray coater has been deployed to deposit a pH sensitive coating over the MCs. Ultrasonic spray coating has been extensively used as a coating technique by many research groups[86]. Bose et al.[87], evaluated the effect of tuning the spray coater parameters on the coating outcome; in particular, a wet and a dry regime were found as extreme cases. In the former regime, the coating manifested the presence of edge peaks whereas the other regime caused the formation of a non-homogenous and rough coating. The optimal regime thereby falls between these two and thus the ideal parameters to use have to be defined whenever a different solution is utilized (e.g. different polymers, concentrations, solvents). To avoid a wet regime it is necessary to reduce the amount of solution deposited per interval time, this can be achieved by reducing the flow rates (e.g. 0.1 mL/min). A different option is to use solvents with high evaporation rate (e.g. dichloromethane, DCM) an issue that can be encountered when using low boiling point solvents is, however, the risk of clogging the spray coater nozzle. This problem has to be taken into consideration during the spray coater processes. Increasing the substrate temperature is also a valid option to avoid the wet regime, however, it is necessary to bear in mind that the temperature of the substrate can affect the behavior of the polymeric coating. Moreover, the temperature of the substrate should be carefully raised also

accounting for the sensitivity of the API to heat. Increasing the distance between the nozzle and the substrate, to obtain a higher evaporation during the travel time of the spray from the nozzle to the sample, is also a possibility. To avoid falling in the dry regime, the same considerations can be made, but, obviously, inverted. When coating an area, the nozzle sprays the solution following a programmed path defined by the operator. To increase the coating thickness, the same area is sprayed repeatedly in loops until the desired thickness is reached. "Passes" is the term used to define the number of times the spray coater coats the same area. Increasing the speed of the nozzle and/or including a waiting time between consecutive passes can also help to avoid either the wet or the dry regimes and allows for the formation of smoother coatings. For more information on the spray coater, please refer to Chapter 4.2.

In Paper I, the parameters used to deposit a pH sensitive coating on SU-8 MCs are described. A solution of 2% w/V of Eudragit L100® (Evonik, Darmstad, Germany, Figure 10) with dibutyl sebacate (5 wt% in respect to Eudragit L100, Figure 11) in 2-propanol was spray coated over 12.8 x 12.8 mm^2 MCs chip.

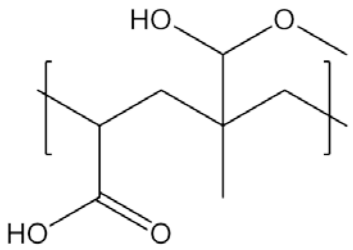

Figure 10 – Chemical structure of Eudragit L100®.

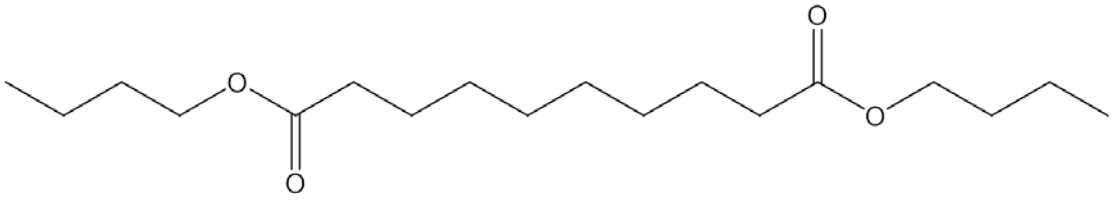

Figure 11 – Chemical structure of dibutyl sebacate.

Each chip was coated with two alternating spray paths with an offset of 2 mm, resulting in a total of 100 passes. The presence of an offset was set to obtain more homogenous coatings (Figure 12).

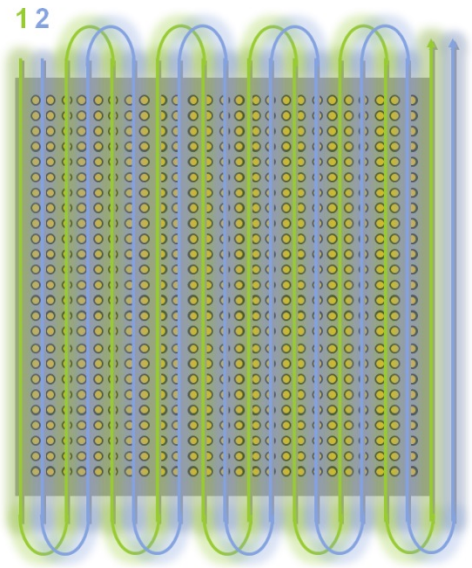

Figure 12 – Schematic representation of the spray coater path utilized for the deposition of the pH sensitive coating based on Eudragit L100® and dibutyl sebacate on a MCs chip.

The resulting coating had a thickness of about 120 μm and allowed for a pH dependent release of ketoprofen from the MCs.

In Paper II and Paper III the focus was kept over the loading process. In particular, in Paper II, the loading technique of $scCO_2$ was performed on PCL filled MCs. PCL was chosen in the attempt of slowing the release of ketoprofen which was seen to be fast in previous studies, where PVP was used[16,18]. PCL is known for its ability of impregnating in supercritical CO_2[64] and for its biodegradability. Not behaving as a solubility enhancer as PVP[88,89], PCL was therefore an optimal choice to slow the release of ketoprofen. In Paper II, two techniques: i) hot punching (HP) of a PCL film into the MCs and consequent loading of ketoprofen using $scCO_2$ impregnation and ii) HP of a premixed PCL and ketoprofen film into the MCs, were, moreover, compared. Surprisingly, the two techniques showed different results. In the former, a burst release, similar to that seen previously with impregnated MCs filled with PVP and loaded with ketoprofen by means of $scCO_2$[18] was seen; In the latter, a much slower release was instead demonstrated, indicating how the different technique approach can influence the release profile of ketoprofen.

In Paper III, the focus was devoted to the $scCO_2$ impregnation technique. In particular, different sizes of MCs (small, medium and large) were fabricated on Si wafers maintaining

the total volume and surface area of the cavities for all samples identical. The MCs were then filled with PVP and impregnated using either ketoprofen or naproxen. An investigation of the API release profile and of the drug distribution in the polymer matrix from these MCs was performed. The results showed no difference among the sizes in terms of release kinetics and in the distribution of APIs in the PVP matrix. The distribution was assessed with a custom-made 3D Raman spectroscope and, interestingly, in all samples investigated (small, medium and large MCs filled with PVP and loaded with ketoprofen or naproxen by means of $scCO_2$ impregnation) the APIs resulted to be present only in the top layer of PVP. This result was extremely important as it allowed defining the reasons behind the burst release seen in previous studies, both using PVP and PCL, when the $scCO_2$ impregnation technique was deployed. The burst release obtained was consequently caused by the selective positioning of the API rather than being influenced by the polymer deployed. To improve the permeation of ketoprofen (or other drugs), in the MCs, an increase in the amount of time the samples are exposed to $scCO_2$ impregnation might be needed.

3.2 Membranes

Membranes (also known as patches) are a common DDS, generally deployed for topical applications. In this work, we designed, developed and characterized a membrane based on the usage of two polysaccharides (AL and CH) suitable for intravaginal applications. Several membranes have been developed in the past years for drug delivery purposes, different materials have been used for their development, encapsulating different APIs and aiming at different objectives. Travan et al.[90], for instance, developed a membrane starting from an AL hydrogel by means of a freeze-drying step. The developed membrane resulted to be able to release hyaluronic acid when in contact with physiological solutions. As a step forward to this publication, Scognamiglio et al.[91], were able to produce a mussle-inspired-mucoadhesive AL membrane by exploiting the known mucoadhesiveness of dopamine[92] which was grafted to AL or deposited as a mucoadhesive coating in the form of NPs[93]. CH was instead deployed by Sacco et al.[94] to develop antimicrobial membranes comprising silver. As previously described, also in this case, a hydrogel was initially prepared, thanks

to the crosslinking of CH with tripolyphosphate pentabasic (TPP)[95] and then freeze-dried to obtain a pliable membrane. Overall, it is clear that the usage of polysaccharides for the development of membranes for drug delivery has been and continues being extensively investigated.

A fundamental step in the design of a membrane as a DDS is to utilize appropriate materials to provide the final formulation with the needed characteristics. In example, a membrane that has to degrade over time should be constituted of biodegradable materials and the degradation of the formulation should be consequently assessed in biorelevant medium. The main results of the work reported in Paper IV are, in fact, consequences of the material choice. The very long degradation time demonstrated by the AL and CH based membrane, able to resist in a simulated vaginal fluid for at least 30 days was achieved by exploiting the presence of Ca^{2+} in vaginal fluids. AL, being crosslinked by divalent cations (e.g. Ca^{2+}), resulted, thereby, a good choice for the fabrication of the membrane.

To enhance the adhesion of the membrane towards the vaginal mucosa, CH was included in the final formulation and was seen to improve the membrane adhesiveness.

The developed membranes possessed good mechanical properties, in line with the results of Jang et al.[96] and were able to encapsulate metronidazole (Figure 13 and Figure 14), chosen as a model class I API and to release it in a simulated vaginal fluid[27].

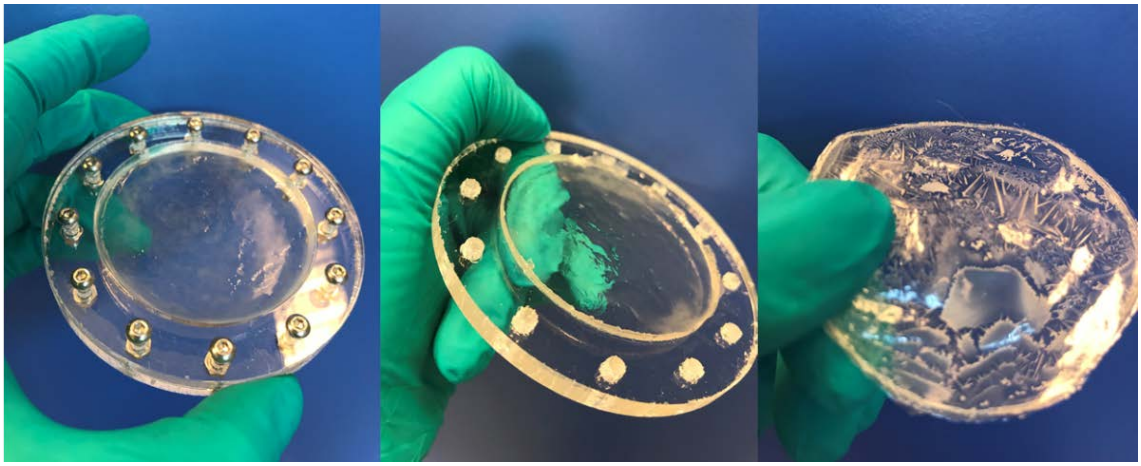

Figure 13 – Fabrication of an AL + metronidazole membrane. From left to right: an AL hydrogel including metronidazole was prepared; the hydrogel was then dried at RT; an AL membrane after complete drying. Crystals of metronidazole are visible in the dry membrane.

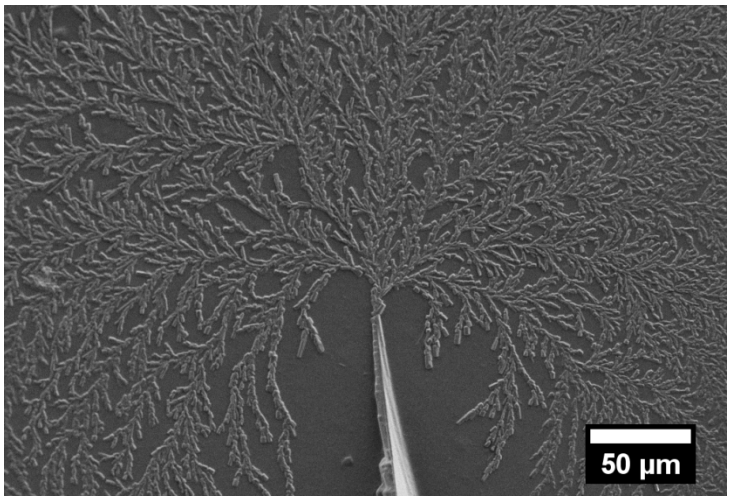

Figure 14 – SEM picture of metronidazole crystals included in the AL/CH membrane.

Finally, the AL/CH + metronidazole membranes were seen to be biocompatible towards an ectocervix epithelial cell line Ect1/E6E7 (ATCC® CRL-2614™) and to be able to kill both S.a. and G.v.

As the AL/CH membrane resulted to degrade slowly, the possible utilization of it as a formulation for birth control drugs was also investigated. Specifically, the encapsulation of ethinyl estradiol (Figure 15) was assessed. Ethinyl estradiol is a hormone, generally used in combination with etonogestrel, deployed in birth control therapies. Although only preliminary, the results demonstrated the possibility of encapsulating sufficient amount of ethinyl estradiol to reach the dosages currently administered in the commercially available medications (15 µg/day of ethinyl estradiol over three weeks). Future works will be dedicated to investigate the release of ethinyl estradiol in a simulated vaginal fluid. The simultaneous encapsulation of ethinyl estradiol and of etonogestrel will also be explored.

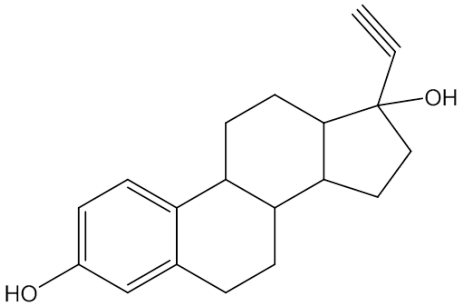

Figure 15 – Chemical structure of ethinyl estradiol.

3.2.1 Fabrication of membranes by means of a dual feed ultrasonic spray coater

During the optimization of the ultrasonic spray coater, performed to obtain the results reported in Paper V, where AL and CH NPs have been fabricated using a dual feed Accumist nozzle (please refer to Chapter 4.2 for the ultrasonic spray coater description), an interesting result was seen. In fact when the spray coater was run with AL and CH solutions both at concentrations above 0.2 mg/mL, the formation of a macroscopic hydrogel was seen. This happening allowed us to discover the possibility of using the ultrasonic spray coater to form a hydrogel coating (e.g. to protect the formulation included in MCs) but also to form membranes (e.g. AL/CH membranes similar to those reported in Paper IV).

Hydrogel coatings of various thicknesses were fabricated using a solution of AL 0.5 mg/mL + TPP 10 µg/mL + metronidazole 1 mM in one of the two feeds and a solution of CH 0.5 mg/mL in the other one. Due to the high polymer concentration, a high generator power had to be deployed: 3 W. The spray coater parameters were then optimized to coat an aluminum foil surface of 25 cm^2 using the following parameters: the flow rate was kept at 0.4 mL/min, the speed of the nozzle was set at 50 mm/sec, the pressure of the focusing air was set at 1 kPa and the temperature of the substrate was maintained at 30ºC. Different thicknesses were obtained by increasing the number of passes: 10, 20, 30 and 45 passes were tested. The thickness of the coatings were 582 ± 34 nm, 1.03 ± 0.1 µm, 2.23 ± 0.2 and 11.5 ± 2.4 µm respectively (measured from SEM pictures, Figure 13). The thickness obtained with 45 passes is much higher than those of the other experiments and does not follow their trend. This might be explained by the increased inhomogeneity. With increased number of passes an increase in the formation of big droplets on the surface, was, in fact, noticed.

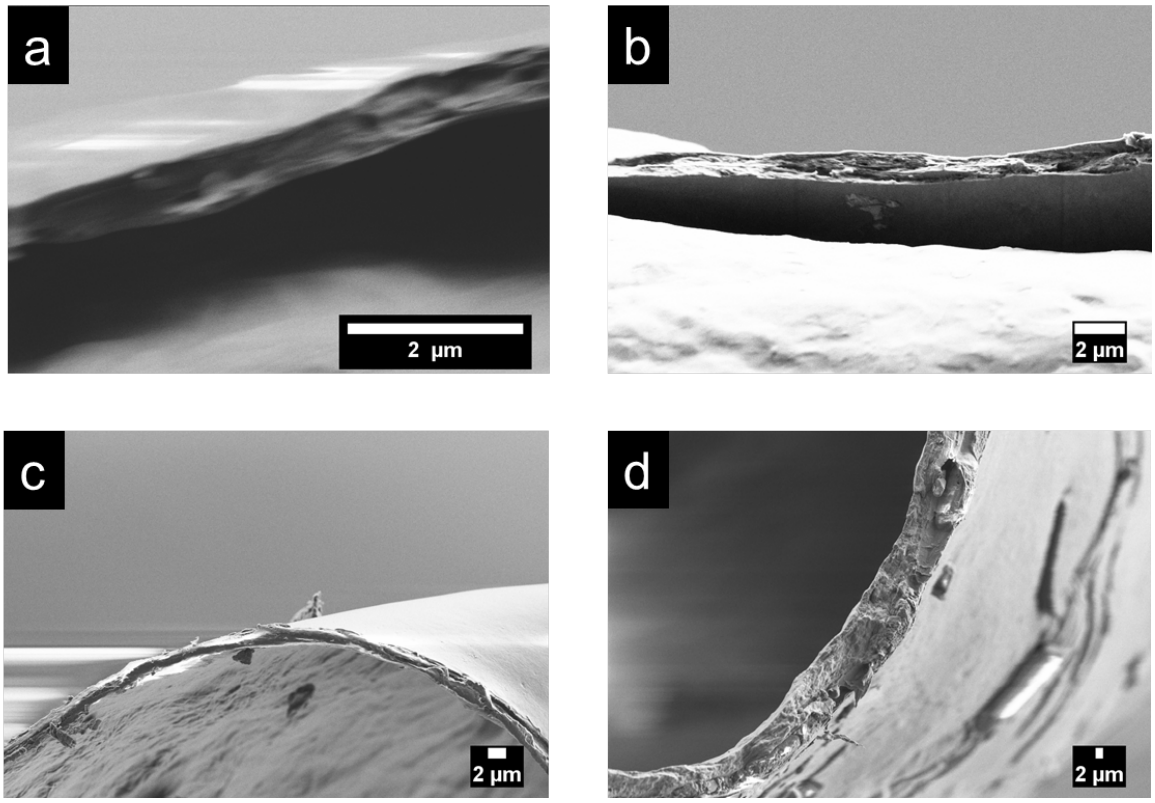

Figure 16 – SEM pictures of AL/CH + metronidazole + TPP coating fabricated by means of a dual feed ultrasonic spray coater: a) 10 passes, b) 20 passes, c) 30 passes and d) 45 passes.

Dissolution studies, performed in phosphate buffered saline (PBS, pH 7.4) showed a fast release of metronidazole from all samples, reaching 100% of release during the first 10 min (Figure 14).

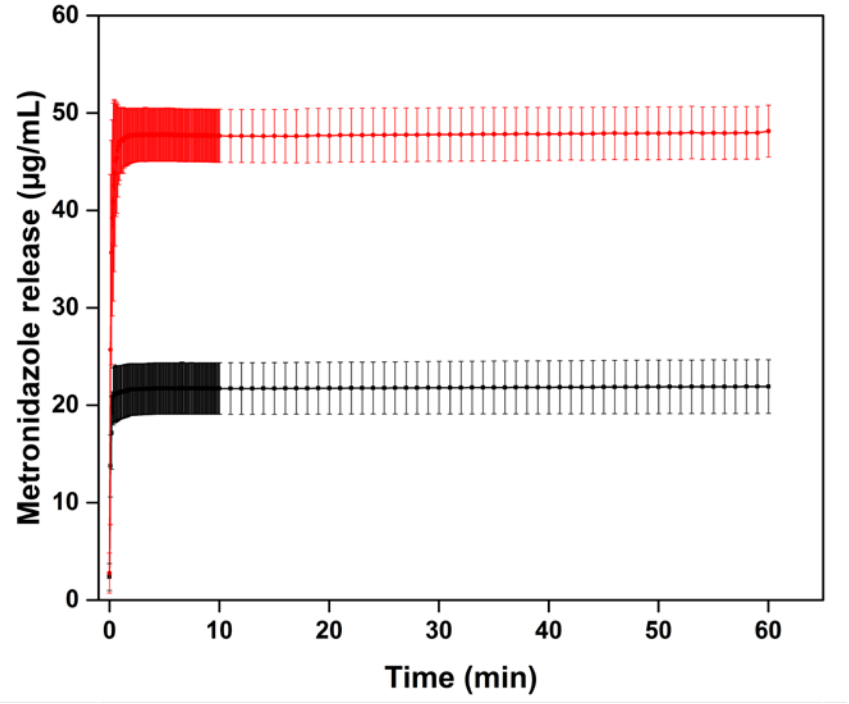

Figure 17 – Release profile from AL/CH + TPP + metronidazole coatings. The result from 10 passes coatings is represented by the black line; the result from 20 passes coatings is depicted by the red line. (N = 4, SD)

3.2.2 Alginate

Alginate is a linear block copolymer of (1-4)-linked β-D-mannuronate (poly M) and its C-5 epimer α-L-guluronate (poly G). AL is an abundant polysaccharide obtained from brown algae[97]; this material has been studied extensively due to its highly interesting properties. AL is, in fact, able to form hydrogels in the presence of calcium and other divalent cations forming structures named egg-boxes[98]. This is possible thanks to the coordination of the divalent cations with the poly G units[99]. In Figure 18, a representation of the chemical structure of AL and its interaction with calcium is depicted.

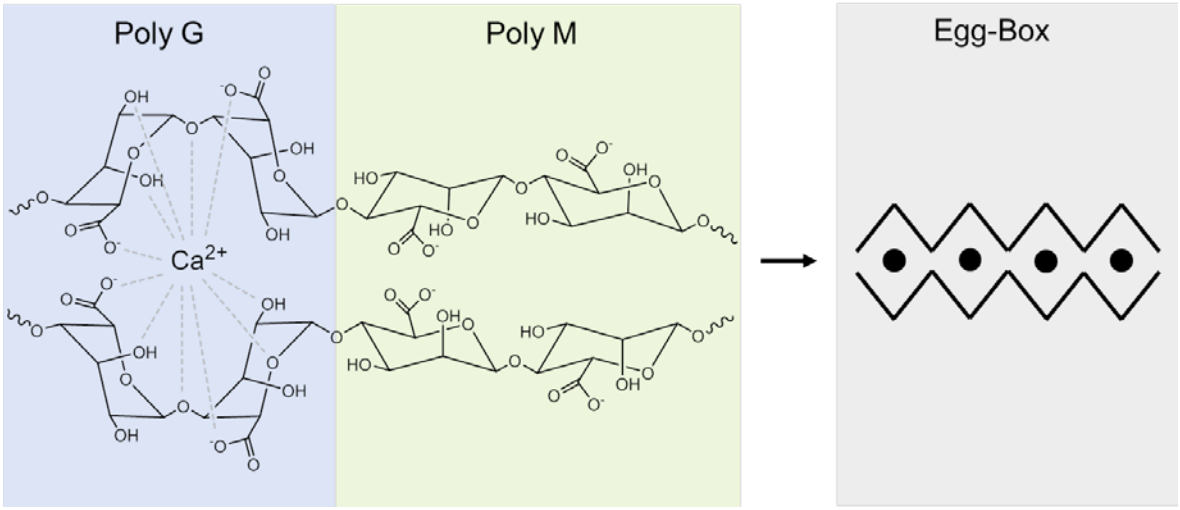

Figure 18 – Chemical structure of AL. The poly G blocks coordinate Ca^{2+} to form the Egg-Box structure.

The ability of AL in forming hydrogels has been extensively investigated and several approaches to obtain these gels have been developed. A common method for obtaining these gels is to simply use a solution of $CaCl_2$ (or other salts of divalent cations), which is mixed to an AL solution. The interaction between the two materials occurs instantaneously and thus the hydrogels formed in this manner may not be homogenous. A different approach was instead proposed by Draget et al.[97]. In their work D-(+)-Glucono-delta-lactone (GDL) is used to slowly acidify a suspension of AL and $CaCO_3$. The insoluble salt solubilizes over time causing the formation of nucleation points for the gelation of AL in a more controlled and homogeneously distributed manner. This approach was also the one utilized in Paper IV for the fabrication of AL/CH membranes for intravaginal applications. Aside from the utilization of AL for the development of membranes and macroscopic gels, this material has been used to fabricate NPs in combination with positively charged polymers for the control release of APIs[100,101].

3.2.3 Chitosan

Chitosan is a linear random copolymer of β-1,4-D-glucose-2-amine and N-acetyl-D-glucose-amine which is derived from chitin upon deacetylation (Figure 19).

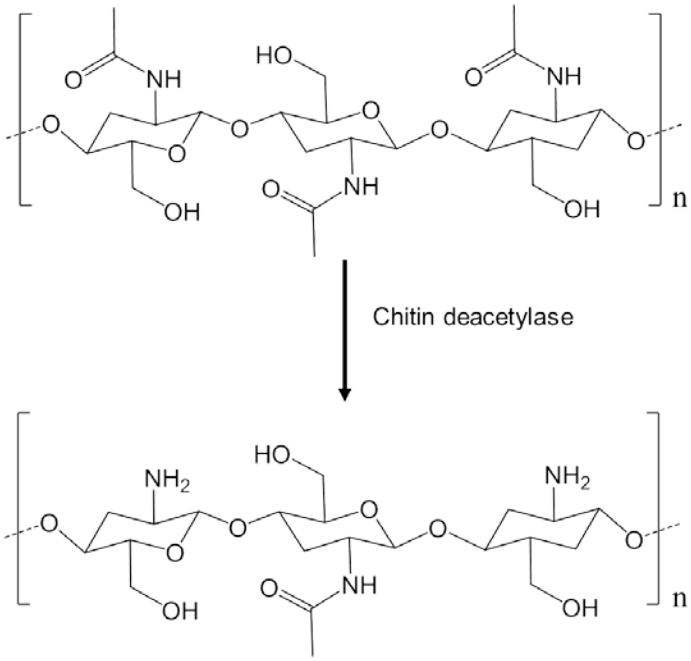

Figure 19 – Chemical structure of chitin (above) and of CH (below).

Chitin is one of the most abundant polysaccharide on Earth and can be found in crustacean shells[102], in insect exoskeletons[103] and in fungal cells[104]. The deacetylation of chitin to obtain CH can be tuned to obtain different forms of CH: different molecular weights and degree of deacetylation can, in fact, be obtained. Tuning these characteristics may greatly affect the behavior of CH. It has been proven, for instance, that fabricating hyaluronic acid/CH NPs deploying CH with higher molecular weights lead to an increase in the NPs average diameter[105]. Greater deacetylation degrees determine, instead, a higher number of primary amines with consequent influences on its solubility and on its interaction with eukaryotic and prokaryotic cells. CH is, in fact, known for its antimicrobial properties, deriving from the presence of the primary amine group[106,107] increasing the deacetylation degree consequently yields an augmented antibacterial effect. Increasing the deacetylation degree also determines the augment of another interesting and extensively investigated characteristic of CH, its mucoadhesiveness[108]. On the other hand, the cytotoxicity of CH was seen to be dependent on the deacetylation degree, lowering the degree of deacetylation reduced the cytotoxicity towards A549 cells (ATCC®)[109]. Overall, CH has been used in

several research areas, such as in tissue engineering[110], in food science[111] but also in the development of smart DDS[112].

Concerning the use of CH in the development of DDS, it has been frequently used in combination with other polymers that present negative charges (e.g. hyaluronic acid and AL). The electrostatic interaction occurring between these materials has been exploited for the development of several DDS, from membranes to nano-particulate systems. CH is also known for its ability to crosslink in the presence of TPP and it has been demonstrated previously that by varying the CH/TPP ratio, the molecular weight of CH, the ionic strength and the pH it is possible to modulate the size, morphology and surface charge of CH based NPs[113]. Moreover, the stability of these nanosystems in different media is highly influenced by these factors[114].

3.3 Nanoparticles

Within the field of drug delivery, NPs represent a very interesting and diversified system. The term NPs has been used historically to refer to "sphere like" particles fabricated with different materials and with highly different sizes. A subtle issue, within the term "nanoparticle", is the suffix "nano". Within the field of nanotechnology, in fact, researches have been using the word "nano" when referring to materials which physical properties manifest a pronounced difference when the size is changed to the nano-scale[115]. An example of this size dependence is, for example, gold NPs. It is in fact known that when the size of gold is changed to the nano-scale its physical and optical properties change significantly compared to those of bulk gold[116]. The term nanoparticle has instead been used to describe any type of particulate DDS in the range of few nm to hundreds of nm, also when the reduction in size was not determining a variation in the physical properties. This is particularly true for, in example, polymeric NPs and liposomes. Nevertheless, according to the directive (2011/696/EU), a NPs can be named as such when 50% or more of the particles lies in the size range of 1 nm to 100 nm. Consequently, for as long as this hallmark is observed, the terminology "nanoparticle" can be freely used to describe particulate DDS.

NPs for drug delivery come in several forms, such as: metallic NPs (e.g. gold NPs), liposomes and polymeric NPs. Although all of these DDS have been extensively studied and all deserve to be mentioned, major focus will be given to polymeric NPs as these constitute the principal work reported in Paper V. Specifically, the focus will be on polymeric NPs that are fabricated by exploiting the electrostatic interaction between oppositely charged polymers.

NPs constituted of biodegradable polymers/polysaccharides are an interesting choice as drug carriers: by using different materials it is in fact possible to tune the properties of the final formulation, leading to a wide range of applications. Mucoadhesivity can be enhanced by using CH. Scavenger abilities towards reactive oxygen species (ROS) can be obtained using, for example, hyaluronic acid[32]. Improved biocompatibility and reduction of protein adhesion can be granted by introducing polyethylenglycol (PEG) in the formulation[117] and enhanced targeting towards specific cells may be granted by modifying the polymers used as carriers by deploying materials able to perform this targeting autonomously (hyaluronic acid and CH ability to bind CD44+ cells in example).

3.3.1 Fabrication of polymeric nanoparticles

Polymeric NPs can be fabricated following several different approaches. A rather common and effective approach is to have a solution of one of the two charged polymers under stirring and to add, dropwise, the second, oppositely charged polymer solution[32,118]. This technique is simple and intuitive but has, however, some weaknesses: being a manual approach, different operators may perform the procedure differently. Moreover, not being a continuous process and being generally performed in small batches, the upscalability of this approach is limited. A different approach is, instead, represented by the usage of an electrospray[119]. In this approach, the polymers are forced out of a nozzle applying a high voltage to the polymeric solution. With this method, the polymers expelled can form micro and NPs. Conversely to the “manual” approach, electrospray can be an upscalable technique and, as the instrumental parameters can be predefined, a reduction in the variations caused by the operator should be expected. Electrospraying may, however,

induce the degradation of some macromolecules due to the working parameters (e.g. thermal stress during drying and shear stress in the nozzle)[120].

In Paper V, the usage of an ultrasonic spray coater, as a novel technique to fabricate NPs exploiting the electrostatic interaction between oppositely charged polysaccharides (AL and CH, Figure 20), was evaluated.

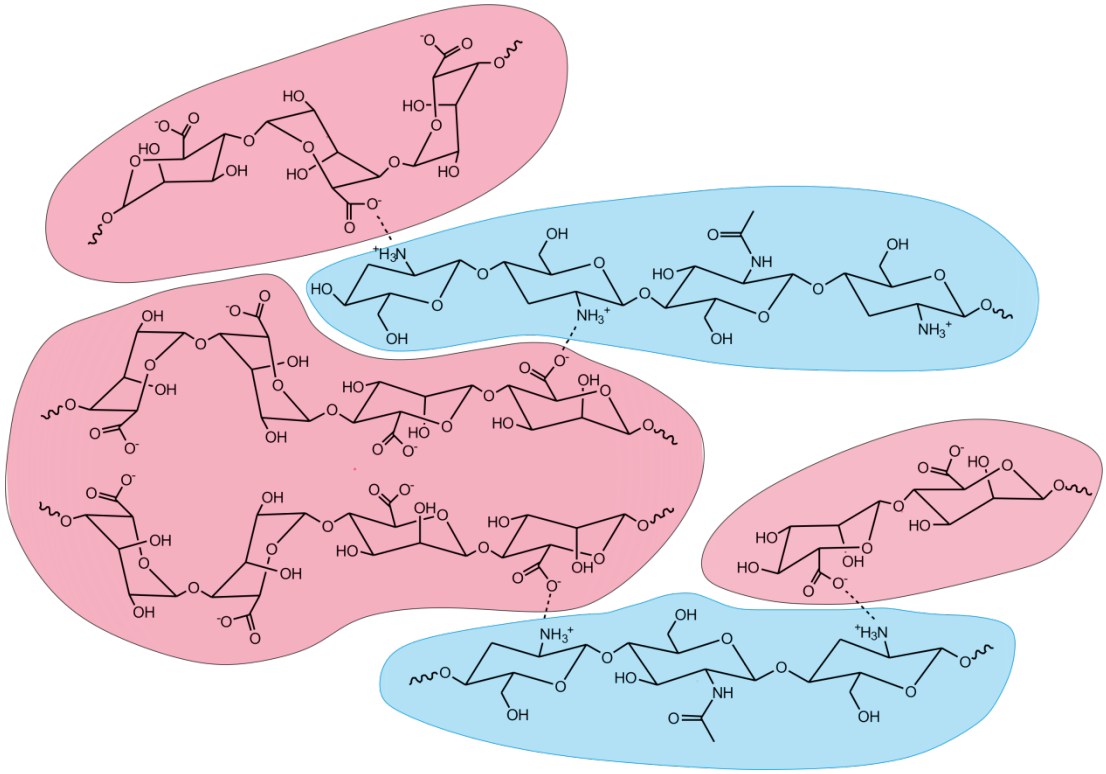

Figure 20 – Schematic representation of AL (red) and CH (blue) electrostatic interaction.

For this, we deployed an ultrasonic spray coater equipped with a dual feed Accumist nozzle. In paper V the two solutions were represented by AL 0.1 mg/mL and CH 0.1 mg/mL. The two solutions were kept separated through the ultrasonic spray coater until the tip of the nozzle was reached. The two polysaccharides were consequently only able to interact at the very interface between the tip of the nozzle and air, meaning once the two solutions were atomized together. Since the nebulization occurs in a *quasi*-instant fashion, AL and CH were only allowed to form electrostatic interaction, driving the formation of NPs, within the atomized droplets.

Apart from defining the spray coater as a viable technique to produce NPs in a controlled and continuous manner, a relation between the applied ultrasound power and the droplet

size distribution was found. As described in Chapter 4.2, in fact, the correlation between ultrasound frequency and droplet size is well known. On the contrary, only indications of a connection between the ultrasound generator power and the droplet size are known. These indications suggest that by increasing the power there is a tendency of forming larger droplets. Indeed, in our study this connection was demonstrated, generating larger NPs by increasing the ultrasound generator power.

To further demonstrate the viability of the ultrasonic spray coater as a technique for producing NPs, the encapsulation of furosemide (BCS II) into AL/CH NPs was performed. A solution of AL 0.1 mg/mL and CH 0.2 mg/mL were used to form blank nanoparticles (BNPs). Furosemide 0.05 mg/mL or 0.001 mg/mL was added to the AL solution to produce loaded nanoparticles (LNPs). The spray coater parameters were set to match the best functioning parameters discovered in Paper V, with the aim of reducing the average size and the polydispersity index (PDI) of NPs. The concentration of CH was increased compared to what reported in Paper V to obtain an outer layer constituted of CH, to grant a higher mucoadhesiveness to the formulation for further works in conjunction with the MCs for oral drug delivery. From the DLS measurements, the average sizes were found to be similar to those obtained in Paper V. Including furosemide in the formulation at the higher concentration caused, however, an increase in the average size. The ζ – potential, on the other hand, resulted positive for both BNPs and LNPs (see Table 1 for the detailed results). It is however worth mentioning that the LNPs comprising furosemide at a concentration of 0.05 mg/mL presented an encapsulation efficiency percentage (EE%, Equation 2) of only 10%. Reducing the concentration of furosemide to 0.001 mg/mL increased the EE% to a final 68%.

$$EE\% = \frac{A-B}{A} \cdot 100 \quad (2)$$

Where A and B represent the concentration of furosemide before and after centrifugation at 5000 g for 10 min.

Table 1 – DLS results of NPs fabricated by means of a dual feed Accumist spray coater. N = 3, SD

Sample	**Size (nm) ± SD**	**PDI**	**ζ – Potential (mV) ± SD**
BNPs	193 ± 4	0.42	42.9 ± 2.0
LNPs (Furosemide 0.05 mg/mL)	239 ± 7	0.44	41.2 ± 0.7
LNPs (Furosemide 0.001 mg/mL)	191 ± 3	0.55	41.3 ± 0.6

4. Experimental methods

In this chapter, the methods and techniques used during the PhD project are described. An explanation of the theory behind each technique is provided and when appropriate, examples taken from the literature are included to highlight the strength and weaknesses of each technique.

4.1 Supercritical carbon dioxide impregnation: overview and theory

In this project, $scCO_2$ impregnation was used to load APIs in SU-8 MCs. With supercritical, a specific state of matter, that occurs when a gas is put at sufficiently high pressures and temperatures, is defined[41]. In Figure 21, the pressure-temperature phase diagram of carbon dioxide is shown.

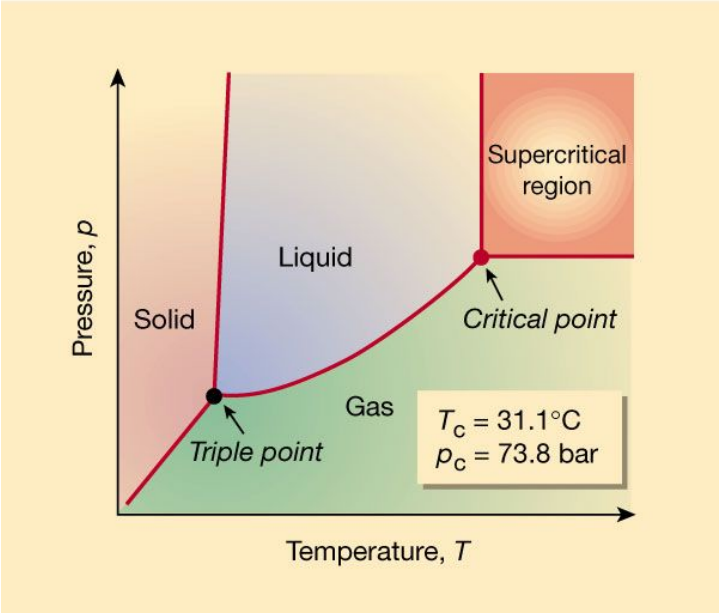

Figure 21 – Pressure/Temperature phase diagram of carbon dioxide, T_c and p_c represents the critical temperature and the critical pressure points respectively. The figure is reprinted from[121], with permission.

As it can be seen, for pressures higher than 73.8 bar and temperatures higher than 31.1 °C, CO_2 reaches its supercritical state. CO_2, in its supercritical state, behaves differently than in its liquid and gaseous counterparts. In fact, the diffusivity and viscosity of CO_2 in its supercritical state is similar to that of gaseous CO_2 whereas its density is similar to that of

liquid CO_2[16]. Thanks to the mild conditions necessary to reach the supercritical state of CO_2, it results in a suitable technique to apply for thermally sensitive molecules, such as APIs[122]. $ScCO_2$ has been, for example, used to impregnate polymers, such as polyvinylpyrrolidone (PVP)[17], PCL[64] and HPMC[123] with different pharmaceuticals. During $scCO_2$ impregnation, the sample that has to be impregnated is placed in a vessel together with a drug and put under pressurized CO_2 at a controlled temperature. Once the supercritical state is reached, the drug is solubilized in the $scCO_2$, which diffuses into the polymer, swelling it and impregnating it with the solubilized molecule. However, to apply this technique, certain conditions have to be satisfied. The polymer, that has to be impregnated, must not be soluble in $scCO_2$ and should be able to swell to allow for the impregnation to occur. It has been shown that the molecular weight of the polymer has a significant effect over its swelling[124]. The longer the polymer chains are, the lower the swelling will be. On the other hand this technique can only be used with APIs that can be solubilized by $scCO_2$. The solubility of molecules in $scCO_2$ was investigated by several research groups. Chrastil, in 1982, evaluated the solubility of several molecules (e.g. stearic acid, cholesterol, α-tocopherol)[125], Yamini et al.[126] evaluated the solubility of dihydroxybenzene isomers, whereas Garmroodi et al.[127] assessed the solubility of different APIs: benzocaine, metrodinazole benzoate and naproxen. Equation 3 can be used to calculate the solubility of molecules in $scCO_2$.

$$\ln\left(\frac{yP}{P_{ref}}\right) = a + \frac{b}{T} + C(\rho - \rho_{ref}) \quad (3)$$

Where y represents the equilibrium mole fraction, P is the pressure, P_{ref} represents a standard pressure of 1 bar, ρ is the density and ρ_{ref} represents a reference density of 700 kg/m^3, a and b are constant at constant temperature[127].

4.2 Ultrasonic spray coating: overview and theory

The ultrasonic spray coater is an instrument capable of atomizing a liquid, generally a polymeric solution, into a fine mist[87]. A scheme of an ultrasonic spray coater is depicted in Figure 22.

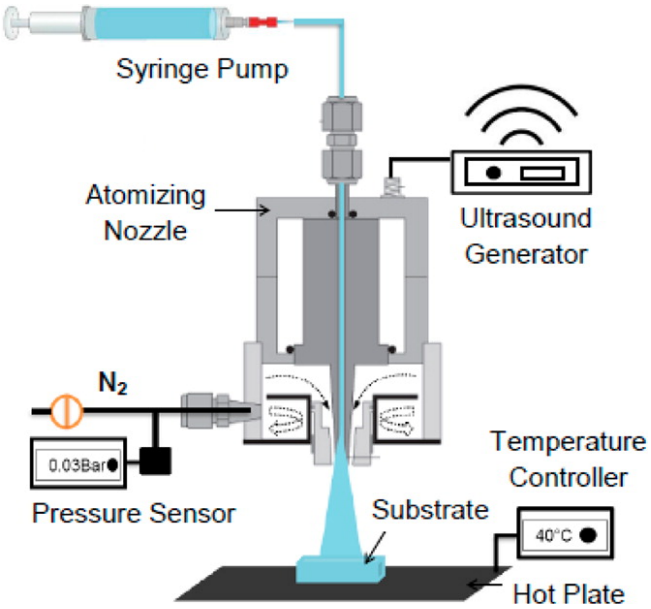

Figure 22 – Schematic representation of an ultrasonic spray coater. Reprinted with permission from[87] . Copyright (2018) American Chemical Society.

The ultrasonic spray coater can be divided into three parts: a pump, a nozzle and an x-y-z movement controller. The pump can be either a syringe pump or a peristaltic pump and it is used to flush, at a controlled flow rate, the liquid that has to be sprayed, bringing it to the spray coater nozzle. The nozzle is constituted of multiple parts: i) the main body, made of Titanium, is resistant to most solvents; ii) the tip of the nozzle presents an inner tube, called microbore, where the liquid passes through before being atomized; iii) pressurized N_2 is used to focus the spray towards the sample. The pressure can be tuned to modify the focus of the spray beam; iv) a piezoelectric transducer is actuated with a power generator, this causes the formation of ultrasonic waves which vibrate the tip of the nozzle. The liquid at the interface between the nozzle and air forms surface capillary waves, portions of the liquid protrusions are then expelled as single droplets[128], causing the atomization of the

liquid. A scheme, representing the liquid at the nozzle/air interface during atomization can be seen in Figure 23. Finally, the x-y-z movement controller is used to define the area that has to be coated with the spray. A variation of the spray coater just described has also been deployed for some of the experiments (Paper V). In this variant, a nozzle (called dual feed Accumist) allows for two solutions to be sprayed simultaneously maintaining the two solutions physically separated until the interface nozzle/air is reached. The two solutions consequently mix when already atomized. In this iteration two syringe pumps are used to flush the polymer solutions towards the spray coater nozzle.

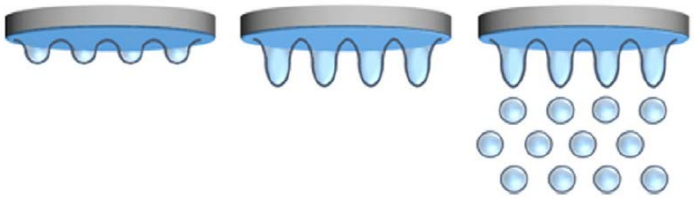

Figure 23 – Atomization of the liquid at the interface between the tip of the ultrasonic spray coater nozzle and air. Figure reprinted from[129] with permission.

The physics behind the atomization of liquids driven by ultrasounds has been investigated by Lang et al.[130]; in their work a correlation between the frequency of the ultrasounds and the size of the droplets formed in the spray, was defined. The formula can be seen in Equation 4.

$$D = 0.34 \cdot \sqrt[3]{\frac{8\pi T}{\rho F^2}} \tag{4}$$

Where T is the liquid surface tension, ρ represent the liquid density and F denotes the frequency.

As a consequence, increasing the frequency determines a reduction in the droplet size. The connection between frequency and droplet size can be further seen in Figure 24.

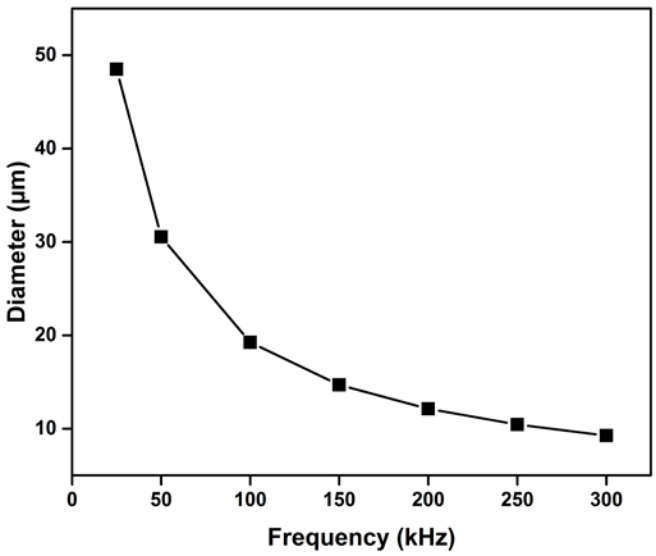

Figure 24 – Droplet size reduction correlated with an increase of the ultrasound frequency generated by an ultrasonic spray coater.

In Paper I and V an ultrasonic spray coater equipped with a 120 kHz ultrasound generator was used. Using Equation 4, it is consequently possible to calculate the average droplet size of the spray coater utilized, equal to roughly 17 µm of diameter (or 2.6 pL).

When operating the ultrasonic spray coater, several parameters, which determine the spray outcome, have to be controlled[87]. The parameters affecting the quality of the spray and its outcome are: i) the choice of the solution (solvent and solute), ii) the flow rate, iii) the applied power of the ultrasounds generator, and iv) the pressure of the focusing nitrogen line. Optimizing these parameters is necessary for the formation of a qualitatively good spray. Other parameters that can be tuned are: v) the distance between the nozzle and the substrate, vi) the temperature of the substrate, vii) the speed of the nozzle, and viii) the number of sprays over the substrate. Depending on the application, some parameters have a higher influence on the outcome than others, as reported in Chapter 3.

4.3 Spin coating

Spin coating is a common technique used to deposit thin layers of materials over surfaces, typically represented by Si wafers[131]. The working principle is simple; the substrate that

has to be coated is placed over a rotating chuck and kept immobile by means of a vacuum pump. A known volume of the material used to form the film is then poured over the substrate, in its center. This material is generally a resin or a polymeric solution at a known concentration[132]. The substrate is consequently put under rotation: the acceleration, rpm and deceleration of the rotating chuck, as well as the duration of the experiment, can all be set to optimize the outcome of the coating in terms of: i) final thickness, ii) surface roughness. The coated substrate is finally left to evaporate the solvent. To increase the rate of evaporation, volatile organic solvents, such as DCM, are frequently used in this technique[133]. A schematic representation of a spin coater can be seen in Figure 25.

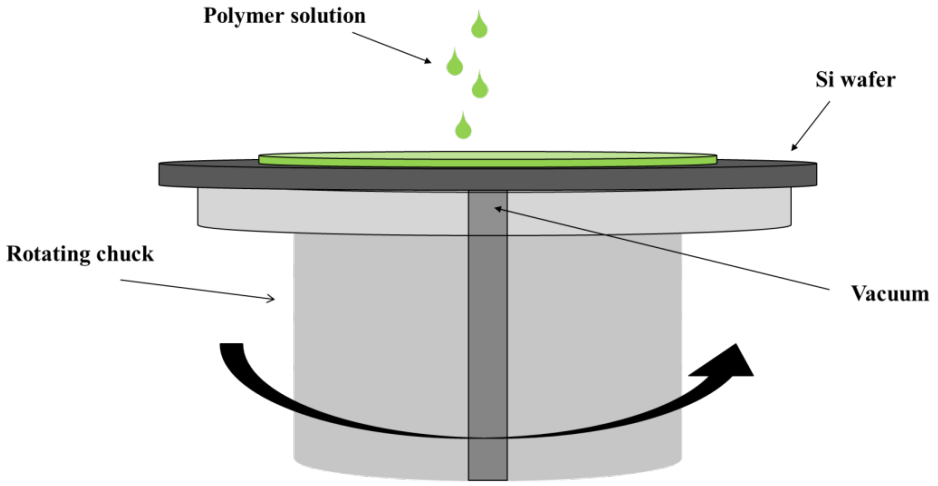

Figure 25 – Schematic representation of a spin coater.

4.4 Hot punching

In hot punching[134] a mold is used to punch out a polymer film, which can be obtained by means of spin coating, and can be used to fill MCs. In the case of MCs filling, the MCs chip is used as mold itself (Figure 26). HP starts with the fabrication of a poly-di-methylsiloxane (PDMS) film over a Si wafer by means of spin coating. Once the PDMS layer is cured, a second layer is made with the desired material. After the complete drying of the second layer, the substrate is ready for HP. The MCs chip, used as a mold, is placed over the substrate; the two are then placed in a hot embosser. Pressure is applied to the mold, together with heat, to allow for the MCs walls to penetrate the polymer film. As the

temperature is risen above the Tg of the polymer, the penetration is facilitated. Once the mold has completely cut through the polymer film, the temperature is slowly brought back to room temperature (RT) and the pressure is finally removed. The film surrounding the mold is then peeled off. The layer of PDMS is necessary in this process as it provides an elastic substrate that: i) prevents mold damage, ii) allows the mold to reach a deeper point in the substrate, effectively cutting the polymer layer. A scheme of the process is depicted in Figure 26.

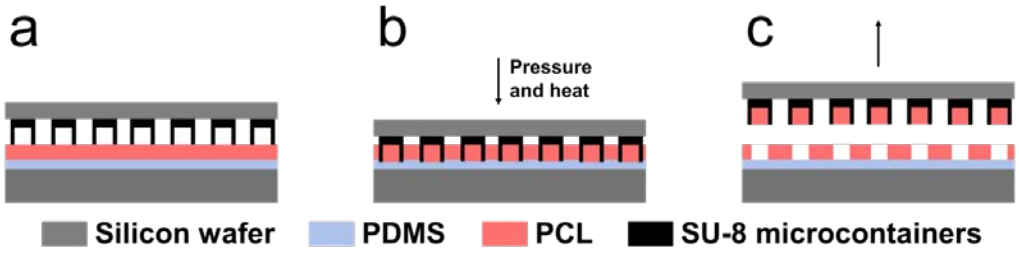

Figure 26 – Schematic representation of the HP of a polymer film into MCs used as mold. The MCs chip is initially positioned on top of a Si wafer, over which a layer of the elastic PDMS and a layer of the polymer that has to be loaded, here PCL, is spin coated (a). The chip is then pressed and heated up with a hot embosser to allow for the penetration of the PCL with the MCs (b). Finally, the temperature is lowered and the chip, with the now filled MCs, is removed (c).

4.5 Raman spectroscopy

Raman spectroscopy is a spectroscopic technique based on the inelastic scattering of light[135]. When a sample is shined with a monochromatic laser, at a known wavelength, the interaction of light with the sample causes the light to scatter in an elastic and inelastic manner. The elastic scattering (Rayleigh scattering) is excluded and the inelastic scattering, possessing a lower energy than that of the laser, is collected. The scattered light spectra are specific and unique for each sample defining a fingerprint of the sample[136]; this is due to the fact that the interaction between the shined laser and the material is based on the vibrational and rotational modes of the molecules that constitute the sample. This technique is highly used to analyze solid[137], liquid[138] and gaseous[139] samples and finds application in various research areas, included pharmacology[140]. In fact, Raman spectroscopy, being a

non-destructive technique, requiring small sample amounts and not needing sample preparation, is suitable for studying new materials (e.g. new APIs) and new formulations. Understanding the solid state of APIs, discerning their crystalline and amorphous forms can be done by means of Raman spectroscopy[16]. This technique can also be used to shed light over possible interactions occurring between the API and any excipient included in the formulation[141]. An example of Raman spectra where the difference between the crystalline and amorphous state of ketoprofen are noticeable can be seen in Figure 27. To obtain these spectra a DXR Raman microscope (Thermo Fisher Scientific, Inc., Waltham, U.S.) has been used, ketoprofen powder was measured over a heating plate at 25°C initially and at 96°C afterwards, causing the melting of the API.

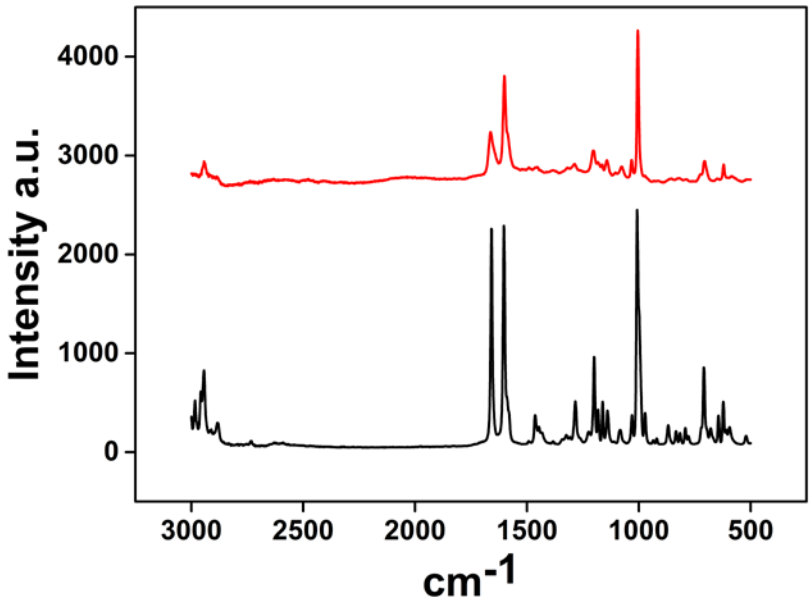

Figure 27 – Raman spectra of crystalline ketoprofen (black) and amorphous ketoprofen (red).

4.6 X-ray powder diffraction

Similarly to Raman spectroscopy, X-ray powder diffraction (XRPD) is a technique frequently used to characterize APIs and formulations[142,143]. In XRPD the substances investigated are hit with monochromatic X-rays that are generated by cathode ray tube, collimated to concentrate and directed towards the sample. The X-rays interact with the

sample and causes the formation of constructive interference when Bragg´s Law (Equation 5) is satisfied[144].

$$n\lambda = 2d \cdot sin\theta \quad (5)$$

Where n represents the "order" of reflection, λ is the wavelength of the incident X-rays, d is the interplanar spacing of the crystal and θ is the angle of incidence.

The diffracted X-rays are then collected and counted. The sample is scanned through a range of angles (2θ) so that all possible diffraction directions of the crystal lattice can be obtained (assuming a stochastic distribution and orientation of the crystals in the analyzed powder). The presence of peaks in the diffractogram is associated with the existence of a crystalline structure. When no peaks are discernible and a halo is instead present, the substance is considered amorphous, that is, no crystal structures are present. Nevertheless, it is important to ensure that the absence of peaks is not caused by an excessively low concentration of an API in a formulation.

XRPD and Raman spectroscopy are frequently coupled to ensure the presence of API in their amorphous solid state and to shed light on possible interactions between APIs and excipients. An example of an XRPD diffractogram where the difference between the crystalline and amorphous state of ketoprofen are noticeable can be seen in Figure 28.

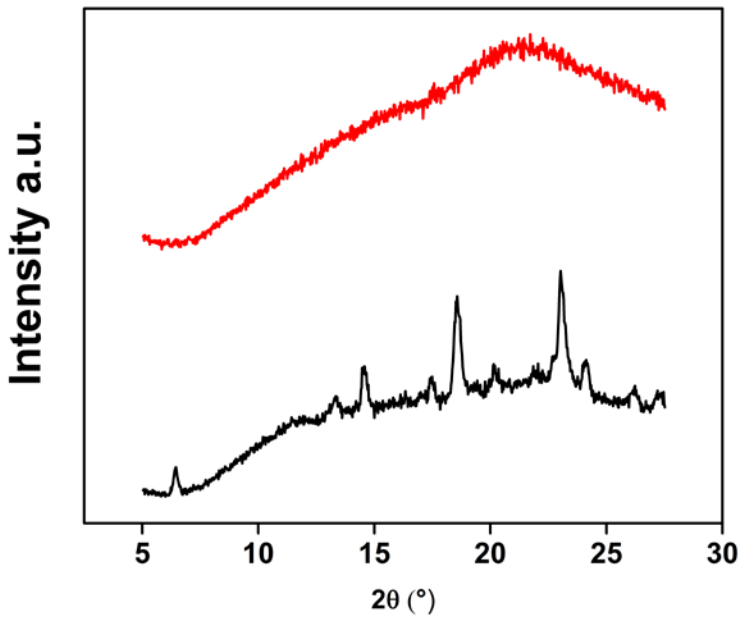

Figure 28 – XRPD diffractograms of a physical mixture of ketoprofen and PVP in weight ratio 1 to 4 (black line) and of a physical mixture of ketoprofen and PVP in weight ratio 1 to 4 after heating at 120°C and quenching in liquid nitrogen.

4.7 UV-Vis spectrophotometry

To evaluate the release of an API from a DDS, being MCs (Paper I, Paper II and Paper III) or membranes (Paper IV), UV-Vis spectrophotometry can be used. This technique is based on the absorbance of light in the range of 200 – 700 nm approximately. When molecules are shined with photons at a sufficient energy their electronic state changes from the fundamental to the excited one. The absorbance of light from a molecule is defined by the Lamber-Beer law (Equation 6)[145].

$$A = \varepsilon \cdot d \cdot [C] \quad (6)$$

Where A is the absorbance, ε is the molar attenuation coefficient (which represents the strength of a molecule in attenuating light at a specific wavelength), d represents the path length and [C] represents the molar concentration of the chemical species. Consequently,

for a given molecule, the absorbance increases linearly when d or [C] increase. A classical spectrophotometer comprises a light source, a sample holder and a detector. The light is shined towards the sample, it interacts with it and the non-absorbed light (transmitted light) is collected by the detector. The absorbance represents indeed the inverse of the transmittance (the difference between the intensity of the light before and after passing through the sample).

Typically, an analysis with a spectrophotometer comprises three steps. If the wavelength of maximum absorbance is not known for the molecule of interest, the sample can be tested over a broad range of wavelengths to identify the appropriate one. Secondly, a calibration step has to be included to perform quantitative measurements. The calibration is performed by adding known amounts of the chemical species in the same solvent in which the sample is to be measured. With increasing concentration, the absorbance increases and a calibration curve can thereby be obtained. Finally, the sample absorbance is measured; this can either be a single measure, for example to evaluate the total amount of API loaded in a DDS, or it can be constituted of a series of measurements over time to obtain the release kinetic of an API from a DDS.

4.8 Dynamic light scattering

Dynamic light scattering[146] is a technique frequently used to evaluate the size of nano-particulate systems[20,25,32,147]. NPs in suspension move due to Brownian motion, following the Stokes-Einstein equation (Equation 7)[148,149]. This motion is dependent on the size of the particles, the viscosity of the liquid and the temperature.

$$R_h = \frac{k_b T}{6\pi\eta D_t} \quad (7)$$

Where k_b represent the Boltzmann constant (1.38064852 x 10^{-23} J/K), T is the temperature in °K, η is the absolute viscosity and D_t represents the translational diffusion coefficient. In DLS measurements, the size of NPs can be determined by measuring particle motion. This

is performed optically. When NPs in suspension are illuminated with a coherent monochromatic light source, scattering occurs.

The light scattered from the NPs in motion present a time-dependent intensity, which derives from the time-dependent position of the scattering element. This time-dependent intensity of the scattered light is considered as either a time phase shift or as a spectral frequency shift from the light source central frequency. The particles in motion are measured over time with a single wavelength and the scattered light is coherently detected at a known angle. The observed scattering fluctuates in its intensity over time due to particles motion. The data analysis is consequently performed as a function of time of the intensity fluctuations to provide information about the particles motion. The time analysis is carried out with a correlator constructing the time autocorrelation function G (Equation 8).

$$G(\tau) = \langle I(t) \cdot I(t+\tau) \rangle \quad (8)$$

Where I(t) represents the intensity of the scattered light fluctuating over time and τ represents the time difference.
For monodispersed particles, the autocorrelation function is represented as an exponential decay of τ, as reported in Equation 9.

$$G(\tau) = A[1 + B^{-2\Gamma\tau}] \quad (9)$$

Where A is a time dependent constant, also identified as “baseline” and B depends on the instrument and represents the intercept of the autocorrelation function. The decay rate Γ (Equation 10) correlates the diffusion coefficient, already expressed in the Stokes-Einstein equation (Equation 7), with the light scattering q^2 (Equation 11).

$$\Gamma = D_t \cdot q^2 \quad (10)$$

$$q = \frac{4\pi n}{\lambda_0} \quad (11)$$

Where n represents the refractive index of the suspension and λ_0 is the wavelength of the laser.

Consequently, the DLS analysis provides the diffusion coefficient distribution that is later used in the Stoke-Einstein equation to obtain information on the size distribution of the suspended particles. In this work, we made use of DLS to evaluate the sizes of AL/CH NPs fabricated by means of an ultrasonic spray coater, please refer to Paper V for more detailed information.

DLS can also be used to obtain information on the Zeta-potential (ζ) of the NPs. The Zeta-potential is an important characteristic of the formulation as it is associated with NPs stability and because it gives information on the outer polymer layer[32,146] (Figure 30).

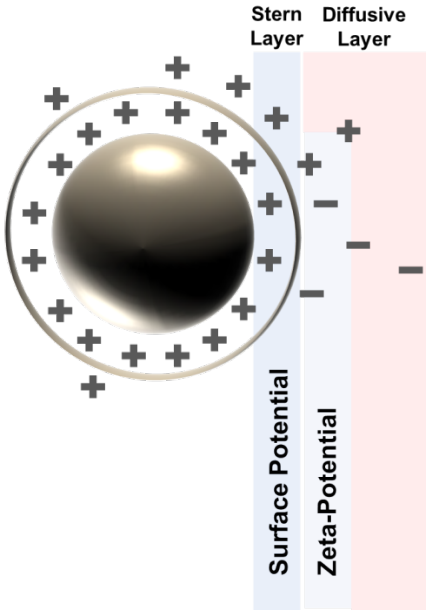

Figure 29 – Schematic representation of a charged NPs. The surface and Zeta-potential are depicted as areas surrounding the NPs.

Zeta-potential values equal or higher than +30 mV or equal or lower than -30 mV are generally associated with improved NPs stability[146], due to the repulsion preventing the aggregation of NPs.

To evaluate the Zeta-potential a Laser Doppler Velocimetry (LDV) technique is used. In LDV a voltage gradient is applied across two electrodes, charged particles are attracted to the oppositely charged electrode and their velocity can be measured. The velocity of a particle in an electric field is commonly referred to as Electrophoretic Mobility (U_E). Using the Henry equation (Equation 12) it is possible to calculate the Zeta-potential of particles in suspension.

$$U_E = \frac{2\varepsilon \cdot Z \cdot f(ka)}{3\eta} \quad (12)$$

Where ε represents the dielectric constant, Z corresponds to the Z-potential, f(ka) is Henry´s function (generally approximated to 1.5 for aqueous suspensions) and η represents the viscosity.

4.9 High-performance liquid chromatography

High-performance liquid chromatography (HPLC) is a technique used to separate compounds in a solution. This technique can either be qualitative, quantitative or semi-preparative for further analyses[150]. A qualitative HPLC is run when the accurate concentration of the samples is not necessary to be known. A quantitative measurement with HPLC gives information on the total amount of the molecule in the solution (e.g. concentration of ketoprofen in plasma samples)[16,151]. A semi-preparative HPLC is run when the goal is to separate the components of the samples[152]. An HPLC is constituted of two main components: i) the mobile phase and ii) the stationary phase. With mobile phase we indicate a solvent that is run in the HPLC. With stationary phase we instead indicate a column, in which the sample is separated with the help of the mobile phase. The separation of the molecule of interest from the medium in which it is solubilized is obtained by exploiting the different affinity between the various molecules in solution with the mobile and with the stationary phase. In a usual HPLC setting the molecule of interest is known and its concentration is not. The solution is then run into a column with high affinity towards the molecule of interest. The mobile phase is flushed in the column to separate the

various chemical species. The molecules with the lower affinity towards the stationary phase and the higher affinity towards the mobile phase exit the column faster than those that, on the contrary, manifest a high affinity to the stationary phase and a low affinity to the mobile phase. The differential affinity between the stationary and mobile phases can be explained by a distribution constant, as described in Equation 13.

$$K = \frac{[M]_s}{[M]_m} \tag{13}$$

Where $[M]_s$ represents the concentration of the molecule in the stationary phase and $[M]_m$ represents the concentration of the molecule in the mobile phase. When $K > 1$ the molecule has higher affinity towards the stationary phase, conversely, the $K < 1$ the affinity between the molecule and the stationary phase is lower.

Considering the distribution constant K, two different types of HPLC can be performed: i) isocratic and ii) in gradient[153]. In the former the chromatographic system, meaning the stationary and the mobile phases, do not change over time and, consequently, the interactions between the molecules with the stationary and mobile phases do not change over time. In the latter, on the contrary, the mobile phase varies over time and the interactions between the molecules with the stationary and mobile phases change, consequently, over time. HPLC experiments run in the gradient mode typically require the usage of a mobile phase constituted of multiple solvents, which ratio is modulated over time.

Designing a HPLC protocol, various types of events can be exploited: i) interactions occurring between the molecules and the stationary and mobile phases (hydrogen bonding, electrostatic interaction, Van der Waals, and hydrophobic interactions) and ii) differential accessibility to the stationary phase, depending on the column pore size and molecule size.

HPLC is generally divided into several subgroups, based on the different stationary phases characteristics: reverse phase (RP-HPLC), ion pair RP-HPLC, hydrophobic interaction chromatography (HIC), ion exchange chromatography, affinity chromatography and size

exclusion chromatography. As relevant to the PhD thesis, RP-HPLC will be further explained in the next paragraph.

During an HPLC experiment, the sample is separated into its components according to the affinity; these exit the column and pass directly to a UV-Vis spectrophotometer or to a fluorimeter where the absorbance (or the emission) at known wavelength is tested. To obtain quantitative measures from an HPLC it is consequently required to perform a calibration step, where known concentrations of the molecule of interest are tested in the same medium as in the final sample to evaluate the signal intensity, similarly to what reported in paragraph 4.7.

4.9.1 Reverse phase high-performance liquid chromatography

Reverse phase high-performance liquid chromatography (RP-HPLC) was utilized in Paper I to evaluate the relative oral bioavailability of ketoprofen after the administration of a microcontainer based formulation.

To perform a RP-HPLC, the usage of a stationary phase constituted of a hydrophobic column is required. This column presents alkyl pendants covalently bound to an inert matrix made of Si. These columns are normally named as “C” with a number, as a suffix, defining the length of the alkyl chains. During this PhD project a C18 column was deployed. The mobile phase generally used in this type of HPLC is a mixture of deionized water (DI-water) and a non-polar solvent (e.g. acetonitrile, methanol or isopropanol)[154]. To the mobile phases, additional chemicals can be included (e.g. formic acid or trifluoroacetate) to tune the pH and to improve the separation of the sample[151]. In Figure 30, the chromatogram of ketoprofen 2.5 µg/mL in rat plasma can be seen.

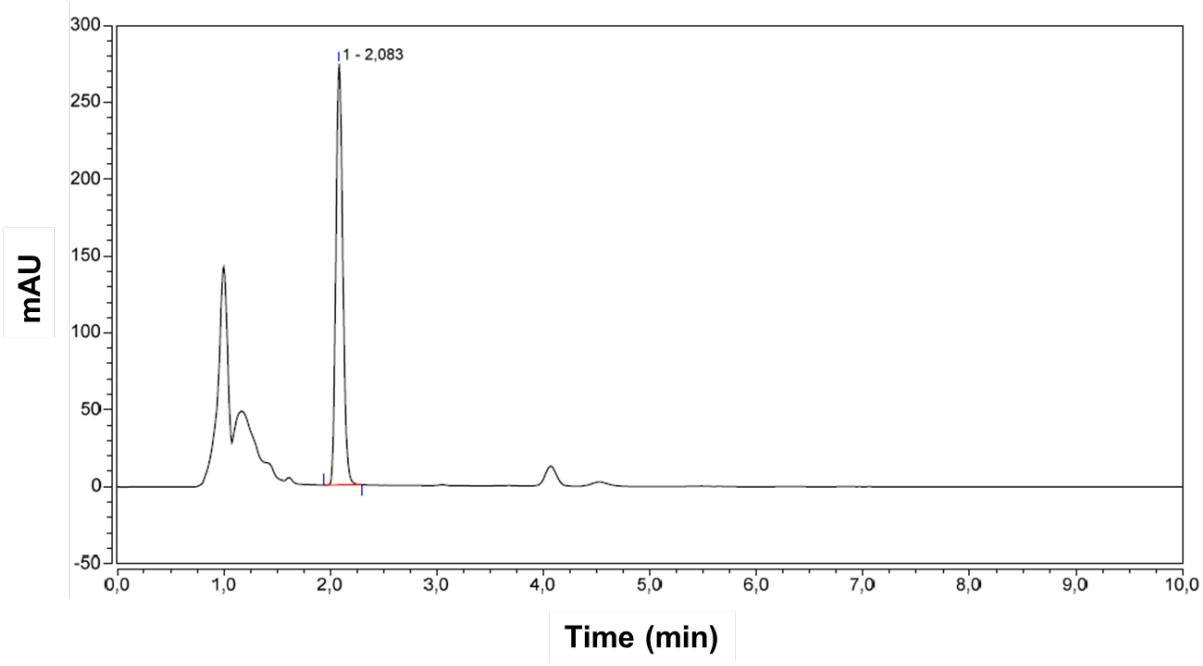

Figure 30 – Chromatrogram of ketoprofen 2.5 µg/mL in rat plasma

4.10 X-ray micro computed tomography

X-ray micro computed tomography (XrµCT) is a powerful technique that allows obtaining a virtual 3D representation of an object from a reconstruction of a series of 2D cross-sections (projection images)[155]. The prefix micro (µ) is included in the name to indicate the resolution of the technique which corresponds to pixel sizes in the 10^{-6} m range. Being a non-destructive technique and requiring minimal sample preparation, XrµCT is suitable for imaging drug formulation[156], large devices[157] and microdevices[16] (e.g. MCs) to evaluate the inner morphology of the samples. In this project, XrµCT was, in fact, used to evaluate the level of filling and the quality of the coating in MCs. An example of a XrµCT image can be seen in Figure 31.

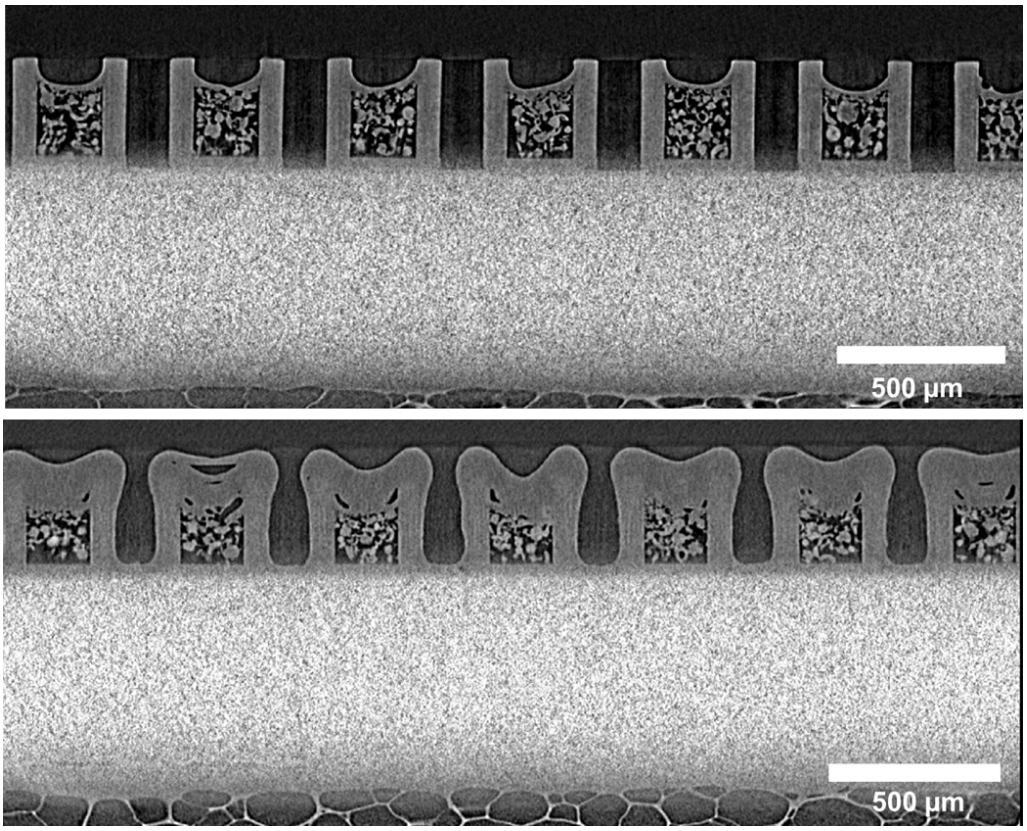

Figure 31 – XrµCT images of an array of MCs filled with PVP K10 and loaded with ketoprofen by means of scCO2 on the top, the same loaded MCs coated with a pH sensitive coating on the bottom. Figure taken from[16].

4.11 Confocal microscopy

Within optimal microscopy, confocal microscopy (CM) is one of the most common and effective microscopy techniques to study biological samples[158]. Conversely to the classic optical microscopy, where the samples are visualized in x-y and the best z focus is used, in CM, a point light source is used to scan the sample of interest in x-y-z. This means that individual x-y stacks at different Z focal points can be obtained and used to reconstruct a 3D image. This is possible as a result of the CM setup, which differs from a classic optical microscope setup (Figure 32).

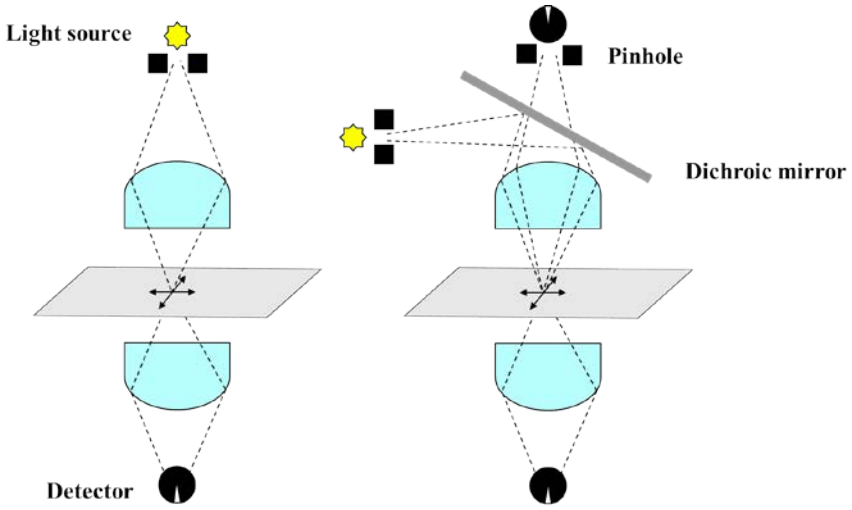

Figure 32 – Schematic representation of a classic transmission optical microscope to the left and of a confocal microscope to the right.

As it can be seen, the light source (typically a laser of known wavelength) is shined and focused on the sample. The samples are generally labeled with one or multiple fluorophores to distinguish different sample components[159]. These fluorophores are excited at the excitation wavelength and emit light at a higher wavelength. This fluorescence is filtered through a dichroic mirror, passes a pinhole and is finally collected by a CCD. The presence of a pinhole allows for a collection of the light coming only from the focal point, the out-of-focus light is, instead, excluded. An example of a CM image can be seen in Figure 33.

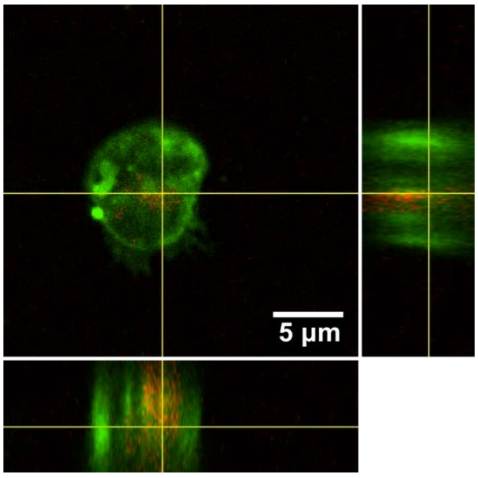

Figure 33 – CM image of a neutrophil labelled in green and polysaccharide based nanoparticles labelled in red.

4.12 Scanning electron microscopy

Scanning electron microscopy is a technique used to visualize samples at high magnification and high resolutions[160]. Compared to optical microscopes, where the limit of resolution is highly dependent on the wavelength of light, in a SEM the sample is shined with an electron beam, which wavelength is dependent on the electron energy. The resolution in an electron microscope is conversely connected to the beam spot size and can be in the order of few nanometers.

A SEM exploits the interaction between an incident beam of electrons at high energy (1 to 40 keV) and the sample. When the electrons hit the sample their interaction causes the formation of several signals that are collected and enhanced by specific detectors. The various signals generated by the interaction of the electrons with the sample are shown in Figure 34.

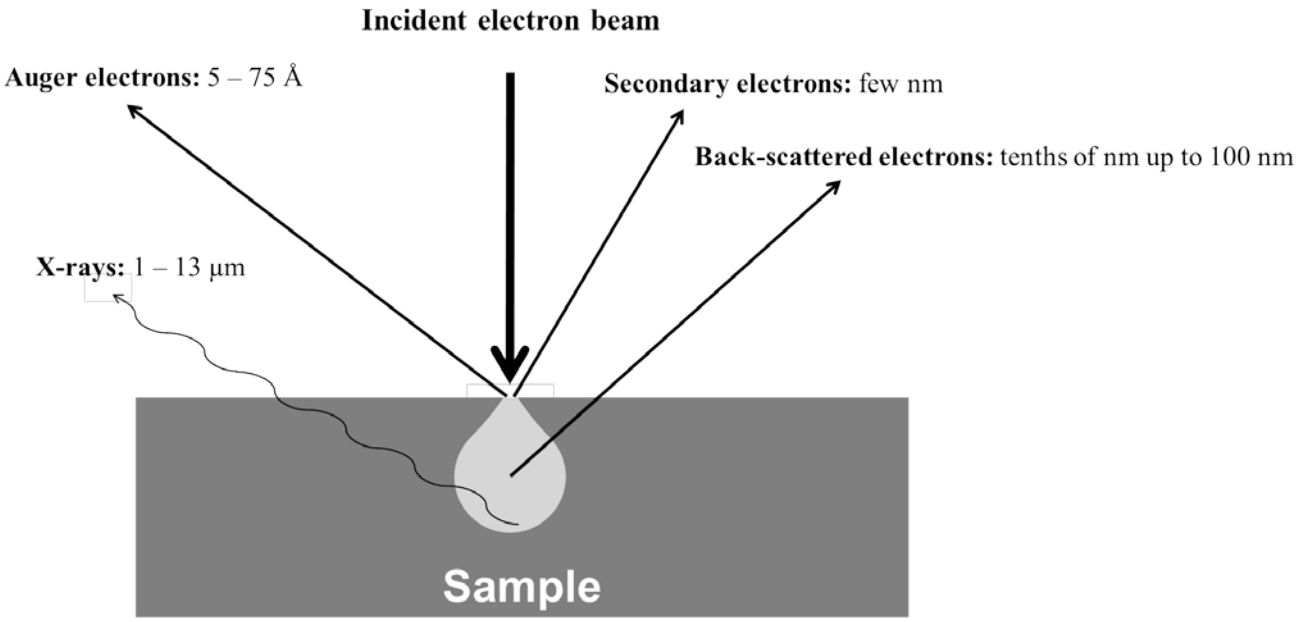

Figure 34 – Interaction between the sample and the incident electron beam in a SEM.

In this work we made use of the secondary electrons (SE) as preferential signal. These electrons have energies < 50 eV and are generated in the proximity of the surface where the electrons from the incident beam ejects the electrons in the orbital k of the atoms hit. Three

types of SE are distinguishable: i) SE-1 are produced as a consequence of the interaction between the incident electron beam and the sample, ii) SE-2 are generated when the backscattered electrons hit the sample and iii) SE-3 are formed due to the interaction between the electron beam and the sample chamber (or analogous). SE-1 are the ones collected and used for the analysis. As the detector for the SE is generally situated laterally in respect of the sample, a shadow effect is generated, the SE originating in the opposite direction from the detector are, in fact, collected in a smaller number than those generated by the detector side. This contrast allows for optimal topographic images of the samples.

4.13 Profilometer

The profilometer is an instrument used to characterize samples surfaces topography. Profilometers can be divided into two categories: i) contact profilometers and ii) non-contact profilometers[161]. During the PhD project, a contact profilometer was used to evaluate the thickness and roughness of various samples. This instrument is based on the usage of a stylus with a sharp diamond tip. The stylus initially positioned over the sample which is positioned over a moving stage (Figure 35). The stylus applies a constant force over the sample during the experiment, so that variations in the height of the sample cause a change in the stylus height (to maintain the same applied force). The variation of the stylus position generates a signal which is consequently converted into a digital signal that is then stored for further analyses. From the profilometer results the thickness of the sample is calculated as the difference between the average height of the sample and the baseline height obtained by measuring outside the sample.

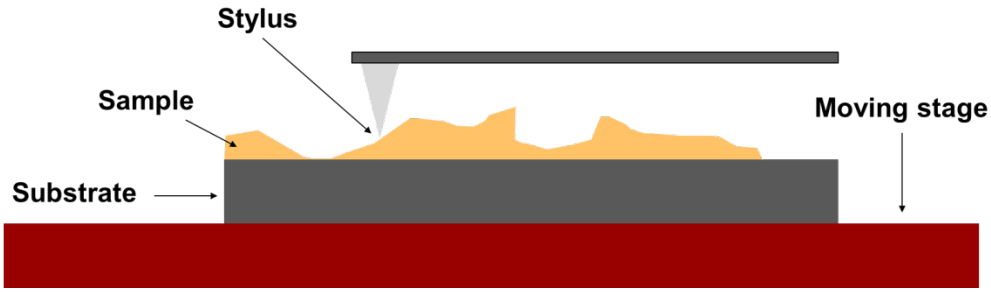

Figure 35 – Schematic representation of a profilometer. The stylus is put in contact with the sample and thanks to the stage movement it scans over the sample to get its surface topography.

4.14 Compressive and tensile stress studies

Studying the mechanical properties of novel materials is crucial to understand their viable applications and how these could be improved. Among the various mechanical properties of a material, in this work, the focus is kept on two: the strength of hydrogels during compression[162] (compressive strength) and the strength of dry membranes during tension (tensile strength).

To perform these mechanical characterizations, two texturometers, equipped with different sample holders, were used. The work principle of a texturometer is to measure the response of the sample during a controlled deformation of it. In regards to the compressive stress study, the moving arm of the texturometer was set to a known speed and, as the sample exerts resistance during its compression, the force of the moving arm increases to maintain the speed of compression constant. This continued until rupture of the sample occurred. When the test was concluded, a stress-strain (σ-ε) graph could be made (Figure 36), where the stress is defined as the force (F) over the initial area of the sample (A_0) (Equation 14) and the strain is the relative change in size of the sample, initially (l_0) and after compression (l) (Equation 15).

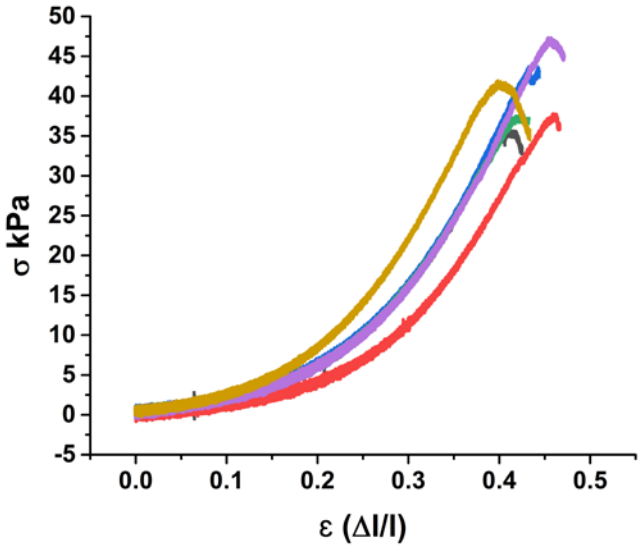

Figure 36 – Compressive stress-strain curve of sodium AL hydrogels after 10 min of soaking in a simulated vaginal fluid. Figure taken from the supplementary information of Paper IV

$$\sigma = \frac{F}{A_0} \tag{14}$$

$$\varepsilon = \frac{l - l_o}{l_0} \tag{15}$$

In the case of the tensile stress study, the sample was held between two clamps, leaving a free portion of the sample with known width and length. The sample was consequently extended until breakage occurred. Similarly to the compressive stress test, the tensile stress test output is expressed as an σ-ε graph.

An image representing a compressive and tensile stress test is shown in Figure 37.

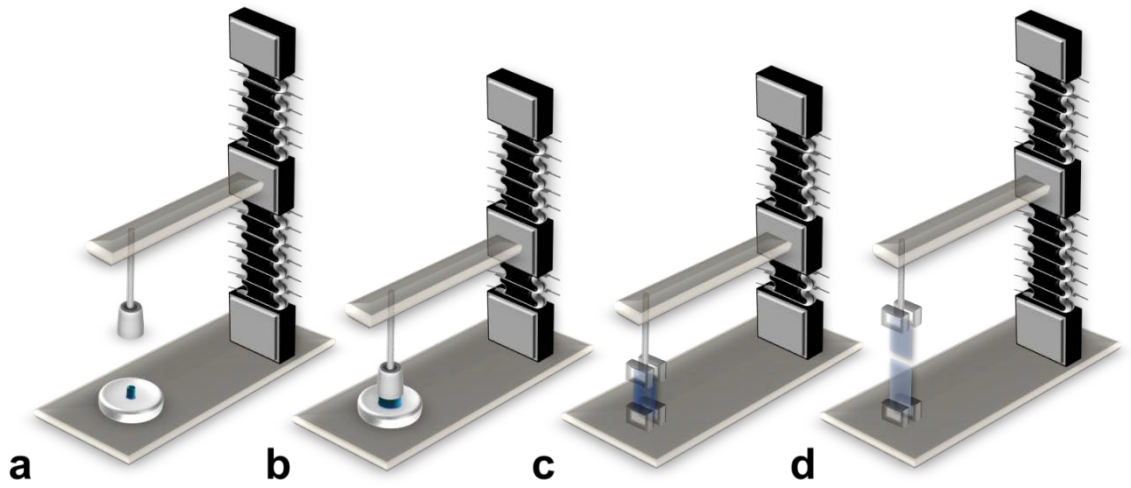

Figure 37 – Schematic representation of a compressive (a and b) and a tensile (c and d) stress study. The compressive stress study begins with the positioning of the sample below the piston of the texturometer (a), the piston is then lowered and the sample in compressed (b). The tensile stress study starts with the clamping of the sample (c), the sample is then extended until breakage happens.

4.15 Adhesion study

Adhesion studies were performed using the Texture Analyzer (TA.XT Plus, Texture Technologies Corp. and Stable Micro Systems, Ltd. Hamilton, MA). The setup of the instrument was similar to that of the compressive stress studies with slight modifications. In

the case of the adhesion studies, a tissue was used as substrate (in this work the tissue deployed was pork vaginal tissue), the sample was then put in contact with the tissue using the piston of the texturometer at known speed and until a specified force was reached. The sample was then kept in contact with the tissue for a desired amount of time. Finally, the piston was retracted. The sample´s adhesive force is the force that has to be applied by the instrument to overcome the interactions between the sample and the tissue. The adhesion can be expressed in terms of Force of adhesion (F_{ad}) and Work of adhesion (W_{ad}). Whereas the former only indicates the maximum force before detachment of the sample from the tissue, the latter is obtained integrating the Force-Distance (Equation 16) and has been seen to be a more robust measure among the two[163].

$$L = \int F \cdot dx \tag{16}$$

4.16 Swelling and Degradation studies

An important characterization for polymer based DDS (e.g. membranes) is to determine their ability of absorbing and retaining water (or another biorelevant media). This happening is commonly referred to as swelling. Swelling is generally calculated as the mass increase over time of a dehydrated material[107] (Equation 17). The dehydrated sample is soaked in the medium for a known amount of time, it is then removed and the excess of liquid is blotted over filter paper. The sample is then weighed and the process is repeated until a plateau is reached.

$$Water\ uptake\ (\%) = \frac{Ww - Wd}{Wd} \cdot 100 \tag{17}$$

Where W_w corresponds to the weight of the wet sample after soaking at each time point and W_d corresponds to the weight of the dry sample.

Related to the swelling, another important property to define is the degradation of the material in water (or another biorelevant media). The degradation is generally calculated as the mass loss over time (Equation 18).

$$Remaining\ weight\ (\%) = \frac{Wn}{Wi} \cdot 100 \quad (18)$$

Where W_n corresponds to the weight of the sample at each time point and W_i corresponds to the weight of the membrane at its highest swelling.

In Paper IV the swelling and the degradation rate of AL/CH membrane was assessed, both in DI-water and in a simulated vaginal fluid.

4.17 Biocompatibility

In this work, a well-established protocol, the AlamarBlue® assay has been used[164]. This test evaluates the level of cytotoxicity and the influence on the proliferation towards mammalian cells. In particular, in Paper IV, this test was carried out on an epithelial ectocervix cell line Ect1/E6E7 (ATCC® CRL-2614™). AlamarBlue is a colorimetric assay based on the reduction of resazurin to resorufin by viable cells, as a consequence to their metabolism (Figure 38)[165]. The latter is a fluorophore that can be excited with light at 544 nm and consequently emits light at 616 nm. As the fluorescence intensity increases with higher amounts of living cells it is possible to use this assay to evaluate the effect of incubating cells with the DDS of interest and to compare it to a negative control (cells incubated only with the medium), in which the cells are allowed to grow normally, and to a positive control (cells treated with the medium + Triton 0.1 % V/V), where cells death is induced. A detailed protocol is described in the "Materials and methods" section of Paper IV.

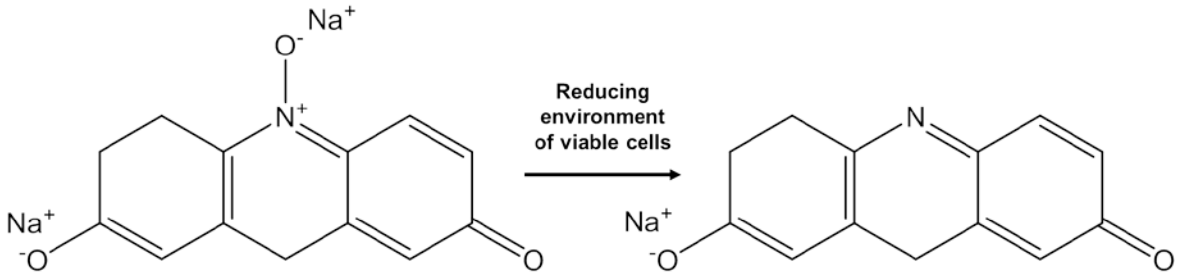

Figure 38 – AlamarBlue® assay principle: resazurin sodium salt, to the left, is reduced to the more fluorescent resorufin sodium salt, to the right, thanks to the reducing environment, typical of viable cells.

4.18 Antimicrobial activity

In this work, antibacterial studies were performed on two different bacteria strains, G.v. and S.a.. To perform this test, a common method, that evaluates the growth of bacteria, incubating them with and without the sample, was used[107]. In this PhD thesis AL and CH membranes comprising metronidazole (used as model antibacterial API, BCS I), were tested[50,166]. Due to the different characteristics of the two strains tested, the antibacterial assays were optimized individually and will be separately discussed in this thesis.

For S.a., bacterial suspensions were made by adding 20 µL of S.a. (in glycerol) to 5 mL of Luria-Bertani (LB) broth, suspensions were then incubated at 37°C overnight. A dilution 1:10 in LB broth was therefore made and incubated for 1.5 h to restore the exponential growth phase (Figure 39).

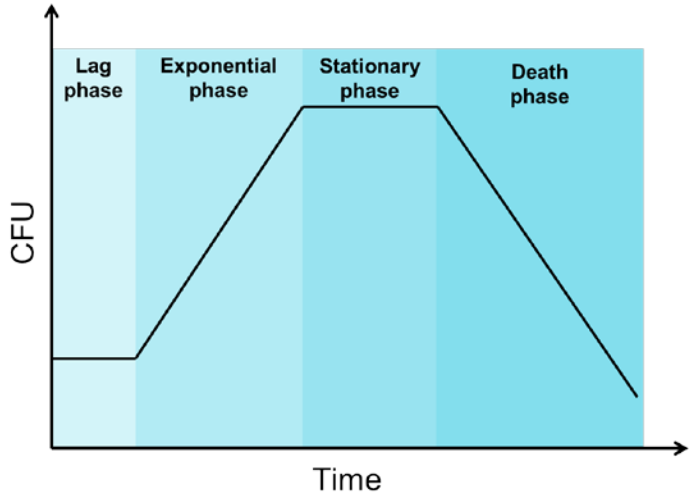

Figure 39 – Bacterial growth over time. In the "lag phase", bacteria interact with the surrounding environment and mature. During the "exponential phase", bacteria doubling occur. In the "stationary phase" the number of new bacteria and the number of dying bacteria matches and, consequently, the total amount of CFU do not increase. Finally, in the "death phase" the number of CFU decreases due to the reduction of nutrients.

The concentration of bacteria in the suspension, represented as colony forming unit in one milliliter (CFU/mL), was measured performing a turbidity measurement[167–169] (Equation 19).

$$0.031 : 4.6 \cdot 10^7 \left(\frac{\mathrm{CFU}}{\mathrm{mL}}\right) = \mathrm{OD} : \mathrm{X} \left(\frac{\mathrm{CFU}}{\mathrm{mL}}\right) \quad (19)$$

By assessing the optical density (OD) at 600 nm with a spectrophotometer, it is possible to obtain an estimate of the bacteria concentration. The strains were consequently incubated with the samples in a diluted culture medium with a final bacterial concentration of $5x10^6$ (CFU/mL). The assay was performed in anaerobic conditions. This was necessary as metronidazole requires absence of oxygen to exert its function[50]. More specifically, metronidazole is a prodrug, meaning that it is not active on its own. Indeed, this API is able to penetrate bacteria and is converted to a free nitroso radical, with short half-life, due to intracellular reduction[51,52]; this radical is only formed in anaerobic conditions, due to the

higher redox potential and interacts specifically with bacterial DNA causing bacterial death (see Chapter 2.1.2 for additional information).

After 24 h of treatment, the bacterial suspensions were vortexed and plated in serial dilutions (from 10^0 to 10^{-5}) and plated in Petri dishes containing LB agar. The plates were then kept at 37°C overnight in aerobic conditions. Aerobic conditions were chosen to increase the grow rate of S.a. and to thereby distinguish the effect of the various treatments more clearly.

In the case of G.v., bacterial suspensions were made by adding 200 µL of G.v. (in glycerol) to 5 mL of Brain-Heart-Infusion (BHI) broth and were incubated at 37°C overnight in a CO_2 enriched atmosphere. A dilution 1:10 in BHI broth was therefore made and incubated for 1.5 h to restore the exponential growth phase (Figure 15). The concentration (CFU/mL) of bacteria in the suspension was assessed as explained above and the treatment of the bacterial suspensions with the samples was performed as previously described for S.a.. However, once plated in Petri dishes at different dilutions, the growth was not performed in aerobic conditions, as described for S.a., but in a CO_2 enriched atmosphere, to allow G.v. to grow[170–172].

The antibacterial effect of the membranes was calculated comparing the number of colonies in each plate adjusting the results for the dilution factor. A detailed protocol and the results are described in Paper IV.

5. Conclusions and future perspectives

The main objective of the PhD project was to develop and characterize DDS for oral and intravaginal applications.

For oral drug delivery, the usage of MCs was investigated. In particular, the addition of a water soluble, sacrificial layer between the MCs base and the Si chip used as a substrate for the fabrication was successful. No interference by the sacrificial layer was, in fact, seen during the various stages of the development of the formulation, that is: i) the sacrificial layer resulted compatible with the $scCO_2$ impregnation technique used to load ketoprofen inside the MCs (previously filled with PVP) and ii) the deposition of the pH sensitive coating over the loaded MCs was not interfering with the ability of the sacrificial layer to dissolve in water. The MCs formulation (loaded with ketoprofen and coated with a pH sensitive coating) was administered to rats orally and the oral bioavailability was compared to a control formulation. Interestingly, the formulation based on MCs resulted in having a faster T_{max} and a higher area under the curve (AUC) within the first 4 h after dosing compared to the control formulation. The detailed results are reported in Paper I.

To further study MCs as a drug delivery platform, two loading techniques were compared. First, MCs were filled with PCL through the HP of a PCL film; ketoprofen was therefore loaded by means of $scCO_2$ impregnation. In the second case, MCs were filled, by means of the HP technique, with a premixed PCL/ketoprofen film. The results obtained from the *in vitro* release studies showed that by using the former method a significantly faster release of ketoprofen was achieved, compared to the other method. This result could imply the possibility of using a different loading method for MCs to achieve slower or faster release kinetics. Please refer to Paper II for more details. An additional finding, reported in Paper II, was the absence of a difference comparing the release profile of ketoprofen loaded in MCs (by means of supercritical CO_2 impregnation) filled with either PVP (well-known solubility enhancer) or PCL. To further understand the motivations behind the absence of a difference, in Paper III, MCs fabricated with different sizes were filled with PVP and impregnated with either ketoprofen or naproxen. All samples were then characterized performing *in vitro* release studies and by mapping the positioning of the API in the

polymeric matrix. The results showed that no difference was discernible between different sizes, both in terms of release profiles and of drug distribution. More specifically, the drug was distributed only in the top layer of the polymer matrix included in the MCs. It is consequently plausible that the usage of different materials did not affect the release from the MCs as the drug was not embedded in the polymeric matrix. The results proved, on the other hand, a non-dependence of the confinement of the polymer matrix, over the loading by means of $scCO_2$ impregnation.

The development of an intravaginal DDS began considering the intravaginal environment: presenting a significant concentration of Ca^{2+}, a membrane based on AL and CH was fabricated (Paper IV). The membrane resulted to be easy to fabricate and was able to resist in a simulated vaginal fluid for an extended period of time, slowly degrading in a *quasi*-linear fashion, due to the stabilization of the calcium ions. The membrane was able to incorporate metronidazole and to effectively kill bacteria strains typical of bacterial vaginosis, a common disease in women in their reproductive age. The AL/CH membrane moreover possessed good mechanical properties both when dry and when swollen in a simulated vaginal fluid and had good adhesion properties.

In the last period of the PhD project, the possibility of deploying a dual feed ultrasonic spray coater for the fabrication of polymeric NPs was assessed. In particular, AL/CH NPs were fabricated changing some of the parameters controlling the ultrasonic spray coater. The results, presented in detail in Paper V, showed that it is possible to fabricate polymeric NPs efficiently and in a continuous and safe manner using an ultrasonic spray coater. Moreover, the possibility of tuning the NPs size distribution by changing the ultrasonic spray coater parameters was verified. The results obtained support the concept by which, an increase in the power of the ultrasound generator determines an increase in the droplet size of the sprayed mist, an occurrence seen previously but not officially reported by the manufacturers of the instrumentation.

In conclusion, the usage of MCs for oral drug delivery is promising, there are, however, issues that have yet to be addressed. First of all, it is necessary to change the material currently used for the fabrication of the MCs. Although SU-8 has been an advantageous

material, thanks to its stability and to the possibility of tuning the shapes and sizes, it is not FDA approved. Additional studies, using MCs fabricated in biodegradable and biocompatible materials, are consequently needed. Secondly, even though we demonstrated (Paper I) that the MCs are able to stick and to be engulfed in the intestinal mucus, efforts must be made to enhance the chances of a correct positioning of the MCs, with the open side directed towards the intestinal epithelium. Finally, in regards of the formulation included in the MCs the possibility of using polymeric NPs (e.g. fabricated by means of ultrasonic spray coating as in Paper V) could be investigated, with the aim of increasing the relative oral bioavailability.

The development of a resistant intravaginal DDS was also successful. In spite of this, additional efforts should be made to evaluate the possibility of using the AL/CH membrane as a DDS for birth control drugs and evaluate the resistance of the membranes to insults, typical of sexual intercourses, and their influence on the drug release kinetic. Finally, the prospect of fabricating hydrogel based membranes using the ultrasonic spray coater to upscale the production could also be investigated.

6. References

[1] G. Tiwari, R. Tiwari, B. Sriwastawa, L. Bhati, S. Pandey, P. Pandey, S. K. Bannerjee, *Int. J. Pharm. Investig.* 2012, *2*, 2.

[2] J. Jin, G. E. Sklar, V. Min Sen Oh, S. Chuen Li, *Ther. Clin. Risk Manag.* 2008, *4*, 269.

[3] D. Eek, M. Krohe, I. Mazar, A. Horsfield, F. Pompilus, R. Friebe, A. L. Shields, *Patient Prefer. Adherence* 2016, *10*, 1609.

[4] M. J. M. Villena, F. Lara-Villoslada, M. A. R. Martínez, M. E. M. Hernández, *Int. J. Pharm.* 2015, *487*, 314.

[5] B. Čalija, N. Cekić, S. Savić, R. Daniels, B. Marković, J. Milić, *Colloids Surfaces B Biointerfaces* 2013, *110*, 395.

[6] C. J. Szymanski, P. Munusamy, C. Mihai, Y. Xie, D. Hu, M. K. Gilles, T. Tyliszczak, S. Thevuthasan, D. R. Baer, G. Orr, P. Northwest, L. Source, L. Berkeley, *Biomaterials* 2016, *62*, 147.

[7] "Ketoprofen," can be found under https://www.drugbank.ca/drugs/DB01009, 2018.

[8] M. Z. I. Khan, Ž. Prebeg, N. Kurjaković, *J. Control. Release* 1999, *58*, 215.

[9] J.-H. Ma, M. Yang, M. Zeng, X.-M. Chen, J. Lan, *Zhongguo Zhong Yao Za Zhi* 2008, *33*, 602.

[10] C. Mazzoni, F. Tentor, S. A. Strindberg, L. H. Nielsen, S. S. Keller, T. S. Alstrøm, C. Gundlach, A. Müllertz, P. Marizza, A. Boisen, *J. Control. Release* 2017, *268*, 343.

[11] L. H. Nielsen, S. S. Keller, A. Boisen, *Lab Chip* 2018, *18*, 2348.

[12] A. Ahmed, C. Bonner, T. A. Desai, *Biomed. Microdevices* 2001, *3*, 89.

[13] H. D. Chirra, T. A. Desai, 2012, 3839.

[14] H. D. Chirra, L. Shao, N. Ciaccio, C. B. Fox, J. M. Wade, A. Ma, T. A. Desai, *Adv. Healthc. Mater.* 2014, *3*, 1648.

[15] C. B. Fox, Y. Cao, C. L. Nemeth, H. D. Chirra, R. W. Chevalier, A. M. Xu, N. A. Melosh, T. A. Desai, *ACS Nano* 2016, *10*, 5873.

[16] C. Mazzoni, F. Tentor, S. A. Strindberg, L. H. Nielsen, S. S. Keller, T. S. Alstrøm, C. Gundlach, A. Müllertz, P. Marizza, A. Boisen, *J. Control. Release* 2017, *268*, 343.

[17] P. Marizza, L. Pontoni, T. Rindzevicius, J. F. Alopaeus, K. Su, J. A. Zeitler, S. S. Keller, I. Kikic, M. Moneghini, N. De Zordi, D. Solinas, A. Cortesi, A. Boisen, *J. Supercrit. Fluids* 2016, *107*, 145.

[18] P. Marizza, S. S. Keller, A. Müllertz, A. Boisen, *J. Control. Release* 2014, *173*, 1.

[19] P. Marizza, S. S. Keller, A. Boisen, *Microelectron. Eng.* 2013, *111*, 391.

[20] Z. Abid, C. Gundlach, O. Durucan, C. von Halling Laier, L. H. Nielsen, A. Boisen, S. S. Keller, *Microelectron. Eng.* 2017, *171*, 20.

[21] L. H. Nielsen, A. Melero, S. S. Keller, J. Jacobsen, T. Garrigues, T. Rades, A. Müllertz, A. Boisen, *Int. J. Pharm.* 2016, *504*, 98.

[22] L. H. Nielsen, S. S. Keller, K. C. Gordon, A. Boisen, T. Rades, A. Müllertz, *Eur. J. Pharm. Biopharm.* 2012, *81*, 418.

[23] E. Baloglu, Z. A. Senyigit, S. Y. Karavana, A. Bernkop-Schnürch, *J. Pharm. Pharm. Sci.* 2009, *12*, 312.

[24] N. B. Dobaria, A. C. Badhan, R. C. Mashru, *AAPS PharmSciTech* 2009, *10*, 951.

[25] A. Abruzzo, F. Bigucci, T. Cerchiara, B. Saladini, M. C. Gallucci, F. Cruciani, B. Vitali, B. Luppi, *Carbohydr. Polym.* 2013, *91*, 651.

[26] A. El-Kamel, M. Sokar, V. Naggar, S. Al Gamal, *AAPS PharmSci* 2002, *4*, 224.

[27] D. H. Owen, D. F. Katz, *Contraception* 1999, *59*, 91.

[28] P. Hay, *Medicine (Baltimore).* 2014, *4*, 359.

[29] G. G. G. Donders, K. Ruban, G. Bellen, *Curr. Infect. Dis. Rep.* 2015, *17*, 1.

[30] Y. Turovskiy, K. S. Noll, M. L. Chikindas, A. A, *J. Appl. Microbiol.* 2011, *110*, 1105.

[31] Y. Barenholz, *J. Control. Release* 2012, *160*, 117.

[32] P. Sacco, E. Decleva, F. Tentor, R. Menegazzi, M. Borgogna, S. Paoletti, K. A. Kristiansen, K. M. Vårum, E. Marsich, *Macromol. Biosci.* 2017, *1700214*, 1700214.

[33] L. H. Nielsen, T. Rades, B. Boyd, A. Boisen, *Eur. J. Pharm. Biopharm.* 2017, *118*, 13.

[34] M. Muller, D. Vehlow, B. Torger, B. Urban, B. Woltmann, U. Hempel, *Curr. Pharm. Des.* 2018, *24*, 1341.

[35] H. Wen, H. Jung, X. Li, *AAPS J.* 2015, *17*, 1327.

[36] "Small Molecule," can be found under https://en.wikipedia.org/wiki/Small_molecule, 2018.

[37] P. K. Patel, C. R. King, S. R. Feldman, *J. Dermatolog. Treat.* 2015, *26*, 299.

[38] "Biopharmaceuticals," can be found under https://en.wikipedia.org/wiki/Biopharmaceutical, 2018.

[39] J. B. Zawilska, J. Wojcieszak, A. B. Olejniczak, *Pharmacol. Reports* 2013, *65*, 1.

[40] H. Chavda, C. Patel, I. Anand, *Syst. Rev. Pharm.* 2010, *1*, 62.

[41] L. Padrela, M. A. Rodrigues, A. Duarte, A. M. A. Dias, M. E. M. Braga, H. C. de Sousa, *Adv. Drug Deliv. Rev.* 2018, *131*, 22.

[42] K. T. Savjani, A. K. Gajjar, J. K. Savjani, *ISRN Pharm.* 2012, *2012*, 195727.

[43] N. J. Babu, A. Nangia, *Cryst. Growth Des.* 2011, *11*, 2662.

[44] J. Sun, F. Wang, Y. Sui, Z. She, W. Zhai, C. Wang, Y. Deng, *Int. J. Nanomedicine* 2012, *7*, 5733.

[45] 2016.

[46] "Naproxen," can be found under https://www.drugbank.ca/drugs/DB00788, 2018.

[47] T. G. Kantor, *Pharmacotherapy* n.d., *6*, 93.

[48] R. N. Brogden, R. C. Heel, T. M. Speight, G. S. Avery, *Drugs* 1979, *18*, 241.

[49] "Metronidazole," can be found under https://www.drugbank.ca/drugs/DB00916, 2018.

[50] S. Löfmark, C. Edlund, C. E. Nord, *Clin. Infect. Dis.* 2010, *50*, S16.

[51] S. A. Dingsdag, N. Hunter, *J. Antimicrob. Chemother.* 2017, 265.

[52] S. N. Moreno, R. P. Mason, R. P. Muniz, F. S. Cruz, R. Docampo, *J. Biol. Chem.* 1983, *258*, 4051.

[53] D. Souza, 1982, 4051.

[54] "Furosemide," can be found under https://www.drugbank.ca/drugs/DB00695, 2018.

[55] L. L. Boles Ponto, R. D. Schoenwald, *Clin. Pharmacokinet.* 1990, *18*, 381.

[56] P. Kanaujia, P. Poovizhi, W. K. Ng, R. B. H. Tan, *Powder Technol.* 2015, *285*, 2.

[57] Y. Hattori, A. Suzuki, M. Otsuka, *Drug Dev. Ind. Pharm.* 2016, *42*, 1851.

[58] Y. Sun, L. Zhu, T. Wu, T. Cai, E. M. Gunn, L. Yu, *AAPS J.* 2012, *14*, 380.

[59] S. Y. Lee, G. Yu, I. W. Kim, *J. Nanomater.* 2013, *2013*, 1.

[60] "Polyvinylpyrrolidone," can be found under https://pubchem.ncbi.nlm.nih.gov/compound/n-vinyl-2-pyrrolidone, 2018.

[61] B. Wang, D. Wang, S. Zhao, X. Huang, J. Zhang, Y. Lv, X. Liu, G. Lv, X. Ma, *Eur. J. Pharm. Sci.* 2017, *96*, 45.

[62] S. J. Gardyne, M. R. Mucalo, M. J. Rathbone, *Results Pharma Sci.* 2011, *1*, 80.

[63] H. Patil, R. V. Tiwari, M. A. Repka, *AAPS PharmSciTech* 2016, *17*, 20.

[64] J. Ivanovic, S. Knauer, A. Fanovich, S. Milovanovic, M. Stamenic, P. Jaeger, I. Zizovic, R. Eggers, *J. Supercrit. Fluids* 2016, *107*, 486.

[65] K. Thanki, R. P. Gangwal, A. T. Sangamwar, S. Jain, *J. Control. Release* 2013, *170*, 15.

[66] J. McLenon, M. A. M. Rogers, *J. Adv. Nurs.* 2018, DOI 10.1111/jan.13818.

[67] I. Iacopetti, A. Perazzi, T. Badon, S. Bedin, B. Contiero, R. Ricci, *BMC Vet. Res.* 2017, *13*, 330.

[68] E. Sjögren, B. Abrahamsson, P. Augustijns, D. Becker, M. B. Bolger, M. Brewster, J. Brouwers, T. Flanagan, M. Harwood, C. Heinen, R. Holm, H.-P. Juretschke, M. Kubbinga, A. Lindahl, V. Lukacova, U. Münster, S. Neuhoff, M. A. Nguyen, A. Van Peer, C. Reppas, A. R. Hodjegan, C. Tannergren, W. Weitschies, C. Wilson, P. Zane, H. Lennernäs, P. Langguth, *Eur. J. Pharm. Sci.* 2014, *57*, 99.

[69] V. V. Khutoryanskiy, *Nat. Mater.* 2015, *14*, 963.

[70] M. T. Cook, G. Tzortzis, D. Charalampopoulos, V. V. Khutoryanskiy, *J. Control. Release* 2012, *162*, 56.

[71] T. Murakami, *Expert Opin. Drug Discov.* 2017, *12*, 1219.

[72] R. A. Cone, *Adv. Drug Deliv. Rev.* 2009, *61*, 75.

[73] M. Boegh, H. M. Nielsen, *Basic Clin. Pharmacol. Toxicol.* 2015, *116*, 179.

[74] F. Bigucci, A. Abruzzo, B. Vitali, B. Saladini, T. Cerchiara, M. C. Gallucci, B. Luppi, *Int. J. Pharm.* 2015, *478*, 456.

[75] A. Hussain, F. Ahsan, *J. Control. Release* 2005, *103*, 301.

[76] C. K. Sahoo, P. K. Nayak, D. K. Sarangi, T. K. Sahoo, *Am. J. Adv. Drug Deliv.* 2013, 043.

[77] W.-Y. Huang, J.-N. Lin, J.-T. Hsieh, S.-C. Chou, C.-H. Lai, E.-J. Yun, U.-G. Lo, R.-C. Pong, J.-H. Lin, Y.-H. Lin, *ACS Appl. Mater. Interfaces* 2016, *8*, 30722.

[78] F. Pozzi, P. Furlani, A. Gazzaniga, S. Davis, I. Wilding, *J. Control. Release* 1994, *31*, 99.

[79] K. Greish, in *Methods Mol. Biol.*, 2010, pp. 25–37.

[80] R. Xu, G. Zhang, J. Mai, X. Deng, V. Segura-Ibarra, S. Wu, J. Shen, H. Liu, Z. Hu, L. Chen, Y. Y. Y. Y. Huang, E. Koay, Y. Y. Y. Y. Huang, J. Liu, J. E. Ensor, E. Blanco, X. Liu, M. Ferrari, H. Shen, *Nat. Biotechnol.* 2016, *34*, 1.

[81] C. von Halling Laier, B. Gibson, M. van de Weert, B. J. Boyd, T. Rades, A. Boisen, S. Hook, L. Hagner Nielsen, *Int. J. Pharm.* 2018, *550*, 35.

[82] B. L. Banik, P. Fattahi, J. L. Brown, *Wiley Interdiscip. Rev. Nanomedicine Nanobiotechnology* 2016, *8*, 271.

[83] K. M. El-Say, H. S. El-Sawy, *Int. J. Pharm.* 2017, *528*, 675.

[84] J. Nagstrup, S. Keller, K. Almdal, A. Boisen, *Microelectron. Eng.* 2011, *88*, 2342.

[85] L. H. Nielsen, T. Rades, B. Boyd, A. Boisen, *Eur. J. Pharm. Biopharm.* 2017, *118*, 13.

[86] L. H. Nielsen, J. Nagstrup, S. Gordon, S. S. Keller, J. Østergaard, T. Rades, A. Müllertz, A. Boisen, *Biomed. Microdevices* 2015, *17*, DOI 10.1007/s10544-015-9958-5.

[87] S. Bose, S. S. Keller, T. S. Alstrøm, A. Boisen, K. Almdal, *Langmuir* 2013, *29*, 6911.

[88] S. M. Patel, R. P. Patel, B. G. Prajapati, *J. Pharm. Bioallied Sci.* 2012, *4*, S104.

[89] K. T. Savjani, A. K. Gajjar, J. K. Savjani, *ISRN Pharm.* 2012, *2012*, 195727.

[90] A. Travan, F. Scognamiglio, M. Borgogna, E. Marsich, I. Donati, L. Tarusha, M. Grassi, S. Paoletti, *Carbohydr. Polym.* 2016, *150*, 408.

[91] F. Scognamiglio, A. Travan, M. Borgogna, I. Donati, E. Marsich, J. W. A. M. Bosmans, L. Perge, M. P. Foulc, N. D. Bouvy, S. Paoletti, *Acta Biomater.* 2016, *44*, 232.

[92] C. Fan, J. Fu, W. Zhu, D. A. Wang, *Acta Biomater.* 2016, *33*, 51.

[93] F. Scognamiglio, A. Travan, G. Turco, M. Borgogna, E. Marsich, M. Pasqua, S. Paoletti, I. Donati, *Colloids Surfaces B Biointerfaces* 2017, *155*, 553.

[94] P. Sacco, A. Travan, M. Borgogna, S. Paoletti, E. Marsich, *J. Mater. Sci. Mater. Med.* 2015, *26*, 1.

[95] P. Sacco, F. Brun, I. Donati, D. Porrelli, S. Paoletti, G. Turco, *ACS Appl. Mater. Interfaces* 2018, *10*, 10761.

[96] J. Jang, Y. J. Seol, H. J. Kim, J. Kundu, S. W. Kim, D. W. Cho, *J. Mech. Behav. Biomed. Mater.* 2014, *37*, 69.

[97] K. I. Draget, G. Skjåk-Bræk, O. Smidsrød, *Int. J. Biol. Macromol.* 1997, *21*, 47.

[98] K. Ingar Draget, K. Østgaard, O. Smidsrød, *Carbohydr. Polym.* 1990, *14*, 159.

[99] A. Haug, J. Bjerrum, O. Buchardt, G. E. Olsen, C. Pedersen, J. Toft, *Acta Chem. Scand.* 1961, *15*, 1794.

[100] M. Gonza, 2002, *239*, 47.

[101] P. Li, Y. N. Dai, J. P. Zhang, A. Q. Wang, Q. Wei, *Int. J. Biomed. Sci.* 2008, *4*, 221.

[102] K. Kurita, *Mar. Biotechnol.* 2006, *8*, 203.

[103] K. J. Kramer, D. Koga, *Insect Biochem.* 1986, *16*, 851.

[104] P. N. Lipke, R. Ovalle, *J. Bacteriol.* 1998, *180*, 3735.

[105] A. Almalik, R. Donno, C. J. Cadman, F. Cellesi, P. J. Day, N. Tirelli, *J. Control. Release* 2013, *172*, 1142.

[106] R. C. Goy, S. T. B. Morais, O. B. G. Assis, *Brazilian J. Pharmacogn.* 2016, *26*, 122.

[107] P. Sacco, A. Travan, M. Borgogna, S. Paoletti, E. Marsich, *J. Mater. Sci. Mater. Med.* 2015, *26*, 1.

[108] I. a. Sogias, A. C. Williams, V. V. Khutoryanskiy, *Biomacromolecules* 2008, *9*, 1837.

[109] M. Huang, E. Khor, L. Y. Lim, *Pharm. Res.* 2004, *21*, 344.

[110] J. K. Suh, H. W. Matthew, *Biomaterials* 2000, *21*, 2589.

[111] F. Shahidi, J. K. V. Arachchi, Y. J. Jeon, *Trends Food Sci. Technol.* 1999, *10*, 37.

[112] M. Garcia-Fuentes, M. J. Alonso, *J. Control. Release* 2012, *161*, 496.

[113] W. Fan, W. Yan, Z. Xu, H. Ni, *Colloids Surfaces B Biointerfaces* 2012, *90*, 21.

[114] H. Jonassen, A. L. Kjøniksen, M. Hiorth, *Biomacromolecules* 2012, *13*, 3747.

[115] P. Satalkar, B. S. Elger, D. M. Shaw, *Sci. Eng. Ethics* 2016, *22*, 1255.

[116] X. Huang, M. A. El-Sayed, *J. Adv. Res.* 2010, *1*, 13.

[117] J. S. Suk, Q. Xu, N. Kim, J. Hanes, L. M. Ensign, *Adv. Drug Deliv. Rev.* 2016, *99*, 28.

[118] X. Deng, M. Cao, J. Zhang, K. Hu, Z. Yin, Z. Zhou, X. Xiao, Y. Yang, W. Sheng, Y.

Wu, Y. Zeng, *Biomaterials* 2014, *35*, 4333.

[119] J. A. Tapia-Hernández, P. I. Torres-Chávez, B. Ramírez-Wong, A. Rascón-Chu, M. Plascencia-Jatomea, C. G. Barreras-Urbina, N. A. Rangel-Vázquez, F. Rodríguez-Félix, *J. Agric. Food Chem.* 2015, *63*, 4699.

[120] R. Sridhar, S. Ramakrishna, R. Sridhar, S. Ramakrishna, 2015, *2535*, 1.

[121] W. Leitner, *Nature* 2000, *405*, 129.

[122] J. R. Falconer, J. Wen, S. Zargar-Shoshtari, J. J. Chen, F. Mohammed, J. Chan, R. G. Alany, *AAPS PharmSciTech* 2012, *13*, 1255.

[123] K. Gong, I. U. Rehman, J. A. Darr, 2008, *48*, 1112.

[124] M. Z. Moghadam, S. Hassanajili, F. Esmaeilzadeh, M. Ayatollahi, M. Ahmadi, *J. Mech. Behav. Biomed. Mater.* 2017, *69*, 115.

[125] J. Chrastil, *J. Chem. Phys.* 1982, *77*, 1512.

[126] Y. Yamini, M. R. Fat'Hi, N. Alizadeh, M. Shamsipur, *Fluid Phase Equilib.* 1998, *152*, 299.

[127] A. Garmroodi, J. Hassan, Y. Yamini, *J. Chem. Eng. Data* 2004, *49*, 709.

[128] Y. Tomita, *Phys. Fluids* 2014, *26*, DOI 10.1063/1.4895902.

[129] J. Stryckers, L. D'Olieslaeger, J. V. M. Silvano, C. K. Apolinario, A. C. G. Laranjeiro, J. Gruber, J. D'Haen, J. Manca, A. Ethirajan, W. Deferme, *Phys. Status Solidi Appl. Mater. Sci.* 2016, *213*, 1441.

[130] R. J. Lang, *J. Acoust. Soc. Am.* 1962, *34*, 6.

[131] N.-T. Nguyen, N.-T. Nguyen, *Micromixers* 2012, 113.

[132] B. C. Shekar, S. Sathish, R. Sengoden, *Phys. Procedia* 2013, *49*, 145.

[133] L. L. Spangler, J. M. Torkelson, J. S. Royal, *Polym. Eng. Sci.* 1990, *30*, 644.

[134] R. S. Petersen, S. S. Keller, A. Boisen, *Lab Chip* 2015, *15*, 2576.

[135] G. S. Bumbrah, R. M. Sharma, *Egypt. J. Forensic Sci.* 2016, *6*, 209.

[136] L. Morelli, K. Zór, C. B. Jendresen, T. Rindzevicius, M. S. Schmidt, A. T. Nielsen, A. Boisen, *Anal. Chem.* 2017, *89*, 3981.

[137] U. Paaver, I. Tamm, I. Laidmäe, A. Lust, K. Kirsimäe, P. Veski, K. Kogermann, J. Heinämäki, *Biomed Res. Int.* 2014, *2014*, 14.

[138] R. Y. Sato-Berrú, E. A. Araiza-Reyna, A. R. Vazquéz-Olmos, *Spectrochim. Acta - Part A Mol. Biomol. Spectrosc.* 2016, *158*, 56.

[139] M. Hippler, *Anal. Chem.* 2015, *87*, 7803.

[140] A. Paudel, D. Raijada, J. Rantanen, *Adv. Drug Deliv. Rev.* 2015, *89*, 3.

[141] L. A. E. B. de Carvalho, M. P. M. Marques, J. Tomkinson, *Biopolymers* 2006, *82*, 420.

[142] G. P. Bettinetti, *Boll. Chim. Farm.* 1989, *128*, 149.

[143] A. W. Newman, S. R. Byrn, *Drug Discov. Today* 2003, *8*, 898.

[144] M. Dudley, X. R. Huang, *Encycl. Mater. Sci. Technol.* 2001, 9813.

[145] D. F. Swinehart, *J. Chem. Educ.* 1962, *39*, 333.

[146] S. Bhattacharjee, *J. Control. Release* 2016, *235*, 337.

[147] J. Tuoriniemi, A.-C. J. H. Johnsson, J. P. Holmberg, S. Gustafsson, J. A. Gallego-Urrea, E. Olsson, J. B. C. Pettersson, M. Hassellöv, *Sci. Technol. Adv. Mater.* 2014, *15*, 035009.

[148] J. Schmidt, J. Skinner, *J. Phys. Chem. B* 2004, 6767.

[149] Y. Matsuura, A. Nakamura, H. Kato, *Anal. Chem.* 2018, *90*, 4182.

[150] B. T. Schaneberg, I. A. Khan, *Pharmazie* 2004, *59*, 819.

[151] L. Vlase, D. Iacob, V. Dorneanu, 2015, *63*.

[152] S. Kongmany, T. T. Hoa, L. T. N. Hanh, K. Imamura, Y. Maeda, L. Van Boi, *J. Chromatogr. B Anal. Technol. Biomed. Life Sci.* 2016, *1038*, 63.

[153] A. P. Schellinger, P. W. Carr, *J. Chromatogr. A* 2006, *1109*, 253.

[154] J. P. B. de Sousa, A. A. da Silva Filho, P. C. P. Bueno, L. E. Gregório, N. A. J. C. Furtado, R. F. Jorge, J. K. Bastos, *Phytochem. Anal.* 2009, *20*, 24.

[155] E. Baird, G. Taylor, *Curr. Biol.* 2017, *27*, R289.

[156] A. Ariyasu, Y. Hattori, M. Otsuka, *Int. J. Pharm.* 2017, *525*, 282.

[157] F. Hindelang, R. Zurbach, Y. Roggo, *J. Pharm. Biomed. Anal.* 2015, *108*, 38.

[158] K. Thorn, *Mol. Biol. Cell* 2016, *27*, 219.

[159] S. Zacchigna, V. Martinelli, S. Moimas, A. Colliva, M. Anzini, A. Nordio, A. Costa, M. Rehman, S. Vodret, C. Pierro, G. Colussi, L. Zentilin, M. I. Gutierrez, E. DIrkx, C. Long, G. Sinagra, D. Klatzmann, M. Giacca, *Nat. Commun.* 2018, *9*, 1.

[160] M. Carter, J. Shieh, *Guid. to Res. Tech. Neurosci.* 2015, 117.

[161] Wikipedia, "Profilometer," can be found under https://en.wikipedia.org/wiki/Profilometer, 2018.

[162] S. Barui, S. Chatterjee, S. Mandal, A. Kumar, B. Basu, *Mater. Sci. Eng. C* 2017, *70*, 812.

[163] J. das Neves, M. H. Amaral, M. F. Bahia, *Eur. J. Pharm. Biopharm.* 2008, *69*, 622.

[164] A. Travan, E. Marsich, I. Donati, M. Benincasa, M. Giazzon, L. Felisari, S. Paoletti, *Acta Biomater.* 2011, *7*, 337.

[165] J. L. Chen, T. W. J. Steele, D. C. Stuckey, *Biotechnol. Bioeng.* 2018, *115*, 351.

[166] S. A. Dingsdag, N. Hunter, *J. Antimicrob. Chemother*. 2017, 265.

[167] A. L. Koch, *Anal. Biochem.* 1970, *38*, 252.

[168] K. Peñuelas-Urquides, L. Villarreal-Treviño, B. Silva-Ramírez, L. Rivadeneyra-Espinoza, S. Said-Fernández, M. B. de León, *Brazilian J. Microbiol.* 2013, *44*, 287.

[169] S. Sutton, *J. Valid. Technol.* 2011, *17*, 46.

[170] P. Braga, M. Sasso, M. Culici, A. Spallino, *Arzneimittelforschung* 2011, *60*, 675.

[171] C. Gottschick, S. P. Szafranski, B. Kunze, H. Sztajer, C. Masur, C. Abels, I. Wagner-Döbler, *PLoS One* 2016, *11*, 1.

[172] F. W. Muli, J. K. Struthers, *J. Med. Microbiol.* 1998, *47*, 401.

Appendix: Pubblications

Paper I

From Concept to *in vivo* testing: Microcontainers for oral drug delivery

C. Mazzoni*, F. Tentor*, S. S. Andersen, L. H. Nielsen, S. S. Keller, T. S. Alstrøm, C. Gundlach, A. Müllertz, P. Marizza, A. Boisen

Journal of Controlled Release, vol. 268, pp. 343–351, 2017

*joint first authorship

Journal of Controlled Release 268 (2017) 343–351

Contents lists available at ScienceDirect

Journal of Controlled Release

journal homepage: www.elsevier.com/locate/jconrel

From concept to *in vivo* testing: Microcontainers for oral drug delivery

Chiara Mazzoni[a,*,1], Fabio Tentor[a,*,1], Sophie Andersen Strindberg[b], Line Hagner Nielsen[a], Stephan Sylvest Keller[a], Tommy Sonne Alstrøm[c], Carsten Gundlach[d], Anette Müllertz[b], Paolo Marizza[a], Anja Boisen[a]

[a] Department of Micro- and Nanotechnology, Technical University of Denmark, Ørsteds Plads 345C, 2800 Kgs. Lyngby, Denmark
[b] Department of Pharmacy, Faculty of Health and Medical Sciences, University of Copenhagen, Universitetsparken 2, 2100 Copenhagen O, Denmark
[c] Department of Applied Mathematics and Computer Science, Technical University of Denmark, Richard Petersens Plads 324, 2800 Kgs. Lyngby, Denmark
[d] Department of Physics, NEXMAP, Technical University of Denmark, Fysikvej 311, 2800 Kgs. Lyngby, Denmark

ARTICLE INFO

Keywords:
Enteric coating
Supercritical impregnation
Oral drug delivery
Microtechnology

ABSTRACT

This work explores the potential of polymeric micrometer sized devices (microcontainers) as oral drug delivery systems (DDS). Arrays of detachable microcontainers (D-MCs) were fabricated on a sacrificial layer to improve the handling and facilitate the collection of individual D-MCs. A model drug, ketoprofen, was loaded into the microcontainers using supercritical CO_2 impregnation, followed by deposition of an enteric coating to protect the drug from the harsh gastric environment and to provide a fast release in the intestine. *In vitro*, *in vivo* and *ex vivo* studies were performed to assess the viability of the D-MCs as oral DDS. D-MCs improved the relative oral bioavailability by 180% within 4 h, and increased the absorption rate by 2.4 times compared to the control. This work represents a significant step forward in the translation of these devices from laboratory to clinic.

1. Introduction

Oral administration of drugs is preferred by patients [1] due to its inherently reduced invasiveness compared to injections and minimal need for trained personnel [2,3]. Moreover, the effective healthcare costs can be diminished avoiding the usage of drugs administered by injections [4,5].

Following oral administration, drug absorption will occur in the gastro-intestinal (GI) tract; primarily in the small intestine due to ahigh surface area provided by the presence of villi and microvilli [6,7]. When delivering drugs through the GI tract, care needs to be taken due to the presence of enzymes and a low gastric pH (1–3.5 in fasted state and 3–6 in fed state) [8]. Both of these can have a negative impact on the administered drug, thereby limiting the effect of the oral formulation.

Traditional oral dosage forms, such as tablets or capsules, can be designed to target the intestine. Enteric coatings can be used to protect the dosage form during transit of the stomach and facilitate the delivery of the drug to the intestinal epithelium for systemic absorption [9,10]. Tablets, capsules as well as micro- and nanoparticulate systems (*i.e.* vesicles, polymeric particles and dendrimers) [11–13], manifest an omni-directional release of the drug in the intestinal lumen. Omni-directional release entails an inevitable loss of the drug in the lumen and therefore a reduction of the drug absorbed into the systemic circulation. Recent and promising approaches focus on reservoir-based microdevices serving as drug carriers, potentially bringing the drug to the desired place of absorption by unidirectional release from the device. An example of such microdevices is microcontainers. Here a polymeric cylinder is situated on a flat surface, defining a container structure with a cavity in the micrometer size [14,15]. Microcontainers provide unidirectional drug release due to their design and a protection of the drug formulation from the acidic environment of the stomach. Previously, they have been suggested as a promising oral drug delivery system, for instance maintaining indomethacin in its amorphous state [16,17] and being suitable for the confinement of spray dried lipid nanoparticles [18]. Furthermore, microcontainers have shown to improve the oral bioavailability of an amorphous salt of furosemide (a class IV drug in the Biopharmaceutics Classification System (BCS)), compared to the same drug loaded into a capsule. It was speculated by the authors that this could be due to the protection of the drug during the passage through the stomach and because of an engulfment of the microcontainers in the intestinal mucus, resulting in a prolonged absorption period [19]. Chirra et al. have illustrated the beneficial effect of using microdevices to improve the relative oral bioavailability of the BCS class III drug, acyclovir compared to a solution of the same drug [20]. Moreover, Fox et al. have shown that nanostraw membranes (porous

* Corresponding authors.
E-mail addresses: chimaz@nanotech.dtu.dk (C. Mazzoni), fabt@nanotech.dtu.dk (F. Tentor).
[1] The authors contributed equally to the work.

http://dx.doi.org/10.1016/j.jconrel.2017.10.013
Received 5 September 2017; Received in revised form 11 October 2017; Accepted 12 October 2017
Available online 18 October 2017
0168-3659/

nanostructured delivery substrates) increase adhesion to the mucus and facilitate the drug loading *via* diffusion [21]. So far, the presented works have only covered part of a device development and/or characterization and, in most cases, not reporting on *in vivo* studies and not characterizing the devices and drugs after individual processing steps. For example, we have previously reported on drug loading of polymer filled microcontainers using supercritical carbon dioxide ($scCO_2$) [22]. However, these containers were not detachable and thus, never used in animal studies. Likewise, we have reported on microcontainers loaded with powder of furosemide [19] where the filled containers were mechanically removed from the carrier substrate introducing a risk of damaging the containers.

Here we present, for the first time, the complete process of developing and characterizing a microcontainer-based oral delivery system. The aim of this work was to translate detachable microcontainers (D-MCs) filled with drug and sealed with a lid, from the concept to the final oral DDS suitable for *in vivo* and *ex vivo* studies. For this purpose, D-MCs have been fabricated on a sacrificial layer, improving handling and facilitating detachment and collection of the individual filled and coated D-MCs. D-MCs were loaded with the BCS class II model drug ketoprofen utilizing $scCO_2$ followed by an enteric coating to prevent release of the formulation during handling, detachment and transit through the stomach. The loaded and coated D-MCs were investigated *in vitro* to assess the functionality of the enteric lid, and *in vivo* and *ex vivo*, to evaluate the potential of microcontainers as an oral DDS.

2. Materials and methods

2.1. Fabrication of detachable microcontainers (D-MCs)

Silicon (Si) wafers (4-in. b100N n-type) were supplied by Okmetic (Vantaa, Finland). SU-8 2075 and SU-8 developer were purchased from Microresist Technology GmbH (Berlin, Germany). Polyacrylic acid 35 wt% aqueous solution (PAA, Mw 100,000) was purchased from Sigma Aldrich (St. Louis, USA) and neutralized with NaOH. A 15 μm thick film of PAA was spin coated on a Si wafer and dried at 80 °C for 10 min. The PAA film served as a water soluble release layer after completed detachable microcontainers (D-MCs) fabrication [23]. D-MCs were fabricated with epoxy-based photoresist SU-8 using a procedure similar to the one described earlier [15,16]. After fabrication, the wafers were cut into square chips containing 625 D-MCs using a laser (microSTRUCT vario, 3D Microac AG, Chemnitz, Germany). The dimensions of the D-MCs were measured using an Alpha-Step IQ Stylus Profilometer (KLA-Tencor Corporation, Milpitas, USA) and optical microscopy.

2.2. Loading of drug formulation into the microcontainers

D-MCs sitting on a Si chip were manually loaded with polyvinylpyrrolidone (PVP) (Mw = 10,000, Sigma Aldrich, St. Louis, USA) blowing away the excess in between the D-MCs using an air gun in a similar setup as described previously [18,19]. The chips were weighted before and after and placed within a supercritical CO_2 chamber (3 chips at a time, see Fig. 1), together with 14.2 ± 0.1 mg (n = 15, SD) of ketoprofen powder (≥ 98% racemate, Sigma Aldrich, St. Louis, USA). The impregnation of the polymer was conducted by bringing CO_2 over its supercritical state at 100 bar and 40 °C, keeping it under stirring for 1 h. During this process ketoprofen solubilizes in supercritical CO_2 and diffuses into the polymer matrix. The pressurization and depressurization rate were 3.9 bar/min and 2.5 bar/min, respectively.

2.3. Enteric coating deposition

A pH sensitive polymer, Eudragit® L100 (Evonik, Darmstad, Germany) was employed for the enteric coating on the cavity of the D-MCs. A solution of 2% w/v Eudragit® L100 and 5% w/w in relation to the polymer of dibutyl sebacate (Sigma Aldrich, St. Louis, USA) was dissolved in isopropanol (Sigma Aldrich, St. Louis, USA).

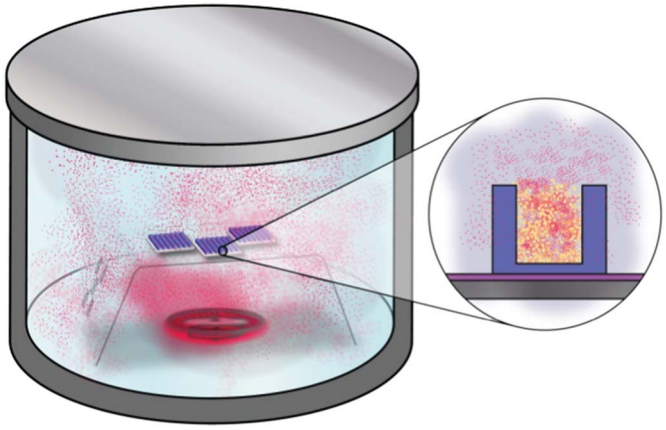

Fig. 1. Schematic representation of the supercritical CO_2 impregnation process. Within the chamber the loading of three D-MCs chips due to the solubilization of ketoprofen in the supercritical CO_2 is depicted. On the right, a zoom in of one D-MC during the loading process is represented.

The solution was sprayed over a chip of drug-loaded microcontainers using an ultrasonic spray coater equipped with an accumist nozzle operating at 120 kHz (Sono-Tek, USA). During the procedure, the flow rate was kept at 0.1 mL/min, together with a 1.5 W generator power. The shaping air was set to 0.02 bar, and the speed of the nozzle was maintained at 5 mm/s, keeping a distance between the tip and the sample of 6.5 cm. The nozzle of the spray coater was positioned above the chip containing loaded D-MCs, following a path in the x-y axis to cover an area defined by the corners of the chip, previously identified using an integrated camera. Each chip was coated with two alternating wavy line spray paths having an offset of 2 mm, resulting in a total of 100 passages. The chips were kept at 40 °C during the spray coating process.

2.4. Morphology characterization

X-ray micro computed tomography (X-ray μCT, Zeiss Xradia 410 versa, Pleasanton, USA) was applied to assess the filling level of the ketoprofen:PVP formulation into the D-MCs and the coating morphology on the cavity of the D-MCs. The 3D tomographic reconstruction was done with the software, provided with the system, based on a FDK algorithm [24]. The chip with D-MCs was investigated using a high voltage of 60 kV and having an effective pixel size of 19.33 μm, taking 1601 projection images. For examining smaller parts of the chip with a higher resolution 60 kV as high voltage and an effective pixel size of 3.02 μm with 3201 projection images was utilized. Three areas from each sample were analyzed to obtain a more representative image of the whole chip.

Capsules filled with D-MCs were scanned to assess the effect of the collection of the D-MCs after their detachment, to assess if they were separated one to each other and if the coating was still intact. For this purpose, scans were recorded with a voltage of 40 kV with a pixel size of either 10.23 μm or 3.36 μm, taking 1601 projection images.

The quality of both the loading and the coating of the D-MCs was investigated using a Zeiss Supra 40VP Field Emission Scanning Electron Microscope (SEM, Carl Zeiss Microscopy GmbH, Jena, Germany). The samples were placed over metallic holders and tilted to 30° prior the analyses, both low and high vacuum modes were used with a variable energy between 4 and 8 keV.

The coating thickness of Eudragit® L100 was measured by contact profilometry (Alpha-Step IQ Stylus Profilometer, KLA-Tencor Corporation, Milpitas, USA). Eudragit® L100 films were sprayed on a SU-8 covered flat silicon chip as described in the above section 'Enteric

coating deposition'. The profiles were measured using a 15.6 mg tip force with a scan speed of 20 μm/s and a sampling rate of 50 Hz.

2.5. Solid state characterization of ketoprofen

X-Ray powder diffraction (XRPD) was used to determine the solid state form of ketoprofen in the D-MCs and of the controls. An X'Pert PRO X-ray diffractometer (PANalytical, Almelo, The Netherlands, MPD PW3040/60 XRD; Cu KR anode, λ = 1.541 Å, 45 kV, 40 mA) was utilized. A starting angle of 5° 2θ and an end angle of 30° 2θ were employed for the scans with a scan speed of 0.67335° 2θ/min and a step size of 0.0262606° 2θ. Data were collected using X'Pert Data Collector software (PANalytical B.V.). The diffractogram of loaded and coated D-MCs was compared to that of crystalline ketoprofen, coated D-MCs loaded with crystalline ketoprofen and D-MCs loaded with 1:4 crystalline ketoprofen:PVP. The diffractograms of D-MCs on the PAA layer, PVP and Eudragit® L100 were also investigated for comparison (data not shown). Moreover, XRPD was used to verify the amorphous form of ketoprofen in the control samples for the *in vivo* studies (described in the 'Capsules preparation' section).

In addition, the solid state form of ketoprofen impregnated into the D-MCs and of control formulations was assessed by means of Raman spectroscopy using a DXR Raman microscope (Thermo Fisher Scientific, Inc., Waltham, USA). The microscope was coupled to a single grating spectrometer with 5 cm^{-1} FWHM spectral resolution and ± 2 cm^{-1} wavenumber accuracy. All spectra were collected using a laser with a wavelength of 780 nm, with a 50 × objective and an estimated laser spot of 3.6 μm diameter. A 50 μm slit was utilized when analyzing bulk powder, whereas a 25 μm pinhole was deployed to analyze the ketoprofen inside the microcontainers the laser power was equal to 10 and 20 mW, respectively. The spectra of: i) pure ketoprofen, ii) pure PVP and iii) microcontainers filled with PVP and impregnated with ketoprofen were compared.

2.6. Release of ketoprofen from D-MCs

The efficacy of the coating and its resistance after the detachment of the D-MCs was evaluated determining the release of the impregnated ketoprofen, both in a Fasted State Simulated Gastric Fluid (FaSSGF pH 1.65 – Biorelevant®, London, UK) and Fasted State Simulated Intestinal Fluid (FaSSIF pH 6.5 – Biorelevant®, London, UK). Impregnated chips either coated or uncoated were individually immersed in 2 mL of deionized water (pH 3.25) to allow the solubilization of the PAA layer (avoiding the coating to dissolve) and hence, the detachment of the D-MCs. Suspended D-MCs were transferred into dialysis bags (MW cut off: 14,000) and placed in 20 mL of FaSSGF in an orbital shaking water bath at 37 °C, 150 rpm (Grant Instrument Ltd., model OLS26, Cambridge, UK) for 2 h. Afterwards, the bags were removed, rinsed with FaSSIF and placed in 20 mL of fresh FaSSIF at 37 °C, 150 rpm for 6 h. 20 μL were collected at 0, 5, 10, 20, 40, 60, 120 min during the release in FaSSGF and after 1, 2, 5, 10, 20, 40, 60, 120, 240 and 360 min during the release in FaSSIF. Samples were analyzed using the UV–Vis spectrophotometer (NanoDrop 2000c, Thermo Fisher Scientific Inc., UK) at 258 nm. The amount of ketoprofen loaded in the D-MCs chips was also investigated as described in the section '*In vitro* release of ketoprofen from coated D-MCs'. The release curves were performed at least in triplicates (n = 3 for the coated and n = 6 for the uncoated D-MCs).

2.7. Capsules preparation

Three chips of D-MCs were impregnated together and coated individually as described above. The solubilization of the sacrificial layer and the subsequent detachment from the Si chip were obtained soaking the chips into 5 mL of deionized water (pH 3.25). After 5 min, the water was removed and the D-MCs were dried at 37 °C for 15 min. Gelatin capsules (Torpac® size 9, Fairfield, USA) were filled with individual D-MCs (258 ± 31 D-MCs per capsule, as visible in Fig. S5 in the Supplementary information) and weighted before and after filling. The concentration of ketoprofen in the capsules was assessed *in vitro* by placing 14 capsules in 20 mL of phosphate buffered saline (PBS, Sigma Aldrich, St. Louis, USA) and kept under stirring (150 rpm) at 37 °C for 24 h. Measurements were done through UV–Vis spectroscopy as described before at a wavelength of 258 nm.

The preparation for the control for the *in vivo* study started with a physical mixture of ketoprofen and PVP powders with the same weight ratio (1:4) as in the D-MCs. The mixture was prepared by heating it up to 120 °C on a heating plate gently mixing the two compounds during the melting of the drug. The heated mixture was immediately quenched using liquid nitrogen followed by grinding to a fine powder. The amorphous form of ketoprofen was confirmed using XRPD as previously described. Gelatin capsules were loaded with 922.4 ± 11.5 μg of the grinded powder, an amount corresponding to that of the D-MCs formulation. Subsequently, the capsules were coated with a solution of 5% w/v Eudragit® L100 and 5% w/w dibutyl sebacate in relation to the polymer in isopropanol. The capsules were coated by dipping half of it into the coating solution and dried for 15 min before coating the other half. This procedure was repeated three times for each capsule.

2.8. In vivo and ex vivo studies

All animal care and experimental studies were performed according to Danish and European laws, guidelines and policies for animal housing, care and experiments at the University of Copenhagen. The *in vivo* experiment was carried out at the Department of Experimental Medicine, University of Copenhagen and approved by the local institutional Animal Welfare Committee under the license number 2015-15-0201-00454. The *ex vivo* study was performed at the Department of Pharmacy, University of Copenhagen under the license number 2016-15-0201-00892. Both studies were carried out in compliance with the Danish laws regulating experiments on animals and EC Directive 2010/63/EU.

Male Sprague-Dawley rats were housed in pairs in cages to acclimatize for a period of one week with a light/dark period of 12/12 h and a temperature of 22 °C with a relative humidity of 55 ± 10%. During this period, the rats had free access to standard pellets and water.

For the *in vivo* study the rats with a weight ranging from 373 to 436 g were randomly divided into two groups. One group was dosed with capsules loaded with D-MCs (n = 11), the second group was dosed with capsules containing the control formulation (n = 6). Both types of capsules were given using a polyurethane feeding tube (Instech Laboratories Inc., Plymouth Meeting, USA), one capsule was dosed per rat. The rats were fastened for 1 h before and after the dosing, and for the rest of period they had free access to water and standard pellets. Blood (200 μL) was sampled through the lateral tail vein at 15, 30, 45, 60, 75, 90, 120 min, 4, 6, 8 and 24 h post dosing and collected in ethylenediaminetetraacetic acid tripotassium salt dihydrate (EDTA, Sigma-Aldrich, St. Louis, USA) coated tubes. Plasma was obtained by immediately spinning the blood samples at 1500 *g* for 10 min. Plasma was stored at − 20 °C until further analyses.

For the *ex vivo* study, two male Sprague–Dawley rats weighting 316 and 319 g were used and were fasted 1 h prior to dosing.

Capsules filled with D-MCs (see the section 'Capsules preparation') were administered to the rats by oral gavage as described previously. After 90 min post-dosing, the rats were sacrificed, and opened at the *linea alba* for retrieving the stomach and small intestine. These were immediately cut open and examined for localizing the D-MCs using a stereo microscope (SteReo Discovery V8, Carl Zeiss MicroImaging GmbH, Jena, Germany).

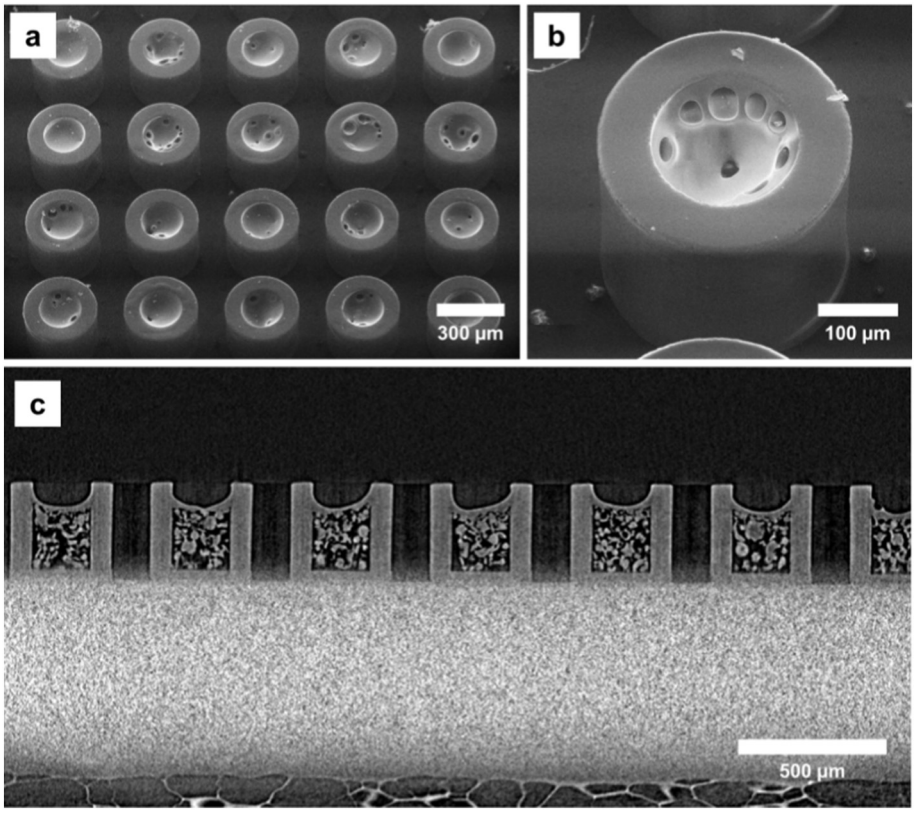

Fig. 2. Morphological characterization of drug loaded D-MCs. (a) and (b): SEM images of D-MCs first manually loaded with PVP and then impregnated with ketoprofen in supercritical CO_2 at 40 °C and 100 bar for 1 h. (c):X-ray μCT cross-sectional view of the loaded D-MCs.

2.9. High Pressure Liquid Chromatography (HPLC) analysis of plasma samples

HPLC analyses were performed using a Dionex Ultimate 3000 Pump equipped with a Dionex ASI-100 Automated Sample Injector and with a UV-VIS lamp.

Ketoprofen was extracted from the plasma samples using a method described elsewhere [25] with minor modifications. Briefly, methanol was added in a 3:1 v/v ratio to the plasma and, after vortexing the mixtures, the samples were centrifuged at 15,000 *g* for 6 min and the supernatants were transferred into HPLC vials.

The HPLC was run in isocratic mode using a method already described in literature with slight modifications [25]. The mobile phases constituted of (A): deionized water with 1% v/v trifluoroacetate (Sigma Aldrich, St. Louis, USA) and (B): 100% acetonitrile (Sigma Aldrich, St. Louis, USA). The ratio of the mobile phase A:B was equal to 45:55 v/v. Samples were run over a Kinetex 5.0 μm XB-C18 100 Å, 100 × 4.6 mm column (Phenomenex ApS, Nordic Region, Værløse, Denmark) at 22 °C. The injected volume was 40 μL with a flow rate of 1 mL/min and a total run time per sample of 10 min. The absorbance was measured at 258 nm.

2.10. Statistics

For the *in vivo* studies, all results were normalized for the averages of rat mass and of the ketoprofen dosed.

To calculate the standard error for the area under the curve (AUC, Table 1), the standard error of the mean of correlated variables is used

$$SE_{\overline{AUC}} = \sqrt{\frac{\sum_{i=1}^{M} var[A_i] + \sum_{i=1}^{M}\sum_{j\neq i}^{M} cov(A_i, A_j)}{N}}$$

where A_i is the AUC for region *i*.

To calculate the average amount of PVP inside a capsule, and the associated standard error, the following formula is derived. To derive the formula, it is assumed that the amount of PVP in each D-MCs in the filling process are independently distributed.

$$SE_{\overline{PVP}} = \sqrt{\frac{1}{N_c}\left(\frac{1}{NM} var[X]\, var[Y] + \frac{1}{N} var[X] E[Y]^2 + \frac{1}{M} var[Y] E[X]^2\right)}$$

where N_c is the total amount of microcontainers per chip, X is the total amount of PVP measured N times, and Y is the number of microcontainers contained inside a capsule, measured M times.

The raw data of the *in vivo* studies can be found in the Supplementary information (Fig. S4).

Moreover, as the sample sizes are different the effect sizes reported in Table 1 uses the Hedges *g* effect size defined as $g = (M_1 - M_2)/SD_{pooled}$ where SD_{pooled} is the weighted standard deviation of the two groups [26–28].

All of the data are expressed as mean and the usage of standard deviation (SD) or standard error of the mean (SE) is defined within the text. Where appropriate, statistical analysis was carried out using Student *t*-tests using GraphPad Prism version 6.05. P-values below 5% ($p < 0.05$) were considered statistically significant.

3. Results

3.1. Fabrication of microcontainers on a sacrificial layer

D-MCs were successfully fabricated in SU-8 on a water soluble layer of PAA. D-MCs had a height of 304 ± 12 μm (n = 8, SD) and a diameter equal to 329 ± 5 μm (n = 8, SD). The inner reservoir had a depth of 272 ± 6 μm (n = 8, SD) and a diameter of 188 ± 4 μm (n = 8, SD) resulting in a container volume of 7.5 ± 0.3 nL (n = 8, SD). D-MCs were adhering well to the PAA layer not impairing the handling. D-MCs were arranged in arrays of 25 × 25 devices on quadratic chips with a side length of 12.8 mm.

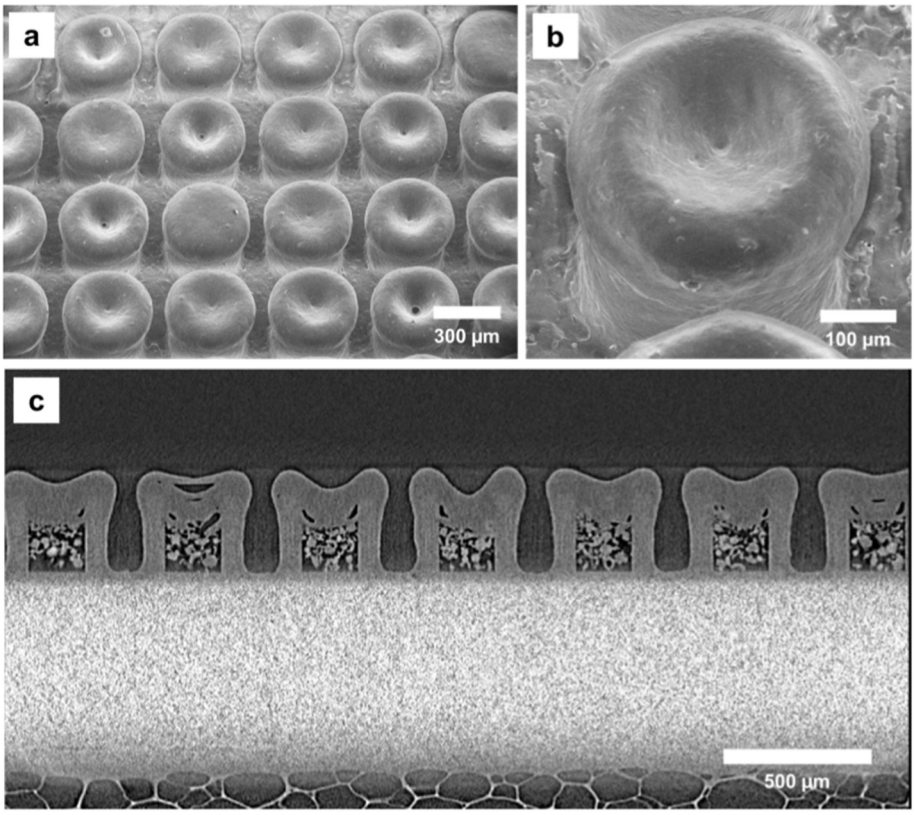

Fig. 3. Morphological characterization of loaded and coated D-MCs. (a) and (b):SEM images of D-MCs coated with Eudragit® L100 onto the cavity of the drug-loaded D-MCs. (c): X-ray µCT cross-sectional view of the drug-loaded and coated D-MCs.

3.2. Loading of D-MCs

Every chip with D-MCs was manually filled with 1.79 ± 0.21 mg (n = 54 chips, SD) of PVP powder followed by loading ketoprofen into the polymer matrix using $scCO_2$. All chips underwent the same supercritical treatment at 40 °C and 100 bar for 1 h. The filled D-MCs on chips were visualized using a SEM (Fig. 2a, b). The cross-sectional X-ray µCT image of the D-MCs loaded with PVP and ketoprofen is shown in Fig. 2c.

3.3. Enteric coating deposition onto drug-loaded D-MCs

The spray coated gastro-resistant lid of Eudragit® L100 was, initially, characterized using contact profilometry to define the coating thickness on two chips. This resulted in thicknesses of 123.0 ± 1.9 and 118.7 ± 3.3 µm (SD describes the roughness of the surface of the coating). X-Ray µCT and SEM were utilized to assess the morphology of the coatings after their deposition on the cavity of the D-MCs. The coatings were homogenous (Fig. 3a, b) and well distinguishable from the impregnated PVP and ketoprofen (Fig. 3c).

3.4. In vitro release of ketoprofen from coated D-MCs

The detachment of the drug-loaded and coated D-MCs from the PAA layer was accomplished by soaking chips in deionized water at pH 3.25 for about 5 min.

The release of ketoprofen was evaluated in human FaSSGF for 120 min (simulating the residence time in the stomach) followed by investigation of the drug release in human FaSSIF for 360 min (simulating the transit time of the small intestine). After 120 min in FaSSGF, 56 ± 14% of the loaded ketoprofen from uncoated D-MCs was released compared to 16 ± 3% from the coated D-MCs (Fig. 4). Upon changing to FaSSIF, a burst release with a significant immediate concentration difference was noticed for the coated microcontainers (p-value = 0.0022). After 6 h in FaSSIF, 100% of the loaded ketoprofen

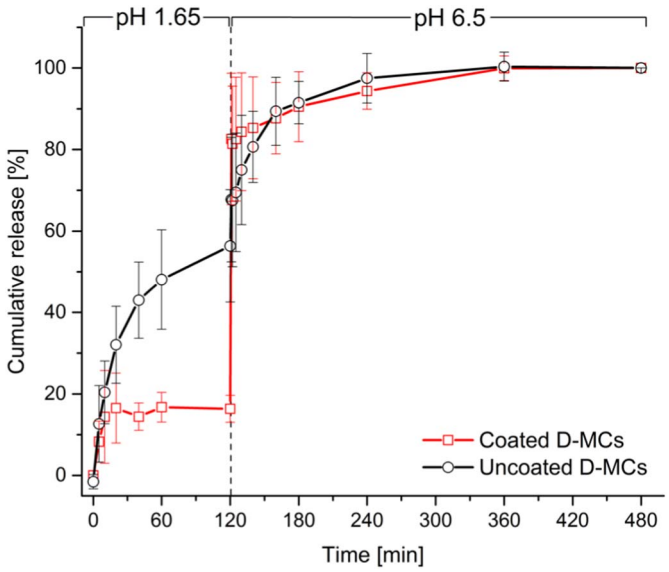

Fig. 4. *In vitro* cumulative release of ketoprofen. Coated (red line) and uncoated (black line) D-MCs. For the first 120 min, the chips were placed in FaSSGF and subsequently in FaSSIF for 360 min. Each release curve is calculated as mean ± standard deviation (n = 6 for the uncoated D-MCs, n = 3 for the coated D-MCs). For the individual profiles refer to Fig. S3 in the Supplementary information. (For interpretation of the references to colour in this figure legend, the reader is referred to the web version of this article.)

was released from both the coated and uncoated D-MCs. The release profile of ketoprofen for the uncoated D-MCs did not present a burst release, but instead followed a first order kinetic. Consequently, statistical significance (p-value = 0.002) was noticeable for the release of ketoprofen after 2 h between coated and uncoated D-MCs. The total amount of ketoprofen loaded into a single chip with 625 D-MCs was 424 ± 10 µg (n = 14, SE) corresponding to a weight ratio of

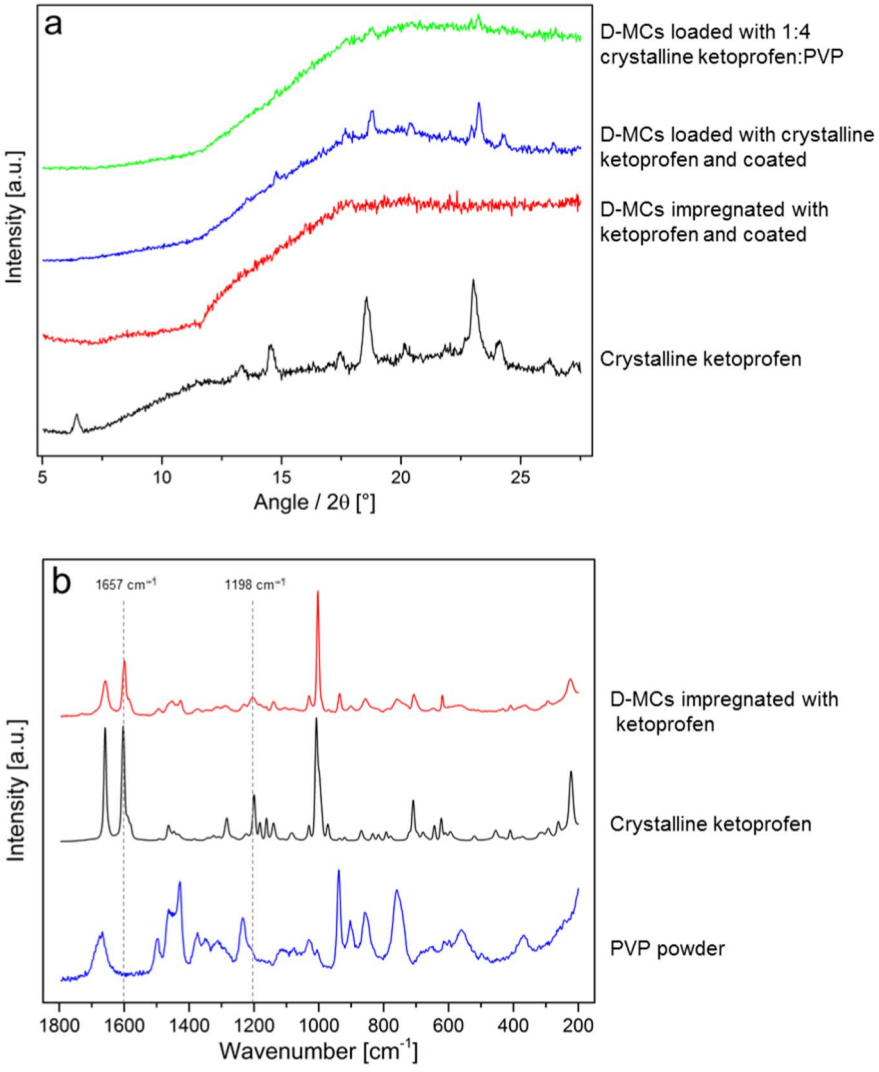

Fig. 5. Solid state characterization of ketoprofen in D-MCs. (a) XRPD diffractograms of crystalline ketoprofen (black), D-MCs impregnated with ketoprofen and coated (red), D-MCs loaded with crystalline ketoprofen and coated (blue) and D-MCs loaded with 1:4 crystalline ketoprofen:PVP (green). (b) Raman scattering profiles of PVP powder (blue), crystalline ketoprofen (black) and D-MCs impregnated with ketoprofen (red). (For interpretation of the references to colour in this figure legend, the reader is referred to the web version of this article.)

ketoprofen to PVP of approximately 1:4 (see the 'Formulation preparation for *in vivo* and *ex vivo* studies' section). The total amount of ketoprofen loaded into the coated and uncoated D-MCs were seen to be very similar. No significant difference was found (p-value = 0.2542).

3.5. Solid state characterization of ketoprofen in D-MCs

The solid state form of ketoprofen in the D-MCs both after $scCO_2$ impregnation and after additional enteric coating deposition was evaluated by means of XRPD. By comparing the diffractograms (Fig. 5a), it was found that the distinct peaks of crystalline ketoprofen were not visible in the final $scCO_2$ impregnated and coated microcontainers. This, together with the typical scattering halo (Fig. 5a, red), indicated the maintenance of ketoprofen in its amorphous form within the D-MCs. The two controls (coated D-MCs loaded with crystalline ketoprofen and D-MCs with a crystalline ketoprofen:PVP mixture in the ratio 1:4) demonstrated that it was possible to measure through the coating and to detect crystalline ketoprofen in the D-MCs in the same quantity as seen in the $scCO_2$ impregnated and coated microcontainers (Fig. 5a, blue and green).

It is worth mentioning that the melted and quenched mixture of ketoprofen:PVP 1:4 (used as control for the *in vivo* studies) was also found to be amorphous in the XRPD diffractograms (see in Supplementary information Fig. S1).

The XRPD results were corroborated by Raman spectroscopy comparing the spectra of pure crystalline ketoprofen, pure PVP and microcontainers filled with PVP and impregnated with ketoprofen (Fig. 5b). As noticeable from the Raman spectra, the characteristic vibrational patterns of ketoprofen were also visible in the impregnated D-MCs. Briefly, the intensity of the peak at 1657 cm^{-1}, which is attributed to the vibrational stretch of the carbonyl ν(C═O), decreased compared to that of crystalline ketoprofen. Moreover, the broadening of the band around 1198 cm^{-1} (CH ring plane bending) together with the lowering of the peak intensities between 1500 cm^{-1} and 1100 cm^{-1}, supported the hypothesis of ketoprofen amorphization due to the impregnation process [29].

3.6. Formulation preparation for in vivo and ex vivo studies

Gelatin capsules were filled with 258 ± 31 (n = 54, SE) $scCO_2$ loaded and coated D-MCs corresponding to 176 ± 14 μg (n = 14, SE) of ketoprofen and 741 ± 52 μg (n = 54, SE) of PVP.

X-ray μCT was employed to visualize the microcontainers inside the capsule. It can be seen that the coating was preserved through all preparation steps and that the microcontainers were intact and separated from each other (Fig. 6).

3.7. In vivo studies

Capsules filled with D-MCs or with the control formulation were

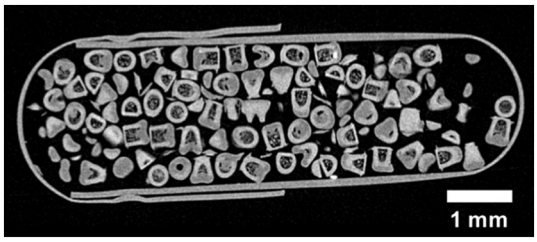

Fig. 6. X-ray μCT image of a gelatine capsule filled with loaded and coated D-MCs.

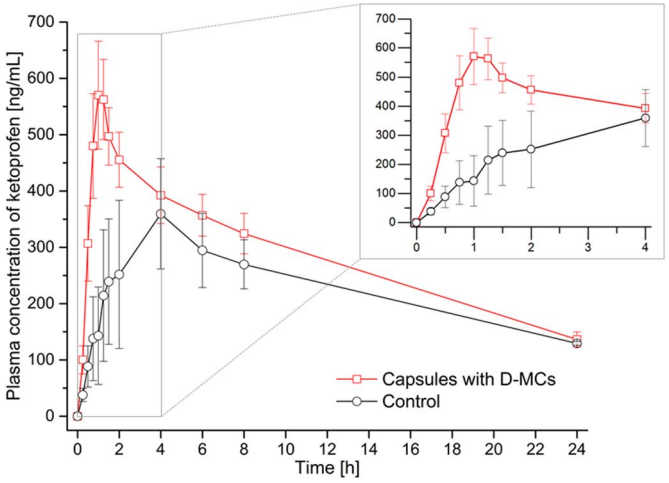

Fig. 7. Plasma concentration of ketoprofen over time. (Red line), capsules with loaded and coated D-MCs (n = 11, SE). (Black line), control capsules filled with melted ketoprofen and PVP and coated (n = 6, SE). The inset represents the same profiles zoomed in the first 4 h. For the individual profiles refer to Fig. S4 in the Supplementary information. (For interpretation of the references to colour in this figure legend, the reader is referred to the web version of this article.)

dosed by oral gavage to rats. The measured plasma concentration of ketoprofen over time is presented in Fig. 7 and key results are summarized in Table 1. The maximum plasma concentrations (C_{max}) are similar for D-MCs and the control. The values were found to be 657 ± 78 ng/mL and 488 ± 105 ng/mL for the formulation with D-MCs and for the control, respectively (p-value = 0.2191). The AUC from 0 to 24 h ($AUC_{0\text{-}24h}$) was calculated to be 406 ± 40 min·ng/mL for the D-MCs formulation and 320 ± 49 min·ng/mL for the control, thereby, no significant difference was observed between the two groups (p-value = 0.2041). The relative bioavailability from 0 to 24 h for ketoprofen in D-MCs compared to the control was found to be 127 ± 23%. However, statistically relevant difference (p-value = 0.0279) was found for the time corresponding to the maximum plasma concentration (T_{max}) when comparing the two formulations (93 ± 17 min for the D-MC and 212 ± 60 min for the control). The $AUC_{0\text{-}4h}$ for the D-MCs formulation was 99 ± 10 min·ng/mL and 55 ± 18 min·ng/mL for the control resulting in a statistically significant difference between the two groups (p-value = 0.0387). According to this, the oral relative bioavailability from 0 to 4 h was 180 ± 62% for the D-MC formulation compared to the control. The absorbance rate of ketoprofen (C_0 to C_{max}) for the rats dosed with D-MCs was 10 ± 2 $ng \cdot min^{-1} \cdot mL^{-1}$, which is significantly higher than for the control (4 ± 1 $ng \cdot min^{-1} \cdot mL^{-1}$) (p-value = 0.0430, Fig. 7, top right).

3.8. Ex vivo study

In order to understand the mechanism of action of the D-MCs, their position in the GI tract of the rats at T_{max} (90 min) was assessed. No D-MCs were found in the stomach of the rats at T_{max}, whereas many were found in the mid-jejunum (see Fig. S2 in the Supplementary information). This indicates that the enteric coating protected the formulation until the intestine was reached, where the ketoprofen was released and absorbed.

4. Discussion

Micro- and nanotechnologies are enabling new possibilities in the world of oral drug delivery. It is a highly complex and multidisciplinary field with focus on fabrication and on the possibilities to integrate novel functionalities into drug delivery systems. *In vivo* studies proving their actual performances [21,30–32] are, however, not always carried out.

In this work, an oral DDS based on microcontainers has been further developed compared to previous ones [19,33]. The complete process, starting from the fabrication of the new D-MCs to the loading and coating, highlighting the subsequent results from the *in vivo* and *ex vivo* investigations, is presented.

D-MCs were filled with PVP in a simple and reproducible manner and $scCO_2$ was used to load the D-MCs with the model drug ketoprofen with a final 1:4 weight ratio of drug to polymer. A single D-MC has a cavity of 7.5 ± 0.3 nL, 178 times larger compared to other similar DDS [34], and each one was loaded with 0.68 μg of ketoprofen, which is considerably more compared to the data presented by Chirra et al. (1.54 ng) [20]. The amount of ketoprofen in a single D-MC corresponds to 1.3% w/w of the total weight of the microdevice. The technique of $scCO_2$ impregnation was preferred over inkjet printing due to the low spotting reproducibility and low loading capacity of the printing process [35,36].

In the loading process, $scCO_2$ acts as a solvent for ketoprofen, but not for PVP, which only swells [22]. The porosity of PVP increased during the impregnation allowing ketoprofen to access the D-MCs. CO_2, in its supercritical state, has a density similar to a liquid, whereas the viscosity and diffusivity are closer to the ones of a gas. These features are exploited during the impregnation process, where ketoprofen is used in relatively high concentration and diffuses easily with the CO_2 into the D-MCs.

Table 1
Non-compartmental model of the *in vivo* study of ketoprofen in D-MCs (n = 11, SE) and for the control formulation (n = 6, SE).

	Capsule with loaded and coated D-MCs	Coated capsules with 1:4 ketoprofen:PVP amorphous mixture (control)	Effect size[b]
C_{max} [ng/mL]	657 ± 78	488 ± 105	0.65
T_{max} [min]	93 ± 17[a]	212 ± 60[a]	1.24
$AUC_{0\text{-}4h}$ [min·ng/mL]	99 ± 10[a]	55 ± 18[a]	1.16
$AUC_{0\text{-}24h}$ [min·ng/mL]	406 ± 40	320 ± 49	0.68
Relative oral bioavailability [%]			
0–4 h	180 ± 62%		
0–24 h	127 ± 23%		

[a] p-value < 0.05.
[b] *Effect size* = $(M_1 - M_2)/SD_{pooled}$ where M_1 and M_2 are the averages of the two populations and SD_{pooled} is the weighted standard deviation of the two groups.

During the $scCO_2$ impregnation, a solid state transition of ketoprofen from its crystalline to its amorphous form was obtained. Ketoprofen is a BCS class II drug meaning that it has a poor solubility in water. Therefore, its aqueous solubility can be increased by exploiting the amorphous form [37–40]. The XRPD diffractograms and the Raman spectra (Fig. 5a and b, respectively) suggested that the amorphous form of ketoprofen was present after impregnation into the D-MCs, confirming previous results [33].

Ketoprofen was kept in its amorphous form for at least 7 days (data not shown) due to the use of $scCO_2$ and to its affinity with PVP [29,41,42]. PVP is a water soluble polymer and has unique properties in prolonging the stability of amorphous forms of drugs, thereby increasing their dissolution rate and solubility [41]. Microcontainers can additionally stabilize the amorphous form of drugs by spatially confining the drug molecules, leading to an improved physical stability of the amorphous drugs [16,17].

In order to avoid premature release of ketoprofen, D-MCs were coated with the gastro-resistant polymer Eudragit® L100. The *in vitro* dissolution studies (Fig. 4) confirmed that this polymer successfully protected the drug during transit through the gastric environment and dissolved quickly upon arrival in the small intestine (where the pH is generally above 6) [19,43–46]. Spray coating by an ultrasonic nozzle was selected as the technology to deposit the coating onto the cavity of the D-MCs. The morphology of PVP and ketoprofen after impregnation (Fig. 2) was suitable for the coating deposition as there was still space for the coating in the top of the cavity of the D-MCs. The deposition of the lid was simple and straightforward, and has the potential of being scaled up. D-MCs were detached from the fabrication platform by soaking them into acidified water. This approach maintains the integrity of the gastro-resistant lid (Fig. 6) and it is a gentler and more controlled procedure than using, for example, mechanical forces. SEM images and X-ray μCT scans of coated D-MCs showed that after spray coating no agglomerates of polymer were present between adjacent microcontainers and that the D-MCs were not attached to each other after dissolution of the PAA sacrificial layer (Figs. 3 and 6).

The *in vitro* release of ketoprofen from the D-MCs in gastric and intestinal simulated media demonstrated the efficacy of the coating. The immediate release of 16 ± 3% of ketoprofen from the coated D-MCs in FaSSGF can be explained by the presence of small pores in the coating (Fig. 3) and/or the possible variation of the polymer morphology (refer to the video in the Supplementary Information for a more detailed view). For the uncoated D-MCs, 56 ± 14% of ketoprofen was released in FaSSGF, showing that nothing efficiently hindered the drug release. Coated D-MCs showed a very significant burst release upon changing to FaSSIF due to the dissolution of Eudragit® L100 followed by a fast release of ketoprofen, together with dissolution of PVP (Fig. 4).

In vivo studies are necessary when testing new drug delivery systems as they provide indications on possible bioavailability improvements after oral administration compared to a control formulation [47,48].

The control formulation used in these studies was designed to have the same ratio of ketoprofen:PVP (1:4) and a total amount of drug and polymer as for the D-MCs formulation to obtain information on the behavior of the D-MCs. The solid state form of a drug has a large influence on the dissolution rate, and can therefore, be of great importance for the bioavailability [49]. It was found that ketoprofen in the D-MCs after $scCO_2$ impregnation was amorphous and consequently, the ketoprofen in the control formulation was also brought to its amorphous form. This was obtained by melting the ketroprofen together with PVP followed by a fast cooling, which is a common method for preparing the amorphous form of a drug, as reported by Enfalt et al. [50].

Compared to the control, the D-MCs formulation did not provide a higher C_{max}. However, a faster T_{max} was observed for the D-MCs formulation being roughly 2.3 times faster than the control. This significant difference resulted in a large value for the effect size (Table 1), in accordance with the classification proposed by Choen [28], where the intervals 0.00–0.20, 0.20–0.50 and 0.50–0.80 correspond to a small, medium or large effect, respectively. This indicates that D-MCs have a large effect on the time of absorption. For the first 4 h of the plasma concentration-time profile (Fig. 7), the absorption of ketoprofen was significantly higher than for the control, again resulting in a large effect size value (Table 1). This difference resulted in a relative oral bioavailability of 180 ± 62% for the first 4 h. In accordance with the difference between the T_{max} values, the absorption rate was significantly higher for the rats administered with D-MCs compared to the control rats. This supports the conclusion that the D-MCs provided a much faster absorption of ketoprofen compared to the control. It can be hypothesized that this, to some extent, is caused by a faster gastric emptying of the rats dosed with the D-MCs compared to the control. Indeed, D-MCs were most likely released from the gelatin capsule in the stomach as no coating was applied to the entire capsule, conversely to the control formulation. From the plasma concentration curve (Fig. 7), it is noticeable that after 4 h the two formulations show more similar kinetics, and the $AUC_{0\text{-}24h}$ is not significantly different. This is reflected in the relative bioavailability of ketoprofen in the D-MCs formulation compared to the control being 127 ± 23%. Choi et al. [51] evaluated the intestinal absorption of a suspension of ketoprofen in rats administering a 2.3 times higher dosage compared to the one used in the present study. The authors report a higher C_{max} (6.12 ± 1.02 μg/mL) and a faster T_{max} (0.42 ± 0.29 h). Indeed, these results might be attributed to the higher dosage and to the fact that ketoprofen was dosed in a suspension form, thus, partially pre-solubilized. An important difference comparing these two studies is the plasma concentration decay over time. The decrease is slower for the D-MCs, indicating a prolonged drug release and absorption time. A possible explanation for this might be provided by the results of our *ex vivo* study where at the time in which the T_{max} was reached (93 ± 17 min), D-MCs were spread in the small intestine, and most of them were found in the mid-jejunum embedded deep into the mucus. This pronounced engulfment might indeed have resulted in a slower release and at the same time allowed prolonged absorption of ketoprofen. It has previously been shown in intestinal perfusion studies in rats that SU-8 microcontainers have mucoadhesive properties showing *i.e.* a high tendency to be engulfed by the mucus [19].

5. Conclusions

In this work, we demonstrated that D-MCs are a promising oral drug delivery system providing a 2.3 times faster T_{max} and a 180% increased $AUC_{0\text{-}4h}$ when compared to the control. These features can be of high importance as it could imply that the administered dose could be reduced. The BCS class II model drug ketoprofen was successfully loaded into D-MCs exploiting the features of $scCO_2$ impregnation maintaining the API in its amorphous form. Enteric coating was employed to protect the drug from the stomach environment and to release ketoprofen in the intestine, as proven by the *in vitro* study. All preparation steps are designed to be compatible with each other maintaining ketoprofen in its amorphous state. *In vivo* and *ex vivo* analyses finally show the potentials of using D-MCs as an oral drug delivery system.

Supplementary data to this article can be found online at https://doi.org/10.1016/j.jconrel.2017.10.013.

Acknowledgments

The authors would like to acknowledge the Danish National Research Foundation (DNRF122) and Villum Fonden (Grant No. 9301) for Intelligent Drug Delivery and Sensing Using Microcontainers and Nanomechanics (IDUN). The 3D Imaging Centre at The Technical University of Denmark is gratefully acknowledged. Line Hagner Nielsen would like to acknowledge Danish Research Council for Technology and Production (FTP), Project DFF 4004-00120B for financial support.

The authors would also like to acknowledge Professor Massimo Borelli, School of PhD Programmes, University 'Magna Graecia', Catanzaro, Italy for his suggestion on the statistical analysis. Nanna Bild, Technical University of Denmark, is acknowledged for the drawing of the schematics.

References

[1] K. Thanki, R.P. Gangwal, A.T. Sangamwar, S. Jain, Oral delivery of anticancer drugs: challenges and opportunities, J. Control. Release 170 (2013) 15–40.
[2] G. Liu, E. Franssen, M.I. Fitch, E. Warner, Patient preferences for oral versus intravenous palliative chemotherapy, J. Clin. Oncol. 15 (1997) 110–115.
[3] C.S. Loh, A.J MacRobert, J. Bedwell, J. Regula, N. Krasner, S.G Bown, Oral versus intravenous administration of 5-aminolaevulinic acid for photodynamic therapy, Br. J. Cancer 68 (1993) 41–51.
[4] Lionel A. Mandell, Michel G. Bergeron, Marie J. Gribble, Peter J. Jewesson, E. Donald, Thomas J. Marrie, Lindsay E. Nicolle, Sequential antibiotic therapy: effective cost management and patient care, Can. J. Infect. Dis. 6 (1995).
[5] P.M.M. Bossuyt, J. Dankert, P. Speelman, Implementation in a Large Teaching Hospital, J. Antimicrob. Chemother. (1999) 601–606.
[6] H.F. Helander, L. Fandriks, Surface area of the digestive tract - revisited, Scand. J. Gastroenterol. 49 (2014) 681–689.
[7] T.T. Kararli, Comparison of the gastrointestinal anatomy, physiology, and biochemistry of humans and commonly used laboratory animals, Biopharm. Drug Dispos. 16 (1995) 351–380.
[8] E. Sjögren, B. Abrahamsson, P. Augustijns, D. Becker, M.B. Bolger, M. Brewster, J. Brouwers, T. Flanagan, M. Harwood, C. Heinen, R. Holm, H.P. Juretschke, M. Kubbinga, A. Lindahl, V. Lukacova, U. Münster, S. Neuhoff, M.A. Nguyen, Peer Av, C. Reppas, A.R. Hodjegan, C. Tannergren, W. Weitschies, C. Wilson, P. Zane, H. Lennernäs, P. Langguth, In vivo methods for drug absorption – comparative physiologies, model selection, correlations with in vitro methods (IVIVC), and applications for formulation/API/excipient characterization including food effects, Eur. J. Pharm. Sci. 57 (2014) 99–151.
[9] D. Schmaljohann, Thermo- and pH-responsive polymers in drug delivery, Adv. Drug Deliv. Rev. 58 (2006) 1655–1670.
[10] T. Yoshida, T.C. Lai, G.S. Kwon, K. Sako, pH- and ion-sensitive polymers for drug delivery, Expert Opin. Drug Deliv. 10 (2013) 1497–1513.
[11] Jonathan F. Lovell, Cheng S. Jin, Elizabeth Huynh, Honglin Jin, Chulhong Kim, John L. Rubinstein, Warren C.W. Chan, Weiguo Cao, Lihong V. Wang, Gang Zheng, Porphysome nanovesicles generated by porphyrin bilayers for use as multimodal biophotonic contrast agents, Nat. Mater. 10 (2011) 324–332.
[12] S.K. Jain, T. Haider, A. Kumar, A. Jain, Lectin-conjugated clarithromycin and acetohydroxamic acid-loaded PLGA nanoparticles: a novel approach for effective treatment of *H. pylori*, AAPS PharmSciTech 17 (2016) 1131–1140.
[13] Rita B. Restani, A. Sofia Silva, Rita F. Pires, Renato Cabral, Ilídio J. Correia, Teresa Casimiro, Vasco D.B. Bonifácio, Ana Aguiar-Ricardo, Nano-in-micro POxylated polyurea dendrimers and chitosan dry powder formulations for pulmonary delivery, Part. Part. Syst. Charact. 33 (2016) 851–858.
[14] J. Nagstrup, S. Keller, K. Almdal, A. Boisen, 3D microstructuring of biodegradable polymers, Microelectron. Eng. 88 (2011) 2342–2344.
[15] P. Marizza, S.S. Keller, A. Boisen, Inkjet printing as a technique for filling of microwells with biocompatible polymers, Microelectron. Eng. 111 (2013) 391–395.
[16] L.H. Nielsen, S.S. Keller, K.C. Gordon, A. Boisen, T. Rades, A. Müllertz, Spatial confinement can lead to increased stability of amorphous indomethacin, Eur. J. Pharm. Biopharm. 81 (2012) 418–425.
[17] L.H. Nielsen, S.S. Keller, A. Boisen, A. Müllertz, T. Rades, A slow cooling rate of indomethacin melt spatially confined in microcontainers increases the physical stability of the amorphous drug without influencing its biorelevant dissolution behaviour, Drug Deliv. Transl. Res. 4 (2014) 268–274.
[18] L.H. Nielsen, T. Rades, B. Boyd, A. Boisen, Microcontainers as an oral delivery system for spray dried cubosomes containing ovalbumin, Eur. J. Pharm. Biopharm. (2016), http://www.sciencedirect.com/science/article/pii/S0939641116309626.
[19] L.H. Nielsen, A. Melero, S.S. Keller, J. Jacobsen, T. Garrigues, T. Rades, A. Müllertz, A. Boisen, Polymeric microcontainers improve oral bioavailability of furosemide, Int. J. Pharm. 504 (2016) 98–109.
[20] H.D. Chirra, L. Shao, N. Ciaccio, C.B. Fox, J.M. Wade, A. Ma, T.A. Desai, Planar microdevices for enhanced in vivo retention and oral bioavailability of poorly permeable drugs, Adv. Healthc. Mater. 3 (2014) 1648–1654.
[21] Cade B. Fox, Yuhong Cao, Cameron L. Nemeth, Hariharasudhan D. Chirra, Rachel W. Chevalier, Alexander M. Xu, Nicholas A. Melosh, Tejal A. Desai, Fabrication of sealed nanostraw microdevices for oral drug delivery, ACS Nano 10 (2016) 5873–5881.
[22] P. Marizza, S.S. Keller, A. Müllertz, A. Boisen, Polymer-filled microcontainers for oral delivery loaded using supercritical impregnation, J. Control. Release 173 (2014) 1–9.
[23] V. Linder, B.D. Gates, D. Ryan, B.A. Parviz, G.M. Whitesides, Water-soluble sacrificial layers for surface micromachining, Small 1 (2005) 730–736.
[24] L.A. Feldkamp, L.C. Davis, J.W. Kress, Practical cone-beam algorithm, J. Opt. Soc. Am. A 1 (1984) 612.
[25] Jean Negru, Daniela-Saveta Popa, Laurian Vlase, Dana Iacob, Marcela Achim, Vasile Dorneanu, High-throughput HPLC method for rapid quantification of ketoprofen in human plasma, Farmacia 63 (2015).
[26] L.V Hedges, Distribution, theory for glass's estimator of effect size and related estimators, J. Educ. Stat. 6 (1981) 107.
[27] S. Sawilowsky, New Effect Size Rules of Thumb, Theor. Behav. Found. Educ. Fac. Publ., 2009.
[28] J. Cohen, Statistical power analysis, Curr. Dir. Psychol. Sci. 1 (1992) 98–101.
[29] L.A.E.B. de Carvalho, M.P.M. Marques, J. Tomkinson, Drug–excipient interactions in ketoprofen: a vibrational spectroscopy study, Biopolymers 82 (2006) 420–424.
[30] D.A. LaVan, T. McGuire, R. Langer, Small-scale systems for in vivo drug delivery, Nat. Biotechnol. 21 (2003) 1184–1191.
[31] W.-J. Zhang, C.-Y. Hong, C.-Y. Pan, Efficient fabrication of photosensitive polymeric nano-objects via an ingenious formulation of RAFT dispersion polymerization and their application for drug delivery, Biomacromolecules (2017) acs.biomac.6b01887 http://pubs.acs.org/doi/abs/10.1021/acs.biomac.6b01887.
[32] S. Sant, S.L. Tao, O.Z. Fisher, Q. Xu, N.A. Peppas, A. Khademhosseini, Microfabrication technologies for oral drug delivery, Adv. Drug Deliv. Rev. 64 (2012) 496–507.
[33] P. Marizza, L. Pontoni, T. Rindzevicius, J.F. Alopaeus, K. Su, J.A. Zeitler, S.S. Keller, I. Kikic, M. Moneghini, N. De Zordi, D. Solinas, A. Cortesi, A. Boisen, Supercritical impregnation of polymer matrices spatially confined in microcontainers for oral drug delivery: effect of temperature, pressure and time, J. Supercrit. Fluids 107 (2016) 145–152.
[34] H.D. Chirra, T.A. Desai, Multi-reservoir bioadhesive microdevices for independent rate-controlled delivery of multiple drugs, Small (2012) 3839–3846.
[35] Cade B. Fox, Cameron L. Nemeth, Rachel W. Chevalier, Joshua Cantlon, Derek B. Bogdanoff, Jeff C. Hsiao, Tejal A. Desai, Picoliter-volume inkjet printing into planar microdevice reservoirs for low-waste, high-capacity drug loading, Bioeng. Transl. Med. (2017) 9–16, http://dx.doi.org/10.1002/btm2.10053.
[36] P. Marizza, S.S. Keller, A. Müllertz, A. Boisen, Polymer-filled microcontainers for oral delivery loaded using supercritical impregnation, J. Control. Release 173 (2014) 1–9.
[37] K. Wlodarski, W. Sawicki, K.J. Paluch, L. Tajber, M. Grembecka, L. Hawelek, Z. Wojnarowska, K. Grzybowska, E. Talik, M. Paluch, The influence of amorphization methods on the apparent solubility and dissolution rate of tadalafil, Eur. J. Pharm. Sci. 62 (2014) 132–140.
[38] S. Mallick, The solid state amorphization of poorly water soluble drugs, Indian J. Pharm. Sci. 66 (2004).
[39] G. Tkalec, M. Pantic, Z. Novak, Z. Knez, Supercritical impregnation of drugs and supercritical fluid deposition of metals into aerogels, J. Mater. Sci. 50 (2015) 1–12.
[40] C. Potter, Y. Tian, G. Walker, C. McCoy, P. Hornsby, C. Donnelly, D.S. Jones, G.P. Andrews, Novel supercritical carbon dioxide impregnation technique for the production of amorphous solid drug dispersions: a comparison to hot melt extrusion, Mol. Pharm. 12 (2015) 1377–1390.
[41] P.S. Yadav, V. Kumar, U.P. Singh, H.R. Bhat, B. Mazumder, Physicochemical characterization and in vitro dissolution studies of solid dispersions of ketoprofen with PVP K30 and d-mannitol, Saudi Pharm. J. SPJ Off. Publ. Saudi Pharm. Soc. 21 (2013) 77–84.
[42] Luigi Manna, Mauro Banchero, Davide Sola, Ada Ferri, Silvia Ronchetti, Silvio Sicardi, Impregnation of PVP microparticles with ketoprofen in the presence of supercritical CO2, J. Supercrit. Fluids 42 (2007) 378–384.
[43] M.O. Besenhard, A. Thurnberger, R. Hohl, E. Faulhammer, J. Rattenberger, J.G. Khinast, Continuous API-crystal coating via coacervation in a tubular reactor, Int. J. Pharm. 475 (2014) 198–207.
[44] D.N. Nguyen, L. Palangetic, C. Clasen, G. Van Den Mooter, One-step production of darunavir solid dispersion nanoparticles coated with enteric polymers using electrospraying, J. Pharm. Pharmacol. 68 (2016) 625–633.
[45] D. Sauer, A.B. Watts, L.B. Coots, W.C. Zheng, J.W. McGinity, Influence of polymeric subcoats on the drug release properties of tablets powder-coated with pre-plasticized Eudragit® L 100-55, Int. J. Pharm. 367 (2009) 20–28.
[46] L.H. Nielsen, J. Nagstrup, S. Gordon, S.S. Keller, J. Østergaard, T. Rades, A. Müllertz, A. Boisen, pH-triggered drug release from biodegradable microwells for oral drug delivery, Biomed. Microdevices 17 (2015) 1–7.
[47] H.D. Chirra, T.A. Desai, Emerging microtechnologies for the development of oral drug delivery devices, Adv. Drug Deliv. Rev. 64 (2012) 1569–1578.
[48] S. Sant, S.L. Tao, O.Z. Fisher, Q. Xu, N.A. Peppas, A. Khademhosseini, Microfabrication technologies for oral drug delivery, Adv. Drug Deliv. Rev. 64 (2012) 496–507.
[49] S. Datta, D.J.W. Grant, Crystal structures of drugs: advances in determination, prediction and engineering, Nat. Rev. Drug Discov. 3 (2004) 42–57.
[50] T. Einfalt, O. Planinšek, K. Hrovat, Methods of amorphization and investigation of the amorphous state, Acta Pharma. 63 (2013) 305–334.
[51] J.-S. Choi, M.J. Jin, H.-K. Han, Intestinal absorption characteristics of ketoprofen in rats, Biopharm. Drug Dispos. 27 (2006) 17–21.

From concept to *in vivo* testing: Microcontainers for oral drug delivery

Chiara Mazzoni[a, *, 1], Fabio Tentor [a, *, 1], Sophie Strindberg Andersen[b], Line Hagner Nielsen[a], Stephan Sylvest Keller[a], Tommy Sonne Alstrøm[c], Carsten Gundlach[d], Anette Müllertz[b], Paolo Marizza[a], Anja Boisen[a]

[1]The authors contributed equally to the work.
*Corresponding authors
[a]Department of Micro- and Nanotechnology, Technical University of Denmark, Ørsteds Plads 345C, 2800 Kgs. Lyngby, Denmark
[b]Department of Pharmacy, Faculty of Health and Medical Sciences, University of Copenhagen, Universitetsparken 2, 2100 København Ø, Denmark
[c]Department of Applied Mathematics and Computer Science, Technical University of Denmark, Richard Petersens Plads 324, 2800 Kgs. Lyngby, Denmark
[d]Department of Physics, NEXMAP, Technical University of Denmark, Fysikvej 311, 2800 Kgs. Lyngby, Denmark

Supplementary Information

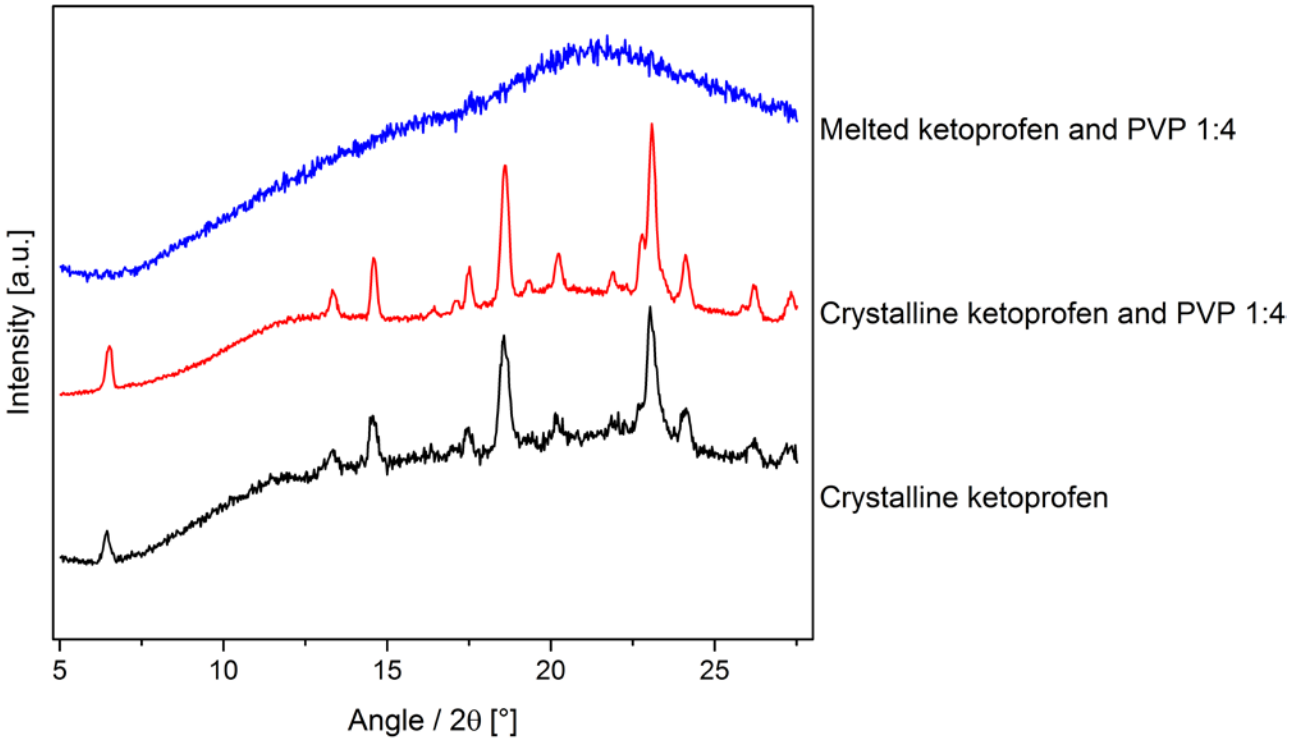

Figure S1: XRPD diffractograms of the control formulation used for the *in vivo* study. Crystalline ketoprofen (**black**), crystalline ketoprofen and PVP 1:4 (**red**) and melted ketoprofen and PVP 1:4 (control for the *in vivo* studies) (**blue**).

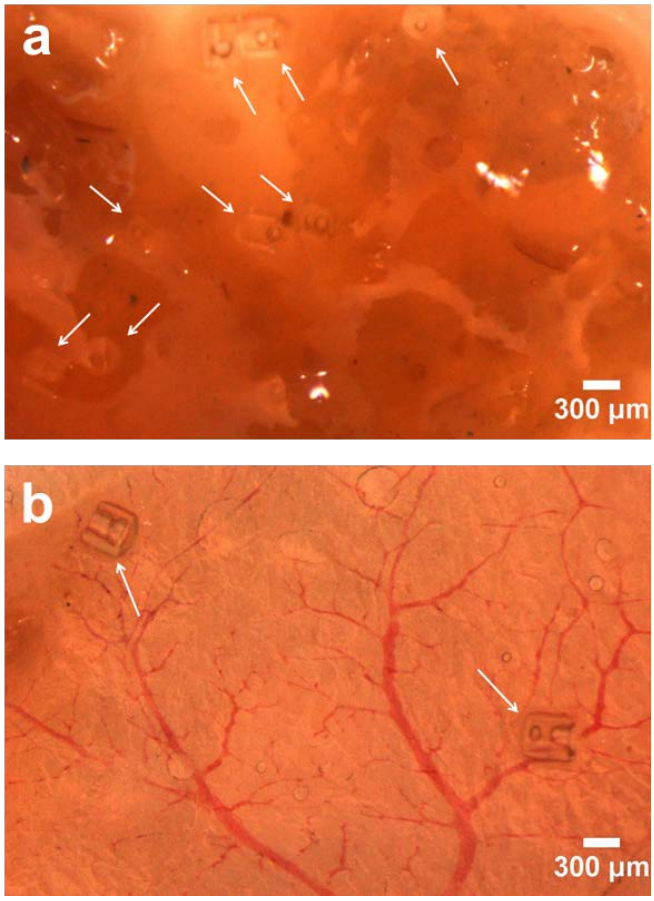

Figure S2: Optical stereoscopy images of the intestinal tissue of oral dosed rats with the D-MCs. D-MCs highlighted with arrows are visible in the intestinal rat tissue, and in (**a**) the engulfment of the D-MCs in the mucus is observed.

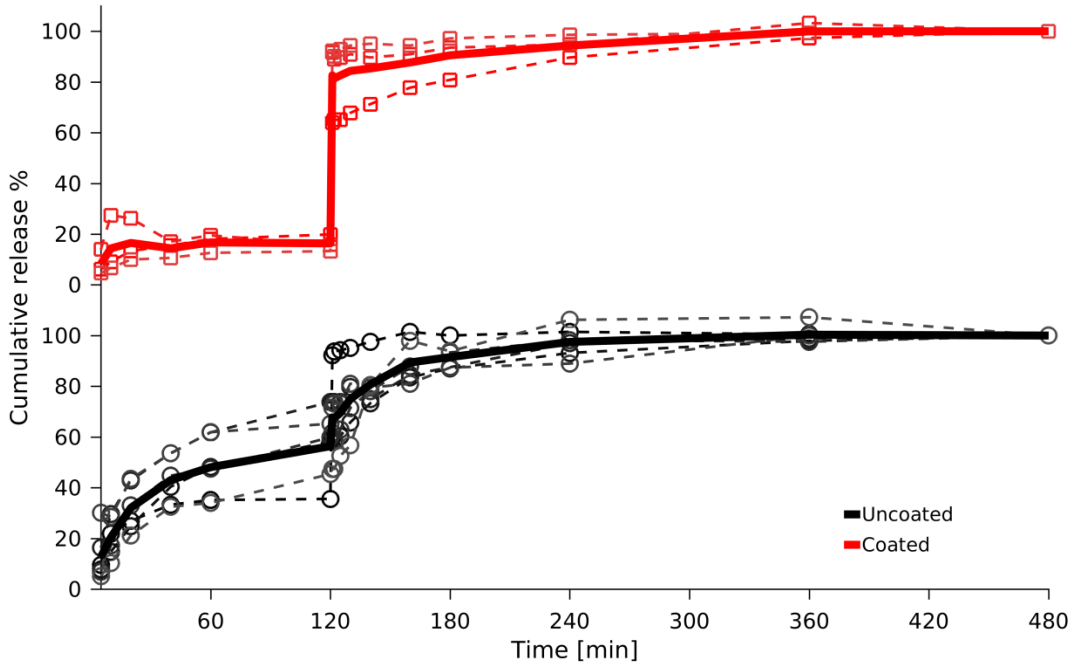

Figure S3: Individual profiles of the *in vitro* cumulative release of ketoprofen. Coated (**red line**) and uncoated (**black line**) D-MCs. For the first 120 min, the chips were placed in FaSSGF and subsequently in FaSSIF for 360 min.

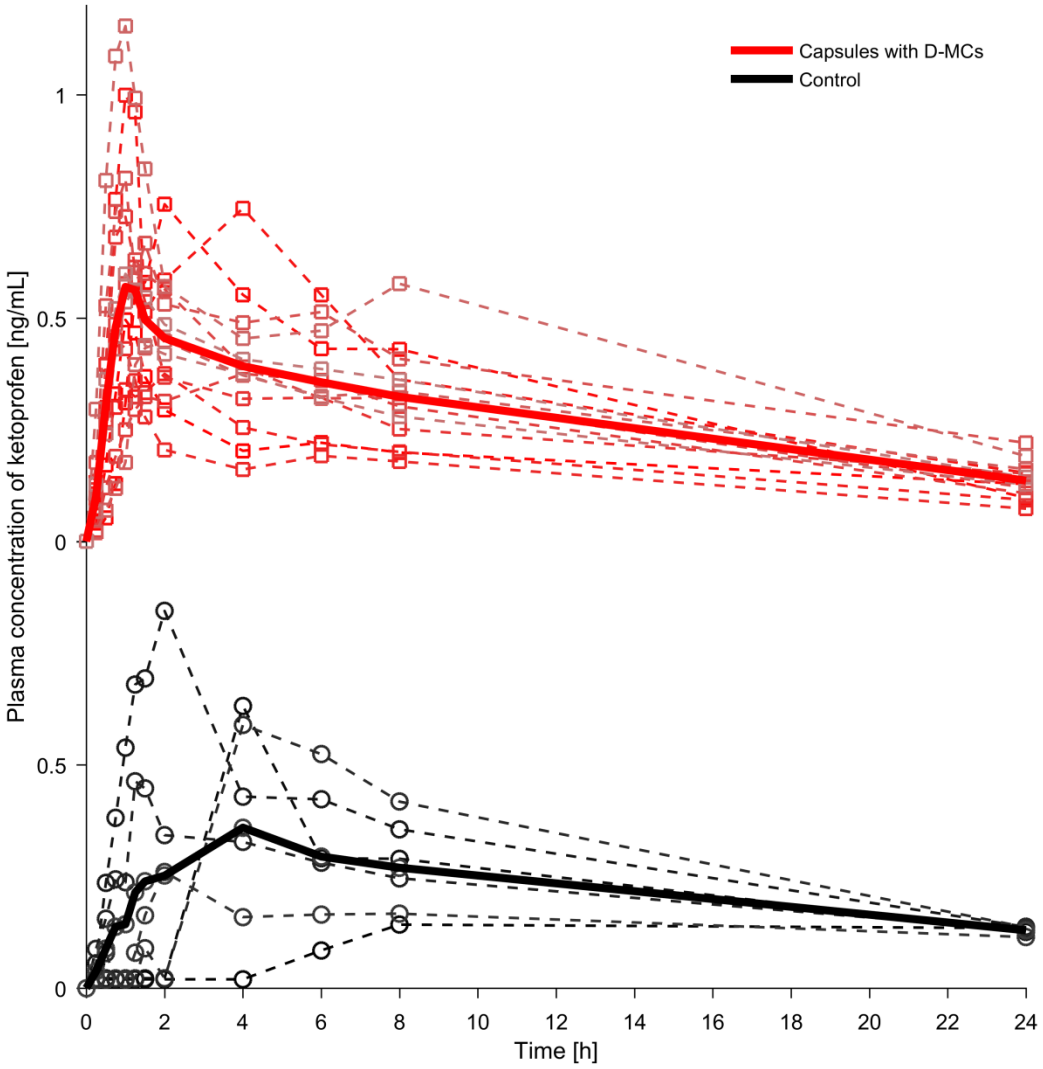

Figure S4: Individual profiles of the *in vivo* plasma concentration of ketoprofen over time. (Red line), capsules with loaded and coated D-MCs**. (Black line)**, control capsules filled with melted ketoprofen and PVP and coated.

Figure S5: Picture of a gelatin capsule filled with loaded and coated D-MCs. Empty D-MCs are positioned outside the capsule for comparison.

Paper II

Release of ketoprofen from microcontainers - influence of the loading method

F. Tentor*, C. Mazzoni*, L. Leonardi, P. Marizza, R. S. Petersen, S. S. Keller, A. Boisen

Manuscript submitted to *Biomedical Microdevice*

*joint first authorship

Release of ketoprofen from microcontainers - influence of the loading method

F. Tentor[#*], C. Mazzoni[#*], L. Leonardi, P. Marizza, R. S. Petersen, S. S. Keller, A. Boisen

The Danish National Research Foundation and Villum Foundation's Center for Intelligent Drug Delivery and Sensing Using Microcontainers and Nanomechanics (IDUN) - Department of Micro- and Nanotechnology, Technical University of Denmark, Kgs. Lyngby, Denmark

[*]Correspondence: fabt@nanotech.dtu.dk, chimaz@nanotech.dtu.dk

[#]these authors contributed equally to the manuscript

Abstract

The oral drug delivery route is the most preferred by patients and has the highest compliance. In the last decade, reservoir based microdevices have been proposed as oral drug delivery systems to overcome the limitations of traditional formulation. Microcontainers are microsized cylindrical reservoirs that can be loaded with a formulation and sealed with a degradable membrane. In this work, we compared two loading techniques for microcontainers: i) hot punching of a poly (ε-caprolactone) (PCL) film coupled with the loading of ketoprofen using supercritical carbon dioxide ($scCO_2$) and ii) hot punching of PCL + ketoprofen film. The drug loading steps were characterized by means of profilometry, scanning electron microscopy and X-ray microtomography. A pronounced difference between the two loading techniques was observed. The hot punching of a PCL + ketoprofen film resulted in a zero-order release kinetic; a burst release was instead obtained from the $scCO_2$ impregnated microcontainers. Finally, X-ray powder diffraction and Raman spectroscopy showed no differences in the solid state of ketoprofen, being amorphous for both loading techniques.

1 Introduction

In the last decades, microfabricated devices (Nielsen et al., 2018) have emerged in the field of oral drug delivery, spurred by the advancements in micro and nanofabrication technologies. These microfabricated devices have been shown to improve traditional formulations. As an example, Chirra et al. have shown that PMMA planar micropatches with three reservoirs improve acyclovir bioavailability by 4.5 fold compared to an acyclovir solution (Chirra et al., 2014). Other microdevices include microcontainers: cylindrical reservoirs with a nanoliter volume cavity that can be loaded with a drug formulation and sealed with a degradable membrane to allow tailoring of the drug release. The main features that these devices provide are: i) protection of the drug from the gastric environment, ii) unidirectional and iii) controlled release. These combined properties aim at reducing drug loss in the intestinal lumen which is a serious issue for many oral dosage forms. Previously, we have shown that microcontainers loaded with ketoprofen and protected with an enteric coating increase the relative oral bioavalability compared to traditional capsules by 180% (Mazzoni et al., 2017). This drug delivery system (DDS) was found to stabilize indomenthacin drug in its amorphous form as a result of the confinement within microcontainers (Nielsen et al., 2012).

One of the main concerns in the field of microfabricated DDS is the loading of the active pharmaceutical ingredient (API) into the reservoirs. Simple diffusion of drug in pre-loaded polymer matrices has been exploited for some microdevices (Fox et al., 2016). However, this technique is not suitable for all devices. Inkjet printing has been investigated as another possible loading techniques (Fox et al., 2017; Marizza et al., 2013; Mchugh et al., 2017). Unfortunately, this method is slow and its use is limited by the viscosity of the printing solutions. A faster technique to load microcontainers with APIs and polymers is powder embossing with a shadow mask, limiting drug deposition to the actual reservoir (Abid et al., 2017) and improving the manual method used previously (Nielsen et al., 2015). Similar to powder embossing, hot punching (Petersen et al., 2017) has been successfully used to load microcontainers with drug. In this case, microcontainers are used as a stamp for the punching of a polymer/drug film pre-deposited on a carrier substrate. This results in the direct transfer of the punched material into the container reservoirs. This process is only suitable for non-thermolabile APIs in combination with a thermoplastic polymer. The absence of a shadow mask and an aligning step make this process upscalable and flexible to every shape and size. The same advantages are achieved by supercritical impregnation with carbon dioxide ($scCO_2$). This technique was used to load a poorly water soluble drug in microcontainers (Marizza et al., 2016; Mazzoni et al., 2017) in an effective and reproducible manner. Nevertheless, $scCO_2$ impregnation only works with APIs that are soluble in CO_2 and with polymers that can swell but not be solubilized in CO_2. In accordance with the strength and weaknesses of each technique, the choice of the loading method highly depends on the API. More than 90% of APIs that are under development for clinical practice belong to either class II or IV in the standard of Biopharmaceutical Classification System (BCS) (Taylor and Zhang, 2016). These two classes are constituted of APIs with poor water solubility. For oral drug delivery this is a serious issue to solve as it causes a reduction in the bioavailability (Dengale et al., 2016; Hörter and Dressman, 2001). There are several options for enhancing the solubility of APIs, two very common methods are: i) including a solubility enhancer (Awasthi et al., 2018) and ii) bringing the API to its amorphous, more soluble state (Grohganz et al., 2014). Finally, the API release kinetic for the DDS under development has also to be considered. Depending on the application, a sustained or zero order release might be preferred to a burst release, or vice-versa (Huang and Brazel, 2001; Tahara et al., 1995). We have previously demonstrated that the combination of ketoprofen with polyvinylpyrollidone (PVP) in microcontainers has led to a burst release, with 87% of the total ketoprofen content being released within the first 30 min (Marizza et al., 2014). The fast release obtained in this case is expected, because i) PVP acts as a solubility enhancer, ii) ketoprofen is in its amorphous state and iii) the polymer swelling during $scCO_2$ impregnation leads to an increase in the polymer matrix porosity.

In this work, we investigated the release of poorly soluble drugs from microcontainers loaded with two different methods. For this study, ketoprofen was chosen as a class II model drug and poly (ε-caprolactone) (PCL) as a slow biodegradable polymer matrix.

The two related techniques were respectively: 1) hot punching of a PCL film into the microcontainers followed by loading of ketoprofen by $scCO_2$ impregnation and 2) loading of a ketoprofen+PCL film into the microcontainers by hot punching. For the loading of ketoprofen in PCL filled microcontainers by $scCO_2$ impregnation two sets of parameters were tested, 2 h at 100 bar and 4 h at 200 bar respectively at a temperature of 40 °C. Throughout this manuscript, we will refer to the samples obtained with the two techniques as: $HPCO_2$-100 and $HPCO_2$-200 for 1) and HP for 2). The differences between $HPCO_2$-100, $HPCO_2$-200 and HP were evaluated in terms of i) solid state of ketoprofen inside the microcontainers, ii) loaded amount of ketoprofen and iii) ketoprofen *in vitro* release kinetics.

2 Materials and Methods

2.1 Materials

Si wafers (4-in. b100N n-type) were supplied by Okmetic (Vantaa, Finland). SU-8 2075 and SU-8 developer were purchased from Microresist Technology GmbH (Berlin, Germany).
Ketoprofen (98%, racemate), poly (ε-caprolactone) (PCL, Mw 80000), poly-di-methylsiloxane (PDMS Sylgard® Sie 184, Dow Corning Corporation, U.S.), dichloromethane (DCM, anhydrous, ≥99.8%) and ethanol (99.9% purity) were purchased from Sigma Aldrich (St. Louise, U.S.).

2.2 Fabrication of SU-8 microcontainers

The microcontainers were fabricated with epoxy-based photoresist SU-8 on Si wafers using a procedure described previously (Marizza et al., 2013). Wafers were diced into square chips (12.8 x 12.8 mm^2), each one containing 625 microcontainers. Each microcontainer has a cavity of about 70 μm in depth and 220 μm in diameter.

2.3 Preparation of polymer films and transfer into microcontainers

The microcontainers were filled with PCL by means of the hot punching technique (Petersen et al., 2015). In Fig. 1, a scheme with the fabrication steps is depicted. At first, a film of PDMS was prepared by spin coating (WS-650, Laurell Technologies Corporation, US): 6 mL of PDMS was prepared mixing the elastomer and the curing agent in a 10:1 weight-to-weight ratio and was thereafter poured on a 4-inch Si wafer fixed to a rotating chuck. The centrifugal forces, induced by the spinning (750 rpm, 60 s), spread the polymer solution on the whole wafer surface. The film was left to crosslink for 12 hours at room temperature (RT). The PDMS layer served as an elastic substrate for the subsequent steps. PCL pellets were then dissolved in DCM (15 %wt.) and the solution was spin coated at different spin rates (500, 1000, 1250 and 1500 rpm) on the PDMS layer. The acceleration and the spinning time were kept constant at 750 rpm/s and 45 sec, respectively. The films were left to dry overnight at RT. The PCL film was then loaded into the microcontainers (used as a mold) using the hot punching technique (Fig. 1a I-II). The embossing procedure was performed with a

bonding press (P/O/Weber, Germany) with plates heated to 65 °C and by applying a pressure of 7.1 MPa for 20 min. The SU-8 microcontainers chip was pressed into the PCL film, which was penetrated by the microcontainers walls until those reached the underlying PDMS layer. After cooling down to 35 °C, the punched PCL film in between the containers was peeled off, resulting in a complete filling of the microcontainers cavities.

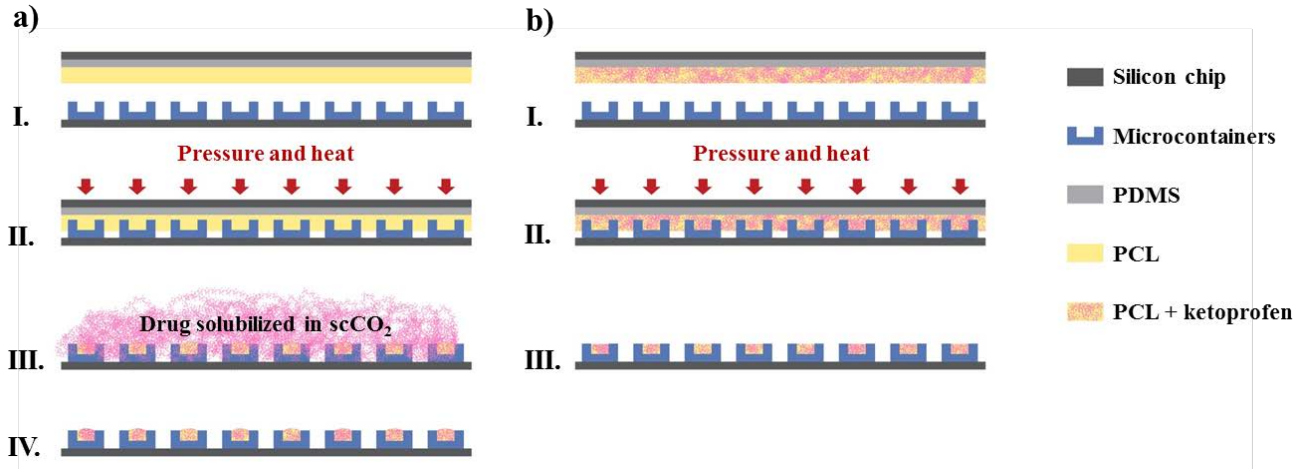

Figure 1. Schematic representation of the loading processes. a) I. Fabrication of microcontainers and preparation of PCL/PDMS films; II. transfer of the polymer film into the microcontainers by hot punching; III. $scCO_2$ impregnation of the polymer-filled microcontainers with ketoprofen; IV. drug loaded microcontainers ($HPCO_2$). b) I. Fabrication of microcontainers and preparation of ketoprofen+PCL/PDMS films; II. transfer of ketoprofen+PCL film into the microcontainers by hot punching; III. Drug loaded microcontainers (HP).

2.4 Supercritical impregnation of PCL filled-microcontainers

The loading of ketoprofen into the PCL-filled microcontainers was performed by means of $scCO_2$ impregnation (Fig. 1a III-IV). In a high-pressure chamber, defined weights of ketoprofen were dissolved in $scCO_2$ at saturation for the specific pressure and temperature used (Macnaughton et al., 1996), as summarized in Table 1. The duration of the experiments was defined by similar results on $scCO_2$ impregnation of PCL (Ivanovic et al., 2016). The microcontainers chip was attached on a metal grid and placed into the chamber, which was then sealed and heated to the desired temperature. Liquid carbon dioxide was then pumped into the chamber at isothermal conditions. During pressurization, ketoprofen was solubilized in the $scCO_2$. When the desired pressure was reached, the $scCO_2$ was put under magnetic stirring (500 rpm). At the end of the experiment, the chamber was depressurized at a controlled rate by a syringe valve and the outlet stream was bubbled through an ethanol solution (99.5%).

Table 1: Parameters of the impregnation process.

Sample	Pressure [bar]	Temperature [°C]	Time [h]	Ketoprofen [mg]
$HPCO_2$-100	100	40	2	4.86 ± 0.02
$HPCO_2$-200	200	40	4	14.16 ± 0.02

2.5 Loading of a ketoprofen+PCL film into microcontainers

In a second approach, microcontainers were directly loaded with ketoprofen+PCL drug polymer matrix without the use of $scCO_2$ impregnation (HP, Fig. 1b). Defined amounts of ketoprofen and PCL were dissolved in DCM and spin coated on a PDMS/Si substrate at the same conditions as described in section 2.3. The drug polymer ratio in the matrix was adjusted to be identical to the one in the microcontainers that were loaded with pure PCL by hot punching and subsequently impregnated with $scCO_2$ ($HPCO_2$). Finally, the ketoprofen+PCL films were transferred into microcontainers by hot punching, following the procedure described in section 2.3.

2.6 Characterization methods

2.6.1 Profilometry

To evaluate the thickness of the polymer layer deposited by spin coating on the PDMS/Si wafer, the films were scratched with a scalpel in three different symmetrical positions with respect to the wafer center and a contact profilometer (Alpha-Step IQ Stylus Profilometer, KLA Tencor) was used. The measurements were performed using a 15.6 mg tip force with a scan speed of 20 µm/sec and a sampling rate of 50 Hz.

2.6.2 X-ray micro computed tomography (XµCT)

XµCT measurements were performed to evaluate the filling of microcontainers after hot punching. A Nanotom S (GE) equipped with a source voltage of 70 kV, a current of 140 µA and a 0.5 mm thick Cu filter to attenuate the high radiation energy was deployed. The sample was measured with a focus object distance (FOD) of 39.9995 mm and a focus detector distance (FDD) of 399.9995 mm. A total of 1400 images were acquired over 360° of rotation each one obtained from the average of 3 separate images. The resulting data acquisition time corresponds to 140 minutes for each sample. The reconstruction of the cross-section images was made using the proprietary software (Phoenix Datos Ix2 acquisition ver. 2.3.2-RTM). Images having an isotropic voxel size of 4.99994 µm were reconstructed using a Feldkamp algorithm for cone beam geometry using the DataViewer MyVGL 3.0.2.

2.6.3 Scanning electron microscopy (SEM)

SEM imaging was used to observe the microcontainers before and after the filling by hot punching and loading of ketoprofen by means of $scCO_2$ impregnation. Moreover, SEM pictures were taken after the *in-*

vitro dissolution studies. The images were obtained using a Zeiss Supra 40VP Field Emission Scanning Electron Microscope (Carl Zeiss Microscopy GmbH, Jena, Germany) in high vacuum mode at 8 keV operating high voltage. The samples were mounted on a metal support and tilted by 30°.

2.6.4 Raman spectroscopy

Raman spectroscopy was performed to evaluate the solid state of ketoprofen loaded with the two different techniques. The spectra were collected using a DXR Raman microscope (Thermo Scientific, Germany) equipped with a 10x objective with a frequency-stabilized single mode diode laser (10 mW, 780 nm) an exposure time of 2 sec and 5 repeated scans.

2.6.5 X-ray powder diffraction (XRPD)

XRPD was performed to corroborate the results obtained with Raman spectroscopy. The analyses were carried out with the X'Pert PRO X-ray diffractometer (PANalytical, Almelo, The Netherlands, MPD PW3040/60 XRD; Cu KR Anode; λ=1.541 Å; 45 kV; 40 mA). All the samples were analysed applying a starting angle of 5° and an end angle of 30°. Data were collected using the X'Pert Data Collector software (PANalytical B.V.).

2.7 *In vitro* drug dissolution tests

The *in vitro* drug dissolution tests were done to elucidate the differences between the loading methods in terms of drug release kinetics. The dissolution of ketoprofen was tested on individual microcontainer chips. Briefly, the chips were glued with carbon pads on Teflon-coated magnetic stirrers and placed into vials filled with 10 mL of milliQ water. The vials were then immersed in a thermostatic bath at 37 °C and put under stirring (100 rpm). At defined times, 50 μL were collected from each vessel and analysed by means of UV-VIS at 259 nm (Nanodrop 2000C, Thermo Scientific, UK). After dissolution, the microcontainers were observed with an optical microscope and SEM (data not shown). The amount of drug loaded by means of $scCO_2$ was estimated by the final concentration value obtained after 24 h of dissolution.

2.8 Statistics

All data is represented as mean and standard deviation. When appropriate a student T test (GraphPad Prism, version 6.05) was used to carry out statistical analyses. P-values below 5% ($p < 0.05$) were considered statistically significant.

3. Results and discussion

3.1 Polymer morphology after hot punching and drug loading

The thickness of PCL films obtained by spin coating on PDMS-coated Si wafers was measured by contact profilometry. In Fig. 2, the thicknesses of the films made with different spin rates are reported.

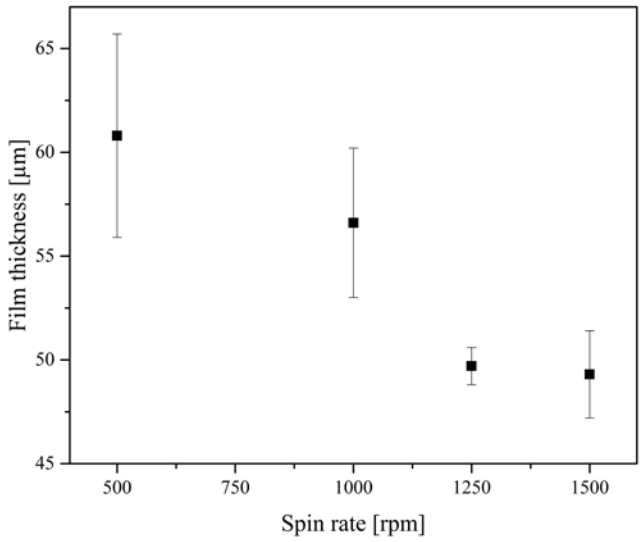

Figure 2: Thicknesses of the PCL films as a function of the spinning rate.

All films prepared showed a thickness lower than that of the microcontainers cavity depth (70 µm) and, therefore, they were found suitable for hot punching. Since the films obtained at 1250 rpm showed the best reproducibility, they were used for the subsequent hot punching. During the punching process, heat was applied on both plates of the press on which the microcontainers chip and the PCL-PDMS or the Ketoprofen+PCL-PDMS films were positioned. The applied temperature of 65 °C is slightly above the melting point of PCL allowing the polymer to reflow and facilitating the penetration of the microcontainers chip through the film. Upon release of the pressure, the punched PCL film was released from the PDMS and confined inside of the SU-8 reservoirs. This transfer occurs due to the higher work of adhesion between PCL and the SU-8 container mold compared to the work of adhesion between PCL and the hydrophobic PDMS layer on the Si carrier substrate.

In Fig. 3, SEM images of microcontainers before and after hot punching are shown. As it can be observed, PCL is homogeneously filled in large arrays of microcontainers with no polymer residues lying in between them.

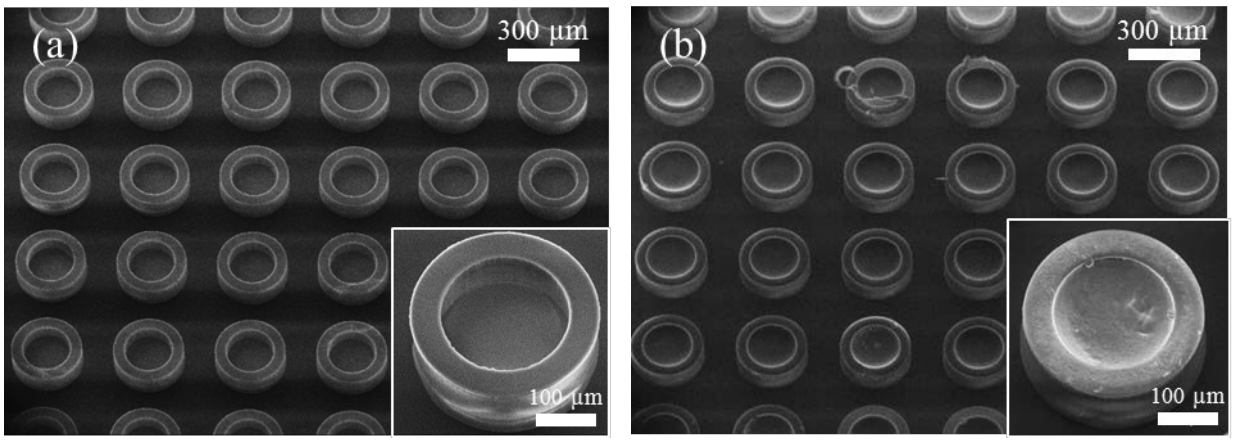

Figure 3. SEM images of SU-8 microcontainers before (a) and after (b) hot punching with PCL.

To visualize the level of polymer filling, microcontainers were scanned by XμCT at different angles (Fig. 4). The contrast of the resulting images was adjusted to distinguish the transferred PCL film from the surrounding SU-8 and the background. As it can be seen in the cross section in Fig. 4, an empty microcontainer was discernible from the ones filled with polymer. The measured thickness of the hot-punched PCL inside the microcontainers was 48 ± 2 μm. This thickness was identical to the one of the spin coated films measured by profilometry and slightly lower than the container cavity depth. Consequently, the film was not deformed during hot punching which supports the hypothesis that the walls of the microcontainers were able to cut through the PCL film.

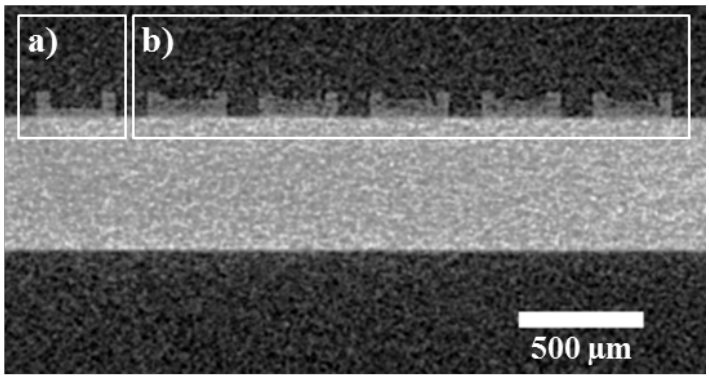

Figure 4. X-ray tomography image of a microcontainer chip after polymer deposition in a cross-sectional view a) empty microcontainer and b) array of microcontainers filled with PCL.

After the hot punching, the PCL-filled microcontainers were loaded with ketoprofen by $scCO_2$ impregnation at 40 ºC. Fig. 5 represents the SEM images of the microcontainers after impregnation performed at 100 bar for 2 hours ($HPCO_2$-100) and 200 bar for 4 hours ($HPCO_2$-200). The two different conditions were chosen to understand their effect on ketoprofen loading, dissolution rate and swelling of the polymer. The comparison of Fig. 3b and Fig. 5 suggests that the polymer underwent substantial morphological changes in the micron scale upon exposure to the compressed fluid. The impregnation at 200 bar caused a more pronounced swelling of the polymer than at 100 bar. Such deformation of PCL was expected as higher pressure causes an increase in the pore dimensions (Moghadam et al., 2017).

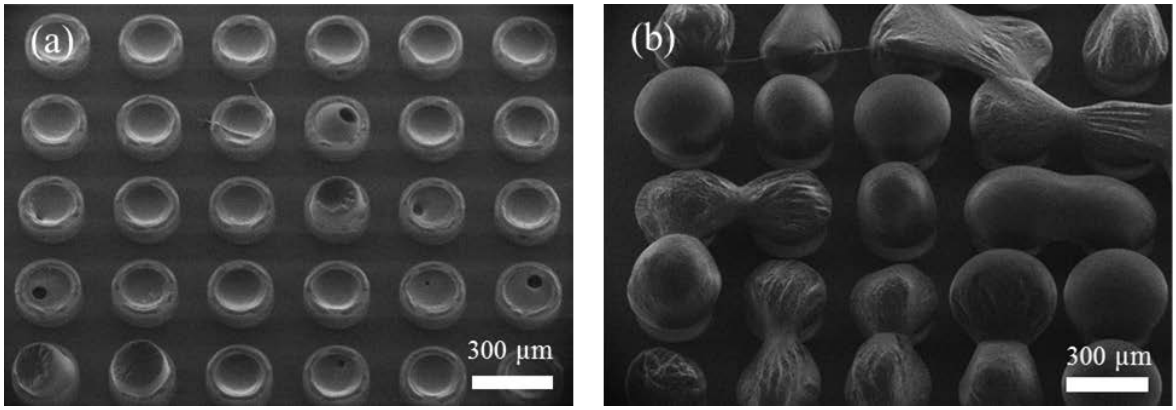

Figure 5. SEM images of PCL filled-microdevices after the supercritical impregnation with ketoprofen at (a) $HPCO_2$-100 (100 bar, 40°C, 2 h) and (b) $HPCO_2$-200 (200 bar, 40°C, 4 h).

3.2 *In vitro* dissolution experiments

The dissolution experiments were carried out on $HPCO_2$-100, $HPCO_2$-200 and HP samples to evaluate the drug release kinetics. Initially, the amount of ketoprofen loaded was assessed for the two $HPCO_2$ samples (Table 2). Indeed, as reported in Table 2, there is no significant difference in the amount of ketoprofen loaded ($p > 0.05$) despite the different pressure and time used for $scCO_2$ impregnation. It is important to notice that at the same $scCO_2$ parameters, the loading of ketoprofen in PCL was lower than what was found for PVP (Marizza et al., 2014), being equal to 0.13 ± 0.07 mg for the former and to 0.58 ± 0.01 mg for the latter. This fact might be explained by a different affinity between ketoprofen and the two polymers. This is in accordance with the results reported by Moghadam et al., where a higher molecular weight leads to lower porosity of the matrix and, consequently, a lower impregnability (Moghadam et al., 2017). As it can be seen in Fig. 6, the $HPCO_2$ samples displayed similar ketoprofen dissolution profiles despite the different swelling of PCL (Fig. 5). The SEM images, combined with the dissolution studies, show that CO_2 was able to permeate the PCL film hot-punched into the microcontainers even at moderate conditions of temperature and pressure (40 °C, 100 bar) and that the drug had been loaded into the polymer matrix. HP samples were prepared with the same ketoprofen/PCL weight ratio (1:10) as the one measured for $HPCO_2$ samples. The release of ketoprofen from HP was significantly slower compared to $HPCO_2$-100 and $HPCO_2$-200 (Fig. 6). During the first 3 h, drug release from HP followed zero-order release kinetics whereas the impregnated samples displayed a burst release. Indeed, after 3 h, only 44.9 ± 9.0 % of the total amount of ketoprofen was released compared to 80.7 ± 9.8 % and 91.8 ± 7.5 % from $HPCO_2$-100 and $HPCO_2$-200 samples, respectively ($p < 0.01$) (Fig. 6, inset). This variation could be attributed to the difference in porosity between $HPCO_2$ and HP due to the $scCO_2$ step in which PCL swells. A similar release profile was seen by T. Potrč et al. for a PCL film loaded with ibuprofen by $scCO_2$ impregnation (Potrč et al., 2015). Another explanation could be differences in distribution of ketoprofen in the PCL matrix. It is plausible that ketoprofen is mostly present in the top layer of the PCL matrix when loaded by $scCO_2$ impregnation. Conversely, the drug distribution in the

ketoprofen+PCL films, that were transferred by hot punching, might be more homogenous, with ketoprofen present in the PCL matrix throughout the complete microcontainers depth.

Table 2: Drug loading of PCL filled microcontainers by means of $scCO_2$ impregnation. Data represented as mean ± SD (N = 3).

Sample	Parameters	Loaded ketoprofen per chip [mg]
$HPCO_2$-100	100 bar 40 °C 2 h	0.1 ± 0.01
$HPCO_2$-200	200 bar 40 °C 4 h	0.13 ± 0.07
HP	-	0.08 ± 0.03

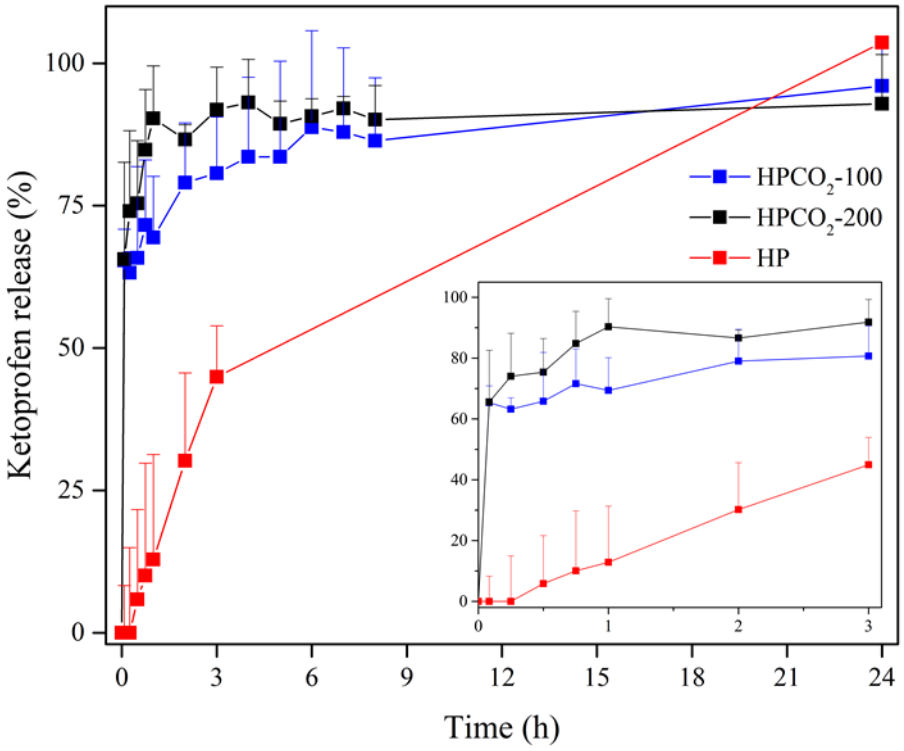

Figure 6: *In vitro* dissolution studies of ketoprofen from $HPCO_2$-100 (blue), $HPCO_2$-200 (black) and HP (red). The inset represents a zoom of the dissolution plots in the first 3 hours.

3.3 Physical state of ketoprofen

APIs included in class II (BCS) are poorly water soluble and highly permeable, this typically entails low oral bioavailability (Dengale et al., 2016). Ketoprofen falls into this class of pharmaceuticals and therefore improving its solubility is crucial. It has been demonstrated that the amorphous state of ketoprofen has a higher solubility and, consequently, a higher oral bioavailability than the crystalline state (Chan et al., 2015). Raman spectroscopy and XRPD analyses were jointly used to evaluate the solid state of ketoprofen in both

HP and $HPCO_2$-200. Fig. 7 depicts the Raman scattering spectra of ketoprofen powder, PCL film, HP and $HPCO_2$-200. All samples with ketoprofen showed two characteristic peaks marked by the dotted lines. The vibrational mode at 1655 cm^{-1} is related to the inter-ring carbonyl [C=O] stretching mode. The peak at 1599 cm^{-1} represents the [C-C] stretching mode of ketoprofen. The [C=O] vibrational mode exhibited a lower intensity and a higher amplitude in all the spectra of the film specimens compared to the pure crystalline drug. As previously observed in the case of ketoprofen impregnated into matrices of poly(vinyl pyrrolidone) (PVP) (Marizza et al., 2016), the Raman intensity of the ketoprofen [C=O] stretching mode exhibited a lower intensity than the [C–C] stretching mode at 1602 cm^{-1}. Moreover, the Full Width at Half Maximum (FWHM) of the [C=O] stretching mode for the drug loaded in microcontainers was larger compared to the crystalline ketoprofen. Such recorded changes might be associated with a rearrangement of ketoprofen into a less organized amorphous state. In the vibrational patterns of both hot punched and impregnated microcontainers no detectable frequency shift of the [C=O] mode was found, suggesting that no formation of hydrogen bonds occurred. The presence of amorphous ketoprofen was confirmed by XRPD spectra (Fig. 8). Both the HP and $HPCO_2$-200 did not show the characteristic peaks of crystalline ketoprofen (Marizza et al., 2014). Conversely, the distinctive patterns of the crystalline PCL (2θ = 22°, 22.5°, 24°) (Kister et al., 2000) could be observed.

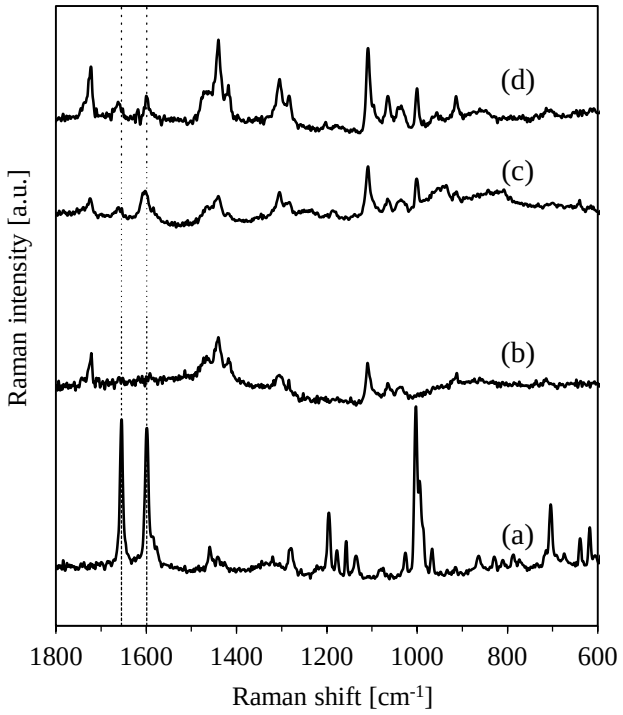

Figure 7. Raman spectra of (a) crystalline ketoprofen; (b) PCL film; (c) HP and (d) $HPCO_2$-200.

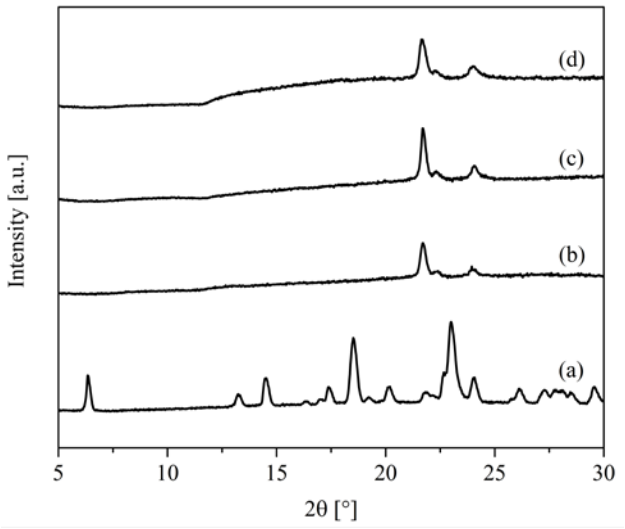

Figure 8. X-ray powder diffraction patterns of (a) crystalline ketoprofen powder; (b) PCL film; (c) HP and (d) $HPCO_2$-200.

4 Conclusions

The use of microfabricated devices for oral drug delivery is becoming more and more popular. Within this field, the development of new drug loading techniques to control the release of active pharmaceutical ingredients is crucial.

In this study two loading techniques were compared: i) hot punching of a PCL film followed by supercritical carbon dioxide impregnation with ketoprofen and ii) hot punching of a ketoprofen+PCL drug polymer film. X-ray powder diffraction and Raman spectroscopy showed that both with $scCO_2$ treatment and only hot punching, the drug was in its amorphous state after loading. Despite a remarkable difference in the polymer morphology between the two $scCO_2$ impregnation setups used, the change of process parameters did not result in any significant differences in terms of ketoprofen loading and release. Conversely, for the ketoprofen+PCL film a slower release profile was exhibited compared to the $scCO_2$ impregnated samples.

Overall, the technique comprising the hot punching of PCL, followed by the loading of drug by $scCO_2$ might be advantageous for APIs where a burst release is needed. On the other hand, the hot punching of a drug+PCL film might be suitable for APIs that require a more sustained or zero-order release.

Acknowledgements

The Danish National Research Foundation (DNRF 122) and the Villum Foundation (grant no. 9301) are greatly acknowledged for funding. From the Technical University of Denmark, the authors would like to thank Zarmeena Abid for her contribution to the project and Nanna Bild for the drawings.

Bibliography

Abid, Z., Gundlach, C., Durucan, O., von Halling Laier, C., Nielsen, L.H., Boisen, A., Keller, S.S., 2017. Powder embossing method for selective loading of polymeric microcontainers with drug formulation. Microelectron. Eng. 171, 20–24. https://doi.org/10.1016/j.mee.2017.01.018

Awasthi, R., Manchanda, S., Das, P., Velu, V., Malipeddi, H., Pabreja, K., Pinto, T.D.J.A., Gupta, G., Dua, K., 2018. Poly(vinylpyrrolidone). Eng. Biomater. Drug Deliv. Syst. 255–272. https://doi.org/10.1016/B978-0-08-101750-0.00009-X

Chan, S.Y., Chung, Y.Y., Cheah, X.Z., Tan, E.Y.L., Quah, J., 2015. The characterization and dissolution performances of spray dried solid dispersion of ketoprofen in hydrophilic carriers. Asian J. Pharm. Sci. 10, 372–385. https://doi.org/10.1016/j.ajps.2015.04.003

Chirra, H.D., Shao, L., Ciaccio, N., Fox, C.B., Wade, J.M., Ma, A., Desai, T.A., 2014. Planar Microdevices for Enhanced In Vivo Retention and Oral Bioavailability of Poorly Permeable Drugs. Adv. Healthc. Mater. 3, 1648–1654. https://doi.org/10.1002/adhm.201300676

Dengale, S.J., Grohganz, H., Rades, T., Löbmann, K., 2016. Recent advances in co-amorphous drug formulations. Adv. Drug Deliv. Rev. 100, 116–125. https://doi.org/10.1016/J.ADDR.2015.12.009

Fox, C.B., Cao, Y., Nemeth, C.L., Chirra, H.D., Chevalier, R.W., Xu, A.M., Melosh, N.A., Desai, T.A., 2016. Fabrication of Sealed Nanostraw Microdevices for Oral Drug Delivery. ACS Nano acsnano.6b00809. https://doi.org/10.1021/acsnano.6b00809

Fox, C.B., Nemeth, C.L., Chevalier, R.W., Cantlon, J., Bogdanoff, D.B., Hsiao, J.C., Desai, T.A., 2017. Picoliter-volume inkjet printing into planar microdevice reservoirs for low-waste, high-capacity drug loading. Bioeng. Transl. Med. 2, 9–16. https://doi.org/10.1002/btm2.10053

Grohganz, H., Priemel, P.A., Löbmann, K., Nielsen, L.H., Laitinen, R., Mullertz, A., Van den Mooter, G., Rades, T., 2014. Refining stability and dissolution rate of amorphous drug formulations. Expert Opin. Drug Deliv. 11, 977–989. https://doi.org/10.1517/17425247.2014.911728

Hörter, D., Dressman, J.., 2001. Influence of physicochemical properties on dissolution of drugs in the gastrointestinal tract1PII of original article: S0169-409X(96)00487-5. The article was originally published in Advanced Drug Delivery Reviews 25 (1997) 3–14.1. Adv. Drug Deliv. Rev. 46, 75–87. https://doi.org/10.1016/S0169-409X(00)00130-7

Huang, X., Brazel, C.S., 2001. On the importance and mechanisms of burst release in matrix-controlled drug delivery systems. J. Control. Release 73, 121–136. https://doi.org/10.1016/S0168-3659(01)00248-6

Ivanovic, J., Knauer, S., Fanovich, A., Milovanovic, S., Stamenic, M., Jaeger, P., Zizovic, I., Eggers, R., 2016. Supercritical CO 2 sorption kinetics and thymol impregnation of PCL and PCL-HA. J. Supercrit. Fluids 107, 486–498. https://doi.org/10.1016/j.supflu.2015.07.001

Kister, G., Cassanas, G., Bergounhon, M., Hoarau, D., Vert, M., 2000. Structural characterization and hydrolytic degradation of solid copolymers of d,l-lactide-co-ε-caprolactone by Raman spectroscopy. Polymer (Guildf). 41, 925–932. https://doi.org/10.1016/S0032-3861(99)00223-2

Macnaughton, S.J., Kikic, I., Foster, N.R., Alessi, P., Cortesi, A., Colombo, I., 1996. Solubility of Anti-Inflammatory Drugs in Supercritical Carbon Dioxide. J. Chem. Eng. Data 41, 1083–1086. https://doi.org/10.1021/je960103q

Marizza, P., Keller, S.S., Boisen, A., 2013. Inkjet printing as a technique for filling of micro-wells with biocompatible polymers. Microelectron. Eng. 111, 391–395.

Marizza, P., Keller, S.S., Müllertz, A., Boisen, A., 2014. Polymer-filled microcontainers for oral delivery loaded using supercritical impregnation. J. Control. Release 173, 1–9.

https://doi.org/10.1016/j.jconrel.2013.09.022

Marizza, P., Pontoni, L., Rindzevicius, T., Alopaeus, J.F., Su, K., Zeitler, J.A., Keller, S.S., Kikic, I., Moneghini, M., De Zordi, N., Solinas, D., Cortesi, A., Boisen, A., 2016. Supercritical impregnation of polymer matrices spatially confined in microcontainers for oral drug delivery: Effect of temperature, pressure and time. J. Supercrit. Fluids 107, 145–152. https://doi.org/10.1016/j.supflu.2015.08.023

Mazzoni, C., Tentor, F., Strindberg, S.A., Nielsen, L.H., Keller, S.S., Alstrøm, T.S., Gundlach, C., Müllertz, A., Marizza, P., Boisen, A., 2017. From concept to in vivo testing: Microcontainers for oral drug delivery. J. Control. Release 268, 343–351. https://doi.org/10.1016/j.jconrel.2017.10.013

Mchugh, K.J., Nguyen, T.D., Yang, D., Behrens, A.M., Rose, S., Tochka, Z.L., Tzeng, S.Y., Norman, J.J., Tomasic, S., Taylor, M.A., Lu, J., Guarecuco, R., Langer, R., 2017. Fabrication of fillable microparticles and other complex 3D microstructures. Sci. 1142, 1138–1142. https://doi.org/10.1126/science.aaf7447

Moghadam, M.Z., Hassanajili, S., Esmaeilzadeh, F., Ayatollahi, M., Ahmadi, M., 2017. Formation of porous HPCL/LPCL/HA scaffolds with supercritical CO2 gas foaming method. J. Mech. Behav. Biomed. Mater. 69, 115–127. https://doi.org/10.1016/J.JMBBM.2016.12.014

Nielsen, L.H., Keller, S.S., Boisen, A., 2018. Microfabricated devices for oral drug delivery. Lab Chip 18. https://doi.org/10.1039/C8LC00408K

Nielsen, L.H., Keller, S.S., Gordon, K.C., Boisen, A., Rades, T., Müllertz, A., 2012. Spatial confinement can lead to increased stability of amorphous indomethacin. Eur. J. Pharm. Biopharm. 81, 418–425. https://doi.org/10.1016/J.EJPB.2012.03.017

Nielsen, L.H., Nagstrup, J., Gordon, S., Keller, S.S., Østergaard, J., Rades, T., Müllertz, A., Boisen, A., 2015. pH-triggered drug release from biodegradable microwells for oral drug delivery. Biomed. Microdevices 17, 55. https://doi.org/10.1007/s10544-015-9958-5

Petersen, R.S., Keller, S.S., Boisen, A., 2017. Loading of Drug-Polymer Matrices in Microreservoirs for Oral Drug Delivery. Macromol. Mater. Eng. 302, 1–6. https://doi.org/10.1002/mame.201600366

Petersen, R.S., Keller, S.S., Boisen, A., 2015. Hot punching of high-aspect-ratio 3D polymeric microstructures for drug delivery. Lab Chip 15, 2576–2579. https://doi.org/10.1039/C5LC00372E

Potrč, T., Baumgartner, S., Roškar, R., Planinšek, O., Lavrič, Z., Kristl, J., Kocbek, P., 2015. Electrospun polycaprolactone nanofibers as a potential oromucosal delivery system for poorly water-soluble drugs. Eur. J. Pharm. Sci. 75, 101–113. https://doi.org/10.1016/j.ejps.2015.04.004

Tahara, K., Yamamoto, K., Nishihata, T., 1995. Overall mechanism behind matrix sustained release (SR) tablets prepared with hydroxypropyl methylcellulose 2910. J. Control. Release 35, 59–66. https://doi.org/10.1016/0168-3659(95)00021-Y

Taylor, L.S., Zhang, G.G.Z., 2016. Physical chemistry of supersaturated solutions and implications for oral absorption. Adv. Drug Deliv. Rev. 101, 122–142. https://doi.org/10.1016/J.ADDR.2016.03.006

Paper III

Where is the drug? - Quantitative 3D distribution analyses of confined drug-loaded polymer matrices

Chiara Mazzoni, Fabio Tentor, Anastasia Antalaki, Rasmus Due Jacobsen, Jacob Mortensen, Roman Slipets, Oleksii Ilchenko, Stephan Sylvest Keller, Line Hagner Nielsen, Anja Boisen

Manuscript submitted to *Advanced Materials Technologies*

DOI: 10.1002/ ((please add manuscript number))
Article type: Full Paper

Where is the drug? - Quantitative 3D distribution analyses of confined drug-loaded polymer matrices

Chiara Mazzoni, Fabio Tentor, Anastasia Antalaki, Rasmus Due Jacobsen, Jacob Mortensen, Roman Slipets, Oleksii Ilchenko, Stephan Sylvest Keller, Line Hagner Nielsen, Anja Boisen**

C. Mazzoni, F. Tentor, A. Antalaki, R. D. Jacobsen, J. Mortensen, R. Slipets, Dr. O. Ilchenko, Ass. Prof. S. S. Keller, Dr. L. H. Nielsen, Prof. A. Boisen
The Danish National Research Foundation and Villum Foundation's Center for Intelligent Drug Delivery and Sensing Using Microcontainers and Nanomechanics (IDUN) - Department of Micro- and Nanotechnology, Technical University of Denmark, Kgs. Lyngby, 2800, Denmark
E-mail: chimaz@nanotech.dtu.dk and anja.boisen@nanotech.dtu.dk

Keywords: polymer matrix, drug distribution, poorly soluble drug, supercritical CO_2 impregnation, Raman spectroscopy

Abstract

To enhance oral bioavailability of poorly soluble drugs, microfabricated devices such as microcontainers can be used. Microcontainers are cylindrical microdevices with only the top side open which can be drug-loaded with supercritical CO_2 ($scCO_2$) impregnation. One main drawback of this technique is the unknown drug distribution in the polymer matrix. The loading of two poorly soluble drugs, naproxen and ketoprofen by $scCO_2$ impregnation into confined polymer matrices is investigated. Three different sizes of microcontainers with different surface areas accessible for impregnation are compared keeping the total surface area per chips constant. From *in vitro* studies, the amount of loaded drug into the different sizes is similar. A custom-made Raman microscope facilitates volumetric Raman maps of an entire microcontainer filled with polyvinylpyrrolidone (PVP) and $scCO_2$ impregnated with either naproxen or ketoprofen. In all microcontainer sizes, the drugs are only detected in the top layer of the polymer matrix. Using X-Ray Powder Diffraction and Raman spectroscopy, the solid state form of the drugs is evaluated showing that ketoprofen is amorphous in all

microcontainer sizes and naproxen is found not to be crystalline. In conclusion, volumetric Raman mapping is a powerful tool for imaging drug distribution in polymer matrices.

1. Introduction

Among the different administration routes of drugs, oral delivery is preferred by the patients since the formulation can be self-administered leading to high compliance.[1] Even though, this route has many advantages, it is often challenging to deliver drugs orally, for example due to the harsh conditions in the stomach and the poor permeability over the intestinal wall.[1] Many drugs are classified as poorly water soluble in the biopharmaceutics classification system (BCS, class II and IV).[2,3] For oral delivery of poorly soluble drugs, solubility and dissolution rate need to be improved to obtain an acceptable bioavailability. One approach for achieving this, is to convert the drug to its amorphous form.[4] Here, the long range order in the crystal lattice is lacking and the disordered structure results in improved solubility and dissolution rate.[4,5] The disadvantage of the amorphous form is its physical and chemical instability and due to that, it can convert back to its metastable or stable counterpart during storage and/or dissolution.[6] There are various techniques to improve the physical stability of the amorphous form e.g. co-amorphization of two drugs[7] or the most common way is the use of polymers as excipients.[8] Another approach for protecting the amorphous drugs is the use of microcontainers.[5,9] Microcontainers are cylindrical, polymeric microdevices with only the top side open. Previously, it has been highlighted that confinement of the amorphous poorly soluble drug indomethacin reduced the re-crystallization rate by 1.8 fold compared to unconfined bulk samples.[5] In particular, using microcontainers with reservoir diameters of 174 µm, 29.0 ± 2.6 % of the amorphous indomethacin crystallized over a period of 30 days compared to microcontainers with diameters of 223 µm where 38.3 ± 1.5 % crystallized. This indicates that microcontainers with smaller diameters enhance the stability of the amorphous drug loaded inside.[5] In addition to the stabilization properties, microcontainers have been

used for improving oral drug delivery by protecting the drug from the harsh gastric environment and providing a release in the small intestine.[10–12] Furthermore, it has been demonstrated that microcontainers adhere to the intestinal mucus layer leading to higher relative oral bioavailability in rats of model drugs such as ketoprofen and furosemide compared to controls.[13,14]

In spite of the advantages of utilizing microdevices for oral drug delivery, loading drugs into the small cavities can be challenging since all of the well-known techniques for preparing oral formulations, such as tableting, cannot be used. Supercritical CO_2 ($scCO_2$) impregnation is one of the techniques that can be used for loading drugs into polymer-filled microcontainers. The critical point of CO_2 is 31.1 °C and 73.8 bar and due to those mild conditions, this technique is suitable for drug loading. In addition, it can be used in combination with various polymers.[15,16] It has previously been demonstrated that the hydrophilic polymer polyvinylpyrrolidone (PVP) could be loaded into microcontainers as a polymer matrix and impregnated by $scCO_2$ with the drug ketoprofen.[17,18] It was found that ketoprofen was in its amorphous form after impregnation in the PVP matrix inside the microcontainers.[14] However, the influence of the size of the confined polymer volumes loaded by supercritical impregnation has never been investigated. One of the main challenges for systematic studies of drug loading with this technique has been the unknown three-dimensional (3D) drug distribution in the polymer matrix after CO_2 impregnation. Therefore, it has not been possible to understand the influence of the parameters on the release profiles and the drug-polymer interactions.[16,17,19]

In the literature, the distribution of impregnated or encapsulated material has been studied with various techniques. Polymeric membranes have been examined with energy dispersive X-ray analyses, obtaining a two-dimensional (2D) map,[19] and this technique has also been successfully used for 3D mapping of nanoparticles.[20] Dispersive X-ray Absorption Spectroscopy (μED-XAS) tomography has been utilized and was able to resolve both 2D and

3D spatial distribution of chemical species from different iron mineral standards.[21] Alternatively, Raman spectroscopy has been used to evaluate the distribution of a drug inside a 3D printed tablet.[22] Previously, a 2D map of a cross section of tablets using Raman spectroscopy has been obtained, understanding the distribution of three different components in an area of 4 x 4 mm.[23] Cross sectional mapping with Raman spectroscopy is a destructive method and in case of a confined polymer matrix (i.e. for microcontainers) this application is not possible. Furthermore, for investigations with Raman spectroscopy, the polymer and drug normally have a relatively low transparency under laser excitation. For reaching an acceptable Raman signal at the bottom of samples as deep as e.g. a microcontainer reservoir, a highly sensitive method for confocal Raman microscope has been developed.

The aim of this study was to investigate the loading of two BCS class II drugs, naproxen and ketoprofen using $scCO_2$ impregnation into confined polymer matrices of different sizes. For this purpose, three different sizes of microcontainers (small, medium and large) and thereby, different surface areas accessible for impregnation were compared. Furthermore, the quantity and solid state form of ketoprofen and naproxen loaded into the microcontainers was evaluated. Finally, the 3D distribution of the drugs in the 300 µm deep polymer matrices was analyzed by confocal Raman microscopy.

2. Results and discussion

2.1. Fabrication of microcontainers

Cylindrical microcontainers with three different sizes were successfully fabricated (**Table 1** and **Figure 1**). The reservoir depth of the microcontainers with the different sizes was kept constant at 225 µm. The number of microcontainers per chip was chosen to keep the total polymer volume and the total surface area exposed to the supercritical CO_2 similar for the different sizes (Table 1). Due to this, it was possible to compare the influence of the

microcontainer size on quantity and distribution of the poorly soluble model drugs loaded with supercritical CO_2 impregnation.

2.2. Loading of ketoprofen or naproxen into the microcontainers using supercritical CO_2 impregnation

Every chip was manually filled with approximately 0.9 mg of PVP powder (**Figure 2**a), the amount varied slightly for the different sizes (**Table 2**). Followed by the filling with PVP, one chip per size was then simultaneously loaded with ketoprofen or naproxen. A SEM image of the medium size microcontainers after $scCO_2$ impregnation with ketoprofen can be seen in Figure 2b. In a previous study, the amount of PVP filled per chip was higher.[14] This is due to the fact that, even if the medium size microcontainers chip has similar dimensions to that used in the reported study, the number of microcontainers is reduced from 625 to 256.

2.3. *In vitro* release of ketoprofen or naproxen from the microcontainers

The quantity of ketoprofen or naproxen loaded into the microcontainers with different sizes was evaluated in order to assess if there was an influence of the dimension of the surface exposed to $scCO_2$. The quantity of the loaded ketoprofen or naproxen in small, medium or large microcontainers was obtained from the release studies (Table 2 and **Figure 3**). The release profiles of the small, medium and large microcontainers loaded with ketoprofen showed similar release profiles without any significant differences (Figure 3a). The same behavior was observed in the case of naproxen (Figure 3b).

The total amount of ketoprofen loaded in the small size of microcontainers compared to the medium and to the large was not significantly different (p-value: 0.4049 and p-value: 0.3667, respectively). No significant difference was observed between the loaded quantity of ketoprofen in the medium and in the large microcontainers (p-value: 0.8098). The same similarities, as observed for ketoprofen, were found for the total amount of naproxen loaded. In fact, the naproxen in the small size was not statistically different compared to the amount of drug in the medium or the large microcontainers (p-value: 0.1071 and p-value: 0.2431,

respectively). Comparing the medium with the large size of microcontainers, the total amount of the loaded naproxen also did not result in statistically different drug loadings (p-value = 0.3286).

Since the solubility of the two drugs in the $scCO_2$ was set to be the same, the release experiments allowed for comparison of loading the two poorly water-soluble drugs into the microcontainers with three different sizes. Within the first 10 min, 90 % of ketoprofen or naproxen was released (Figure 3) from all sizes of microcontainers. No statistical difference in the loaded amount of ketoprofen or naproxen was discernible independent of the size of the microcontainers. Indeed, comparing the loaded amount of ketoprofen and naproxen in the small sizes, the p-value was equal to 0.4374. For the medium and large sizes, the p-values corresponded to 0.0642 and 0.1351, respectively.

Consequently, there was no difference in loading a BCS class II drug such as ketoprofen or naproxen in a polymer matrix (PVP) having smaller or larger surface exposed to the $scCO_2$. This suggests that the size of the microcontainer opening had no influence on the quantity of drug loaded into the microcontainers. Furthermore, both BCS class II drugs were released with similar kinetics from the different sizes of microcontainers demonstrating the versatility of the method.

2.4. Three-dimensional distribution of the drugs in microcontainers

It was possible to obtain 3D maps of polymer and drug-loaded microcontainers down to a depth of 270 µm (the entire height of the microcontainer) using our custom-made Raman microscopy technique. To avoid heating of the sample due to relatively high absorption of the laser, the temperature was kept constant at 8°C. To distinguish the various materials (PVP, ketoprofen/naproxen, SU-8 or Si) in the samples, a chemical decomposition was performed on the spectra (Figure 4). In Figure 4, the same microcontainer 3D map reconstruction is shown in three different perspectives; an overview, a cross section view and a top view.

For all sizes of microcontainers loaded with either ketoprofen or naproxen, the drug was mainly impregnated in the top layers of the polymer matrix confined within the microcontainers walls. The results obtained in the *in vitro* release studies showed that both drugs reached 90 % of release within 10 min. The fast release could be explained by the fact that the drugs were mostly on top of the polymer matrix and not deeply inside the microcontainer reservoir. It is important to notice that the drug was distributed with the same morphology as PVP. It can therefore be speculated that in a more porous polymer matrix, the drug could have penetrated deeper during the supercritical impregnation. In the top view of the microcontainers, it is possible to notice that both drugs were homogenously distributed in the PVP. Furthermore, ketoprofen and naproxen were absent on the edge of the SU-8 microcontainers meaning that both drugs were preferentially deposited in the PVP matrix and not on SU-8. This technique can be useful to analyze polymer matrices for drug delivery in tissue engineering since the drug depth in the polymer matrix affects the release kinetic of the drug.[24]

2.5. Solid state analyses of the drugs loaded into the microcontainers

It has previously been shown that loading ketoprofen in a PVP matrix led to its conversion into its amorphous form.[14,18] In **Figure 5**a, the diffractograms from XRPD of the small, medium and large size of microcontainers loaded with ketoprofen showed a halo, distinctive of an amorphous form. This indicated that the loaded ketoprofen was amorphous. In the case of naproxen loaded into the PVP matrix in the different sizes of microcontainer, the diffractograms also showed a halo for the small microcontainers (Figure 5b). For the medium and large microcontainers, the halo still appeared, but with a few peaks comparable to those of the crystalline diffractogram of naproxen. Probably, a low crystallization of the drug occurred in the medium and large microcontainers. In the literature, studies showed that when naproxen has been combined with excipients or other drugs, a stable amorphous form could be obtained[25,26] despite the high tendency of naproxen to recrystallize.[27] In particular, Liu et

al. showed that naproxen was amorphous even after 4 months when it was thermally treated and combined with PVP.[25] A connection between the microcontainers size and the stability of naproxen amorphous form may therefore exist. This confirms what has previously been shown: smaller sizes of microcontainers prolonged the stability of the amorphous form of indomethacin (BCS class II drug).[5]

The results obtained by means of XRPD were confirmed by Raman spectroscopy for both drugs (**Figure 6**). The spectra from the microcontainers loaded with ketoprofen resulted to be the same as the amorphous ketoprofen spectrum confirming that ketoprofen is amorphous when loaded in PVP matrices by $scCO_2$ impregnation (Figure 6a). Due to the instability of naproxen, it was not possible to obtain a Raman spectrum of its amorphous form therefore, the peak-shifts were analyzed (Figure 6b). In particular, the peaks at 1626, 1390 and 740 cm^{-1} in the crystalline naproxen spectrum are shifted to 1630-1632, 1387-1389 and 742 cm^{-1} in the spectra corresponding to microcontainers loaded with naproxen meaning that naproxen loaded in the microcontainers is not in its crystalline form. Previously, the same peak-shifts have been considered, together with other techniques, to show the amorphous state of naproxen when co-milled with cimetidine.[28]

3. Conclusion

In this study, the influence of the surface exposed to $scCO_2$ was evaluated when loading two poorly water soluble drugs in a PVP polymer matrix confined in microcontainers. The release studies showed that the amount of loaded naproxen or ketoprofen was the same, when keeping the total surface area constant, and the release profiles were similar having 90 % of the drug released within 10 min. For microcontainers of different sizes, the loaded amount of drug nicely correlated with the surface area of the PVP matrix exposed to supercritical CO_2 during impregnation. To evaluate the 3D distribution of the drug in the polymer matrix in the microcontainers, a custom-made Raman microscope allowed obtaining volumetric Raman maps of the complete microcontainer volume. In the small, medium and large microcontainers,

ketoprofen or naproxen were impregnated on top of the polymer matrix explaining the fast release obtained in the release studies. Moreover, the solid state form of the drugs was evaluated showing that ketoprofen was amorphous in all microcontainers sizes and naproxen, despite its instability, was found not to be crystalline.

4. Experimental Section

Materials: Silicon (Si) wafers (4-in, b100N n-type) were provided by Okmetic (Vantaa, Finland). SU-8 2075 and SU-8 developer were purchased from Microresist Technology GmbH (Berlin, Germany). Polyvinylpyrrolidone (PVP) (Molecular weight of 10,000 Da), ketoprofen powder (≥98 %, racemate) and phosphate buffer saline (PBS) were obtained from Sigma-Aldrich (St. Louis, MO, USA). Naproxen was purchased from Fagron (Newcastle upon Tyne, England). Deionized water (18.2 mΩ) was acquired from Merck KGaA (Darmstadt, Germany).

Fabrication of microcontainers: Squared chips of microcontainers with dimensions of 12.8 x 12.8 mm^2 were fabricated on Si wafers in the epoxy-based photoresist SU-8 using a similar procedure as described previously.[5] Three different sizes of microcontainers were produced having three different cavity diameters (small, medium and large) and the same cavity height. The number of microcontainers per chip for the three different sizes was chosen to keep the total polymer surface exposed to the $scCO_2$ per chip constant, and thereby also the total polymer volume constant. The dimensions of the microcontainers were measured using an Alpha-Step IQ Stylus Profilometer (KLA-Tencor Corporation, Milpitas, USA) and an optical microscope.

Loading of naproxen and ketoprofen into the microcontainers using supercritical CO_2 impregnation: The microcontainers on Si chips were manually filled with PVP blowing away the excess powder in between the microcontainers using an air gun in a similar setup as described previously.[14] One chip of each size (small, medium and large) was placed within a supercritical CO_2 chamber, together with 4.8 ± 0.1 mg (n=3) of ketoprofen powder or 6.0 ±

0.03 mg (n=3) of naproxen. The impregnation with ketoprofen was conducted by bringing CO_2 to its supercritical state at 120 bar and 45°C keeping it under stirring for 1 h. The impregnation with naproxen was performed bringing CO_2 to 100 bar and 40°C. These parameters were chosen to have a solubility in the supercritical CO_2 of 0.06 g/L for both drugs.[29,30] The pressurization and depressurization rate were 3.9 bar/min and 2.5 bar/min, respectively, for both drugs. The chips with microcontainers were weighed before and after filling with PVP to determine the amount of polymer loaded into the microcontainers. A tabletop Scanning Electron Microscope (SEM) TM3030Plus (Hitachi High-Technologies, Tokyo, Japan) was used to visualize the microcontainers after filling with PVP and after the impregnation process.

In vitro release of ketoprofen or naproxen from the microcontainers: For determining the release of ketoprofen or naproxen over time, a μ-Diss profiler (pION INC, Woburn, MA), equipped with in situ UV probes with a path length of 10 mm for ketoprofen and 5 mm for naproxen was used. The release studies were performed in PBS at pH 6.5 for 120 min. Standard curves of either ketoprofen or naproxen were obtained before each release experiment. In order to prepare the standard curves, aliquots of a stock solution of ketoprofen (5 mg/mL in ethanol) or naproxen (3 mg/mL in ethanol) were added to known volumes of PBS, and the absorbance was assessed in a range of 250-260 nm for ketoprofen and at a wavelength of 230 nm for naproxen.

For the release experiments, the chips with drug-loaded microcontainers were attached to cylindrical magnets and placed inside glass vials. 10 mL of PBS buffer were added to the vials immediately before starting the experiment. All the release studies were run at 37°C stirring the chips at 100 rpm. The experiments were performed in triplicates for each drug and for each size of microcontainers, the data are presented as mean (normalized by the quantity of PVP filled) ± SD.

Three-dimensional distribution of the drugs in microcontainers: Volumetric Raman microscopy was used to evaluate the distribution of ketoprofen or naproxen in the microcontainers with the three different sizes. The microscope collected Raman spectra in the range of 350-2400cm^{-1} with a spectral resolution of 2.5 cm^{-1} under the excitation of a 785 nm laser. The laser power was 35 mW, and the diffraction limited spot size was equal to 1.7 µm with the usage of a 100x/0.75 HD DIC Zeiss microscope objective. The chip of microcontainers was placed on the surface of a custom-made Peltier stage and kept at 8°C during the Raman measurements. With the usage of this custom-designed Raman microscope, it was possible to acquire a spectrum for each point of the sample. These Raman spectra were studied performing a non-negative least squares analysis to obtain quantitative chemical response, visualized as voxel based 3D images.[31,32]

Solid state analyses of the drugs loaded into microcontainers: X-Ray Powder Diffraction (XRPD) was used to determine the solid state form of ketoprofen or naproxen in the microcontainers. An X'Pert PRO X-ray diffractometer (PANalytical, Almelo, The Netherlands, MPD PW3040/60 XRD; Cu KR anode, λ = 1.541 Å, 45 kV, 40 mA) was utilized. A starting angle of 5° 2θ and an end angle of 28° 2θ were employed for the scans with a scan speed of 0.67335° 2θ /min and a step size of 0.0262606° 2θ. Data were collected using X'Pert Data Collector software (PANalytical B.V.). The diffractogram of naproxen or ketoprofen loaded in the microcontainers were compared to the pure crystalline drugs. In addition, Raman microscopy was used to investigate the solid state form of the drugs. The spectra measured from the naproxen or ketoprofen loaded into the microcontainers were collected as described in "Three-dimensional distribution of the drugs in microcontainers" section. For the spectra of crystalline and amorphous ketoprofen, naproxen and PVP the laser power was 35 mW and the exposure time was 2 s. The amorphous ketoprofen was prepared by melting the crystalline ketoprofen powder at 98°C on a heating plate followed by immediately measurements of the sample.

*Statistics:*All of the data are expressed as mean ± standard deviation (SD). Statistical analysis were carried out, where relevant, using Student t-tests (GraphPad Prism, La Jolla, CA, USA, version 7.04). P-values below 5 % ($p < 0.05$) were considered statistically significant.

Acknowledgements

The authors would like to acknowledge the Danish National Research Foundation (DNRF122) and Villum Fonden (Grant No. 9301) for Intelligent Drug Delivery and Sensing Using Microcontainers and Nanomechanics (IDUN). Nanna Bild, DTU Nanotech, is acknowledged for the drawings of the table of content.

Received: ((will be filled in by the editorial staff))
Revised: ((will be filled in by the editorial staff))
Published online: ((will be filled in by the editorial staff))

References

[1] M. W. Tibbitt, J. E. Dahlman, R. Langer, *J. Am. Chem. Soc.* **2016**, *138*, 704.

[2] G. L. Amidon, H. Lennernäs, V. P. Shah, J. R. Crison, *Pharm. Res.* **1995**, *12*, 413.

[3] M. Davis, G. Walker, *J. Control. Release* **2018**, *269*, 110.

[4] H. Grohganz, P. A. Priemel, K. Löbmann, L. H. Nielsen, R. Laitinen, A. Mullertz, G. Van den Mooter, T. Rades, *Expert Opin. Drug Deliv.* **2014**, *11*, 977.

[5] L. H. Nielsen, S. S. Keller, K. C. Gordon, A. Boisen, T. Rades, A. Müllertz, *Eur. J. Pharm. Biopharm.* **2012**, *81*, 418.

[6] X. Liu, L. Zhou, F. Zhang, *Mol. Pharm.* **2017**, *14*, 658.

[7] I. Petry, K. Löbmann, H. Grohganz, T. Rades, C. S. Leopold, *Int. J. Pharm.* **2018**, *544*, 172.

[8] J. M. Ting, W. W. Porter, J. M. Mecca, F. S. Bates, T. M. Reineke, *Bioconjug. Chem.* **2018**, *29*, 939.

[9] L. H. Nielsen, S. S. Keller, A. Boisen, A. Müllertz, T. Rades, *Drug Deliv. Transl. Res.* **2014**, *4*, 268.

[10] C. B. Fox, Y. Cao, C. L. Nemeth, H. D. Chirra, R. W. Chevalier, A. M. Xu, N. A. Melosh, T. A. Desai, *ACS Nano* **2016**, *10*, 5873.

[11] C. B. Fox, C. L. Nemeth, R. W. Chevalier, J. Cantlon, D. B. Bogdanoff, J. C. Hsiao, T. A. Desai, *Bioeng. Transl. Med.* **2017**, *2*, 9.

[12] L. H. Nielsen, J. Nagstrup, S. Gordon, S. S. Keller, J. Østergaard, T. Rades, A. Müllertz, A. Boisen, *Biomed. Microdevices* **2015**, *17*, 55.

[13] L. H. Nielsen, A. Melero, S. S. Keller, J. Jacobsen, T. Garrigues, T. Rades, A. Müllertz, A. Boisen, *Int. J. Pharm.* **2016**, *504*, 98.

[14] C. Mazzoni, F. Tentor, S. A. Strindberg, L. H. Nielsen, S. S. Keller, T. S. Alstrøm, C. Gundlach, A. Müllertz, P. Marizza, A. Boisen, *J. Control. Release* **2017**, *268*, 343.

[15] I. Kikic, F. Vecchione, *Curr. Opin. Solid State Mater. Sci.* **2003**, *7*, 399.

[16] M. Champeau, J.-M. Thomassin, T. Tassaing, C. Jérôme, *J. Control. Release* **2015**, *209*, 248.

[17] P. Marizza, L. Pontoni, T. Rindzevicius, J. F. Alopaeus, K. Su, J. A. Zeitler, S. S. Keller, I. Kikic, M. Moneghini, N. De Zordi, et al., *J. Supercrit. Fluids* **2016**, *107*, 145.

[18] P. Marizza, S. S. Keller, A. Müllertz, A. Boisen, *J. Control. Release* **2014**, *173*, 1.

[19] S. Cardea, M. Scognamiglio, E. Reverchon, *Mater. Sci. Eng. C* **2016**, *59*, 480.

[20] T. J. Slater, E. A. Lewis, S. J. Haigh, *J. Vis. Exp* **2016**, 52815.

[21] D. F. Sanchez, A. S. Simionovici, L. Lemelle, V. Cuartero, O. Mathon, S. Pascarelli, A. Bonnin, R. Shapiro, K. Konhauser, D. Grolimund, et al., *Sci. Rep.* **2017**, *7*, 16453.

[22] S. J. Trenfield, A. Goyanes, R. Telford, D. Wilsdon, M. Rowland, S. Gaisford, A. W. Basit, *Int. J. Pharm.* **2018**, *549*, 283.

[23] M. Cerea, A. Maroni, L. Palugan, M. Bellini, A. Foppoli, A. Melocchi, L. Zema, A. Gazzaniga, *J. Control. Release* **2018**, *287*, 247.

[24] V. V Gaikwad, A. B. Patil, M. V Gaikwad, *Int. J. Pharm. Sci. Nanotechnol.* **2008**, *1*, 113.

[25] X. Liu, L. Zhou, F. Zhang, *Mol. Pharm.* **2017**, *14*, 658.

[26] A. Beyer, H. Grohganz, K. Löbmann, T. Rades, C. S. Leopold, *Eur. J. Pharm. Biopharm.* **2016**, *109*, 140.

[27] J. Sibik, K. Löbmann, T. Rades, J. A. Zeitler, *Mol. Pharm.* **2015**, *12*, 3062.

[28] M. Allesø, N. Chieng, S. Rehder, J. Rantanen, T. Rades, J. Aaltonen, *J. Control. Release* **2009**, *136*, 45.

[29] S. S. T. Ting, S. J. Macnaughton, D. L. Tomasko, N. R. Foster, *Ind. Eng. Chem. Res.* **1993**, *32*, 1471.

[30] A. Garmroodi, J. Hassan, Y. Yamini, *J. Chem. Eng. Data* **2004**, *49*, 709.

[31] O. Ilchenko, Y. Pilgun, T. Makhnii, R. Slipets, A. Reynt, A. Kutsyk, D. Slobodianiuk, A. Koliada, D. Krasnenkov, V. Kukharskyy, *Vib. Spectrosc.* **2016**, *83*, 180.

[32] O. O. Ilchenko, Y. V. Pilgun, A. S. Reynt, A. M. Kutsyk, *Ukr. J. Phys.* **2016**, *61*, 519.

Table 1. Numbers showing the dimensions of the SU-8 microcontainers, amount of microcontainers per silicon chip and total polymer surface area per chip. The data represents mean ± SD in 8 replicates.

Sample	Internal microcontainer diameter [µm]	Number of microcontainers per chip	Total polymer surface area exposed to $scCO_2$ per chip [mm^2]
Small	97 ± 6	1024	31 ± 4
Medium	191 ± 9	256	30 ± 3
Large	413 ± 5	64	34 ± 1

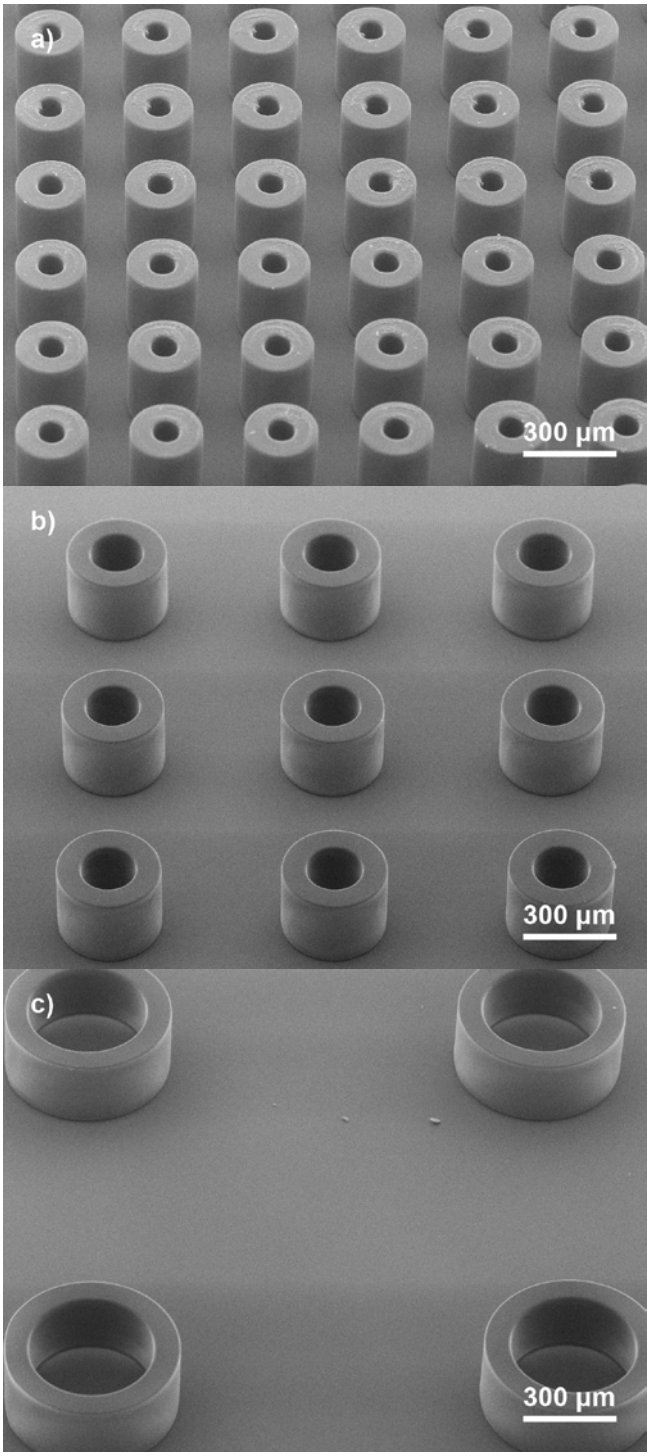

Figure 1. SEM images of SU-8 microcontainers in the size of a) small, b) medium and c) large having an internal diameter of 97 ± 6 µm, 191 ± 9 µm and 413 ± 5 µm, respectively.

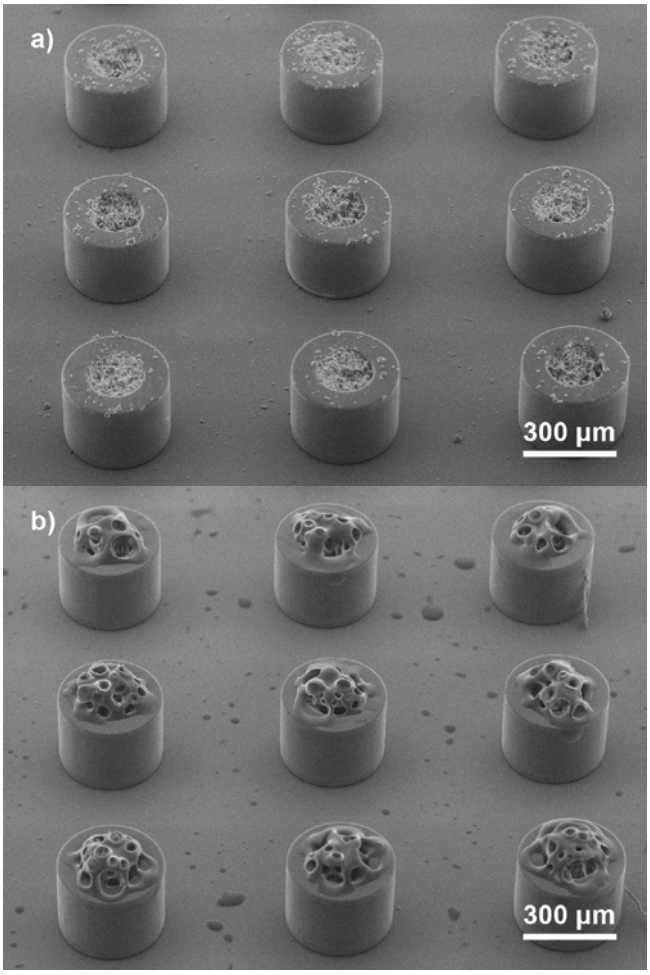

Figure 2. SEM images of medium sized microcontainers a) filled with PVP and b) loaded with ketoprofen using $scCO_2$ impregnation. These images are representative examples of the PVP filling and the drug loading with the supercritical impregnation method.

Table 2. Amount of ketoprofen or naproxen loaded in the three different sizes of microcontainers. The data represents mean ± SD in triplicates.

Sample	Amount of PVP filled per chip [mg]	Total amount of ketoprofen loaded per chip [µg]	Total amount of naproxen loaded per chip [µg]
Small	0.94 ± 0.36	128.3 ± 65.9	89.7 ± 40.95
Medium	0.82 ± 0.1	91.3 ± 20.1	160.54 ± 42.8
Large	1.03 ± 0.17	86.1 ± 28.7	128.23 ± 26.50

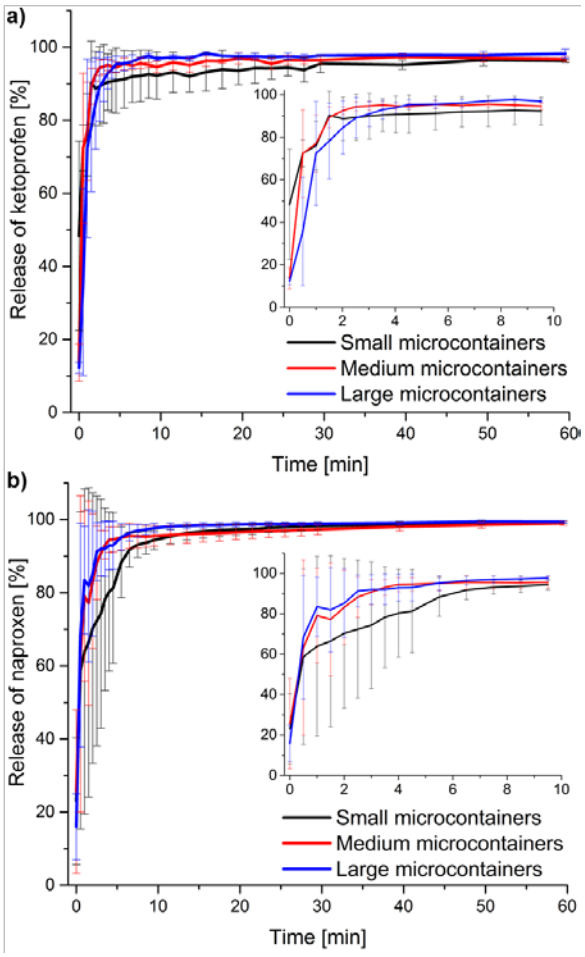

Figure 3. Release profiles of a) ketoprofen) and b) naproxen from small, medium and large microcontainers performed on a µ-Diss profiler in PBS at pH 6.5. The inserts represent the same profiles zoomed in on the first 10 min. The graphs represent mean ± SD in triplicates.

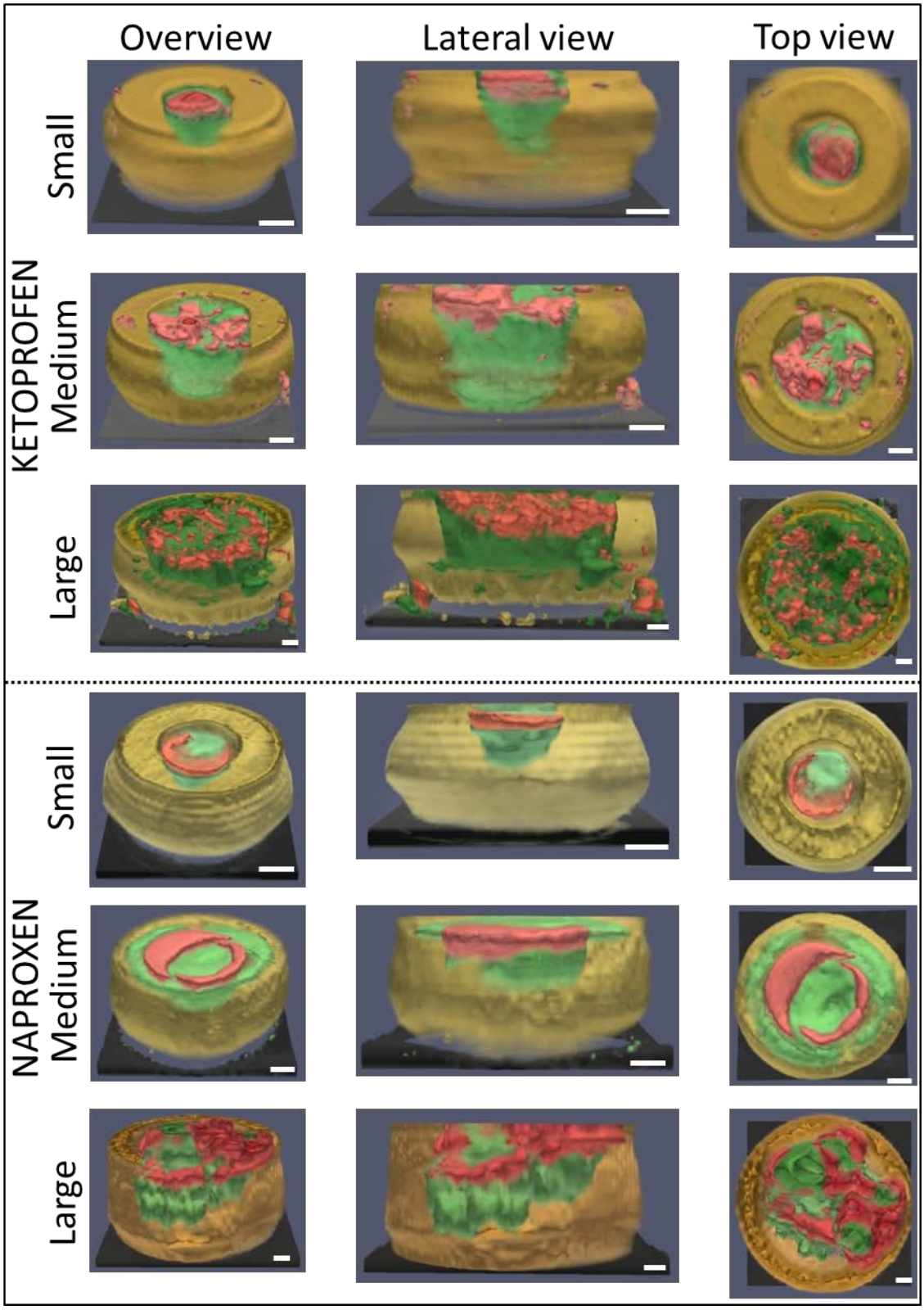

Figure 4. Volumetric Raman maps of ketoprofen or naproxen loaded into the microcontainers. The overview, the lateral view and the top view can be seen from left to right for each of the different sizes of microcontainers: small, medium and large from top to bottom. Ketoprofen or naproxen are represented in red, PVP in green, SU-8 in yellow and Si in black. The scale bars correspond to 50 µm.

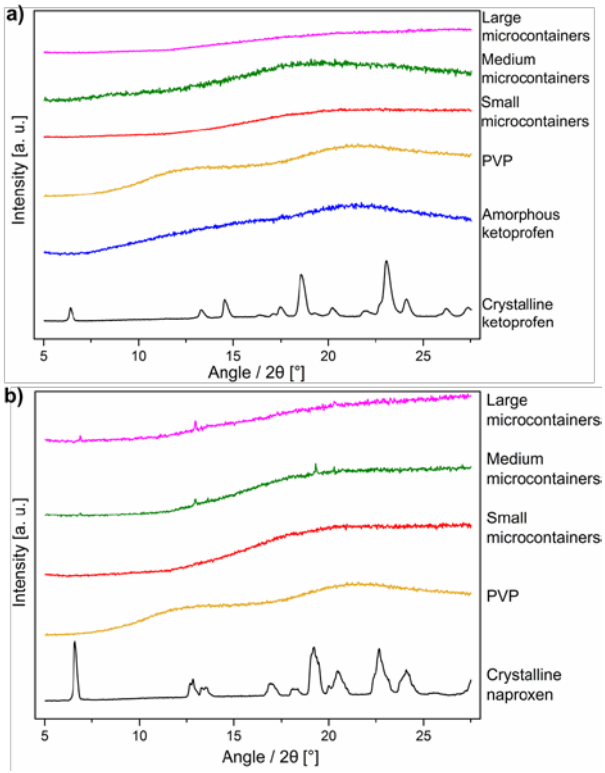

Figure 5. (a) XRPD diffractograms of crystalline and amorphous ketoprofen, PVP, small, medium and large microcontainers filled with PVP followed by impregnation with ketoprofen. (b) XRPD diffractograms of crystalline naproxen, PVP, small, medium and large microcontainers filled with PVP and followed by impregnation with naproxen.

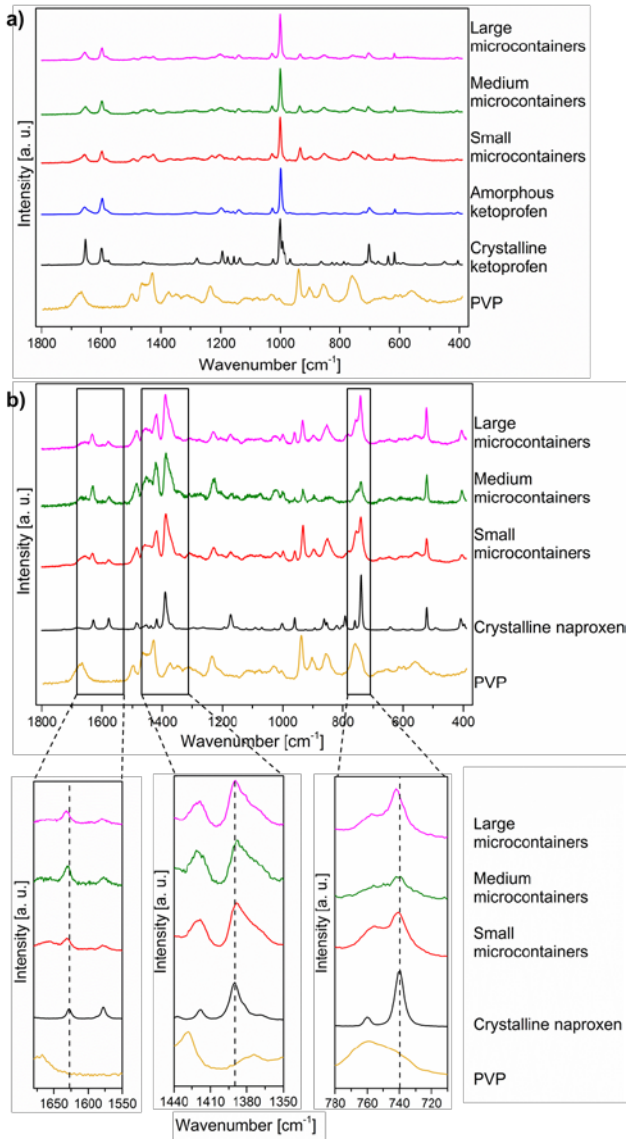

Figure 6. a) Raman spectra of PVP, crystalline and amorphous ketoprofen, small, medium and large microcontainers filled with PVP followed by impregnation with ketoprofen. b) Raman spectra of PVP, crystalline naproxen, small, medium and large microcontainers filled with PVP followed by impregnation with naproxen. The zoom-in areas show the peak-shifts in naproxen loaded in microcontainers compared to its crystalline form.

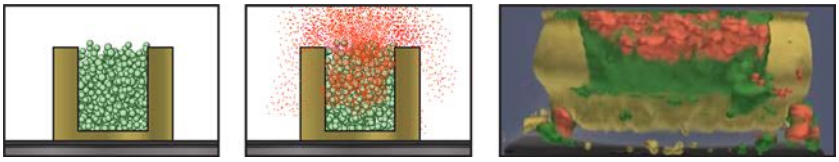

Three different sizes of polymeric confined matrices are drug loaded with supercritical CO_2 impregnation. With a custom-made Raman microscope, volumetric maps of an entire confined polymer matrix loaded with drug are obtained allowing for a drug distribution analysis. For the first time, a 3D distribution analysis has been done on a micrometer size object without bulky, destructive or expensive techniques.

Keyword polymer matrix, drug distribution, poorly soluble drug, supercritical CO_2 impregnation, Raman spectroscopy

C. Mazzoni*, F. Tentor, A. Antalaki, R. D. Jacobsen, J. Mortensen, R. Slipets, O. Ilchenko, S. S. Keller, L. H. Nielsen, Prof. A. Boisen*

Where is the drug? - Quantitative 3D distribution analyses of confined drug-loaded polymer matrices

Paper IV

Long lasting mucoadhesive membrane based on AL and CH for intravaginal drug delivery

Fabio Tentor, Giorgia Siccardi, Pasquale Sacco, Danilo Demarchi, Eleonora Marsich, Kristoffer Almdal, Sanjukta Bose Goswami, Anja Boisen

Manuscript submitted to *ACS Biomaterials science and engineering*

Long lasting mucoadhesive membrane based on alginate and chitosan for intravaginal drug delivery.

Fabio Tentor[1,*], Giorgia Siccardi[2], Pasquale Sacco[3], Danilo Demarchi[2], Eleonora Marsich[4], Kristoffer Almdal[1], Sanjukta Bose Goswami[1], Anja Boisen[1]

[*]Corresponding author, fabt@nanotech.dtu.dk; Fax: 45887762
[1]Department of Micro- and Nanotechnology, Technical University of Denmark, Ørsteds Plads 345C, 2800 Kgs. Lyngby, Denmark
[2]Department of Electronics and Telecommunications, Politecnico di Torino, Corso Duca degli Abruzzi, 24, 10129 Torino, Italy
[3]Department of Life Sciences, University of Trieste, via L. Giorgieri 5, I-34127 Trieste, Italy
[4]Department of Medicine, Surgery and Health Sciences, University of Trieste, Piazza dell'Ospitale 1, I-34129 Trieste, Italy

Keywords

Alginate, Chitosan, Drug delivery, Membrane, Intravaginal, Antimicrobial.

Abstract

The intravaginal route of administration can be exploited to treat local diseases and for systemic delivery. In this work, we developed an alginate/chitosan membrane sufficiently stable in a simulated vaginal fluid, which degrade over time at a very slow and linear rate. The membrane demonstrated good mechanical properties both in its swollen and dry form. As a study case, we evaluated the viability of this potential drug delivery system for the treatment of bacterial vaginosis, a common disease affecting women in their reproductive age. Metronidazole was effectively included in the alginate/chitosan membrane and its bactericide effect was demonstrated against *Staphilococcus aureus* and *Gardnerella vaginalis*, simultaneously showing good biocompatibility with a cervix epithelial cell line. Since this alginate/chitosan membrane is stable in a simulated vaginal environment, is easy to fabricate and can be used for controlled release of a model drug, it is a promising drug delivery system for local intravaginal applications.

1. Introduction

Drug delivery systems (DDS) are used to improve the performances of active pharmaceutical ingredients (APIs). DDS can be used to control the time and site of drug release[1,2]; they can implement mucoadhesive properties to the formulations[3] and can be used to lower the risk of adverse effects during treatment[4] while increasing the bioavailability[5]. Tailoring DDS, taking into account the administration route, is crucial: different materials can be used to address specific issues for different administration routes. The DDS developed in this work was tailored for intravaginal drug delivery. The vaginal route of administration can be used to treat diseases systemically[6], avoiding the first pass metabolism, and also for the treatment of local diseases[7]. Conventional formulations (i.e. suppositories), however, generally have short residence times which means that the medication does not persist at the site of application, reducing its bioavailability[8]. So far, many DDS have been developed to address local diseases in the vaginal cavity improving the intravaginal residence time[9,10]. Dobaria et al.[10], for instance, developed a bioadhesive membrane, constituted of hydroxypropyl cellulose, with the aim of retaining a formulation in the vaginal cavity for 8 h.

The development of intravaginal DDS consisting of bioadhesive and biocompatible materials has been extensively investigated. Alginate and chitosan have shown promising advantages as materials for

intravaginal applications[11,12]. Alginate is a well-known polysaccharide commonly used in many DDS due to its ability to form hydrogels in the presence of calcium and other divalent cations[13–17]. Chitosan, on the other hand, is known for its intrinsic mucoadhesive properties[18] which have been successfully applied in many DDS. Chitosan has been frequently used in combination with negatively charged polymers (i.e. alginate and hyaluronic acid), exploiting their electrostatic interactions[19] to form micro/nanoparticles[3,13] and membranes[20–22].
Regarding intravaginal DDS, El-Kamel et al.[11] developed a glutaraldheyde-crosslinked alginate and chitosan intravaginal tablet which was able to incorporate metronidazole, a commonly used antibiotic to treat Bacterial Vaginosis (BV). Abruzzo et al.[12], developed an alginate and chitosan complex to be used as a vaginal insert for the controlled release of chlorhexidine digluconate, a common antiseptic. These reported studies, however, lack a characterization of the degradation of the respective DDS in a simulated vaginal fluid[23].

In this work, we have developed an alginate (AL) and chitosan (CH) mucoadhesive membrane capable of encapsulating metronidazole (Met) which is a model class I drug according to the Biopharmaceutical Classification System (BCS)[24,25]. Met is an antibiotic used to treat Bacterial Vaginosis (BV)[26]. This disease is a common infection in women in their reproductive age, with a prevalence of 10 – 50%, worldwide; its main symptoms are vaginal discharge, risk of miscarriage and preterm birth[27]. Although the etiology of BV is not completely understood this disease is frequently associated with a disturbance of the normal vaginal flora and an abnormal growth of *Staphilococcus aureus* (*S.a*) and *Gardnerella vaginalis* (*G.v.*)[28–30]. We pursued ´an easy to fabricate` approach to develop the membranes used in this work which showed good mechanical properties. The most characteristic feature of the developed membranes is their ability to withstand a simulated vaginal fluid, where the membranes slowly degrade in a *quasi*-linear fashion during 30 days of investigation. A biocompatible and mucoadhesive DDS, made of alginate and chitosan and which is able to tolerate an intravaginal environment at least one month, could be exploited for sustained drug release. To evaluate the capability of the developed DDS to deliver Met, dissolution studies were performed in a simulated vaginal fluid. The bactericide ability of the membranes, towards both *S.a.* and *G.v.*, was demonstrated. Finally, the DDS was seen to be biocompatible with a cervix epithelial cell line.

2. Experimental section

2.1. Materials

Sodium Alginate (AL, medium molecular weight, Mn 110 kDa, PDI = 4.309) was purchased from Sigma Aldrich (St. Louis, USA). Chitosan chlorohydrate (CH, Mn 158.3 kDa, deacetylation = 83.6%) was purchased from Microresist Technology GmbH (Berlin, Germany). $CaCO_3$, D-(+)-Glucono-delta-lactone (GDL), Metronidazole (Met), NaCl, KOH, $Ca(OH)_2$, Bovine Serum Albumin (BSA), lactic acid, acetic acid (99.8% v/v), glycerol, urea, D-glucose, hydrochloric acid (32% v/v), fluorescein isothiocyanate (FITC), $NaHCO_3$, $CaCl_2$, Triton™ X-100, Luria Bertani (LB) broth/agar, Brain Hearth Infusion (BHI) broth and Phosphate Buffered Saline (PBS) were all purchased from Sigma Aldrich (St. Louis, USA). Streptomycin and Penicillin were purchased from EuroClone (Milan, Italy). Rozex® 0.75% metronidazole (Met) was purchased from Nomeco (Copenhagen, Denmark). Keratinocyte-serum free medium (K-SFM), Epidermal Growth Factor 1-53 (EGF 1-53), Bovine Pituitary Extract (BPE), Oxoid™ AnaeroGen™ 2.5L Sachet and AlamarBlue® were purchased from Thermo Fisher Scientific (Waltham, MA, USA). All solutions were prepared using milliQ water (18.2 mΩ).

2.2. Membrane fabrication

Membranes were fabricated in a round shaped poly(methyl methacrylate) (PMMA) mold having a flat base over which a PMMA ring ($Ø_i$ = 55 mm) was screwed tightly. The first part of the membrane development consisted of the fabrication of an alginate (AL) hydrogel. To obtain a smooth and homogenous hydrogel we followed, with slight modifications, the approach reported first by Draget and coworkers[31] and used frequently thereafter[32]. Briefly, a suspension of AL 3.16% w/v (AL) and $CaCO_3$ 23.3 mM was kept under stirring for 24h. 3.92 g of the suspended mixture was poured into the PMMA mold. Then, 2.16 mL of an 84.3 mM GDL solution was added, gently mixing the suspension with a pipette tip for a few seconds. The addition of GDL caused the dissociation of $CaCO_3$, followed by the crosslinking of AL to form the hydrogel membrane. To obtain drug loaded membranes, metronidazole 4 wt% was added to the alginate/CaCO3 suspension and the same procedure was applied. The total amount of API present in the final membrane corresponded to 16 mg. The hydrogel was consequently kept at room temperature (RT) overnight to crosslink completely. The ring was removed and the AL hydrogel was left to dry at RT. Once dry, the AL membrane was soaked in chitosan chlorohydrate 0.5% w/v to form a polyelectrolyte complex (PEC). This was done by firstly pouring 2 mL of the CH solution on a petri dish and placing the AL membrane over it. Finally an additional 1.5 mL of the CH solution was poured over the AL membrane. The membrane was then left to absorb the CH solution overnight and was kept at RT until dry. Once ready, the membranes were cut manually into 4 quarters. For the sake of clarity, the abbreviations AL and AL/CH will be used to represent one membrane quarter comprised of only alginate and alginate/chitosan respectively throughout the manuscript. AL+Met and AL/CH+Met will be used to represent membrane quarters comprising alginate and alginate/chitosan with the addition of 4 mg of metronidazole respectively.

2.3. Swelling studies

The swelling of AL and AL/CH membranes was assessed both in deionized water (DI) and in simulated vaginal fluid (SVF). The simulated vaginal fluid was made in accordance with the recipe proposed by Owen et al.[23]: NaCl 3.51 g, KOH 1.40 g, $Ca(OH)_2$ 0.222 g, Bovine Serum Albumin (BSA) 0.018 g, lactic acid 2 g, acetic acid 1 g, glycerol 0.16 g, urea 0.4 g and D-glucose 5 g were mixed in 1 L of milliQ water, the pH of the solution was then adjusted to 4.2. AL and AL/CH membranes were first dried overnight at 37 °C and then soaked in 5 mL of DI water or SVF at 37 °C for the studies. After each time point the excess of medium was blotted away using filter paper and the samples were weighed. The water uptake was calculated according to Equation 1.

$$Water\ uptake\ (\%) = \frac{Ww - Wd}{Wd} \cdot 100 \qquad (1)$$

Where W_w corresponds to the weight of the wet sample after soaking at each time point and W_d corresponds to the weight of the dry sample.

2.4. Mechanical characterization

The mechanical properties of the developed membranes were evaluated both in their dry and swollen state. The aim was to understand the effect of the inclusion of chitosan and metronidazole in the formulation, in terms of both compressive modulus (E) and compressive strength at break (σ). A tensile stress test was used to characterize the dry membranes. Compression studies were instead conducted to characterize the swollen membranes. The results of the tensile and compression studies are, consequently, not comparable.

2.4.1. Tensile stress test

To characterize the mechanical properties of the membranes in their dry state, tensile tests were performed.
The tensile stress test was performed using an INSTRON 5967 (Tensile & Compression Testers, Cambridge, Massachusetts, USA) equipped with a 500 N load cell following the ASTM D882-12. AL+Met and AL/CH+Met membranes were cut to obtain rectangles of 3x1 cm and held vertically between two clamps exposing 1 cm of the membrane in between the clamps. The thickness of the AL+Met membrane was 49 ± 2 μm and that of AL/CH+Met was 46 ± 4 μm. The test was carried out at room temperature using a stretching rate of 0.5 mm/min until fracture. The Young´s Modulus (E) and the tensile stress at break (σ) were measured.

2.4.2. Compression studies

To characterize the mechanical properties of the membranes swelled in SVF we performed a compression study. The compressive modulus (E) and the compressive strength at break (σ) of the membranes were determined using a Texture Analyzer (TA.XT Plus, Texture Technologies Corp. and Stable Micro Systems, Ltd. Hamilton, MA) equipped with a 5 kg load cell. The samples were obtained by punching out cylinders (Ø = 6 mm) from each membrane tested: AL, AL/CH and AL/CH+Met. Investigation on each type of membranes was repeated thrice. The cylinders were kept in SVF for 10 min at T = 37 °C to reach equilibrium swelling prior to the analysis. The samples were then removed and quickly tested at RT. The texture analyzer probe was moved towards the sample until a trigger force of 2.0 g was measured. Uniaxial compression force was from thereafter applied with a displacement rate of 0.01 mm/sec until gel rupture occurred.
The compressive modulus was calculated from the slope of the stress–strain curve (σ-ε) at the target strain of 20%[33].

2.5. Morphological investigation

Scanning Electron Microscopy (SEM) was used to evaluate the morphology of the prepared membranes and to evaluate the distribution of the metronidazole within them. Cross-sectional views of AL, AL+Met, AL/CH and AL/CH+Met membranes were obtained using a Zeiss Supra 40VP Field Emission Scanning Electron Microscope (SEM, Carl Zeiss Microscopy GmbH, Jena, Germany) in high vacuum mode with an energy of 2 KeV.

2.6. Confocal microscopy

Confocal Microscopy (CM) was used to evaluate the adsorption of chitosan within the alginate membrane. Chitosan was labeled with Fluorescein isothiocyanate (FITC) according to a previous published procedure[34]. Briefly, 90 mg of chitosan was dissolved in 30 mL of milliQ water (pH = 4.7). 200 μL of a Fluorescein isothiocyanate solution 0.5 mg/mL in sodium bicarbonate buffer (50 mM) was then added to the chitosan solution. The reaction mixture was then kept at RT in a dark environment for 24h under constant stirring. Later, the mixture was dialyzed in a dark environment in a dialysis bag (cut-off = 12 kDa, Sigma Aldrich, St. Louis, USA). The dialysis was initially performed against $NaHCO_3$ 50 mM (V = 2 L, t = 24 h), continued against NaCl 100 mM (V = 2 L, t = 24 h) and concluded against deionized water until the conductivity of the external solution resulted to be lower than 3 μS/cm at 4 °C. The pH of the solution was finally adjusted to 4.5 and the solution was then freeze-dried.
The Fluorescein labeled chitosan (CH-FI) was used to prepared AL/CH-FI membranes using the same approach described in the “Membrane fabrication” section with slight modifications: a solution of CH 0.45%

w/V + CH-FI 0.05% w/V was, in fact, used instead of the CH 0.5% w/V solution. Once dry, the AL/CH-FI membrane was positioned transversally over a microscope slide. Confocal microscopy analyses were performed using a Nikon Eclipse C1-si confocal laser-scanning microscope with a Nikon Plan Apochromat 40x as objective. The resulting stacks of images were analyzed using the Fiji software.

2.7. *In vitro* Mucoadhesion

The mucoadhesiveness of AL+Met and AL/CH+Met membranes was evaluated using gilt´s vagina (obtained from a slaughter school, Roskilde, Denmark) as a model tissue. The measurements were conducted by means of a texture analyzer (TA.XT Plus, Texture Technologies Corp. and Stable Micro Systems, Ltd. Hamilton, MA) equipped with a 500 g load cell. The mucoadhesion was evaluated by means of a tensile stress test. The work of adhesion (W_{ad}) and detachment force (F_{de}) required to detach a membrane sample from the tissue were taken into consideration to represent the mucoadhesiveness. Following the protocol suggested by Neves et al.[35], with slight modifications, the tissues were washed with PBS and cut in half exposing the mucosa. After rinsing, the tissues were frozen at -20 °C until further use.
Prior to the adhesion studies, the tissues were defrosted in PBS for 60 min at 37 °C. The excess of liquid was blotted away using filter paper; the tissue was finally placed flat on a support to be used for analysis. Before starting the measurements, to maintain physiological conditions, the tissue was wetted with 50 µL of SVF. The excess of liquid was carefully removed with filter paper. The membranes were cut in pieces (Ø = 10 mm) and attached to the probe by means of adhesive tape.
The probe was put in contact with the tissue with a speed of 0.50 mm/sec. Intimate contact between the sample and the vaginal tissue was ensured pressing the vaginal tissue with the probe until the applied force was equal to 0.05 N. The membrane was kept in contact with the tissue for 60 seconds. The probe was thereafter pulled to its initial position at a speed of 2.50 mm sec^{-1}. All experiments were carried out at 37 ± 1 °C. Each sample was tested on fresh tissue portions. The experiments were conducted at the Technical University of Denmark under the license number 2018-12-711-07152.

2.8. Membrane degradation

To evaluate the stability of the AL/CH+Met membranes in an intravaginal environment, degradation studies were conducted in SVF at 37 °C. AL/CH+Met dry membranes were placed in 5 mL of SVF and kept at 37 °C. The weight of the samples was measured at 0, 15, 30, 60, 120, 240, 360 min and, subsequently, until 30 days at the time points depicted in Figure 4. The excess of water was removed using filter paper prior to the measure. The remaining weight percentage was thereby calculated according to Equation 2.

$$Remaining\ weight\ (\%) = \frac{Wn}{Wi} \cdot 100 \qquad (2)$$

Where W_n corresponds to the weight of the sample at each time point and W_i corresponds to the weight of the membrane at its highest swelling.

2.9. Dissolution of metronidazole

The release of metronidazole from the AL/CH+Met membranes was evaluated using a µ-Diss profiler (pION INC, Woburn, MA, USA). The dissolution profiles were then compared to that of the pure API in the same concentration and of a commercially available metronidazole gel (Rozex® 0.75% metronidazole, GALDERMA). The instrument was initially calibrated in SVF using a stock solution of metronidazole. The dissolution was therefore conducted for 24h in 25 mL of SVF. The dissolution medium was kept at 37 °C

under constant stirring (30 rpm). Dip style probes with 1 mm path length were used. The absorption was evaluated in the wavelength range of 320 – 325 nm with a baseline correction at 500 nm.
To further evaluate the release kinetics from the membranes, the *in vitro* dissolution of metronidazole from AL/CH+Met membranes was also assessed in a custom flow system. This setup was meant at mimicking the physiological production of vaginal fluid better. The membranes were positioned at an angle of 30° and SVF was poured over the membranes at a flow rate of 5 mL/h. The medium was collected every 5 min for 1h and analyzed using a Varioskan LUX Multimode Microplate Reader (Thermo Fisher Scientific, Waltham, MA, USA) at 322 nm.

2.10. Cell culture

Cervix epithelial cells Ect1/E6E7 (ATCC® CRL-2614™), kindly provided by Dr. Chiara Agostinis (University of Trieste, Italy), were used for the *in vitro* studies. The cell line was cultured in Keratinocyte-SFM, complemented with EGF 1-53 0.1 ng/mL, BPE 0.05 mg/mL, streptomycin 100 µg/mL, penicillin 100 µg/mL and $CaCl_2$ 0.4 mM. Cells were grown in a humidified atmosphere (5% CO_2) at 37 °C in 75 cm^2 flasks. The medium was changed every 2-3 days.

2.11. Biocompatibility assay

An AlamarBlue® assay was conducted on AL/CH and AL/CH+Met membranes to assess their biocompatibility. The epithelial ectocervix cell line Ect1/E6E7 (ATCC® CRL-2614™) was used for this purpose. AL/CH and AL/CH+Met membranes were sterilized under UV for 5 min on each side and placed in 5 mL of Keratinocyte-SFM for 24h at 37 °C. 200 µL of cell suspensions were seeded into 96-well plates (10,000 cells/well). The well plate was kept overnight at 37 °C (5% CO_2) to allow for cell adhesion. The medium was consequently removed from the wells and the cells rinsed using PBS. Finally, 200 µL/well of: i) AL/CH membrane extract, ii) AL/CH+Met membrane extract, iii) complete keratinocyte-SFM (control) and iv) keratinocyte-SFM + Triton 0.1 % V/V, were added. The cells were incubated at 37 °C (5% CO_2) for 24h and 48h. After the incubation, the wells were rinsed with PBS and incubated with 300 µL/well of AlamarBlue® reagent (10% V/V in complete keratinocyte-SFM) for 5h at 37 °C. At the end of this time frame, 150 µL of the treatment media were transferred in a black 96-well plate. The fluorescence was measured using a FLUOStar Omega-BMG Labtech spectrofluorometer (λex = 544 nm; λem = 590 nm). Each sample was analyzed at least in triplicate. The cells viability is expressed as the ratio % between the fluorescence intensity of sample and of the untreated cells (control) after 24h and 48h. The reported results correspond to an average of three independent experiments.

2.12. Antimicrobial activity of the membranes

The antimicrobial activity of the AL/CH+Met membranes was evaluated against *Staphilococcus aureus* (*S.a.*, ATCC® 25923™) and *Gardnerella vaginalis* (*G.v.* DSM No. 4944, Leibniz-Institut DSMZ, Germany). AL/CH was used as negative control; pure metronidazole was used as positive control. AL/CH and AL/CH+Met membranes were sterilized under UV for 5 min on each side. For the experiments on *S.a.*, each membrane and the pure metronidazole were placed in 15 mL tubes, where 500 µL of PBS/LB broth 90%/10% v/v was added to allow the membranes to swell. Bacterial suspensions were prepared by adding 20 µL of *S.a.*, preserved in glycerol, to 5 mL of Luria-Bertani (LB) broth. The obtained suspensions were incubated at 37 °C overnight. 500 µL of the bacterial suspension was poured in 9.5 mL of LB broth and grown for 90 min at 37 °C to restore the exponential growth phase. The *S.a.* concentration was assessed by means of optical density (OD) at 600 nm. The suspension was consequently diluted in a solution of PBS/LB broth 90%/10% V/V to obtain a final concentration of $5x10^6$ bacteria/mL. 5 mL of the *S.a.* suspension was

poured in the tubes containing the samples: AL/CH, AL/CH+Met and pure metronidazole. All tubes were placed in a 2.5 L jar containing an Oxoid™ AnaeroGen™ 2.5L Sachets to create anaerobic conditions. The test was carried out at 37 °C for 24h. After the incubation, bacterial suspensions from each treatment were vortexed and collected. The *S.a.* suspensions were consequently diluted in PBS (10^{-1} to 10^{-5}). 25 µL of the suspensions and the dilutions were plated on LB agar and incubated overnight at 37 °C in aerobic conditions. The colony forming units (CFU) were counted the day after. Bacterial suspensions of *G.v.* were prepared by adding 200 µL of *G.v.*, preserved in glycerol, to 5 mL of Brain Heart Infusion (BHI) broth. The obtained suspensions were incubated at 37 °C in CO_2 enriched atmosphere overnight. The concentration of *G.v.* was assessed as described for *S.a.*. The suspension was consequently diluted in a solution of PBS/BHI broth 90%/10% V/V to obtain a final concentration of $5x10^6$ bacteria/mL. 5 mL of the *G.v.* suspension was poured in the tubes containing the samples. All tubes were placed in a 2.5 L jar containing an Oxoid™ AnaeroGen™ 2.5L Sachets to create anaerobic conditions. The test was carried out at 37 °C for 24h. After the incubation, bacterial suspensions from each treatment were vortexed and collected. The *G.v.* suspensions were consequently diluted in PBS (10^{-1} to 10^{-5}). 25 µL of the suspensions and the dilutions were plated on Columbia blood agar base (Oxoid) supplemented with 5% V/V horse blood defibrinated (ThermoFisher) and incubated three days at 37 °C in CO_2 enriched atmosphere. The colony forming units (CFU) were counted at the end of experiments. The data are presented as LogCFU/mL of 3 independent replicates.

2.13. Statistical Analysis

All data are expressed as mean ± standard deviation (SD). T-student was used for all parametric data. Mann-Whitney U Test was instead used to analyze the work of adhesion results.
Differences between the samples were considered statistically significant when the p-value resulted lower than 0.05. P-values lower than 0.05 are indicated as ´*´, p-values lower than 0.01 as ´**´, p-values lower than 0.001 as ´***´ and p-values lower than 0.0001 as ´****´.

3. Results and Discussions

3.1. Membrane Fabrication

Alginate was chosen for its ability to make biodegradable hydrogels that are crosslinked and stabilized by the presence of divalent cations, such as Ca^{2+}, commonly present in the vaginal fluid[23]. The second polysaccharide, chitosan, was included to improve the mechanical and biological properties of the membrane. Chitosan was selected because of its ability to interact with alginate *via* electrostatic interactions and due to its known antimicrobial and mucoadhesive properties[3,36]. In addition, chitosan has been proven to reduce the concentration of Reactive Oxygen Species (ROS) produced by stimulated neutrophils: this can be exploited to improve the wound healing process[3]. In Figure 1 an AL/CH+Met dry membrane is depicted. As it can be noticed, crystals of metronidazole are visible to the naked eye as the concentration is relatively high compared to the weight of the membrane (about 8.5 wt%). The API, once solubilized in the hydrogel, crystallizes during the drying process and is encapsulated within the membrane. The fabrication of the AL/CH membrane with or without metronidazole was found to be simple and upscalable. A scheme, depicting the workflow, is shown in Figure 1.

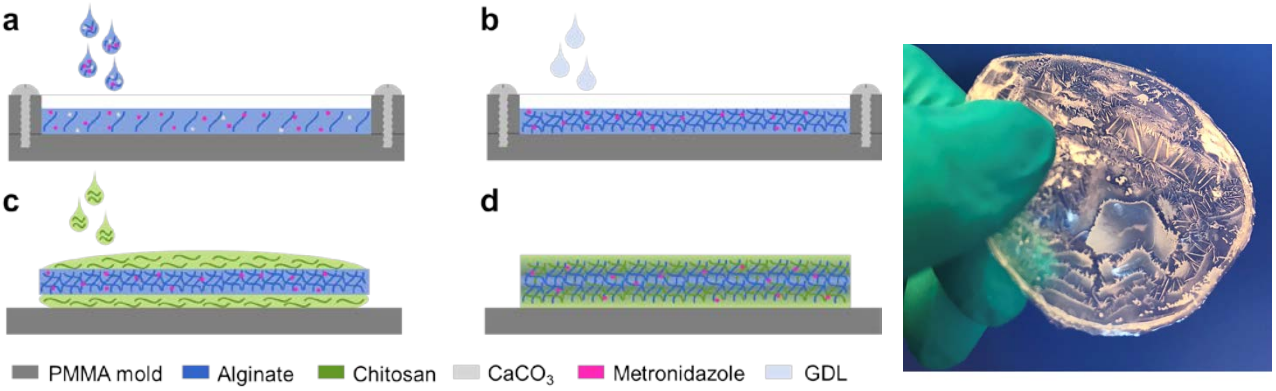

Figure 1 – Scheme of the AL/CH+Met membrane fabrication. To the left, the steps of the AL/CH+Met membrane fabrication are depicted: a) a solution of alginate+$CaCO_3$+Met is poured in a PMMA mold, b) D-(+)-Glucono-delta-lactone is added to the mold to induce the gelation of alginate, c) the mold is opened to dry the hydrogel, the dry film is then allowed to swell in chitosan, d) chitosan penetrates in the alginate film to form the alginate/chitosan + metronidazole membrane (AL/CH+Met). To the right, an example of an AL/CH+Met membrane dried at room temperature is shown; metronidazole crystals are visible as white aggregates in the membrane.

3.2. Swelling Studies

Understanding the swelling properties of the developed membranes is of high importance as it gives an idea of: i) the volume the material would occupy, ii) how much medium the material is able to absorb and iii) the absorption rate. The membranes were tested on two different media: a) DI water, as a reference and b) SVF, already reported as a valid medium by Owen et al.[23]. When swelled in milliQ water, the AL membrane water uptake (Figure 2a), was higher than that of the AL/CH membrane. For both the AL and AL/CH membranes their respective highest swelling point was reached after 10 min. When swollen in DI water, the weight of the membranes started to drop right after the peak was reached; this was probably due to the high volume variation the membranes encountered during the swelling and consequent disaggregation. The membranes were completely disrupted after 2h (AL membranes) and 1h (AL/CH membranes). When exposed to the SVF for both membranes (Figure 2b) the highest water uptake point remained the same (10 min), as observed in the case of milliQ water. The mass-swelling ratio was observed to be approximately 40 in case of milliQ water whereas it was equal to around 10 in case of SVF. Similar swelling behaviors have also been reported by Baysal et al.[37]. It is worth noticing how both the AL and AL/CH membranes maintained the same weight after about 10 min of swelling in the SVF. This observation can be attributed to the presence of Ca^{2+} in the SVF medium - which is expected to strengthen the alginate-based membrane - and due to the lower pH of the solution where both polysaccharides behave as oppositely charged polyelectrolytes, meaning that electrostatic interactions are fostered.

An important difference noticed during the swelling studies was the thickness of the membranes: once swollen, the AL membranes were thicker than the AL/CH membranes with thicknesses of 2.2 ± 0.2 mm and 1.1 ± 0.1 (N = 3, SD) mm respectively. This is probably due to the attractive interactions between AL and CH, which increase the stiffness of the swollen network and reduce the swelling. The presence of metronidazole had no effect in terms of both water uptake and thickness (data not reported). As the thickness of the AL/CH membrane was significantly lower (***$p < 0.0001$), this DDS is preferred over membrane constituted of only AL.

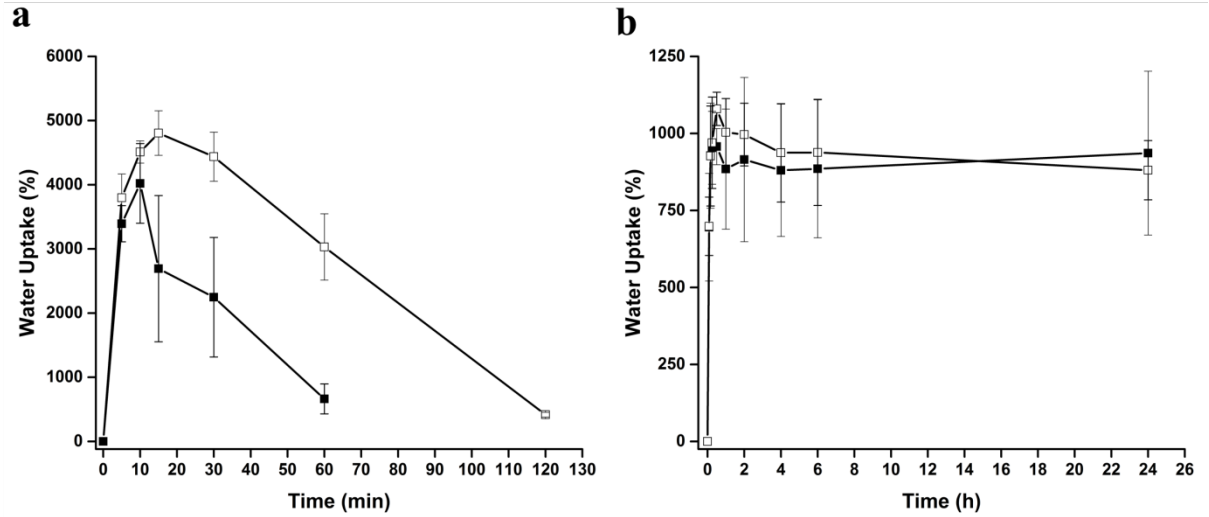

Figure 2 – Water Uptake (%). The graphs represent the water uptake % of AL (**empty squares**) and AL/CH (**full squares**) membranes in deionized water (**a**) and in a simulated vaginal fluid (**b**). (N = 3, SD).

3.3. Mechanical characterization

3.3.1. Tensile stress test

The prepared AL/CH membranes are aimed to be used for intra vaginal drug delivery which should be applied in the vaginal cavity manually or with the help of a tampon. Thus, it is important to obtain a membrane that is mechanically stable and flexible. Both AL and AL/CH membranes were folded more than 200 times manually without any breakage to confirm the flexibility of the dry membranes. To further assess the mechanical properties of the dry membranes, tensile stress tests were performed. The results are summarized in Table 1. In the dry state, the AL/CH+Met membranes could resist high tensile stress before reaching the break point; that is, the membranes are sufficiently tough and flexible to be folded. These results support the use of this membrane as an intravaginal DDS that can be wrapped around a dispenser using a place in the desired site without risking breaking it.

3.3.2. Compression Studies

By means of compression studies we evaluated the mechanical properties of the membranes swollen in SVF and assessed the effect of the presence of CH and Met in terms of E and σ. The test was performed after swelling the membranes in the SVF for 10 min at 37 °C, in accordance to the swelling behavior reported in Paragraph 3.5 “Swelling Studies”. The results are summarized in Table 1.

Table 1 – Mechanical Characterization.

Tensile Stress Test (dry membranes)		
Sample	**E (MPa) ± SD, (N = 3)**	**σ (MPa) ± SD, (N = 3)**
AL+Met	446 ± 240	5.7 ± 3.2
AL/CH+Met	235 ± 154	9.7 ± 0.4
Compression Studies (swollen membranes)		
Sample	**E (kPa) ± SD, (N ≥ 3)**	**σ (kPa) ± SD, (N ≥ 3)**
AL	25.4 ± 4.4	34.9 ± 6.9
AL/CH	38.9 ± 8.7*	93.3 ± 4.2***
AL/CH+Met	32.3 ± 7.8	100.4 ± 20.3**

The compressive modulus (E) of the AL hydrogel is in line with the data presented by Jang and coworkers[33]. By introducing CH in the DDS the E increases significantly (*p = 0.0426). By including Met in the AL/CH membrane the compressive modulus of the DDS tends to be a little lower. This can be due to the presence of metronidazole interfering with the electrostatic interactions occurring between AL and CH and thereby reducing the synergistic contribution shown by AL/CH membranes. In a similar manner to the compressive modulus, the compressive strength at break (σ) results are higher for both AL/CH (****p < 0.0001) and AL/CH+Met (**p = 0.0011) compared to only AL membranes.

3.4. Morphological Investigation

SEM was used to understand the morphology of the prepared membranes, as shown in Figure 3.

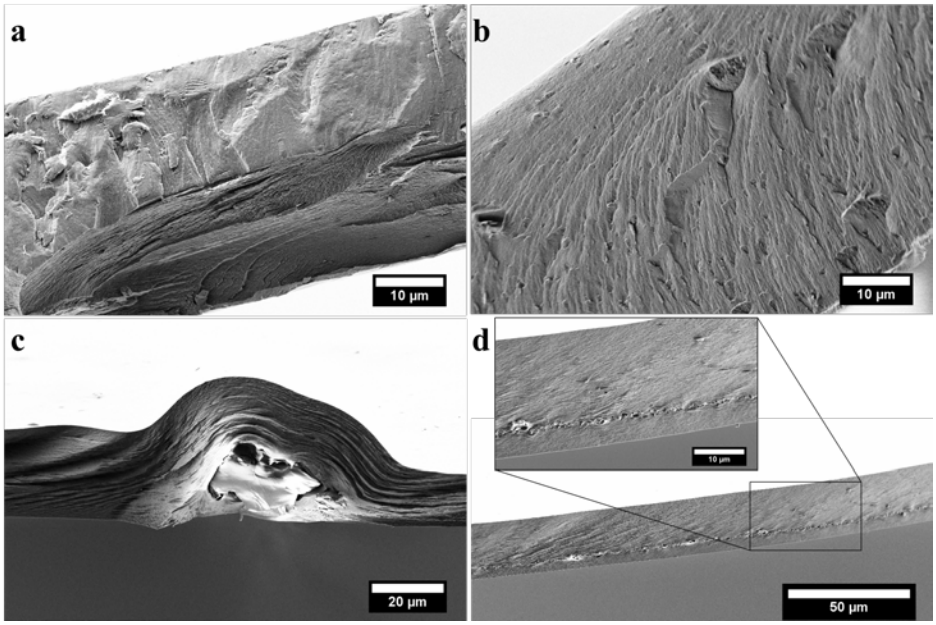

Figure 3 – SEM images of the membranes: cross-section view. The images represent: a) AL, b) AL/CH, c) AL+Met and d) AL/CH+Met. The inset highlights the layer of metronidazole.

By comparing the SEM images of AL (Figure 3a) and AL/CH (Figure 3b) no phase separation is observed, indicating homogeneous mixing between AL and CH. This observation also complements the results obtained from confocal microscopy measurements. Metronidazole appears as blocks of crystals both in the AL+Met and AL/CH+Met membranes (Figure 3c and 3d respectively). However, when the two polysaccharides are mixed a more homogenous layer of the drug can be seen, as in Figure 3d; this could derive from the interaction between metronidazole and both AL and CH causing its localization during the penetration of CH into the AL membrane. It is worth noticing how the drug is included within the membrane and not present on the surface of it.

Confocal microscopy was deployed to evaluate the distribution of FITC-labeled chitosan in the AL/CH membrane during its fabrication, as shown in Figure 4. While swelling, CH penetrates within the AL membrane. As it can be seen from the Fluorescein (FI) intensity % (Figure 4), the concentration of CH is higher at the borders than at the center of the membrane. This observation also supports the plausible electrostatic interactions between AL and CH which consequently improves the mechanical properties of the membranes. Having a higher concentration of CH on the borders is also beneficial for the DDS as a higher mucoadhesion can thereby be achieved. In terms of the application of the DDS, it is worth noticing that by having a membrane with two highly similar border layers, the patient would not have to worry which of the two sides is being applied.

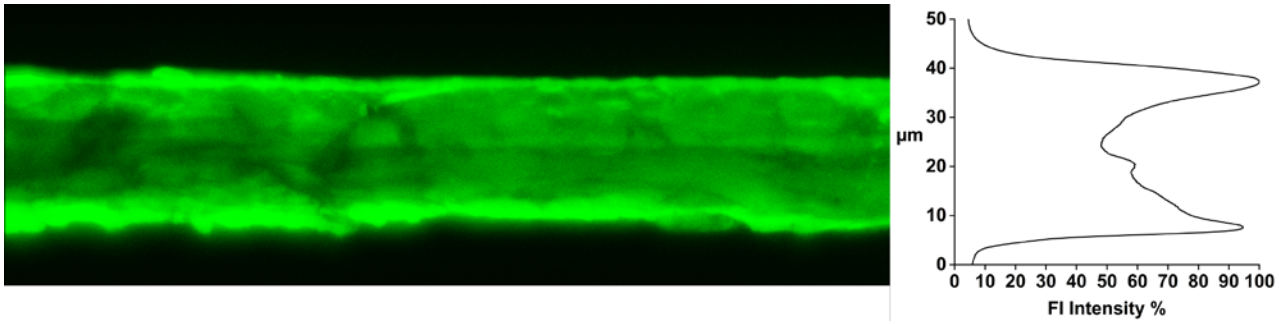

Figure 4 – Confocal microscopy of an AL/CH-FI membrane. To the left a cross-section image of an AL/CH-FI membrane (Z-stack average) shows the penetration of the fluorescein-labeled CH within the AL membrane. The Fluorescein (FI) intensity %, reported in the graph to the right, shows the maximum signal intensity on the borders of the membrane with a progressive reduction of the signal reaching the center of the membrane.

3.5. *In vitro* Mucoadhesion

Mucoadhesiveness is an important feature for a membrane to be used as a vaginal DDS. Chitosan was chosen to implement its intrinsic adhesive properties in the DDS and simultaneously strengthen the membrane due to its interactions with alginate. The mucoadhesiveness of AL/CH membranes was assessed with an adhesion study using a texture analyzer. Gilt´s vagina was used as a model tissue. The results, reported in Table 2, represent the force of adhesion and work of adhesion. Both the force and the work of adhesion were increased by adding CH to the DDS and the values are in line with what has previously been presented by Neves et al[35] for a 1% (w/w) Carbopol® 974P gel. The parameters chosen for the analysis were aimed at minimizing the plateau effect[35]. Specifically, the contact force and the contact time were kept at the lowest values suggested. The probe speed was instead chosen to minimize the plateau effect and the variance.

Table 2 – Mucoadhesion studies.

Mucoadhesion studies		
Sample	**F_{dt} (N) ± SD (N = 12)**	**W_{dt} (mJ) ± SD (N = 12)**
AL+Met	0.050 ± 0.006	0.202 ± 0.053
AL/CH+Met	0.077 ± 0.019***	0.497 ± 0.215**

Comparing the results obtained from AL+Met and AL/CH+Met, both the force of detachment and the work of adhesion were higher for the samples comprising CH. The observed difference was extremely significant for the detachment force (***p = 0.0003) whereas it was very significant for the work of adhesion (**p = 0.00138). It can be noticed that the variance is higher when considering the work of adhesion. Due to the high difference in terms of variance between the W_{ad} of AL+Met and AL/CH+Met the statistical analysis was performed using the Mann-Whitney U test. Overall, CH improved the adhesion of the membrane towards the vaginal tissue and demonstrated again the benefits of including this polysaccharide in the developed vaginal DDS.

3.6. Degradation

Understanding the degradation rate of a biodegradable membrane is highly important. The results of the degradation study performed depicted in Figure 5 show how AL/CH+Met membranes last for a long period in a simulated vaginal fluid at 37 °C. After 30 days, the membranes were almost disintegrated and the measurements were stopped. Such a long degradation time (50% of weight remaining after 30 days) opens up for the possibility of delivering pharmaceuticals over an extended period of time.

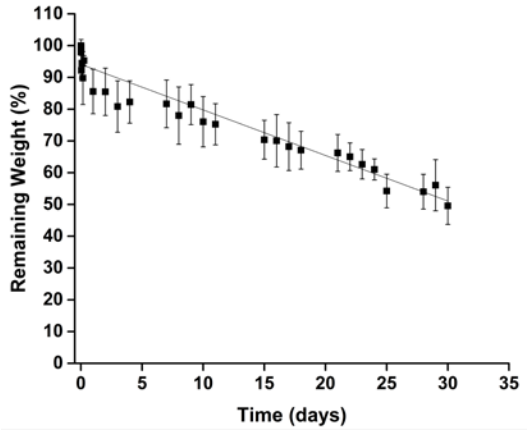

Figure 5 – Degradation of AL/CH+Met in a simulated vaginal medium. The linear fit, starting from 6 h of degradation, shows that the degradation follows a *quasi*-linear behavior. (R^2 = 0.97, N = 3, SD).

3.7. Dissolution of metronidazole

The release of metronidazole from AL/CH+Met membranes was evaluated with two different setups. In the first one the dissolution of the API included in the membranes and that of the free drug were compared (Figure 6a). The release obtained from the membranes results significantly different in the first hour compared to the one of the pure API (***p = 0.0004) and follows a typical diffusive kinetic. Due to the high amount of metronidazole included in the membranes, it was necessary to increase the volume used for the experiment to 25 mL. This volume is, however, not representative of the physiological vaginal environment,

where the average daily production of vaginal fluid is around 5 mL/day[23]. Nevertheless AL/CH+Met showed a more prolonged release than the pure API. Indeed, after 10 min in the dissolution medium, 98.5 ± 1.9 % of the pure metronidazole was dissolved, whereas only 70.4 ± 9.9 % of the metronidazole contained in the AL/CH+Met membrane was released (**p = 0.0085). A second comparison was made by assessing the dissolution of metronidazole from a commercially available formulation and that of AL/CH+Met membranes. The results reported in Figure 6, b showed that the release profile was similar for the two samples; the variance was instead higher for the commercial formulation.
The second setup tested was aimed at resembling the vaginal environment. SVF was poured at a flow rate of 5 mL/h over a tilted membrane. As the membrane became swollen, the drug was solubilized by the SVF. The results (Figure 6c) showed a much slower release compared to the previous setup, reaching 18.3 ± 2.3 % of the total metronidazole included in the membranes after 60 min. It is also worth noticing that the profile follows a *quasi*-zero order kinetic (R^2 = 0.97). With this simulation AL/CH+Met behaves as a prolonged DDS, in line with its very long degradation time.

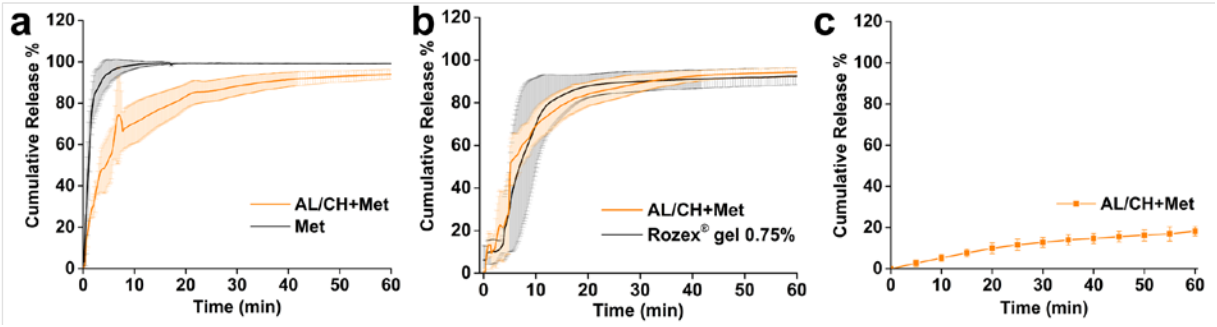

Figure 6 – Dissolution of metronidazole. The dissolution of metronidazole is expressed as cumulative release %, where 100% corresponds to the real amount of API present during in the samples. (a) release of metronidazole from AL/CH+Met compared to the puyre API, (b) release of metronidazole from AL/CH+Met compared to a commercial gel formulation, (c) release of metronidazole from AL/CH+Met (flow rate of the SVF = 5 mL/h). N ≥ 3, SD.

3.8. Biocompatibility assay

To evaluate the feasibility of the AL/CH+Met membrane as an intravaginal DDS, membrane *in vitro* toxicity was assessed on cervix epithelial cells Ect1/E6E7 using the AlamarBlue® assay[38]. The membranes were incubated in the cell culture medium for 24h to allow for a partial degradation and solubilization of the matrix componets. The extracts were consequently used to treat the cells for 24h and 48h (according to ISO 10993-5: Biological Evaluation of Medical Devices-Part 5: Tests for in Vitro Cytotoxicity, 2nd ed.; 1999). As shown in Figure 7, the cells treated with AL/CH or AL/CH+Met extracts showed no significant reduction of viability with respect to the control cells, both after 24h and 48h, indicating no toxic effects following the contact of the cells with the membrane components.

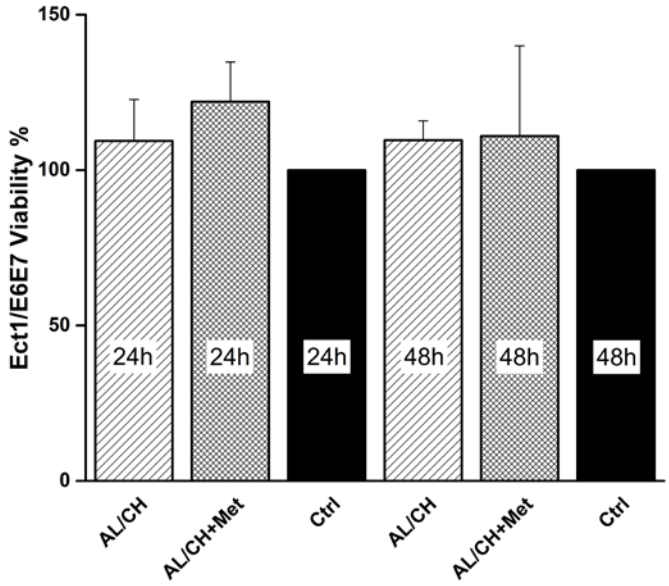

Figure 7 – Biocompatibility assay. AL/CH and AL/CH+Met membranes were tested and compared to the control, corresponding to 100% of viability. N = 3, SD.

3.9. Antimicrobial activity of the membranes

The antibacterial activity of AL/CH+Met membranes was assessed against *Staphilococcus aureus* and *Gardnerella vaginalis.* These two strains are mainly responsible for bacterial vaginosis, the model disease considered to evaluate the AL/CH DDS. As metronidazole is less effective in the presence of oxygen[26], the strains were treated in an oxygen deprived environment for 24h. After the treatment, the strains were seeded on petri dishes. *G.v.*was let to grow in a CO_2 enriched environment. The growth of both *S.a.* and *G.v.* is limited in anaerobic conditions but as metronidazole kills the bacteria, the difference between AL/CH, AL/CH+Met and Met could be evaluated over the petri dish. The results, reported in Figure 8, show how metronidazole is effective in killing both *S.a.* and *G.v.*. No statistical significance was found when comparing the results of AL/CH+Met and Met.

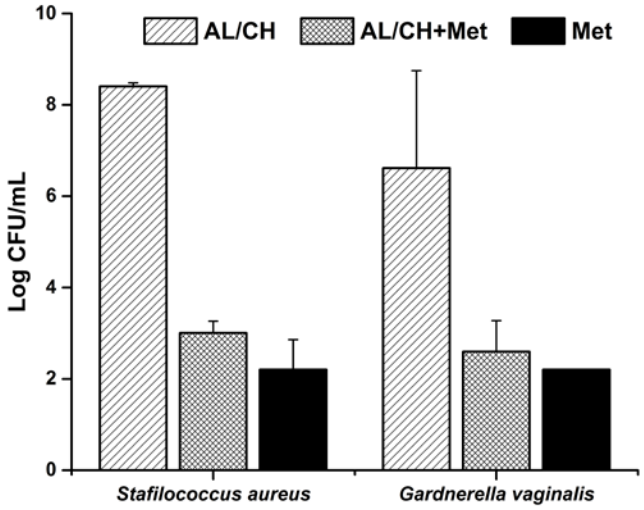

Figure 8 – Histogram representing the antibacterial activity of the membranes. To the left, the results obtained by treating *Staphiloccoccus aureus* with AL/CH, AL/CH+Met and Met are presented. To the right, the results from treating *Gardnerella vaginalis* with AL/CH, AL/CH+Met and Met are shown. N = 3, SD.

Compared to the control, both AL/CH+Met and Met reduced the CFU/mL count by > 4 logs for *S.a.*. In the case of *G.v.* the reduction resulted > 3 logs, instead.

4. Conclusions

In this work we fabricated an alginate/chitosan membrane as a potential drug delivery system to treat local vaginal diseases. The resulting fabrication is simple, highly tunable and upscalable. The developed DDS was sufficiently strong to endure handling both in the dry and in the swollen state. When dry, the membranes remained pliable and flexible. These membranes could be particularly effective for intravaginal administration due to their stability in a simulated vaginal fluid, where the swelling was seen to be limited and where the degradation occurred in a very slow fashion. The good mechanical properties of the swollen membrane together with the demonstrated mucoadhesiveness, enhanced by the addition of chitosan, make these membranes a promising intravaginal DDS. The ability of slowing the API release could find potential applications within medications requiring prolonged releases e.g. birth control APIs. Overall, the membrane represents a DDS suitable for intravaginal drug delivery. It is able to resist the vaginal environment and can attach to the tissue releasing metronidazole over time until its complete degradation.

5. Acknowledgements

The authors would like to acknowledge the Danish National Research Foundation (DNRF122) and Villum Fonden (Grant No. 9301) for Intelligent Drug Delivery and Sensing Using Microcontainers and Nanomechanics (IDUN). The authors would also like to acknowledge Claudio Cecone, Nicola Labovitis and Ho Duy Khiet for their initial help during the 2017 Summer School in Drug Delivery held at the Technical University of Denmark. Nanna Bild, Technical University of Denmark, is acknowledged for the drawing of the schematics.

6. Declaration of interest

None.

7. Data availability

The raw/processed data required to reproduce these findings are available to download from https://zenodo.org/record/1418734#.W5uUR84zbDB (DOI: 10.5281/zenodo.1418734).

8. References

(1) Pozzi, F.; Furlani, P.; Gazzaniga, A.; Davis, S.; Wilding, I. The Time Clock System: A New Oral Dosage Form for Fast and Complete Release of Drug after a Predetermined Lag Time. *J. Control. Release* 1994, *31* (1), 99–108.

(2) Mazzoni, C.; Tentor, F.; Strindberg, S. A.; Nielsen, L. H.; Keller, S. S.; Alstrøm, T. S.; Gundlach, C.; Müllertz, A.; Marizza, P.; Boisen, A. From Concept to in Vivo Testing: Microcontainers for Oral Drug Delivery. *J. Control. Release* 2017, *268* (September), 343–351.

(3) Sacco, P.; Decleva, E.; Tentor, F.; Menegazzi, R.; Borgogna, M.; Paoletti, S.; Kristiansen, K. A.; Vårum, K. M.; Marsich, E. Butyrate-Loaded Chitosan/Hyaluronan Nanoparticles: A Suitable Tool for Sustained Inhibition of ROS Release by Activated Neutrophils. *Macromol. Biosci.* 2017, *1700214*, 1700214.

(4) Barenholz, Y. Doxil®--the First FDA-Approved Nano-Drug: Lessons Learned. *J. Control. Release*

2012, *160* (2), 117–134.

(5) Lopes, C. M.; Bettencourt, C.; Rossi, A.; Buttini, F.; Barata, P. Overview on Gastroretentive Drug Delivery Systems for Improving Drug Bioavailability. *Int. J. Pharm.* 2016, *510* (1), 144–158.

(6) Hussain, A.; Ahsan, F. The Vagina as a Route for Systemic Drug Delivery. *J. Control. Release* 2005, *103* (2), 301–313.

(7) Bigucci, F.; Abruzzo, A.; Vitali, B.; Saladini, B.; Cerchiara, T.; Gallucci, M. C.; Luppi, B. Vaginal Inserts Based on Chitosan and Carboxymethylcellulose Complexes for Local Delivery of Chlorhexidine: Preparation, Characterization and Antimicrobial Activity. *Int. J. Pharm.* 2015, *478* (2), 456–463.

(8) Baloglu, E.; Senyigit, Z. A.; Karavana, S. Y.; Bernkop-Schnürch, A. Strategies to Prolong the Intravaginal Residence Time of Drug Delivery Systems. *J. Pharm. Pharm. Sci.* 2009, *12* (3), 312–336.

(9) Ceschel, G. C.; Maffei, P.; Lombardi Borgia, S.; Ronchi, C.; Rossi, S. Development of a Mucoadhesive Dosage Form for Vaginal Administration. *Drug Dev. Ind. Pharm.* 2001, *27* (6), 541–547.

(10) Dobaria, N. B.; Badhan, A. C.; Mashru, R. C. A Novel Itraconazole Bioadhesive Film for Vaginal Delivery: Design, Optimization, and Physicodynamic Characterization. *AAPS PharmSciTech* 2009, *10* (3), 951–959.

(11) El-Kamel, A.; Sokar, M.; Naggar, V.; Al Gamal, S. Chitosan and Sodium Alginate—Based Bioadhesive Vaginal Tablets. *AAPS PharmSci* 2002, *4* (4), 224–230.

(12) Abruzzo, A.; Bigucci, F.; Cerchiara, T.; Saladini, B.; Gallucci, M. C.; Cruciani, F.; Vitali, B.; Luppi, B. Chitosan/Alginate Complexes for Vaginal Delivery of Chlorhexidine Digluconate. *Carbohydr. Polym.* 2013, *91* (2), 651–658.

(13) LIU, P.; KRISHNAN, T. R. Alginate-Pectin-Poly-L-Lysine Particulate as a Potential Controlled Release Formulation. *J. Pharm. Pharmacol.* 1999, *51* (2), 141–149.

(14) Patel, N.; Lalwani, D.; Gollmer, S.; Injeti, E.; Sari, Y.; Nesamony, J. Development and Evaluation of a Calcium Alginate Based Oral Ceftriaxone Sodium Formulation. *Prog. Biomater.* 2016, *5* (2), 117–133.

(15) Agulhon, P.; Markova, V.; Robitzer, M.; Quignard, F.; Mineva, T. Structure of Alginate Gels: Interaction of Diuronate Units with Divalent Cations from Density Functional Calculations. *Biomacromolecules* 2012, *13* (6), 1899–1907.

(16) Haug, A.; Bjerrum, J.; Buchardt, O.; Olsen, G. E.; Pedersen, C.; Toft, J. The Affinity of Some Divalent Metals for Different Types of Alginates. *Acta Chemica Scandinavica.* 1961, pp 1794–1795.

(17) Draget, K. I.; Skjåk-Bræk, G.; Smidsrød, O. Alginate Based New Materials. *Int. J. Biol. Macromol.* 1997, *21* (1–2), 47–55.

(18) Sogias, I. a.; Williams, A. C.; Khutoryanskiy, V. V. Why Is Chitosan Mucoadhesive? *Biomacromolecules* 2008, *9* (7), 1837–1842.

(19) Lawrie, G.; Keen, I.; Drew, B.; Chandler-Temple, A.; Rintoul, L.; Fredericks, P.; Grøndahl, L. Interactions between Alginate and Chitosan Biopolymers Characterized Using FTIR and XPS. *Biomacromolecules* 2007, *8* (8), 2533–2541.

(20) Bierhalz, A. C. K.; Moraes, ï¿½ngela M. Tuning the Properties of Alginate—chitosan Membranes by Varying the Viscosity and the Proportions of Polymers. *J. Appl. Polym. Sci.* 2016, *133* (46), 1–11.

(21) Caetano, G. F.; Frade, M. A. C.; Andrade, T. A. M.; Leite, M. N.; Bueno, C. Z.; Moraes, Â. M.; Ribeiro-Paes, J. T. Chitosan-Alginate Membranes Accelerate Wound Healing. *J. Biomed. Mater. Res. - Part B Appl. Biomater.* 2015, *103* (5), 1013–1022.

(22) Wang, L.; Khor, E.; Wee, A.; Lim, L. Y. Chitosan-Alginate PEC Membrane as a Wound Dressing: Assessment of Incisional Wound Healing. *J. Biomed. Mater. Res.* 2002, *63* (5), 610–618.

(23) Owen, D. H.; Katz, D. F. A Vaginal Fluid Simulant. *Contraception* 1999, *59* (2), 91–95.

(24) Reddy, N. H. S.; Patnala, S.; Löbenberg, R.; Kanfer, I. In Vitro Dissolution of Generic Immediate-Release Solid Oral Dosage Forms Containing BCS Class I Drugs: Comparative Assessment of Metronidazole, Zidovudine, and Amoxicillin Versus Relevant Comparator Pharmaceutical Products in South Africa and India. *AAPS PharmSciTech* 2014, *15* (5), 1076–1086.

(25) Dingsdag, S. A.; Hunter, N. Metronidazole: An Update on Metabolism, Structure–cytotoxicity and Resistance Mechanisms. *J. Antimicrob. Chemother.* 2017, No. June, 265–279.

(26) Löfmark, S.; Edlund, C.; Nord, C. E. Metronidazole Is Still the Drug of Choice for Treatment of Anaerobic Infections. *Clin. Infect. Dis.* 2010, *50* (s1), S16–S23.

(27) Hay, P. Bacterial Vaginosis. *Medicine (Baltimore).* 2014, *4* (4), 359–363.

(28) Donders, G. G. G.; Ruban, K.; Bellen, G. Selecting Anti-Microbial Treatment of Aerobic Vaginitis. *Curr. Infect. Dis. Rep.* 2015, *17* (5), 1–7.

(29) Schwebke, J. R.; Muzny, C. A.; Josey, W. E. Role of Gardnerella Vaginalis in the Pathogenesis of Bacterial Vaginosis: A Conceptual Model. *J. Infect. Dis.* 2014, *210* (3), 338–343.

(30) Turovskiy, Y.; Noll, K. S.; Chikindas, M. L.; A, A. The Etiology of Bacterial Vaginosis. *J. Appl. Microbiol.* 2011, *110* (5), 1105–1128.

(31) Ingar Draget, K.; Østgaard, K.; Smidsrød, O. Homogeneous Alginate Gels: A Technical Approach. *Carbohydr. Polym.* 1990, *14* (2), 159–178.

(32) Porrelli, D.; Travan, A.; Turco, G.; Marsich, E.; Borgogna, M.; Paoletti, S.; Donati, I. Alginate-Hydroxyapatite Bone Scaffolds with Isotropic or Anisotropic Pore Structure: Material Properties and Biological Behavior. *Macromol. Mater. Eng.* 2015, *300* (10), 989–1000.

(33) Jang, J.; Seol, Y. J.; Kim, H. J.; Kundu, J.; Kim, S. W.; Cho, D. W. Effects of Alginate Hydrogel Cross-Linking Density on Mechanical and Biological Behaviors for Tissue Engineering. *J. Mech. Behav. Biomed. Mater.* 2014, *37*, 69–77.

(34) Sacco, P.; Brun, F.; Donati, I.; Porrelli, D.; Paoletti, S.; Turco, G. On the Correlation between the Microscopic Structure and Properties of Phosphate-Cross-Linked Chitosan Gels. *ACS Appl. Mater. Interfaces* 2018, *10* (13), 10761–10770.

(35) das Neves, J.; Amaral, M. H.; Bahia, M. F. Performance of an in Vitro Mucoadhesion Testing Method for Vaginal Semisolids: Influence of Different Testing Conditions and Instrumental Parameters. *Eur. J. Pharm. Biopharm.* 2008, *69* (2), 622–632.

(36) Kong, M.; Chen, X. G.; Xing, K.; Park, H. J. Antimicrobial Properties of Chitosan and Mode of Action: A State of the Art Review. *Int. J. Food Microbiol.* 2010, *144* (1), 51–63.

(37) Baysal, K.; Aroguz, A. Z.; Adiguzel, Z.; Baysal, B. M. Chitosan/Alginate Crosslinked Hydrogels: Preparation, Characterization and Application for Cell Growth Purposes. *Int. J. Biol. Macromol.* 2013, *59* (April), 342–348.

(38) Travan, A.; Marsich, E.; Donati, I.; Benincasa, M.; Giazzon, M.; Felisari, L.; Paoletti, S. Silver-Polysaccharide Nanocomposite Antimicrobial Coatings for Methacrylic Thermosets. *Acta Biomater.* 2011, *7* (1), 337–346.

Long lasting mucoadhesive membrane based on alginate and chitosan for intravaginal drug delivery.

F. Tentor[1,*], G. Siccardi[2], P. Sacco[3], D. Demarchi[2], E. Marsich[4], K. Almdal[1], S. Bose Goswami[1], A. Boisen[1]

[*]Corresponding author, fabt@nanotech.dtu.dk; Fax: 45887762

[1]Department of Micro- and Nanotechnology, Technical University of Denmark, Ørsteds Plads 345C, 2800 Kgs. Lyngby, Denmark

[2]Department of Electronics and Telecommunications, Politecnico di Torino, 10129 Torino, Italy

[3]Department of Life Sciences, University of Trieste, via L. Giorgieri 5, I-34127 Trieste, Italy

[4]Department of Medicine, Surgery and Health Sciences, University of Trieste, Piazza dell'Ospitale 1, I-34129 Trieste, Italy

Supporting information

Here we report additional information about the mechanical properties of the samples investigated. We moreover share the raw and processed data of the swelling, degradation and antibacterial studies.

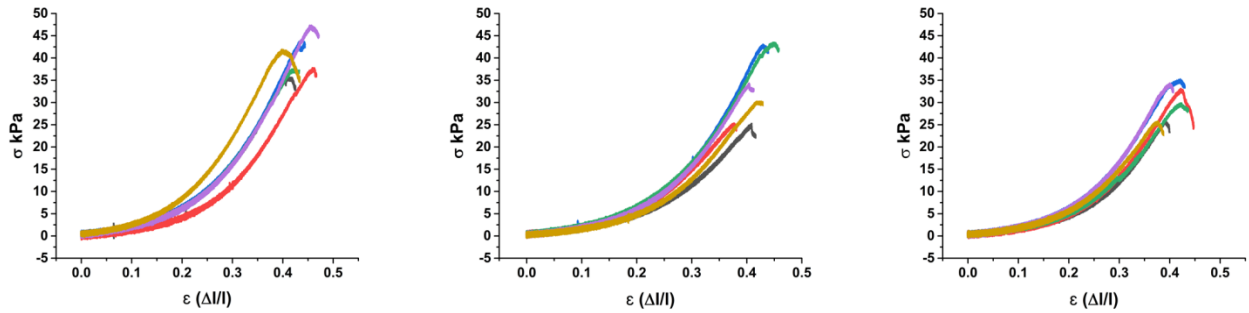

Figure S1 – Stress strain curves of three indipendent AL membranes samples after 10 min of soaking in simulated vaginal fluid.

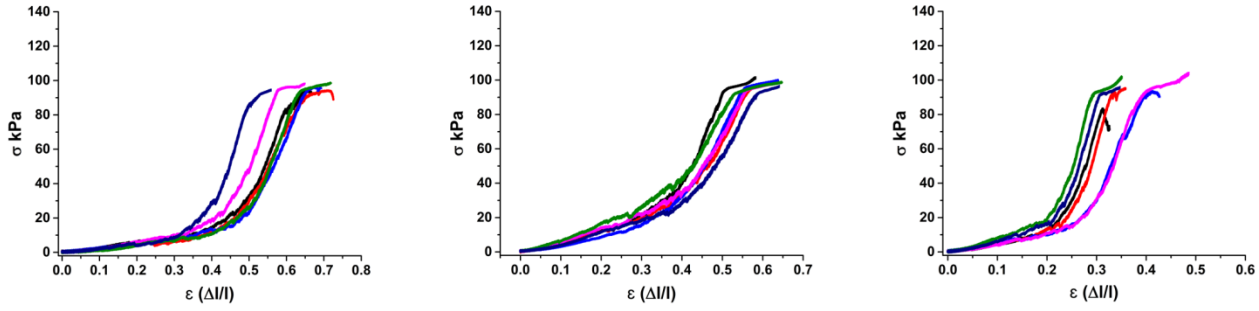

Figure S2 – Stress strain curves of three indipendent AL/CH membranes samples after 10 min of soaking in simulated vaginal fluid.

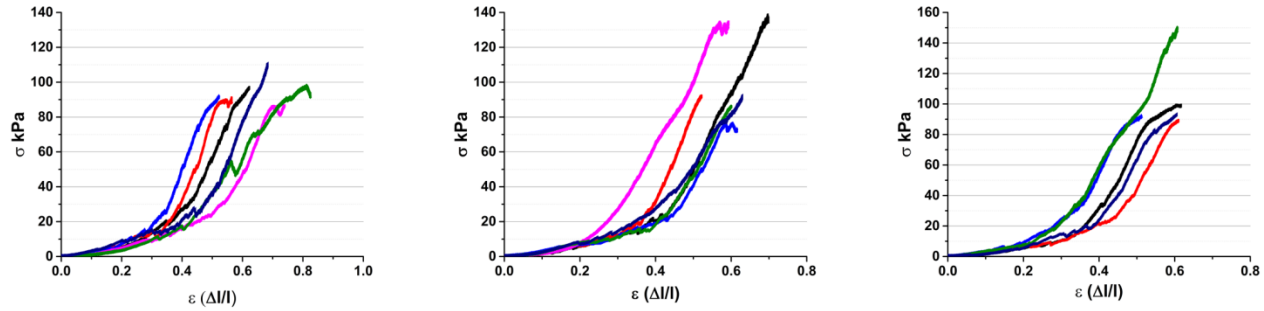

Figure S3 – Stress strain curves of three indipendent AL/CH+Met membranes samples after 10 min of soaking in simulated vaginal fluid.

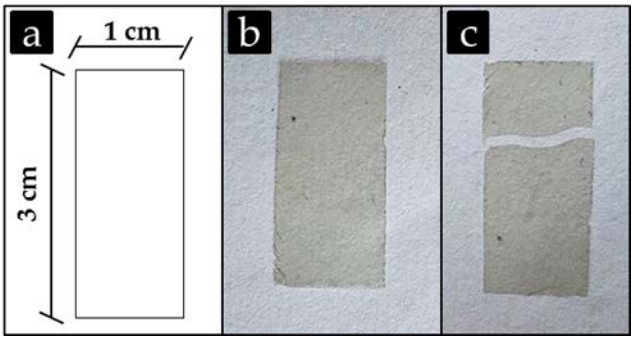

Figure S4 – Tensile stress test: a) schematic representation of the sample, b) an AL/CH+Met sample, c) membrane sample after rupture.

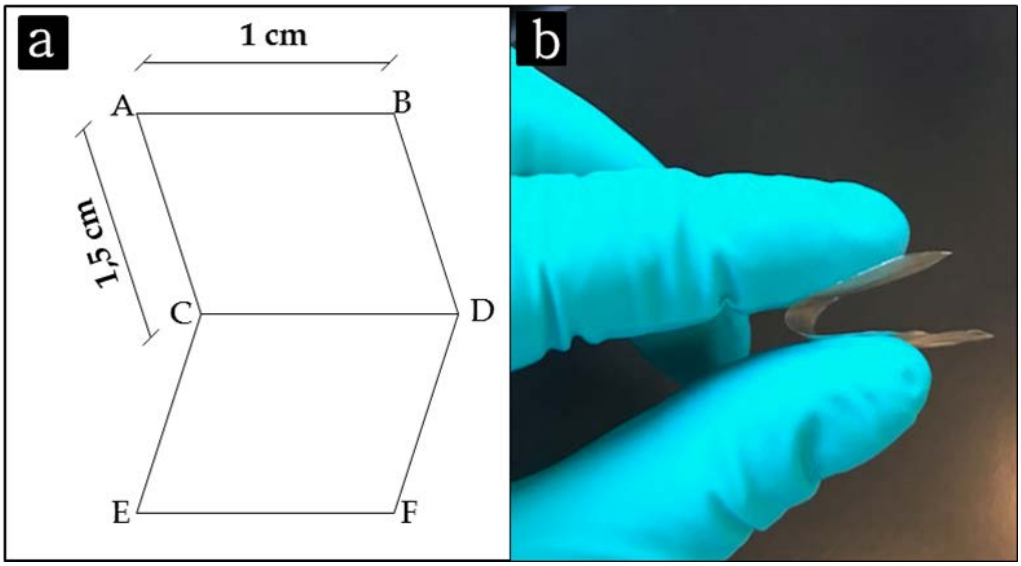

Figure S5 – Flexibility of the AL/CH+Met membrane. A schematic representation of the AL/CH+Met sample is depicted in a). A sample being flexed manually can be seen in b).

Swelling in Simulated Vaginal Fluid

AL Sample

Time (min)	Sample 1	Sample 2	Sample 3	Water Uptake %	Water Uptake %	Water Uptake %	Time (min)	Average	Standard deviation
0	32.289	33.978	30.806	0	0	0	0	0	0
5	286.6	274.8	215.4	787.6087832	708.7586085	599.2144387	5	698.5272768	94.61298729
10	374.5	365.2	260.6	1059.837716	974.8131144	745.9391028	10	926.8633109	162.3498461
15	390	370.1	281.1	1107.84168	989.2342104	812.4845809	15	969.8534904	148.6292811
30	361.1	414.5	370.1	1018.337514	1119.906999	1101.38934	30	1079.877951	54.09385292
60	363.3	408.1	303.4	1025.15098	1101.071281	884.8730767	60	1003.698446	109.6839749
120	353.3	407.4	306.8	994.1806807	1099.011125	895.9098877	120	996.3672311	101.568272
240	325.6	410.8	275.3	908.3929512	1109.0176	793.6570798	240	937.0225435	159.6176824
360	353.8	399.1	260.2	995.7291957	1074.583554	744.6406544	360	938.3178014	172.3009878
1440	314.2	367.1	273.7	873.0868097	980.4049679	788.4632864	1440	880.651688	96.19419326

Swelling in Simulated Vaginal Fluid

AL/CH Sample

Time (min)	Sample 1	Sample 2	Sample 3	Water Uptake %	Water Uptake %	Water Uptake %	Time (min)	Average	Standard deviation
0	34.565	26.096	17.861	0	0	0	0	0	0
5	214.5	207.7	173.3	520.5699407	695.9074188	870.2704216	5	695.5825937	174.8504667
10	300	263.1	215.7	767.929987	908.2004905	1107.659146	10	927.9298744	170.7217378
15	325.6	271.6	210.3	841.9933459	940.7725322	1077.425676	15	953.3971847	118.2228062
30	350.2	270.1	200.7	913.1636048	935.0245248	1023.677286	30	957.2884718	58.52419087
60	340.1	206.1	210.7	883.9432952	689.7762109	1079.665192	60	884.4615662	194.9450074
120	319.8	210.1	234.9	825.2133661	705.1042305	1215.155926	120	915.157841	266.656501
240	329.8	203.5	215.6	854.1443657	679.8129982	1107.099267	240	880.3522101	214.8453563
360	315.4	210.5	220.8	812.4837263	706.6370325	1136.212978	360	885.1112456	223.8078208
1440	364.7	198.7	230.8	955.1135542	661.4193746	1192.200885	1440	936.2446045	265.8933636

Swelling in milliQ water

AL Sample

Time (min)	Sample 1	Sample 2	Sample 3	Water Uptake %	Water Uptake %	Water Uptake %	Time (min)	Average	Standard deviation
0	20.26	24.27	23.72	0	0	0	0	0	0
5	704.7	980.1	990.8	3378.28233	3938.318912	4077.065767	5	3797.889003	369.9526898
10	909.6	1100.1	1140.8	4389.634748	4432.756489	4709.443508	10	4510.611582	173.5381001
15	984.2	1280.1	1087.4	4757.847976	5174.412855	4484.317032	15	4805.525955	347.5096453
30	1000.52	1092	990.5	4838.40079	4399.381953	4075.801012	30	4437.861252	382.7533117
60	754	670.9	689.1	3621.618954	2664.318088	2805.143339	60	3030.360127	516.8638002
120	102	135.6	115.5	403.4550839	458.7144623	386.93086	120	416.3668021	37.59329379
240							240		
360							360		
1440							1440		

Swelling in milliQ water

AL/CH Sample

Time (min)	Sample 1	Sample 2	Sample 3	Water Uptake %	Water Uptake %	Water Uptake %	Time (min)	Average	Standard deviation
0	27.51	19.71	29.1	0	0	0	0	0	0
5	920.7	752.4	964.35	3246.782988	3717.351598	3213.917526	5	3392.684037	281.6501437
10	1001.9	950.7	1134.6	3541.948382	4723.439878	3798.969072	10	4021.452444	621.3732186
15	989.4	648.6	433	3496.51036	3190.715373	1387.972509	15	2691.732747	1139.394889
30	800.6	563.5	370.2	2810.214467	2758.954845	1172.164948	30	2247.11142	931.2836976
60	203.6	198.7	157.6	640.0945111	908.1177067	441.580756	60	663.2643246	234.1299037
120							120		
240							240		
360							360		
1440							1440		

Degradation Studies in Simulated Vaginal Fluid

Time (days)	Membrane 1 Weight (mg)	Membrane 2 Weight (mg)	Membrane 3 Weight (mg)	Membrane 1 Remaining Weight %	Membrane 2 Remaining Weight %	Membrane 3 Remaining Weight %	Time (days)	Average Remaining Weight %	Standard Deviation Remaining Weight %
0.00694	517.78	624.6	598.6	100	100	100	0.00694	100	0
0.01042	501	601.3	604	96.75924138	96.26961255	100.9021049	0.01042	97.97698628	2.545029146
0.02083	527.81	620.5	580.4	101.9371161	99.34357989	96.95957234	0.02083	99.41342279	2.489506804
0.04167	488.27	559.3	555.8	94.30066824	89.545309	92.84998329	0.04167	92.23198684	2.437170508
0.08333	459.2	601.4	587.4	88.68631465	96.2856228	98.12896759	0.08333	94.36696835	5.005182296
0.16667	513.5	520.7	519.9	99.17339411	83.36535383	86.8526562	0.16667	89.79713471	8.305179086
0.25	502.5	587.12	567.7	97.0489397	93.99935959	94.83795523	0.25	95.29541817	1.575417081
1	470.3	484.7	528.5	90.83008227	77.60166507	88.2893418	1	85.57369638	7.019886252
2	466.1	480.1	535.6	90.01892696	76.86519372	89.4754427	2	85.45318779	7.442383717
3	448.2	447	505	86.56186025	71.56580211	84.36351487	3	80.83039241	8.0983119
4	446.5	465.8	514.6	86.23353548	74.57572847	85.96725693	4	82.25884029	6.65510192
7	453	457.2	504.8	87.4888949	73.19884726	84.33010358	7	81.67261524	7.506533722
8	446.5	427	475.1	86.23353548	68.3637528	79.36852656	8	77.98860495	9.014456222
9	429.2	465.6	520.1	82.8923481	74.54370797	86.88606749	9	81.44070786	6.297928562
10	427.9	420	468.3	82.64127622	67.24303554	78.2325426	10	76.03895145	7.930027463
11	420.7	427.2	455.7	81.25072425	68.39577329	76.12763114	11	75.25804289	6.47144333
15	400.73	421.4	396.6	77.39387385	67.46717899	66.25459405	15	70.3718823	6.111371739
16	409.8	393.5	407.2	79.14558307	63.0003202	68.02539258	16	70.05709862	8.262157725
17	388.2	375.4	416.3	74.97392715	60.10246558	69.54560641	17	68.20733305	7.525511546
18	381.5	388	392.1	73.67994129	62.11975664	65.50283996	18	67.10084596	5.943457297
21	373.5	378	395.2	72.13488354	60.51873199	66.020715	21	66.22477684	5.810763732
22	353.7	375.1	399	68.31086562	60.05443484	66.65552957	22	65.00694334	4.368127713
23	346.1	360.2	379.7	66.84306076	57.6689081	63.43133979	23	62.64776955	4.636998597
24	325.7	357.3	377.1	62.90316351	57.20461095	62.99699298	24	61.03492248	3.317478832
25	290.6	301.5	349.1	56.12422264	48.27089337	58.31941196	25	54.23817599	5.283091939
28	300.4	298.4	336.8	58.01691838	47.77457573	56.26461744	28	54.01870385	5.478091972
29	333.4	301.9	332.1	64.39028159	48.33493436	55.47945205	29	56.06822267	8.043850557
30	290.2	300.1	267.1	56.04696976	48.04674992	44.62078182	30	49.5715005	5.863709654

G. vaginalis
Starting bacteria concentration 5 * 10^6

AL/CH	CFU/plate	Diluition factor	bacteria in 25 µl	CFU/mL	log10	Average	Standard deviation
24 h	NC	1	#VALUE!	#VALUE!	#VALUE!		
	NC	10	#VALUE!	#VALUE!	#VALUE!		
	49	100	4900	196000	5.292256071		
	11	1000	11000	440000	5.643452676		
	0	10000	0	0	#NUM!		
	0	100000	0	0	#NUM!	5.467854374	0.248333501

AL/CH + metronidazole 4 mg	CFU/plate	Diluition factor	bacteria in 25 µl	CFU/mL	log10	Average	Standard deviation
24 h	4	1	4	160	2.204119983		
	0	10	0	0	#NUM!		
	0	100	0	0	#NUM!		
	0	1000	0	0	#NUM!		
	0	10000	0	0	#NUM!		
	0	100000	0	0	#NUM!	2.204119983	#DIV/0!

Metronidazole 4 mg	CFU/plate	Diluition factor	bacteria in 25 µl	CFU/mL	log10	Average	Standard deviation
24 h	4	1	4	160	2.204119983		
	0	10	0	0	#NUM!		
	0	100	0	0	#NUM!		
	0	1000	0	0	#NUM!		
	0	10000	0	0	#NUM!		
	0	100000	0	0	#NUM!	2.204119983	#DIV/0!

Sample	Log CFU/mL	Standard deviation
AL/CH	5.5	0.2
AL/CH + metronidazole 4 mg	2.2	#DIV/0!
Metronidazole 4 mg	2.2	#DIV/0!

AL/CH	CFU/plate	Diluition factor	bacteria in 25 µl	CFU/mL	log10	Average	Standard deviation
24 h	NC	1	#VALUE!	#VALUE!	#VALUE!		
	NC	10	#VALUE!	#VALUE!	#VALUE!		
	27	100	2700	108000	5.033423755		
	9	1000	9000	360000	5.556302501		
	0	10000	0	0	#NUM!		
	0	100000	0	0	#NUM!	5.294863128	0.369731107

AL/CH + metronidazole 4 mg	CFU/plate	Diluition factor	bacteria in 25 µl	CFU/mL	log10	Average	Standard deviation
24 h	4	1	4	160	2.204119983		
	0	10	0	0	#NUM!		
	0	100	0	0	#NUM!		
	0	1000	0	0	#NUM!		
	0	10000	0	0	#NUM!		
	0	100000	0	0	#NUM!	2.204119983	#DIV/0!

Metronidazole 4 mg	CFU/plate	Diluition factor	bacteria in 25 µl	CFU/mL	log10	Average	Standard deviation
24 h	4	1	4	160	2.204119983		
	0	10	0	0	#NUM!		
	0	100	0	0	#NUM!		
	0	1000	0	0	#NUM!		
	0	10000	0	0	#NUM!		
	0	100000	0	0	#NUM!	2.204119983	#NUM!

Sample	Log CFU/mL	Standard deviation
AL/CH	5.3	0.4
AL/CH + metronidazole 4 mg	2.2	#DIV/0!
Metronidazole 4 mg	2.2	#NUM!

AL/CH	CFU/plate	Diluition factor	bacteria in 25 µl	CFU/mL	log10	Average	Standard deviation
24 h	NC	1	#VALUE!	#VALUE!	#VALUE!		
	NC	10	#VALUE!	#VALUE!	#VALUE!		
	NC	100	#VALUE!	#VALUE!	#VALUE!		
	NC	1000	#VALUE!	#VALUE!	#VALUE!		
	NC	10000	#VALUE!	#VALUE!	#VALUE!		
	300	100000	30000000	1200000000	9.079181246	9.079181246	#VALUE!

AL/CH + metronidazole 4 mg	CFU/plate	Diluition factor	bacteria in 25 µl	CFU/mL	log10	Average	Standard deviation
24 h	18	1	18	720	2.857332496		
	4	10	40	1600	3.204119983		
	3	100	300	12000	4.079181246		
	0	1000	0	0	#NUM!		
	0	10000	0	0	#NUM!		
	0	100000	0	0	#NUM!	3.380211242	0.863977536

metronidazole 4 mg	CFU/plate	Diluition factor	bacteria in 25 µl	CFU/mL	log10	Average	Standard deviation
24 h	4	1	4	160	2.204119983		
	0	10	0	0	#NUM!		
	0	100	0	0	#NUM!		
	0	1000	0	0	#NUM!		
	0	10000	0	0	#NUM!		
	0	100000	0	0	#NUM!	2.204119983	#DIV/0!

Sample	Log CFU/mL	Standard deviation
AL/CH	9.1	#VALUE!
AL/CH + metronidazole 4 mg	3.4	0.9
metronidazole 4 mg	2.2	#DIV/0!

Sample	Log CFU/mL	Log CFU/mL	Log CFU/mL	Average Log CFU/mL	Standard Deviation
AL/CH	5.467854374	5.294863128	9.079181246	6.613966249	2.136690251
AL/CH + metronidazole 4 mg	2.204119983	2.204119983	3.380211242	2.596150402	0.679016605
Metronidazole 4 mg	2.204119983	2.204119983	2.204119983	2.204119983	0

S. aureus
Starting bacteria concentration 5 * 10^6

AL/CH	CFU/plate	Diluition factor	bacteria in 25 µl	CFU/mL	log10	Average	Standard deviation
24 h	NC	1	#VALUE!	#VALUE!	#VALUE!		
	NC	10	#VALUE!	#VALUE!	#VALUE!		
	NC	100	#VALUE!	#VALUE!	#VALUE!		
	NC	1000	#VALUE!	#VALUE!	#VALUE!		
	528	10000	5280000	211200000	8.324693914		
	-	100000	#VALUE!	#VALUE!	#VALUE!	**8.324693914**	**#DIV/0!**

AL/CH + metronidazole 4 mg	CFU/plate	Diluition factor	bacteria in 25 µl	CFU/mL	log10	Average	Standard deviation
24 h	9	1	9	360	2.556302501		
	3	10	30	1200	3.079181246		
	0	100	0	0	#NUM!		
	0	1000	0	0	#NUM!		
	0	10000	0	0	#NUM!		
	0	100000	0	0	#NUM!	**2.817741873**	**0.369731107**

Metronidazole 4 mg	CFU/plate	Diluition factor	bacteria in 25 µl	CFU/mL	log10	Average	Standard deviation
24 h	0	1	0	0	#NUM!		
	2	10	20	800	2.903089987		
	0	100	0	0	#NUM!		
	0	1000	0	0	#NUM!		
	0	10000	0	0	#NUM!		
	0	100000	0	0	#NUM!	**2.903089987**	**#DIV/0!**

Sample	Log CFU/mL	Standard deviation
AL/CH	8.3	#DIV/0!
AL/CH + metronidazole 4 mg	2.8	0.4
Metronidazole 4 mg	2.9	#DIV/0!

AL/CH	CFU/plate	Diluition factor	bacteria in 25 µl	CFU/mL	log10	Average	Standard deviation
24 h	NC	1	#VALUE!	#VALUE!	#VALUE!		
	NC	10	#VALUE!	#VALUE!	#VALUE!		
	NC	100	#VALUE!	#VALUE!	#VALUE!		
	NC	1000	#VALUE!	#VALUE!	#VALUE!		
	240	10000	2400000	96000000	7.982271233		
	173	100000	17300000	692000000	8.840106094	**8.411188664**	**0.606580848**

AL/CH + metronidazole 4 mg	CFU/plate	Diluition factor	bacteria in 25 µl	CFU/mL	log10	Average	Standard deviation
24 h	31	1	31	1240	3.093421685		
	8	10	80	3200	3.505149978		
	0	100	0	0	#NUM!		
	0	1000	0	0	#NUM!		
	0	10000	0	0	#NUM!		
	0	100000	0	0	#NUM!	**3.299285832**	**0.291135868**

Metronidazole 4 mg	CFU/plate	Diluition factor	bacteria in 25 µl	CFU/mL	log10	Average	Standard deviation
24 h	1	1	1	40	1.602059991		
	1	10	10	400	2.602059991		
	0	100	0	0	#NUM!		
	0	1000	0	0	#NUM!		
	0	10000	0	0	#NUM!		
	0	100000	0	0	#NUM!	**2.102059991**	**0.707106781**

Sample	Log CFU/mL	Standard deviation
AL/CH	8.4	0.6
AL/CH + metronidazole 4 mg	3.3	0.3
Metronidazole 4 mg	2.1	0.7

AL/CH	CFU/plate	Diluition factor	bacteria in 25 µl	CFU/mL	log10	Average	Standard deviation
24 h	NC	1	#VALUE!	#VALUE!	#VALUE!		
	NC	10	#VALUE!	#VALUE!	#VALUE!		
	NC	100	#VALUE!	#VALUE!	#VALUE!		
	NC	1000	#VALUE!	#VALUE!	#VALUE!		
	446	10000	4460000	178400000	8.25139485		
	127	100000	12700000	508000000	8.705863712	**8.478629281**	**0.321358014**

AL/CH + metronidazole 4 mg	CFU/plate	Diluition factor	bacteria in 25 µl	CFU/mL	log10	Average	Standard deviation
24 h	4	1	4	160	2.204119983		

	0	10	0	0	#NUM!		
	1	100	100	4000	3.602059991		
	0	1000	0	0	#NUM!		
	0	10000	0	0	#NUM!		
	0	100000	0	0	#NUM!	**2.903089987**	**0.98849286**

metronidazole 4 mg	**CFU/plate**	**Diluition factor**	**bacteria in 25 µl**	**CFU/mL**	**log10**	**Average**	**Standard deviation**
24 h	1	1	1	40	1.602059991		
	0	10	0	0	#NUM!		
	0	100	0	0	#NUM!		
	0	1000	0	0	#NUM!		
	0	10000	0	0	#NUM!		
	0	100000	0	0	#NUM!	**1.602059991**	**#DIV/0!**

Sample	Log CFU/mL	Standard deviation
AL/CH	8.5	0.3
AL/CH + metronidazole 4 mg	2.9	1.0
metronidazole 4 mg	1.6	#DIV/0!

Sample	**Log CFU/mL**	**Log CFU/mL**	**Log CFU/mL**	**Average Lo**	**Standard Deviation**
AL/CH	8.32469391	8.411188664	8.478629281	8.4048373	0.077163977
AL/CH + metronidazole 4 mg	2.81774187	3.299285832	2.903089987	3.0067059	0.25695007
Metronidazole 4 mg	2.90308999	2.102059991	1.602059991	2.2024033	0.656293647

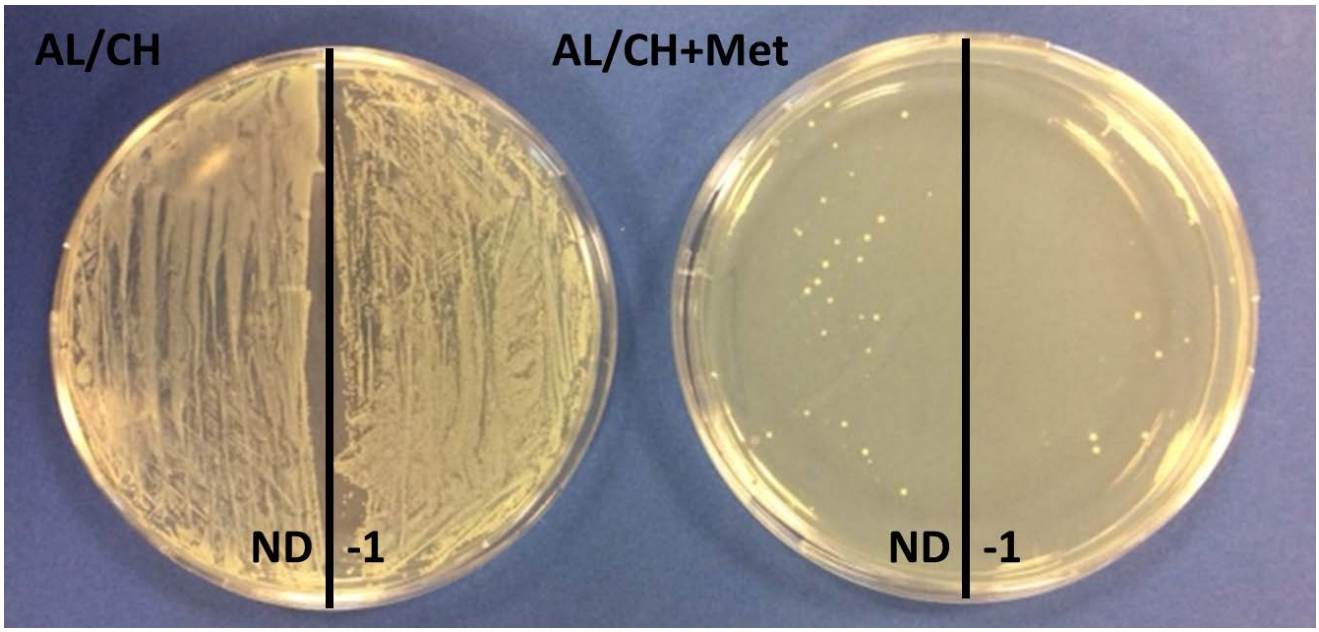

Figure S6 – Example of a *Staphilococcus aureus* growth treated with the control samples, AL/CH, to the left and with AL/CH+Met to the right. For both Petri dishes the not diluted (ND) sample and the sample diluted ten times are shown.

Paper V

Ultrasonic spray coating: a novel, continuous and tunable method for the fabrication of polymeric nanoparticles

F. Tentor, P.E. Larsen, S. Basak, N. Kamaly, K. Almdal, S.B. Goswami, A. Boisen

Manuscript to be submitted to *Lagmuir*

Controlling the size distribution of polymeric nanoparticles using an ultrasonic spray coater: a continuous and tunable fabrication process.

F. Tentor*, P.E. Larsen, S. Basak, N. Kamaly, K. Almdal, S.B. Goswami, A. Boisen

*Corresponding author, fabt@nanotech.dtu.dk
Department of Micro- and Nanotechnology, Technical University of Denmark, Ørsteds Plads 345C, 2800 Kgs. Lyngby, Denmark

Keywords: Ultrasonic spray coater, Nanoparticles, Dynamic light scattering, Size distribution, Polyelectrolyte copmplexes.

Abstract

Polymeric nanoparticles, fabricated exploiting the electrostatic interaction between oppositely charged polymers, have been extensively studied as potential drug delivery systems. In particular, several research groups devoted their attention to the development of polymeric nanoparticles using novel materials, with the aim of providing the formulation with specific properties. Polymeric nanoparticles have been fabricated using different techniques, each one bestowing advantages and disadvantaged. In this contribution, the usage of an ultrasonic spray coater, as continuous and tunable method for the fabrication of polymeric nanoparticles, has been investigated. The influence of the parameters controlling the atomization induced by the ultrasonic spray coater on the size distribution of the fabricated nanoparticles was assessed by means of dynamic light scattering. The results demonstrated the possibility of tuning the nanoparticles size distribution modifying the parameters of the ultrasonic spray coater and supported the theory by which an increase in the power of the ultrasounds causes the formation of bigger droplets in the atomized solutions.

1. Introduction

Within the field of nanomaterials, nanoparticles represent a highly interesting material. The term nanoparticle is considered appropriate, as defined by the directive (2011/696/EU), only when 50% or more of the particles lies in the size range of 1 nm to 100 nm[1]. Nanoparticles have been, and still represent, a topic in which many research groups focus their attention[2–6]. This is due to their application in different fields, from photonics[7] to drug delivery[6]. There are several different types of nanoparticles that can be made, depending on their application. Metallic nanoparticle, such as gold nanoparticles, have been used in spectroscopy for enhancing Raman signals[8]. Silver nanoparticles have been used for their antibacterial properties[9]. Liposomes and polymeric nanoparticles have been extensively studied for drug delivery purposes, instead. There are many advantages of using liposomes and nanoparticles as drug delivery systems (DDS) compared to traditional formulations: i) they can encapsulate an active pharmaceutical ingredient (API)[6,10] and ii) control its release overtime[11], they

can be used to iii) reduce the chances of side effects[12] and iv) increase bioavailability[13,14]. They are v) highly tunable, several research groups have in fact demonstrated how it is possible to modify their surface to target specific cell lines[15,16]. The interest on polymeric nanoparticles also comes from the fact that they can be fabricated using very different materials[6,14,16]. These materials can have specific properties able that enhance the final formulation, in examples: adhesiveness (i.e. chitosan)[17], stealthiness towards the immune system (i.e. poly-ethylenglycol)[18] and pH controlled release (i.e. Eudragit® S100)[19].

In this manuscript we focus our attention on polymeric nanoparticles, and, specifically, to those that are constituted of positively and negatively charged polymer and that exploit the electrostatic interaction between them to form nanoparticles. Several techniques have been proposed to fabricate polymeric nanoparticles, each one having benefits and drawbacks. The "manual" approach may be the easiest[6,20]. It consists of having two solutions, one including a negatively charged polymer and the other one including a positively charged polymer. One of the two is kept under stirring whilst the other is added dropwise to the former. This technique is certainly the most intuitive and the easiest, it is however non-upscalable, it is done in small batches and the results can differ significantly based on the operator. An alternative common method to fabricate nanoparticles is the emulsification-solvent evaporation technique[5,21]. Briefly, a polymer and the molecule that has to be encapsulated are dissolved in organic solvent, water and surfactants are then added to create an emulsion. Sonication is often deployed in this technique to induce the formation of nanosized droplets. After complete evaporation the nanoparticles are generally collected *via* centrifugation and freeze-drying. A different approach is instead represented by electrospray[22]. The principle of this technique is to force the polymer out from a syringe in the form of micro and nanoparticles by applying a high voltage to the polymeric solution. Conversely to the "manual" approach, electrospray is suitable for upscaling and the instrument parameters can be predefined to reduce the variations caused by the operator. Electrospray may, however, induce degradation of some macromolecules due to the working parameters (i.e. thermal stress during drying, shear stress in the nozzle)[23].

In this work, we propose the use of an ultrasonic spray coater for the continuous and controlled production of polysaccharide nanoparticles.

The working principle of an ultrasonic spray coater is simple: a solution is flushed at a controlled flow rate through a nozzle. At the nozzle tip, ultrasound waves, at known frequencies, vibrate the layer of solution at the interface between nozzle and air. The ultrasound waves induce the formation of surface capillary waves that protrude the liquid outwards. Portions of the liquid are consequently expelled, forming a mist. The size of the droplets in the mist is mainly depended on the frequency of the ultrasound[24], as reported in Equation 1.

$$D = 0.34 \cdot \sqrt[3]{\frac{8\pi T}{\rho F^2}} \quad (1)$$

Where D represents the droplets diameter, T is the liquid surface tension, ρ represent the liquid density and F denotes the frequency. Ultrasonic spray coating has been extensively studied for coating surfaces[25] and we recently deployed it to cover microcontainers with a pH sensitive coating for oral drug delivery[26]. Ultrasonic spray coating has also been used to form layer of preformed particles in suspension, in their work, Stryckers et al.[27] noticed how the ultrasonic waves were able to remove particles aggregate, demonstrating the potential of this technique in connection with nanoparticles.
We evaluated the possibility of directly using an ultrasonic spray coater to fabricate alginate and chitosan nanoparticles instead of using preformed nanoparticles and evaluated the effect of tuning the spray coater parameters (generator power, flow rate of the two solutions, distance between nozzle and substrate and pressure of the focusing air) in terms of shifts in the size distribution. To the authors knowledge it is the first time this has been done.

2. Materials and Methods

2.1. Materials

Sodium Alginate (AL, medium molecular weight, Mn 110 kDa, PDI = 4.309) was purchased from Sigma Aldrich (St. Louis, USA). Chitosan chlorohydrate (CH, Mn 158.3 kDa, deacetylation = 83.6%) was purchased from Microresist Technology GmbH (Berlin, Germany).

2.2. Fabrication of nanoparticles

To fabricate the nanoparticles we made use of an ultrasonic spray coater (Sono-Tek, NY, U.S.) equipped with a dual feed Accumist nozzle and a 120 kHz ultrasounds generator. At first, a 0.1 $mg \cdot mL^{-1}$ solution of sodium alginate in deionized water and a 0.1 $mg \cdot mL^{-1}$ solution of chitosan chlorohydrate were made. Both solutions were then filtered through a 0.22 µm filter. The two solutions were then pumped in the spray coater at controlled flow rates, maintaining the ratio between the two solutions 1:1. The overall flow rates tested were: 0.5 $mL \cdot min^{-1}$, 1.0 $mL \cdot min^{-1}$, 1.5 $mL \cdot min^{-1}$. The alginate and chitosan solutions were then sprayed together, with a generator power of: 1 W, 2 W and 3 W. The spray beam was controlled with pressurized nitrogen at pressures of: 0.050 kPa, 0.075 kPa and 0.100 kPa. The samples obtained from the spray were collected in a vessel placed underneath the spray coater nozzle, at varying distances: 80, 55 and 30 mm. The starting parameters were selected on the basis of a visual assessment of the spray and corresponded to: 1.0 $mL \cdot min^{-1}$, 1 W, 0.075 kPa and 30 mm. Once collected, the samples were transferred to 1.5 mL vials for the subsequent characterization. The combination of parameters can be found in Table 1. As a reference sample, a nanoparticle suspension of alginate and chitosan was obtained following the “manual” protocol. Briefly, 1 mL of sodium alginate 0.1 $mg \cdot mL^{-1}$ was poured in a becker and placed under stirring, 1 mL of chitosan chlorohydrate 0.1 $mg \cdot mL^{-1}$ was consequently poured into the becker and kept under stirring for 5 min. The suspension was then collected for further analyses. A scheme, depicting the formation of polymeric nanoparticles using an ultrasonic spray coater, can be seen in Figure 1.

Table 1 – Ultrasonic spray coater parameters combinations used to obtain different nanoparticles samples.

	S1	S2	S3	S4	S5	S6	S7	S8	S9
Power (W)	1	2	3	1	1	1	1	1	1
Flow rate (mL·min^{-1})	1.0	1.0	1.0	0.5	1.5	1.0	1.0	1.0	1.0
Distance (mm)	30	30	30	30	30	55	80	30	30
Air pressure (kPa)	0.075	0.075	0.075	0.075	0.075	0.075	0.075	0.050	0.100

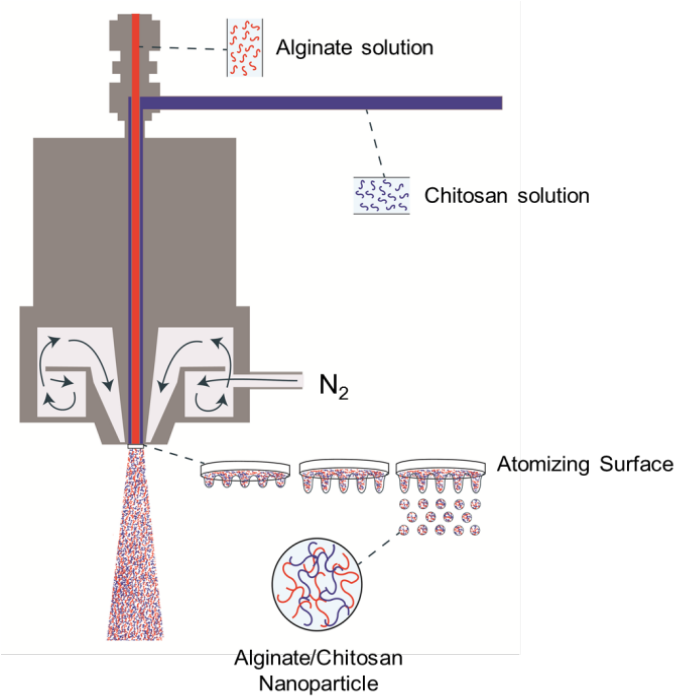

Figure 1 – Schematic representation of the ultrasonic spray coater nozzle. The two solutions are flushed simultaneously through the spray coater nozzle, kept separated until the tip of the nozzle is reached. Ultrasounds vibrate the tip of the nozzle inducing the atomization of the two solutions that are therefore being mixed in individual droplets. With the help of pressurized air the spray is focused towards a vessel to collect the nanoparticles suspension.

2.3. Dynamic light scattering

Dynamic light scattering (DLS) is an established method for size characterization of monodispersed particles in the sub-micron range. Measurements are based on the size dependent hydrodynamic mobility of particles in suspension and its effect on the transient modulation of the intensity of the scattered light.

The instrument used in this study to perform the DLS and ζ-potential measurements was a Zetasizer Nano ZS (Malvern Panalytical, Worcestershire, UK). Machine parameters relevant for DLS

measurements are the laser wavelength λ and the refraction angle θ, being equal to 633 nm and 173°, respectively. All measurements were performed at 25 °C. The dynamic viscosity η (0.89 mPas) and refractive index n (1.33) of deionized water were assumed for the measurements. All samples were measured right after spraying and tested in triplicate.

2.3.2. Particle size fitting from DLS autocorrelation function

Many different approaches on how to extract the particle size from the DLS measurements have been used and all have their own set of advantages and limitations. In the cases where a distribution is being calculated through fitting, the challenges often revolve around the large numbers of freedom introduced through the many parameters. In the cases where analytical calculation methods are employed, the complex mathematics can pose a bottleneck. On top of that, a more fundamental limitation of DLS measurements is the struggle to differentiate small size differences in a particle population.
The proposed method of extracting the particle size distribution in this paper aims at addressing these challenges. From a physics perspective, it is reasonable to assume that the particle sizes x obtained with this fabrication method follow a Gaussian distribution (hypothesis confirmed by scanning electron microscopy measurements). To avoid nonsensical negative particle sizes, a slightly modified Gaussian distribution was utilized: a Gamma distribution.

(…)

2.4. Scanning electron microscopy

The size of the alginate-chitosan nanoparticles was further investigated by means of scanning electron microscopy (SEM). Samples were prepared following the protocol of Schütz et al. with slight modifications. Briefly, a sample of nanoparticles was obtained using the parameters as in S1 (Table 1), the suspension was then poured over a clean glass slide and was freeze-dried overnight. The sample was subsequently coated with gold using a Cressington 208HR sputter coater, equipped with a gold target. The samples were finally visualized using a Zeiss Supra 40VP Field Emission SEM (Carl Zeiss Microscopy GmbH, Jena, Germany) in high vacuum mode at 10 keV.

4. Results and Discussion

4.1. Nanopoarticles characterization

To evaluate the possibility of using an ultrasonic spray coater to fabricate polymeric nanoparticles, and to evaluate the effect of changing the spray coater parameters on the size distribution of the nanoparticles, we used a well know combination of polysaccharides: alginate and chitosan. These two materials have been already seen forming nanoparticles by many research groups[6,28,29] and constituted, therefore, a nice case study. Alginate and chitosan are, nevertheless, very interesting materials. Alginate is known for its ability of forming hydrogels in the presence Ca^{2+} or other divalent ions[30,31]. Chitosan has proven to be mucoadhesive[17], to possess antibacterial properties[9] and to dampen the

formation of reactive oxygen species (ROS) in stimulated human neutrophils[6]. Both materials have been extensively studies as promising materials for drug delivery purposes.

During the process, the two solutions (alginate and chitosan) are physically separated until they reach the tip of the nozzle. Once the two solutions reached the tip of the nozzle they were atomized into a mist constituted of droplets of around 2.6 pL. The two polymers got consequently mixed in their atomized phase. Once collected into the vessel, electrostatic repulsion (see the ζ-potential in Table 2) inhibited aggregation.

Initially, we evaluated which concentration was suitable for the usage of ultrasonic spray coating. We tested various concentrations of alginate and chitosan and found out that 0.1 $mg \cdot mL^{-1}$ (for both solutions) allowed for the formation of fine sprays. Concentrations above 0.2 $mg \cdot mL^{-1}$ (for both solutions) caused the formation of a macroscopic hydrogel in the vessel. Once the concentrations were defined the spray coater parameters where varied to understand their effect on the nanoparticles size distribution. The results of the DLS analyses, reported in Table 2, show the effect on the size distribution caused by the changes in the parameters.

Table 2 – DLS results represented as hydrodynamic diameter (D_H), poly dispersity index (PDI) and ζ-potential (ζ) ± standard deviation (SD). N = 3.

	S1	S2	S3	S4	S5	S6	S7	S8	S9	Ctrl
D_H (nm) ± SD	162 ± 5	227 ± 20	241 ± 37	198 ± 7	237 ± 14	170 ± 3	230 ± 5	217 ± 4	189 ± 4	162 ± 3
PDI	0.385	0.376	0.406	0.390	0.520	0.321	0.453	0.492	0.427	0.211
ζ (mV) ± SD	-32 ± 1	-34 ± 0	-33 ± 0	-36 ± 2	-41 ± 1	-37 ± 1	-33 ± 3	-38 ± 2	-38 ± 1	-27 ± 3

Following the results in Table 2, when the power was varied between 1 W, 2 W and 3 W (S1 *vs* S2 *vs* S3) the average hydrodynamic diameter increased together with the PDI of the individual suspensions. This effect could be explained by hypothesizing that in each droplet of the spray one, and only one nanoparticle, is formed. Consequently, bigger droplets would cause the formation of bigger nanoparticles. Changing the power might, in fact, have an influence on the size of the droplets. Conversely to the frequency, where it´s influence on the droplets size is well understood, the effect of the ultrasounds generator power over the droplets size is not. A tendency of causing the formation of bigger droplets and a less homogenous spray has, however, been seen. We hypothesize that, by increasing the power of the ultrasound generator, the liquid protrusions at the interface with air become more pronounced and bigger portions of these are thereby expelled in the spray leading to the formation of bigger nanoparticles.

Comparing the samples obtained using different flow rates (S1 *vs* S4 *vs* S5) it is possible to notice how both reducing the flow rate to 0.5 $mL \cdot min^{-1}$ (S4) and increasing it to 1.5 $mL \cdot min^{-1}$ (S5) caused an

increase in the nanoparticle average hydrodynamic diameter. The differences are less pronounced compared to the variation caused by tuning the generator power. When the flow rate was reduced, a thinner spray was formed. This spray resulted more affected by the inbuilt ventilation system of the spray coater compared to S1, causing a loss in the smaller droplets. Moreover, comparing to S1, twice the power-flow rate ratio applied was doubled, an excessive power for that volume of solution might have caused a similar effect to that explained previously for sample S2 and S3. When the flow rate was instead increased (S5) the average hydrodynamic diameter also increased. The level of power deployed for that flow rate (1 W) probably was too low. Indeed, from a qualitative point of view, the spray looked thicker and larger droplets where distinguishable. Shifting the attention to the distance between the nozzle and the substrate (S1 *vs* S6 *vs* S7), it is possible to notice how moving further away causes an increase in the size distribution of the alginate-chitosan nanoparticles. Whereas the difference between S1 and S6 was only limited, it resulted more evident when S7 was considered. As the spray had to travel a longer distance the influence of the ventilation system was more prominent. The spray itself was, in fact, seen to wobble due to the suction; it is probable that the smaller droplets were being influenced more by this effect and, consequently, the average size shifted towards higher hydrodynamic diameters. It is consequently possible to define a range of nozzle-substrate distances in which the effect on the nanoparticles hydrodynamic size is limited. This would be useful when casting a coating of nanoparticles, in fact, as Bose Goswami et al.[25] demonstrated, the distance between the nozzle and the substrate that has to be coated is the most important parameters to control for achieving a uniform coating layer. Finally comparing the air pressure (S1 *vs* S8 *vs* S9) is not trivial. A reduction in the pressure from 0.075 kPa to 0.050 kPa (S1 *vs* S8) caused an increase in the average size of the nanoparticles. This was caused by a very poor level of the spray beam focus, which tended to wobble significantly more, collecting the sample resulted in fact more difficult. As seen for the variation in the distance between nozzle and substrate, again the ventilation might have had a greater effect on the smaller droplets in the spray. Increasing the air pressure, from 0.075 kPa to 0.100 kPa (S1 *vs* S9) also resulted in bigger dimensions of nanoparticles. In this case the resulted highly focused and not affected by the ventilation system in any manner. It is possible, however, that the high pressure caused the merging of multiple droplets in bigger ones. Following the initial hypothesis, where one and only one nanoparticle is formed in each droplet, we can assume that bigger nanoparticles would form in case of droplets merging. Overall, we can say that, among the tested parameters, the nanoparticles size distribution was mostly effected by changes in ultrasound power. The other parameters had, instead, a minor influence: power > flow rate > distance > air pressure. Regarding the ζ-potential, the differences resulted much more limited instead. All samples presented a net negative charge of around -35 mV. This net negative charge is justified by the excess of charged groups present in alginate compared to chitosan, as only 83.6% of the total chitosan monomers were deacetylated and thereby presented a net positive charge. From the point of view of a drug delivery system, having nanoparticles with a ζ-potential of ± 30 mV or higher is generally associated with highly stable formulations, thanks to their reciprocal repulsion. It is nevertheless interesting to notice how the control (Ctrl, Table 2) which represent the “manual” method of fabrication, tended to give nanoparticles with a lower size and with

the smaller PDI among all sample tested. This makes sense considering that the two polysaccharides, in the control, are able to freely interact all together. The nanoparticles formation is consequently purely driven by a reduction in free energy as the two oppositely charged, alginate and chitosan, interact. Using the ultrasonic spray coater, instead, the nanoparticles formation was forced to happen in the individual droplets forming the spray. The droplets volumetric distribution is consequently driving the size distribution of the nanoparticles.

As reported in Figure 2a and b, the alginate-chitosan nanoparticles were also investigated by means of SEM. After freeze drying, the nanoparticles tended to form agglomerates around NaCl crystals; this was expected as the suspensions were not dialyzed against deionized water to remove the counter ions of sodium alginate and chitosan chlorohydrate. The nanoparticles diameter resulted lower to that seen from the DLS analysis, resulting equal to 41 ± 8 nm (N = 120, SD), this result is appropriate as the nanoparticles were not hydrated. The size distribution resulted moreover to fit a Gaussian distribution (data not shown).

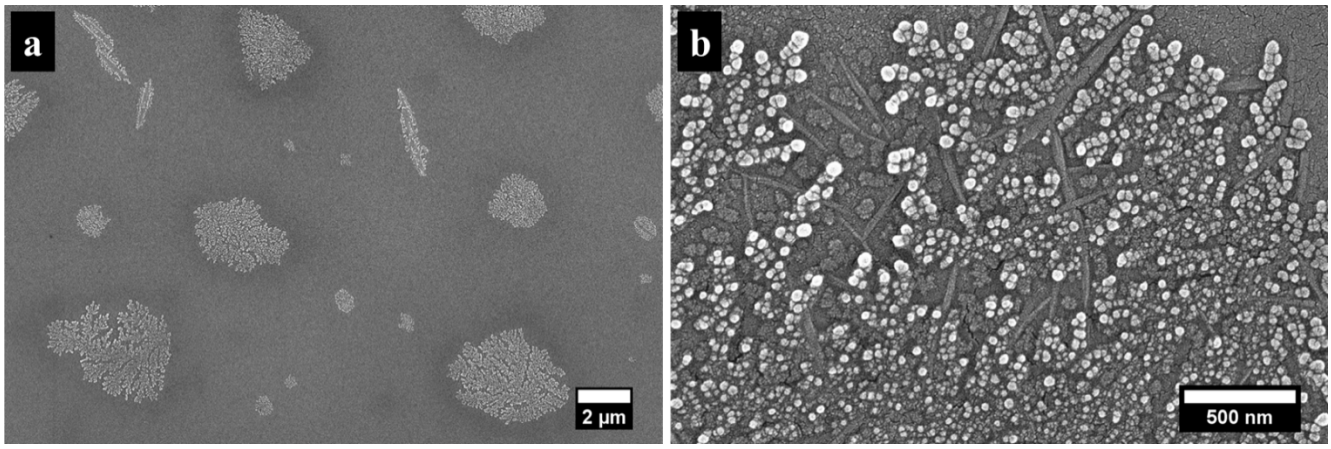

Figure 2 – SEM pictures of nanoparticles (sample S1). Overview of the nanoparticles clustered around NaCl crystals (a). Zoom in on a nanoparticles cluster (b)

5. Conclusions

In this work ultrasonic spray coating was successfully used to fabricate nanoparticles constituted of alginate and chitosan. This technique has a great potential due to its intrinsic up-scalability, safety and simplicity. The fabrication process can be moreover easily modified to obtain nanoparticles with different materials. The ability of tuning the size of nanoparticles by changing the instrumentation parameters is a powerful tool that can be exploited to obtain population of nanoparticles with the desired sizes without modifying the formulation. In this regards, a variation in the frequency of the ultrasounds deployed should be further investigated as a parameter to modulate the size distribution of nanoparticles, since its effect on droplet size is well established. Finally, this work, reports for the first time, an actual indication of an increase in droplet size from an ultrasonic spray coater caused by an increase in the ultrasound generator power.

Acknowledgment

The Danish National Research Foundation (DNRF 122) and the Villum Foundation (grant no. 9301) are greatly acknowledged for funding. Ellen Vallentin Christiansen is acknowledge for drawing the schematics.

References

[1] S. Bhattacharjee, *J. Control. Release* **2016**, *235*, 337.

[2] F. J. Heiligtag, M. Niederberger, *Mater. Today* **2013**, *16*, 262.

[3] B. L. Banik, P. Fattahi, J. L. Brown, *Wiley Interdiscip. Rev. Nanomedicine Nanobiotechnology* **2016**, *8*, 271.

[4] N. Han, L. Pang, J. Xu, H. Hyun, J. Park, Y. Yeo, *Mol. Pharm.* **2017**, *14*, 1538.

[5] K. M. El-Say, H. S. El-Sawy, *Int. J. Pharm.* **2017**, *528*, 675.

[6] P. Sacco, E. Decleva, F. Tentor, R. Menegazzi, M. Borgogna, S. Paoletti, K. A. Kristiansen, K. M. Vårum, E. Marsich, *Macromol. Biosci.* **2017**, *1700214*, 1700214.

[7] M. S. Schmidt, J. Hübner, A. Boisen, *Adv. Mater.* **2012**, *24*, 11.

[8] L. Morelli, K. Zór, C. B. Jendresen, T. Rindzevicius, M. S. Schmidt, A. T. Nielsen, A. Boisen, *Anal. Chem.* **2017**, *89*, 3981.

[9] P. Sacco, A. Travan, M. Borgogna, S. Paoletti, E. Marsich, *J. Mater. Sci. Mater. Med.* **2015**, *26*, 1.

[10] C. von Halling Laier, B. Gibson, M. van de Weert, B. J. Boyd, T. Rades, A. Boisen, S. Hook, L. Hagner Nielsen, *Int. J. Pharm.* **2018**, *550*, 35.

[11] M. Matbou Riahi, A. Sahebkar, K. Sadri, S. Nikoofal-Sahlabadi, M. R. Jaafari, *Int. J. Pharm.* **2018**, *540*, 89.

[12] Y. Barenholz, *J. Control. Release* **2012**, *160*, 117.

[13] L. Jia, **2009**, *1*, 237.

[14] M. Morgen, C. Bloom, R. Beyerinck, A. Bello, W. Song, K. Wilkinson, R. Steenwyk, S. Shamblin, *Pharm. Res.* **2012**, *29*, 427.

[15] M. Salvalaio, L. Rigon, D. Belletti, F. D'Avanzo, F. Pederzoli, B. Ruozi, O. Marin, M. A. Vandelli, F. Forni, M. Scarpa, R. Tomanin, G. Tosi, *PLoS One* **2016**, *11*, 1.

[16] M. Gupta, G. Chashoo, P. R. Sharma, A. K. Saxena, P. N. Gupta, G. P. Agrawal, S. P. Vyas, *Mol. Pharm.* **2014**, *11*, 697.

[17] I. a. Sogias, A. C. Williams, V. V. Khutoryanskiy, *Biomacromolecules* **2008**, *9*, 1837.

[18] J. S. Suk, Q. Xu, N. Kim, J. Hanes, L. M. Ensign, *Adv. Drug Deliv. Rev.* **2016**, *99*, 28.

[19] S. Chen, F. Guo, T. Deng, S. Zhu, W. Liu, H. Zhong, H. Yu, R. Luo, Z. Deng, *AAPS PharmSciTech* **2017**, *18*, 1277.

[20] X. Deng, M. Cao, J. Zhang, K. Hu, Z. Yin, Z. Zhou, X. Xiao, Y. Yang, W. Sheng, Y. Wu, Y. Zeng, *Biomaterials* **2014**, *35*, 4333.

[21] J. P. Rao, K. E. Geckeler, *Prog. Polym. Sci.* **2011**, *36*, 887.

[22] J. A. Tapia-Hernández, P. I. Torres-Chávez, B. Ramírez-Wong, A. Rascón-Chu, M. Plascencia-Jatomea, C. G. Barreras-Urbina, N. A. Rangel-Vázquez, F. Rodríguez-Félix, *J. Agric. Food Chem.* **2015**, *63*, 4699.

[23] R. Sridhar, S. Ramakrishna, R. Sridhar, S. Ramakrishna, **2015**, *2535*, 1.

[24] R. J. Lang, *J. Acoust. Soc. Am.* **1962**, *34*, 6.

[25] S. Bose, S. S. Keller, T. S. Alstrøm, A. Boisen, K. Almdal, *Langmuir* **2013**, *29*, 6911.

[26] C. Mazzoni, F. Tentor, S. A. Strindberg, L. H. Nielsen, S. S. Keller, T. S. Alstrøm, C. Gundlach, A. Müllertz, P. Marizza, A. Boisen, *J. Control. Release* **2017**, *268*, 343.

[27] J. Stryckers, L. D'Olieslaeger, J. V. M. Silvano, C. K. Apolinario, A. C. G. Laranjeiro, J. Gruber, J. D'Haen, J. Manca, A. Ethirajan, W. Deferme, *Phys. Status Solidi Appl. Mater. Sci.* **2016**, *213*, 1441.

[28] M. A. Azevedo, A. I. Bourbon, A. A. Vicente, M. A. Cerqueira, *Int. J. Biol. Macromol.* **2014**, *71*, 141.

[29] R. C. Nagarwal, R. Kumar, J. K. Pandit, *Eur. J. Pharm. Sci.* **2012**, *47*, 678.

[30] A. Haug, J. Bjerrum, O. Buchardt, G. E. Olsen, C. Pedersen, J. Toft, *Acta Chem. Scand.* **1961**, *15*, 1794.

[31] K. I. Draget, G. Skjåk-Bræk, O. Smidsrød, *Int. J. Biol. Macromol.* **1997**, *21*, 47.